

**Structural and biochemical studies of the regulation
and catalytic mechanism of ATP synthase**

by

Matthew William Bowler

A dissertation submitted to the University of Cambridge in
candidature for the degree of Doctor of Philosophy

Lent Term 2005

Medical Research Council Dunn Human Nutrition Unit

and

Girton College, Cambridge University

Declaration

The work described in this thesis was carried out at the Medical Research Council Dunn Human Nutrition Unit between October 2001 and January 2005. Except where specifically stated, this dissertation is the outcome of my own work and not the result of any collaboration. No part of this thesis has been submitted for a qualification at any other university.

Matthew W. Bowler

January 2005

Acknowledgements

I thank Prof. Sir John Walker for supervising my research; it has been a fascinating and inspiring three years. I am grateful for his continued support. I would also like to thank Dr. A. G. W. Leslie for teaching me crystallography and for being extremely generous with his time and knowledge.

Analytical centrifugation was carried out in the Laboratory of Molecular Biology under the guidance of Dr. P. J. G. Butler. I am very grateful for the time and effort given to showing me the technique. I thank Prof. D. M. Mueller for the yeast strain with a histidine tagged ATP synthase β subunit. I received much advice on cloning, expressing, purifying and crystallising proteins from Mr. M. G. Montgomery and Mr. M. J. Runswick, I am extremely grateful for their efforts.

For proofreading and invaluable comments on the manuscript I thank Dr. I. M. Fearnley, Dr. M. G. Bowler, Dr. A. G. W. Leslie, Dr. V. R. Smith, Mr. M. G. Montgomery and Mr. M. J. Runswick. Many thanks are due to Mr. M. G. Montgomery for help with all things Macintosh. I also thank Mary for excellent proofreading.

I would like to thank all the members of the Walker group for making my time here incredibly enjoyable, in particular Dr. V. R. Smith, Dr. J. L. Rubinstein, Mr. M. G. Montgomery, Mr. M. J. Runswick and Miss C. Terry.

I thank Mary for her tireless support, timely advice and tolerance of numerous late nights.

This thesis is dedicated to Mary and to the memory of PMB.

Matthew W. Bowler, January 2005.

“I hate quotations. Tell me what you know.”

Ralph Waldo Emerson

Contents

Abstract	xii
Abbreviations	xiii
Chapter One: Introduction	1
1.1 The mitochondrion and bioenergetics	1
1.1.1 The mitochondrion	1
1.1.2 Bioenergetics	7
1.2 The electron transport chain and oxidative phosphorylation	9
1.3 The ATP synthase	15
1.3.1 Introduction	15
1.3.2 The subunits of the ATP synthase	16
1.3.3 The minor subunits	19
1.3.4 The peripheral stalk	20
1.3.5 Proton translocation by the F_o domain	22
1.3.6 The structure of bovine mitochondrial F_1 -ATPase	26
1.3.7 The catalytic mechanism	29
1.3.8 Direct observation of rotation	31
1.3.9 Structures of F_1 -ATPase	32

1.4 The inhibitor protein of the ATP synthase	34
1.4.1 Regulation of the ATP synthase	34
1.4.2 The bovine mitochondrial IF ₁	36
1.4.3 The inhibitor protein of <i>Saccharomyces cerevisiae</i>	38
1.5 Metallofluorides as analogues of nucleotides and of the transition state of phosphoryl transfer	39
1.5.1 The chemistry of phosphoryl transfer	41
1.5.2 Aluminium and beryllium fluoride	44
1.5.3 Transition states in the catalytic cycle of F ₁ -ATPase	45
1.5.3.1 The structure of bovine F ₁ -ATPase with all three catalytic sites occupied	45
1.5.3.2 The structure of bovine F ₁ -ATPase with two sites occupied by ATP	48
1.5.4 Magnesium fluoride	50
1.6 Aims of this work	52
Chapter Two: Materials and methods	54
2.1 Materials	54
2.1.1 Chemicals	54
2.1.2 Chromatography	55
2.1.3 Bacterial strains and growth media	55
2.1.4 <i>Saccharomyces cerevisiae</i> strains and growth media	56
2.1.5 Synthetic oligonucleotides	56

2.2 Biochemical methods	56
2.2.1 Agarose gel electrophoresis	56
2.2.2 SDS-PAGE	57
2.2.3 Western blotting	58
2.2.3.1 Protein transfer	58
2.2.3.2 Immuno-detection of proteins	58
2.2.4 Measurement of protein concentration	59
2.2.5 Preparation of competent cells	59
2.2.5.1 Electro-competent cells	59
2.2.5.2 Chemically competent cells	59
2.2.6 Transformation of bacteria	60
2.2.6.1 Electroporation	60
2.2.6.2 Heat shock transformation	60
2.2.7 Calibration of gel filtration columns	61
2.2.8 Activity assays	61
2.2.9 Construction of expression plasmids bearing wild type and mutant IF₁	62
2.2.9.1 Polymerase chain reaction (PCR)	63
2.2.9.2 Restriction digestions	64
2.2.9.3 Vector preparation	65
2.2.9.4 Vector screening and preparation	65
2.2.9.5 DNA sequence analysis	66
2.2.10 Purification of inhibitor proteins	66
2.2.10.1 Overexpression	66

2.2.10.2 Purification of yeast IF ₁	67
2.2.11 Purification of F₁-ATPase from <i>S. cerevisiae</i>	67
2.2.11.1 Cell growth and purification of mitochondria from <i>S. cerevisiae</i>	67
2.2.11.2 Preparation of submitochondrial particles	68
2.2.11.3 Purification of <i>S. cerevisiae</i> F ₁ -ATPase	68
2.2.12 Purification of bovine mitochondrial F₁-ATPase	69
2.2.12.1 Purification of bovine heart mitochondria	69
2.2.12.2 Purification of bovine F ₁ -ATPase	70
2.2.13 Inhibition of F₁-ATPases by inhibitor proteins	71
2.2.14 Analysis of the oligomeric state of <i>S. cerevisiae</i> IF₁	72
2.2.14.1 Gel filtration chromatography	72
2.2.14.2 Covalent cross-linking	72
2.2.14.3 Analytical centrifugation	72
2.2.15 Inhibition of bovine F₁-ATPase with ADP and magnesium fluoride	73
2.2.16 Protein crystallisation	74
2.2.16.1 Crystallisation of F ₁ -ATPase inhibited by ADP and magnesium fluoride	74
2.2.16.2 Harvesting and cryoprotection	75
2.2.17 X-ray crystallography analysis	76
2.2.17.1 Crystal screening	76
2.2.17.2 Data collection	77
2.2.17.3 Data processing	77
2.2.17.4 Molecular replacement	79
2.2.17.5 Model refinement	80

2.2.17.5.1 Refinement using Refmac5	80
2.2.17.5.2 Manual rebuilding	81
2.2.17.6 Structure validation	81
2.2.17.7 Figure preparation	82

Chapter Three: Mechanism of action of the F-ATPase

inhibitor protein IF₁ from *Saccharomyces cerevisiae* 83

3.1 Results 83

3.1.1 Purification of recombinant inhibitor proteins 83

3.1.2 Inhibitory activity of *S. cerevisiae* inhibitor proteins 86

3.1.3 Covalent crosslinking of inhibitor proteins 88

3.1.4 Oligomeric state of the *S. cerevisiae* F₁-YIF₁ complex 90

3.1.4.1 Gel filtration analysis 90

3.1.4.2 Analytical ultracentrifugation 92

3.2 Discussion 94

3.2.1 Active and inactive states of the *S. cerevisiae* inhibitor proteins 94

3.2.2 Structure and mechanism of action of the inhibitor proteins 95

3.2.3 Dimerisation of F-ATPases 98

Chapter Four: The structure of bovine mitochondrial F₁-ATPase inhibited with ADP and magnesium fluoride	99
4.1 Results	99
4.1.1 Introduction	99
4.1.2 Inhibition of bovine F ₁ -ATPase with ADP and magnesium fluoride	99
4.1.3 Crystallisation of bovine F ₁ -ATPase inhibited with ADP and magnesium fluoride	101
4.1.4 Cryoprotection of crystals	102
4.1.4.1 Harvesting solution	102
4.1.4.2 Cryoprotectant	102
4.1.4.3 Screening of crystals	104
4.1.5 Structure determination	104
4.1.5.1 Data collection	104
4.1.5.2 Structure solution	106
4.1.5.3 Structure validation	110
4.1.6 Molecular architecture of the ADP and magnesium fluoride inhibited bovine F ₁ -ATPase	113
4.1.7 The nucleotide binding sites	115
4.1.8 The nucleotide occupancy of F ₁ -ATPase in crystal 22	118
4.2 Discussion	121
4.2.1 Comparison of the F ₁ -MgF ₃ ⁻ structure with previously solved structures	121
4.2.2 The catalytic sites	124

4.2.3 Why does the β_E subunit bind nucleotide?	125
4.2.4 Implications for the catalytic mechanism	130
4.3 Conclusion	132
Appendix A: Crystallographic theory	135
A.1 Introduction	135
A.2 X-ray sources	136
A.2.1 Rotating anode X-ray tubes	136
A.2.2 Synchrotron radiation	138
A.3 X-ray detectors	140
A.3.1 Image plates	140
A.3.2 CCD detectors	142
A.4 Crystals	144
A.5 Scattering of X-rays by protein crystals	149
A.6 The Ewald sphere and reciprocal space	152
A.7 Structure solution and the phase problem	153
A.8 The molecular model	158
Appendix B: Supplementary figures	160
References	167

Abstract

Structural and biochemical studies of the regulation and catalytic mechanism of ATP synthase

Matthew W. Bowler

ATP synthase (F_1F_0 -ATPase) catalyses the production of ATP from ADP and orthophosphate by using the proton motive force established across a membrane by photosynthesis or oxidative phosphorylation. The ATP synthase of eukaryotic mitochondria is located in the inner membrane and is comprised of two domains. The globular F_1 domain protrudes into the matrix and it contains the catalytic sites for ATP synthesis. The membrane bound F_0 domain contains a proton channel. The two domains are connected by central and peripheral stalks. When F_1 is removed from the complex, it can hydrolyse ATP but not synthesise it. It is composed of nine subunits with the stoichiometry $\alpha_3\beta_3\gamma\delta\epsilon$. The α and β subunits are arranged alternately round the asymmetric γ subunit, which, with the δ and ϵ subunits, forms the central stalk. Catalysis occurs by a rotary mechanism where rotation in F_0 , induced by the passage of protons, is transmitted to F_1 via the central stalk. The rotation of the γ subunit induces conformational changes in the catalytic β subunits that lead to the synthesis of ATP. The three catalytic sites proceed through three major and well defined conformations sequentially, and no two sites are the same at any one time. The peripheral stalk counters the tendency of the $\alpha_3\beta_3$ subcomplex to rotate with the γ subunit. The ATP synthase of mitochondria is regulated by an inhibitor protein, IF_1 , that prevents hydrolysis of ATP when the proton motive force collapses.

Saccharomyces cerevisiae has two inhibitor proteins, YIF_1 and STF_1 . The states of oligomerisation of their active and inactive forms have been investigated. In contrast to bovine IF_1 , which is active as a dimer, the yeast inhibitors are active as monomers around pH 7.0. Like the bovine protein, they form inactive oligomers at higher pH values.

While many of features of the mechanism of catalysis of the ATP synthase are well understood, it is now clear that there are many sub-steps within the cycle. Some of them have been revealed by analogues of phosphoryl transfer. Bovine mitochondrial F_1 -ATPase inhibited with ADP and magnesium fluoride forms a transition state analogue complex. Its structure was solved to 2.5 Å resolution. The β_{TP} and β_{DP} catalytic sites both contain ADP and MgF_3^- . The β_E subunit binds ADP, despite being in an essentially open conformation. The structure represents a new sub-step in the catalytic cycle just before the release of the substrates of ATP hydrolysis.

Abbreviations

Structures:

1. Reference structure: bovine F_1 -ATPase containing AMP-PNP in the β_{TP} subunit and ADP in the β_{DP} subunit (Abrahams *et al.*, 1994). The structure used is taken from a single crystal cooled to 100K (Braig *et al.*, 2000).
2. (ADP·AlF₃)-F₁: The structure of bovine F_1 -ATPase inhibited with ADP and aluminium fluoride. The structure contained AMP-PNP in the β_{TP} subunit and ADP·AlF₃ in the β_{DP} subunit (Braig *et al.*, 2000).
3. (ADP·AlF₄⁻)₂-F₁: The structure of bovine F_1 -ATPase inhibited with ADP and aluminium fluoride. The structure contained ADP·AlF₄⁻ in the β_{TP} subunit and the β_{DP} subunit and the β_E subunit contained ADP and sulphate (mimicking phosphate) and adopted a 'half-closed' conformation (Menz *et al.*, 2001b).
4. F₁-DCCD: The structure of bovine F_1 -ATPase inhibited with dicyclohexylcarbodiimide (DCCD) (Gibbons *et al.*, 2000).
5. BeF₃⁻-F₁: The structure of bovine F_1 -ATPase inhibited with ADP and beryllium fluoride. The structure contained ADP·BeF₃⁻ in the β_{TP} subunit and the β_{DP} subunit (Kagawa *et al.*, 2004).
6. F₁-MgF₃⁻: The structure of bovine F_1 -ATPase inhibited with ADP and magnesium fluoride.

Å	Ångström (1 Å = 0.1 nm)
$\Delta\psi$	transmembrane potential
ϵ ACA	ϵ -amino-N-caproic acid
ADP	adenosine diphosphate
AlF_3	aluminium trifluoride
AlF_4^-	aluminium tetrafluoride
AMP-PNP	adenylylimidodiphosphate
ANT	adenine nucleotide transporter
ATP	adenosine triphosphate
ATPase	adenosine triphosphatase
BCA	bicinchoninic acid
BeF_3^-	beryllium trifluoride
BIF_1	bovine inhibitor protein
bp	base pairs
BSA	bovine serum albumin
ca	circa
CCD	charge coupled device
CM-sepharose	carboxy-methyl sepharose
CoA	coenzyme A
C-terminal	carboxy terminal
Da	Dalton
DCCD	dicyclohexylcarbodiimide

DMS	dimethyl suberimidate
DNA	deoxyribonucleic acid
DTT	dithreothreitol
EDTA	ethylenediaminetetraacetic acid
F ₁	factor 1
F ₆	factor 6
FAD	flavin adenine dinucleotide
FADH ₂	reduced flavin adenine dinucleotide
F _C	calculated structure factors
FMN	flavin mononucleotide
FMNH	reduced Flavin mononucleotide
F _o	oligomycin sensitivity factor
F _O	observed structure factors
g	relative centrifugal force
GDP	guanosine diphosphate
GTP	guanosine triphosphate
hrs	hours
HPLC	high performance liquid chromatography
IBTP	iodobutyltriphenylphosphonium
IF ₁	inhibitor protein of ATP synthase
IPTG	isopropyl-β-D-thiogalactopyranoside
J	Joule

K_{av}	partition coefficient
LDH	lactate dehydrogenase
M	molar
MES	2-(N-morpholino)-ethanesulphonic acid
MgADP	magnesium salt of adenosine diphosphate
MgATP	magnesium salt of adenosine triphosphate
MgF_3^-	magnesium trifluoride
MgF_4^{2-}	magnesium tetrafluoride
min	minutes
NAD^+	nicotinamide adenine dinucleotide
NADH	reduced nicotinamide adenine dinucleotide
NH_4F	ammonium fluoride
NMR	nuclear magnetic resonance
NTA	nitrilotriacetic acid
N-terminus	amino terminus
NTP	nucleotide triphosphate
OD_{xxx}	optical density at wavelength XXX nm
OSCP	oligomycin sensitivity conferral protein
PAB	p-amino benzamidine
PAGE	polyacrylamide gel electrophoresis
PCR	polymerase chain reaction
PDB	protein data bank

PEG	polyethylene glycol
PEP	phosphoenol pyruvate
Pi	inorganic phosphate
PK	pyruvate kinase
pmf	proton motive force
PMSF	phenyl methyl sulphonyl fluoride
PVDF	poly-(vinylidene difluoride)
Q	coenzyme Q (quinone)
Q [•]	semiquinone
QH ₂	reduced Coenzyme Q (quinol)
rmsd	root mean square deviation
rpm	revolutions per minute
S	Svedbergs
SDS	sodium dodecylsulphate
SMP	submitochondrial particle
STF ₁	stabilising factor 1
STF ₂	stabilising factor 2
STF ₃	stabilising factor 3
TCA	tricarboxylic acid
TIM	translocase of the inner membrane
TOM	translocase of the outer membrane
Tris	2-amino-2-(hydroxymethyl)-1,3-propanediol

TY	tryptone yeast broth
U	units of enzyme activity
UV	ultra violet
v/v	volume per volume
V_0	void volume
V_e	elution volume
V_t	total volume
w/v	weight per volume
YIF ₁	inhibitor protein of ATP synthase from <i>S. cerevisiae</i>

CHAPTER 1: INTRODUCTION

1.1 The mitochondrion and bioenergetics

Mitochondria are often referred to as the power plant of eukaryotic cells, as they are the site of oxidative metabolism and produce the energy used by the cell in the form of adenosine triphosphate (ATP). Almost all energetic processes within biological cells require ATP, mostly produced by the membrane bound multimeric complex ATP synthase. This complex, and the complexes associated with the production of energy, are located in the inner membrane of mitochondria.

ATP synthase is also found in the energy transducing membranes of prokarya, archaea and eukarya. These membranes are the plasma membrane of eubacteria and archaea, and the thylakoid membrane of chloroplasts. Some of the protein complexes found in these membranes perform essentially the same functions and are structurally very similar as they share the same evolutionary origin: Mitochondria and chloroplasts are the evolutionary legacy of endosymbiotic events when non-respiring or photosynthetic eukaria ingested, or were invaded by, prokaryotes (Altmann, 1890; Gray *et al.*, 1999).

1.1.1 The mitochondrion

Mitochondria are eukaryotic cellular organelles present throughout the cytosol of most cells (Figure 1.1). Their size and morphology vary according to tissue type but they are generally ellipsoidal in shape, with dimensions of about 1.5 μm in diameter and 2 μm in length. They are bounded by two membranes, a smooth outer membrane and a highly folded inner membrane (Mannella *et al.*, 1997). The outer membrane is freely permeable to ions and small molecules via a non-specific channel VDAC [voltage dependent anion channel, or

porin]. The invaginated inner membrane provides an enormous surface area for energy transduction [(Palade, 1953) Figure 1.2]. These invaginations, or cristae, are impermeable to metabolites, macromolecules and protons but they are freely permeable to oxygen and carbon dioxide. The cristae contain the proteins of oxidative phosphorylation (Saraste, 1999) and transporters that import necessary metabolites and export metabolic products (Walker and Runswick, 1993).

The cristae split the mitochondria into two compartments: the matrix, which is bounded by the inner membrane, where the citric acid cycle, fatty acid oxidation and ATP synthesis take place; and the intermembrane space.

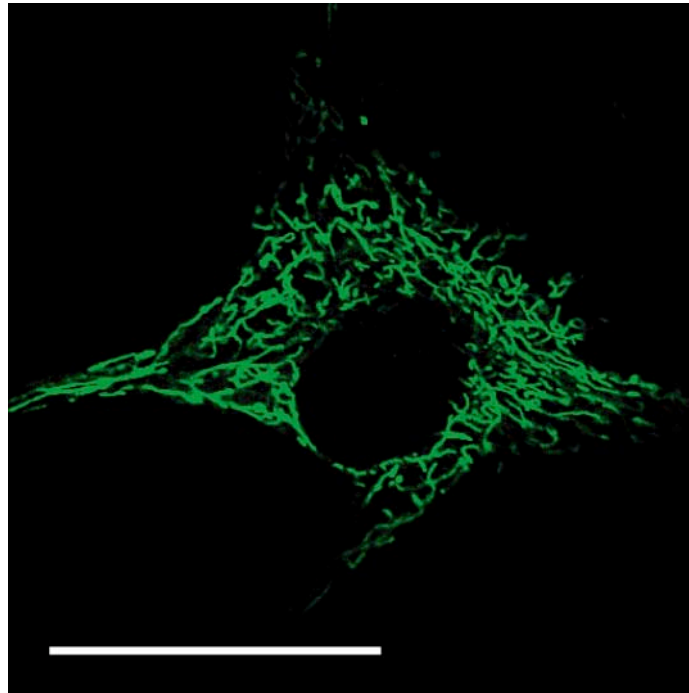


Figure 1.1. Mitochondria of a human fibroblast. A human fibroblast was incubated with iodobutyltriphenylphosphonium (IBTP), fixed, and visualised with anti-IBTP antiserum and an Oregon green linked secondary antibody. IBTP accumulates in mitochondria driven by the membrane potential and reacts covalently with free protein thiols in the matrix. The scale bar represents 50 μm . [Figure courtesy of Meredith Ross, MRC Dunn Human Nutrition Unit]

Electron tomography of mitochondria has revealed that the cristae are, in turn, differentiated into two sections: the inner membranes and the cristae membranes. The inner membranes closely follow the outer membranes and the cristae membranes fill most of the mitochondrion, and are connected to the inner membranes by tubular structures referred to as cristae junctions [Figure 1.3 (Frey *et al.*, 2002)]. This effectively splits the inner membranes into two sections.

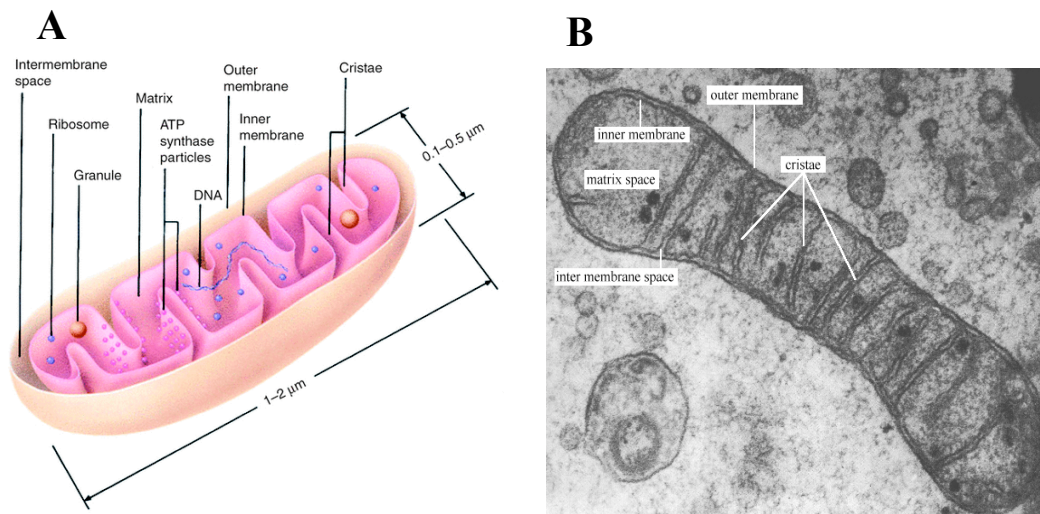


Figure 1.2. The mitochondrion. **A:** Schematic of the mitochondrion showing the major features. [From (Lodish *et al.*, 2000)]. **B:** Cross-section of a mitochondrion taken by electron microscopy in negative stain.

Mitochondria are semi-autonomous as they possess their own DNA, and independent machinery to replicate and transcribe it and to translate the transcripts into proteins. The human mitochondrial genome is a closed circular molecule of 16,596 bp that contains 37 genes. Of these genes, 13 encode proteins of the respiratory chain and the ATP synthase, 22 encode transfer RNAs and the remaining two encode the 12 and 16 S ribosomal RNAs (Figure 1.4). The proteins encoded by the genome are as follows: seven subunits of complex

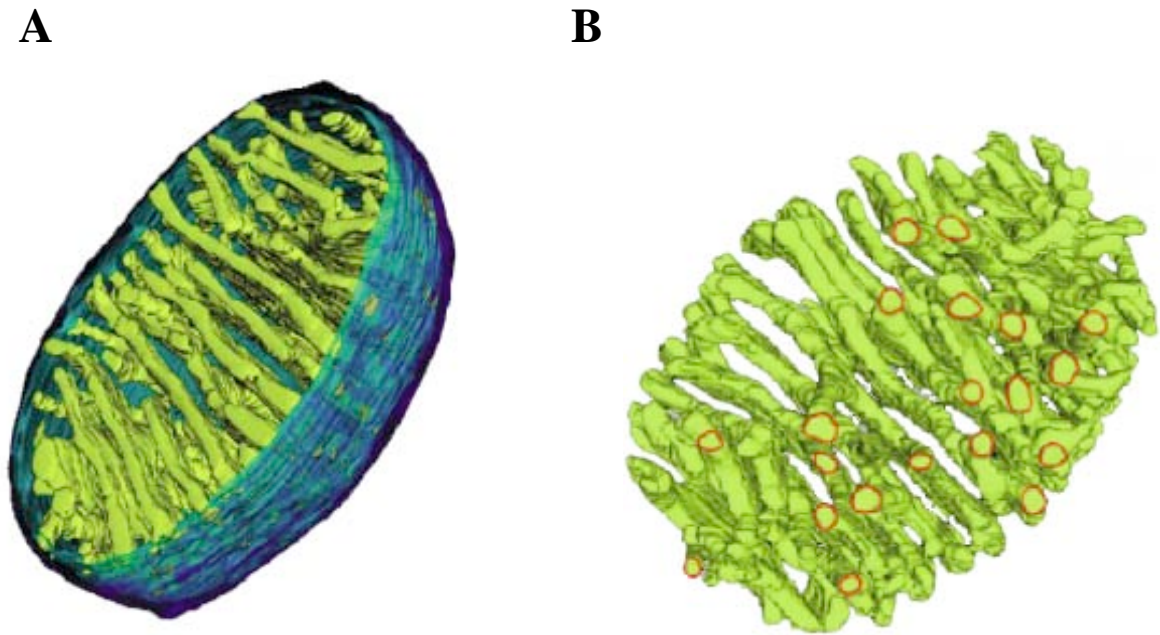


Figure 1.3. Electron tomography of a chick cerebellar mitochondrion. **A:** A three-dimensional model of a mitochondrion. The outer membrane is coloured dark blue, the inner membrane light blue and the cristae green. **B:** The isolated cristae from A shown from behind. The cristae junctions are outlined in red [adapted from (Frey *et al.*, 2002)].

I (ND1-6 and 4L), cytochrome b of complex III, three subunits of complex IV (COX I-III) and subunits a and A6L of the ATP synthase. All of these subunits are highly hydrophobic. The size of the genome varies with the species, with more complex organisms having a smaller number of proteins encoded in the mitochondrial genome. The size of mitochondrial genomes varies from 6000 bp in *Plasmodium* to over 200,000 bp in some plant mitochondrial genomes. Sequencing of the genomes has revealed the closest relative to the prokaryotes that were involved in the endosymbiotic events. Comparison of bacterial genomes with those of mitochondria has identified the intracellular parasite genus *Rickettsia* (the causative agent of typhoid) as having a genome most similar to mitochondria (Gray and Spenser, 1996).

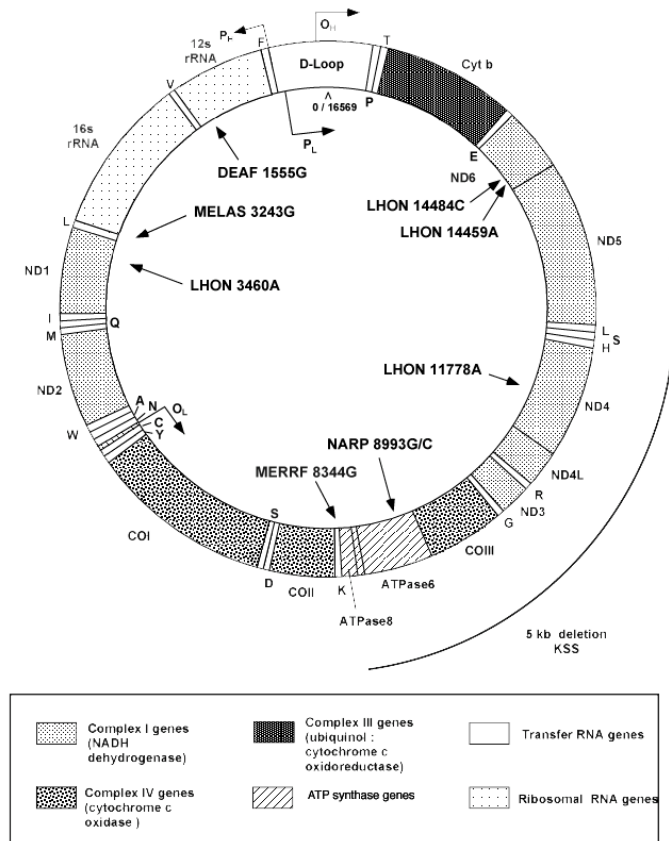


Figure 1.4 The human mitochondrial genome. The proteins and tRNAs that are encoded are shown, as well as disease causing mutations. All the proteins encoded in the human mitochondrial genome are integral membrane subunits of the complexes of the electron transport chain and the ATP synthase. Single letter codes for amino acids indicate their corresponding tRNAs, O_H and O_L are the replication origins of the light and heavy chains respectively and P_H and P_L are the transcription sites. [Adapted from MITOMAP: A Human Mitochondrial Genome Database, <http://www.mitomap.org>]

The vast majority of the proteins present in mitochondria are imported from the cytoplasm where nuclear encoded proteins are synthesised and directed to the mitochondria. Many, but not all of these proteins, contain a targeting sequence, containing positively charged residues that help to carry the protein into the matrix, driven by the negative membrane potential difference. The presequence is cleaved during the process (von Heijne, 1986).

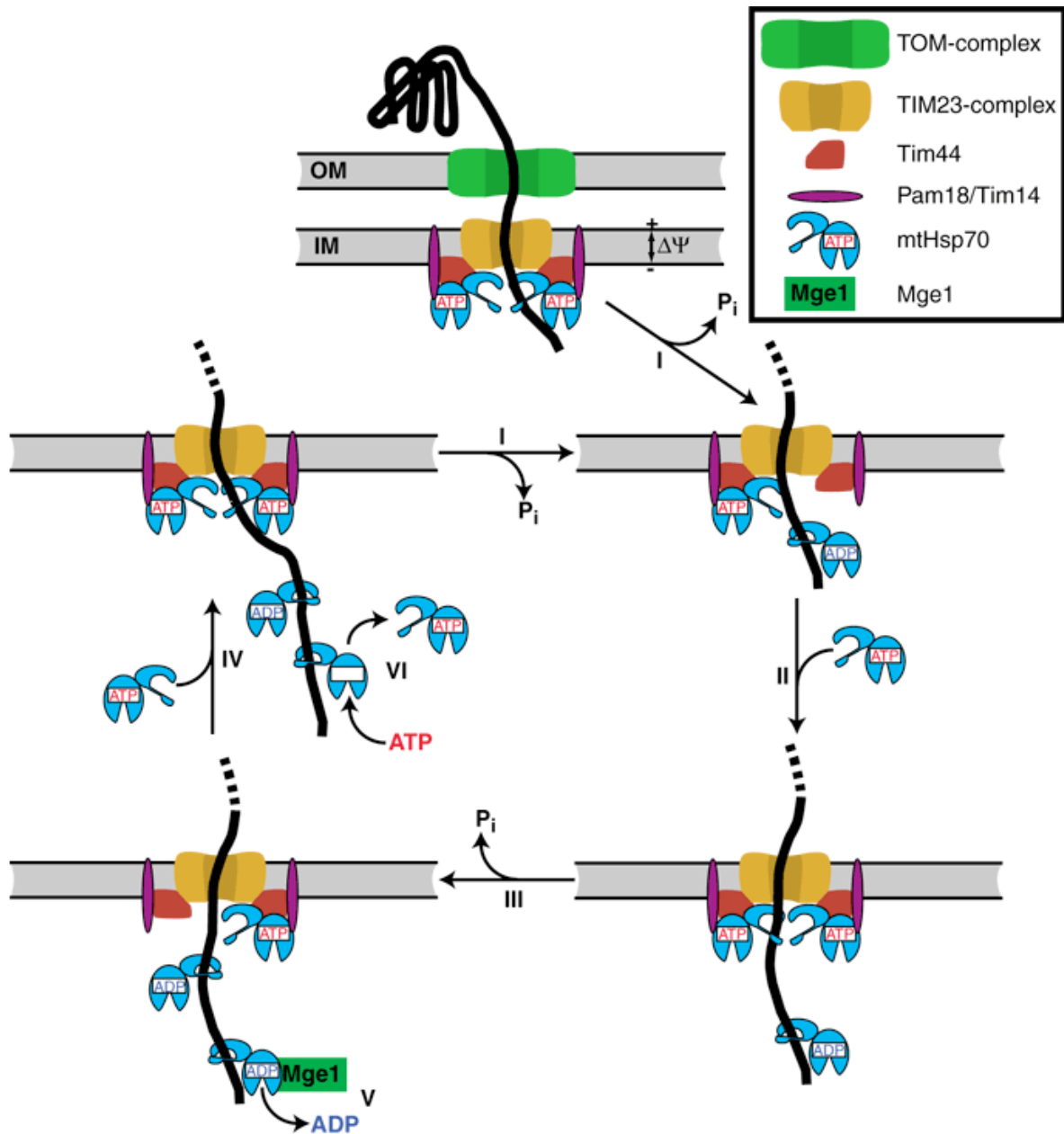


Figure 1.5 The import of proteins containing a presequence into the mitochondrial matrix. The presequence is recognised by the TOM complex and directed to the TIM complex. The positively charged residues of the presequence move through the TIM channel due to the membrane potential ($\Delta\psi$) and passes into the matrix. Binding of the peptide by Hsp70 and Pam18/Tim14 causes ATP hydrolysis leading to Hsp70 release from Tim44 (I). A free Hsp70 with ATP bound is then able to bind to Tim44 (II). The polypeptide moves into the matrix by Brownian motion and is continuously bound by Hsp70 until the complete polypeptide is imported (III and IV). The soluble protein Mge1 causes the release of ADP from peptide bound Hsp70 and the rebinding of ATP (V) inducing the release of the bound polypeptide (VI). [After (Mayer, 2004)].

Many of the proteins of the inner and outer membranes contain the targeting information within the mature protein. However, how this targeting occurs is largely unknown, but some experiments with the adenine nucleotide transporter (ANT) of *S. cerevisiae* (a protein imported without presequence) suggest a possible mechanism. The ANT (and other members of the transporter superfamily) contains three homologous domains. These domains may contain the targeting information, as each can form a complex with a Tom70 dimer. The domains would then pass through the outer membrane sequentially (Wiedemann *et al.*, 2001).

Proteins are imported through two translocases; the Translocase Outer Membrane (TOM) and the Translocase Inner Membrane (TIM) (Jensen and Dunn, 2002; Paschen and Neupert, 2001). The TOM complex consists of protein import receptors and the import channel itself. The receptors, Tom20, 22, 37 and 70, bind the precursor protein and initiate the transport of the protein through the channel [consisting of Tom40 and some smaller subunits Tom5, 6 and 7 (Lithgow, 2000)]. Proteins containing a targeting sequence pass the inner membrane through the TIM23 pore (made up of Tim23 and 17 and the translocation motor composed of Tim44, hsp70 and mGrpE). This process is energy dependent and utilises ATP and the proton motive force [pmf (Figure 1.5)]. Insertion of proteins into the inner membrane is facilitated by the TIM22 complex. Precursor proteins are brought into the membrane by a membrane bound insertion complex (composed of Tim10, 12, 18, 22 and 54), again this process utilises energy from the pmf.

1.1.2 Bioenergetics

All biochemical reactions within the cell require energy and many of these reactions, such as the maintenance of large gradients across membranes or the synthesis of ATP, are

thermodynamically unfavourable. The energy required for these reactions is provided by the oxidation of nutrients or by photosynthesis. These energy producing processes are coupled by the formation of a proton electrochemical gradient across the inner membrane of mitochondria, a concept first proposed in the chemiosmotic theory (Mitchell, 1961). The protein complexes of the electron transport chain generate a proton electrochemical gradient across the inner mitochondrial membrane (detailed in Section 1.2) converting a redox potential difference to a chemiosmotic potential difference. This gradient is called the proton motive force (pmf) and has two components: the differences in pH (ΔpH) and in electrical potential ($\Delta\psi$) across the membrane as shown in equation 1.1:

$$\Delta \tilde{\mu}_{H^+} = -F\Delta\psi + 2.3RT\Delta\text{pH} \quad (1.1)$$

where $\Delta \tilde{\mu}_{H^+}$ is the proton motive force in kJM^{-1} , $\Delta\psi$ is the membrane potential in mV, F is the Faraday constant, R is the gas constant, T is the temperature in Kelvin and ΔpH is the pH difference across the membrane.

The maintenance of the proton electrochemical gradient far from equilibrium is used by the ATP synthase to convert ADP and orthophosphate to ATP. The maintenance of the ATP to ADP ratio up to 1000 fold away from equilibrium results in the high potential chemical energy. This potential is utilised by the cell to fuel thermodynamically unfavourable reactions. The ΔG of hydrolysis of ATP (to ADP and Pi) is given by equation 1.2:

$$\Delta G = -RT \ln \frac{K}{\Gamma} \quad (1.2)$$

where K is the equilibrium constant and Γ is the observed mass action ratio (the ratio of reactant to product, in this case $[\text{ATP}]/[\text{ADP}]$). In the cytoplasm, the mass action ratio is maintained as low as 10^{-5} M whereas the equilibrium constant is as high as 10^5 M. At this displacement from equilibrium the hydrolysis of ATP typically liberates 57 kJ M^{-1} of free energy (Nicholls and Ferguson, 2002).

1.2 The electron transport chain and oxidative phosphorylation

Glycolysis, fatty acid oxidation and the citric acid cycle produce high energy electrons bound to nicotine adenine dinucleotide (NADH) and flavin adenine dinucleotide (FADH_2). These electrons are used to reduce oxygen to water, releasing large amounts of free energy. The electrons are passed down a series of membrane bound protein complexes that pump protons out of the mitochondrial matrix as redox energy is abstracted during electron transport. The accumulation of protons in the intermembrane space generates the pmf that is used to drive the synthesis of ATP (Figure 1.6).

Complex I (NADH-Q oxidoreductase), the first enzyme in the electron transport chain, oxidises NADH to NAD^+ . It passes its electrons to a flavin mononucleotide (FMN) prosthetic group becoming FMNH_2 (FMN binds protons when reduced). Then the electrons are passed through a series of iron-sulphur clusters to reduce coenzyme-Q (Q) to quinol (QH_2) in the lipid bilayer.

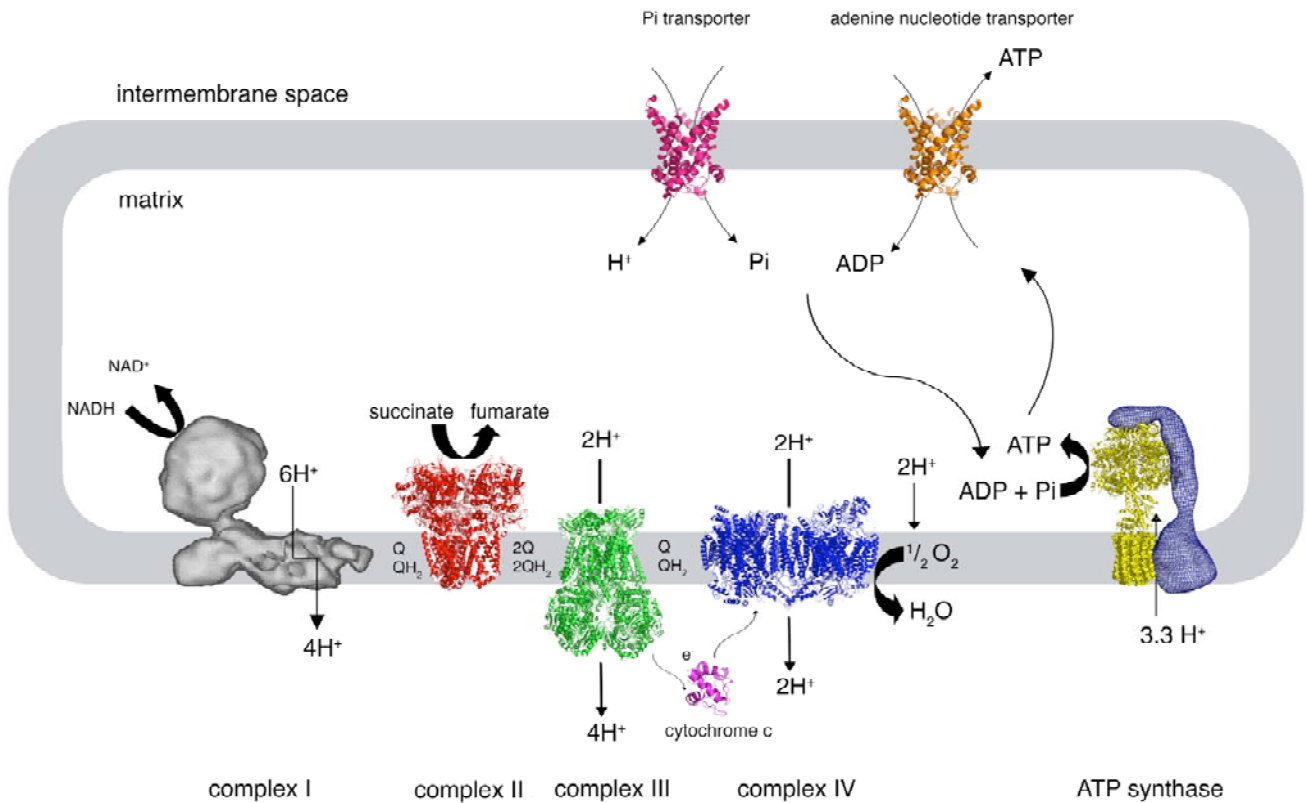


Figure 1.6. The protein complexes of oxidative phosphorylation in mitochondria. Complex I (NADH-Q oxidoreductase) oxidises NADH. Two electrons are passed to coenzyme Q, which is reduced from ubiquinone (Q) to ubiquinol (QH₂), and 4 protons are pumped into the intermembrane space. Electrons also enter the chain from complex II (succinate-Q reductase), which oxidises succinate to fumarate, and passes the electrons to Q but does not pump any protons. Complex III (cytochrome reductase) shuttles electrons from Q to cytochrome c and transfers 4 protons to the intermembrane space. In the final stage, 4 electrons from cytochrome c are passed to complex IV (cytochrome c oxidase) to reduce molecular oxygen to water with the concomitant pumping of 4 protons from the matrix. The resultant proton gradient is used by the ATP synthase to power the production of ATP from ADP and Pi. The adenine nucleotide transporter shuttles synthesised ATP out of the matrix and ADP in and the phosphate transporter imports orthophosphate (with a proton, maintaining electroneutrality). Structures and references: complex I from bovine heart mitochondria (Grigorieff, 1998), complex II from *E. coli* [PDB 1NEN, (Yankovskaya *et al.*, 2003)], complex III from bovine heart mitochondria [PDB 1BE3, (Iwata *et al.*, 1998)], complex IV from *Paracoccus denitrificans* [PDB 1AR1, (Ostermeier *et al.*, 1997)], ATP synthase: a chimera between bovine F₁-ATPase [PDB 1E79, (Gibbons *et al.*, 2000)], the c-ring from yeast mitochondrial ATP synthase [PDB 1Q01, (Stock *et al.*, 1999)] and the peripheral stalk, and remaining F₀ subunits, from bovine ATP synthase [a 3-D reconstruction from electron cryomicroscopy of single particles in ice (Rubinstein *et al.*, 2003)]. Cytochrome c is from horse heart mitochondria [PDB 1HRC, (Bushnell *et al.*, 1990)] and ANT from bovine heart mitochondria [PDB 10KC, (Pebay-Peyroula *et al.*, 2003)]. The phosphate transporter is modelled from the ANT coordinates. Their sequences are highly homologous (Walker and Runswick, 1993) and they probably adopt a similar fold. The structures are not shown to scale.

Accompanying the transfer of two electrons, four protons are removed from the matrix. Two of them are pumped into the intermembrane space and the other two are passed to Q in the membrane.

Complex II (succinate-Q reductase) oxidises FADH₂, from succinate dehydrogenase, to FAD⁺. Again the electrons are passed through a series of iron sulphur clusters to Q in the membrane, contributing to the pool of QH₂. Unlike the other electron transfer complexes no protons are pumped into the intermembrane space at this site. Complex III (cytochrome c reductase) transfers electrons from the reduced Q pool, through three haem irons and a Rieske centre (a two iron cluster bound by sulphurs and two histidines that maintains the irons with a higher reduction potential ensuring initial electron transfer is to the Rieske iron) to the soluble protein, cytochrome c, in the intermembrane space. This reduction is associated with the pumping of four protons, two from the matrix and two from the Q pool (see Figure 1.7).

The final stage of the electron transport chain is catalysed by complex IV (cytochrome c oxidase). This complex transfers an electron from reduced cytochrome c, to a binuclear centre. Then the electron is shuttled through two haem groups to a final copper centre. At this stage a second electron enters the protein from cytochrome c, passing down the same pathway, but stopping at the second haem iron as the final copper is already reduced. This iron is then able to bind oxygen (freely permeable in the membrane) as it is in the Fe²⁺ state. The electron bound to the copper, reduces the iron oxygen, forming a peroxide bridge between the metals. A further electron from cytochrome c, and a proton from the matrix, cleaves this bond, reducing the copper oxygen. A fourth electron and another matrix proton reduce the iron oxygen and the addition of another two protons from the matrix releases two water molecules into the intermembrane space, and the protein returns to the oxidised form. The end result of complex IV activity is that four protons are removed from the matrix and enter the cytosol in the form of water (see Figure 1.8). Complex IV also

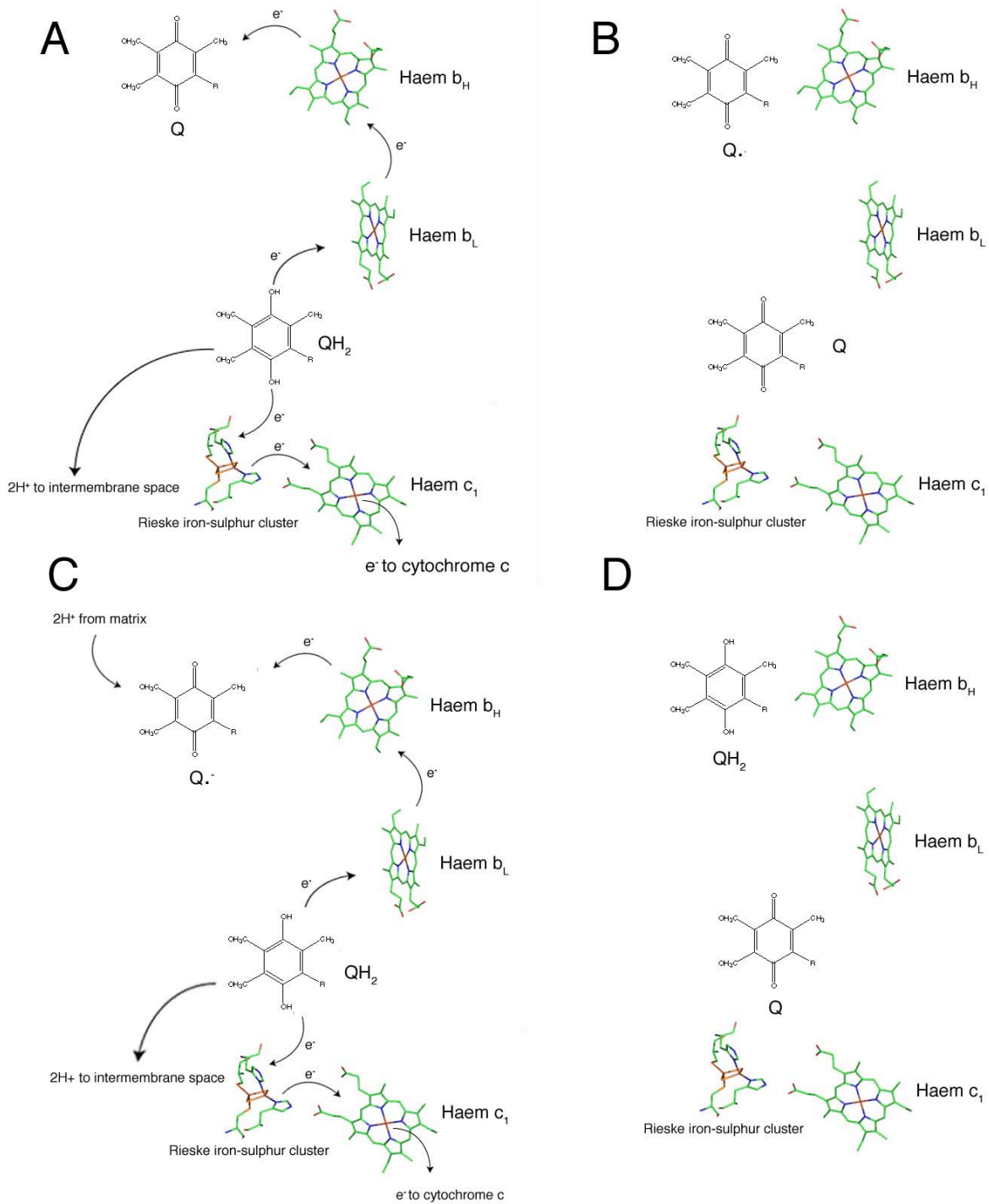


Figure 1.7 The Q cycle in mitochondria. **A:** Two electrons from a bound QH₂ are transferred, one to cytochrome c and the other to a bound Q (forming semiquinone, Q•), **B:** **C:** The newly formed Q is released and a new QH₂ diffuses in from the membrane and transfers its electrons, one to cytochrome c the other reduces semiquinone to QH₂. This last step leads to the uptake of two protons from the matrix. **D:** Newly formed QH₂ and Q diffuse back into the membrane.

pumps four protons from the matrix per oxygen molecule reduced, although the mechanism of this pump is unclear.

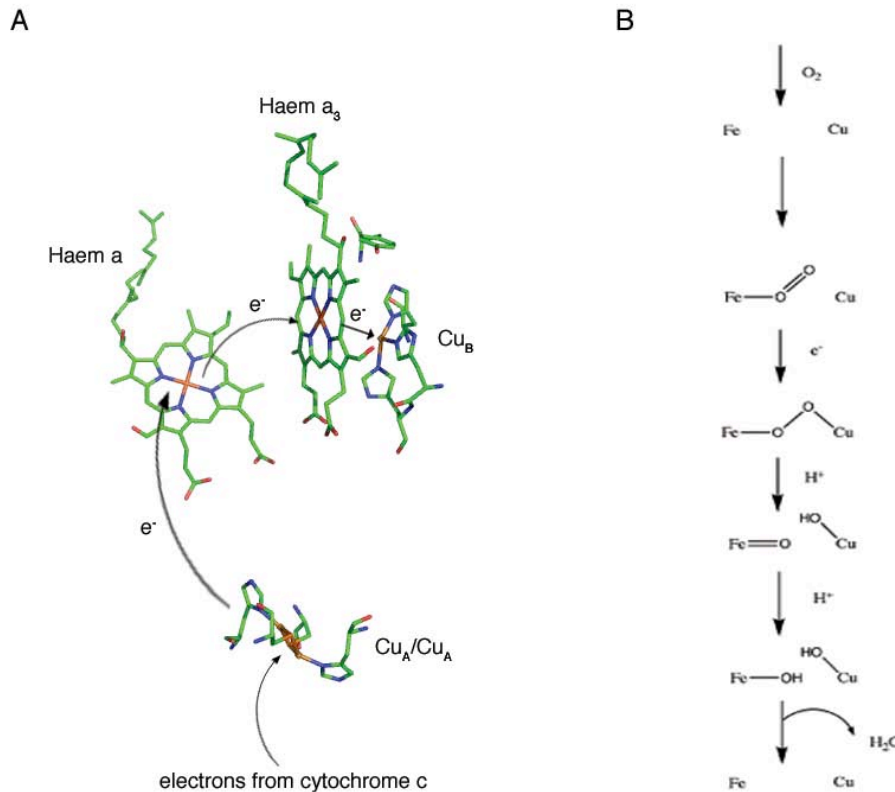


Figure 1.8 The mechanism of complex IV. **A:** The prosthetic groups of complex IV as arranged in the protein. Electrons from cytochrome c proteins are transferred to the Cu_A/Cu_A cluster, through the haem groups to reduce Cu_B. A second electron reduces the haem a₃ iron enabling it to bind oxygen. **B:** The reduction of oxygen to water. Oxygen binds the reduced iron and a further two electrons from cytochrome c are transferred to the oxygen forming a peroxide bridge between the iron and Cu_B. Another electron breaks this bond and leads to the uptake of a proton from the matrix. Another electron and a further three protons from the matrix generates two water molecules that are released into the intermembrane space and leave the enzyme in the reduced state.

The proton electrochemical gradient across the inner mitochondrial membrane is used not only in the production of ATP by the ATP synthase (Section 1.3) but also in the transport of some metabolites in and out of the matrix. The adenine nucleotide translocase (ANT)

catalyses the antiport of one ADP into the matrix and an ATP out. In the presence of a pmf, it will preferentially transport ATP out, and vice versa, as ATP has an additional negative charge, in effect repelling it from the matrix. The phosphate carrier transports orthophosphate into the matrix with a proton, maintaining electroneutrality. Around 30% of the pmf is utilised in removing ATP and importing ADP and phosphate. The combined effect of these transporters provides the ATP synthase with reactants, and the cytosol with ATP. A large family of these transporters exist to provide the mitochondria with metabolites and they all share a common structure (Walker and Runswick, 1993).

The mechanisms of many of the complexes involved in ATP generation in mitochondria has been illuminated by high resolution crystal structures which have provided information about the position and number of prosthetic groups. High resolution structures exist for, complex III (Hunte *et al.*, 2000; Iwata *et al.*, 1998; Lange and Hunte, 2002), complex IV (Ostermeier *et al.*, 1997; Soulimane *et al.*, 2000; Svensson-Ek *et al.*, 2002; Yoshikawa *et al.*, 1998) and parts of the ATP synthase (Abrahams *et al.*, 1994; Carbajo *et al.*, 2004; Gibbons *et al.*, 2000; Stock *et al.*, 1999) from mitochondria. The structure of the ANT inhibited with carboxyatractyloside has provided the first glimpse of the transporter family (Pebay-Peyroula *et al.*, 2003). There are also structures for the eubacterial complex II (Yankovskaya *et al.*, 2003) and complex IV (Ostermeier *et al.*, 1997; Soulimane *et al.*, 2000). Complex I, the largest and most complicated of the complexes, is known only at low resolution (Grigorieff, 1998). A high resolution structure will be required to help to explain its mechanisms of electron transport and proton pumping.

1.3 The ATP synthase

1.3.1 Introduction

The ATP synthase (F_1F_0 -ATPase) is common to eubacteria, chloroplasts and mitochondria. The archaeal H^+ ATPase (A-type ATPase) is similar to the F-type ATPases but has a greater resemblance to the ATPases found in the vacuoles of eukaria (V-type ATPases) which are also related to the F-ATPases, pointing to a common evolutionary origin for F, V and A-type ATPases. ATP synthase was first observed by electron microscopy as spherical structures of unknown function attached by a stalk to the membrane of inside-out vesicles made from mitochondrial inner membranes (Figure 1.9) [sub-mitochondrial particles (SMPs)] (Fernandez-Moran, 1962). It was found subsequently that the spheres could synthesise ATP while SMPs were respiring, but, when removed from the membrane by treatment with urea, they were only able to hydrolyse ATP (Pullman *et al.*, 1960). However, the particles could be reconstituted with the membranes with subsequent restoration of ATP synthetic activity (Kagawa and Racker, 1966c). The depleted membranes were also found to be unable to respire and were highly permeable to protons.

Further experiments demonstrated that there were two major parts to this enzyme: the soluble F_1 (factor 1) domain (Kagawa and Racker, 1966b), where ATP synthesis occurs and the integral membrane domain F_0 (Kagawa and Racker, 1966a) where the proton channel is located (oligomycin blocks proton flow and ATP synthesis). These experiments were the first in a long line that have revealed much about the structure and mechanism of this enzyme. The current state of knowledge is outlined in the following sections.

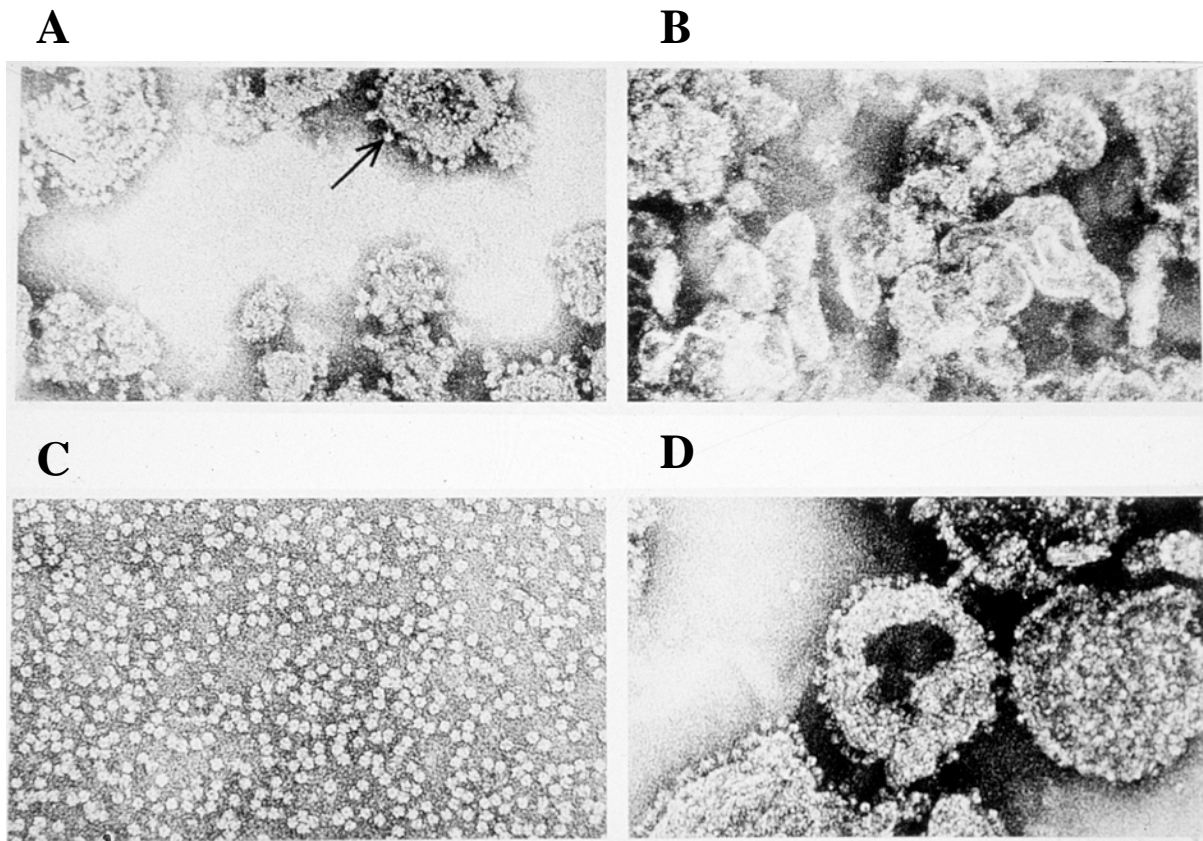


Figure 1.9 Electron micrographs of submitochondrial particles (175,000 x magnification). **A:** SMPs – ATP synthase is visible as spheres protruding from the membrane (arrow). **B:** SMPs after treatment with urea. The membranes are smooth as the F_1 portion has been removed. **C:** The water soluble F_1 -ATPase removed from the membrane, the particles are unable to synthesise ATP but will hydrolyse it. **D:** SMPs reconstituted with F_1 particles – they regain the ability to synthesise ATP in the presence of a pmf. [Image from (Weissmann and Claiborne, 1975)]

1.3.2 The subunits of the ATP synthase

The ATP synthase is a large multimeric complex. The bacterial enzyme from *Escherichia coli* is representative of the most simple form, being composed of eight different subunits with the stoichiometry: $\alpha_3\beta_3\gamma\delta\epsilon ab_2c_{9-11}$. The genes for these proteins are contained

in a single operon (Foster and Fillingame, 1982; Walker *et al.*, 1984a; Walker *et al.*, 1984b). Subunits $\alpha\beta\gamma\delta\epsilon$ form F_1 and a, b and c form the F_0 portion. The number of c subunits is uncertain in *E. coli* as crosslinking and radiolabelling experiments are not conclusive, but the value is likely to be in the range 9 to 12 (Foster and Fillingame, 1982; Jones *et al.*, 2000) and 10 has been decided on (Jiang *et al.*, 2001). The subunit composition and nomenclature varies with the species (Table 1.1); but the overall architecture of the enzyme is likely to be the same throughout. Figure 1.10 shows a comparison of the subunits and their roles in the complex. The ATP synthase from chloroplasts (Süss and Schmidt, 1982) and photosynthetic bacteria (Cozens and Walker, 1987; Falk *et al.*, 1985; Tybulewicz *et al.*, 1984; van Walraven *et al.*, 1984; van Walraven *et al.*, 1993) have similar subunits in the stoichiometry of $\alpha_3\beta_3\gamma\delta\epsilon ab b' c_{9-12}$ where b and b' are homologous and replace the b dimer found in other species (Cozens and Walker, 1987; Dunn *et al.*, 2000; Falk *et al.*, 1985).

The ATP synthase from mitochondria is the most complex and contains the largest number of subunits. The best characterised of these protein complexes are those from bovine heart and yeast mitochondria. The bovine enzyme comprises 16 subunits that combine to form a complex of 583.6 kDa containing 28 separate polypeptides (Walker *et al.*, 1991). The stoichiometry of subunits in the F_1 domain is $\alpha_3\beta_3\gamma\delta\epsilon$ (Walker *et al.*, 1985) and in F_0 subunits $abc_{10}defgOSCPF_6$ and A6L (Collinson *et al.*, 1994b; Collinson *et al.*, 1996; Walker *et al.*, 1987; Walker *et al.*, 1991). Subunits a and c form the proton channel and the other subunits are in the peripheral stalk (see Section 1.3.4) or in F_0 (see Section 1.3.3). The F_0 subunits are all present in a 1:1 ratio (Collinson *et al.*, 1994b; Collinson *et al.*, 1996) except for subunit c, where many copies are found. The yeast enzyme has two additional subunits (i and k), but it adopts essentially the same arrangement as the bovine protein (Velours and Arselin, 2000), see Table 1.1. Both enzymes are regulated by one or more inhibitor proteins (see Section 1.4).

Table 1.1 The subunits of ATP synthase from various species. Subunit equivalence is based on sequence homology. A dash indicates no homologous subunit is present. Bold subunits are encoded in the mitochondrial or chloroplast genomes (the chloroplast genome sampled was that of *Arabidopsis thaliana*).

Mitochondria		Chloroplasts and photosynthetic bacteria	<i>E. coli</i> and some other eubacteria
bovine	yeast		
α	α	α	α
β	β	β	β
γ	γ	γ	γ
δ	δ	ϵ	ϵ
ϵ	ϵ	-	-
OSCP	OSCP	δ	δ
<i>a</i>	<i>a</i> (6)	<i>a</i> (IV)	<i>a</i>
<i>b</i>	<i>b</i> (4)	<i>b</i> and <i>b'</i> (I and II)	<i>b</i>
<i>c</i>	<i>c</i> (9)	<i>c</i> (III)	<i>c</i>
<i>d</i>	<i>d</i>	-	-
<i>e</i>	<i>e</i>	-	-
<i>f</i>	<i>f</i>	-	-
<i>g</i>	<i>g</i>	-	-
F ₆	<i>h</i>	-	-
A6L	8	-	-
IF ₁	IF ₁	-	-
-	STF ₁ (9 kDa)	-	-
-	STF ₂ (15 kDa)	-	-
-	<i>i</i>	-	-
-	<i>k</i>	-	-

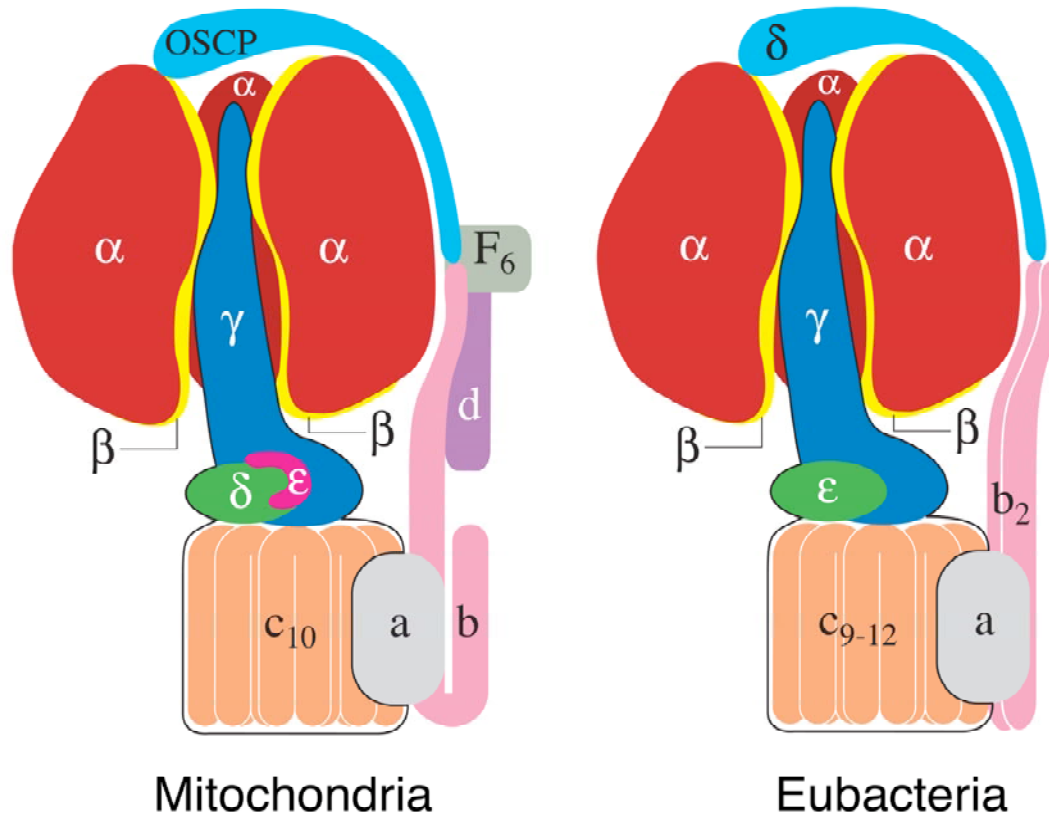


Figure 1.10 Models of mitochondrial and eubacterial ATP synthase. The models are based on structural and biochemical information and show all the bacterial subunits and the major mitochondrial subunits (subunits e, f, g, i, k, A6L and IF₁ are not shown). A β subunit has been removed in order to expose the central stalk. The rotary assembly ($\gamma\delta\epsilon$) is outlined in black.

1.3.3 The minor subunits

The bovine subunits e, f, g, A6L, IF₁ and the yeast subunits e, f, g, 8, i, and k are not found in the bacterial or chloroplast complexes and are generally collectively termed the minor subunits. While yeast subunits e, g and k are not considered necessary for a fully functioning ATP synthase, they have been implicated in yeast ATP synthase dimer formation, as has subunit i (Arnold *et al.*, 1998; Paumard *et al.*, 2002a; Paumard *et al.*, 2000). They are thought to be in the membrane and to form homodimeric parallel α -helical coiled-coils between complexes that may lead to ‘supra-molecular’ complexes (Schägger and

Pfeiffer, 2000). The presence and levels of e and g have also been observed to have an affect on formation of cristae (Arselin *et al.*, 2004; Paumard *et al.*, 2002b). It has been proposed that the formation of dimers of ATP synthase controls cristae morphology. A subunit f null yeast mutant was shown to have much lower ATPase activity and a role for it in complex assembly has been postulated (Roudeau *et al.*, 1999; Vaillier *et al.*, 1999). Subunit A6L (8 in yeast) is hydrophobic and may play a role in energy transduction (Fearnley and Walker, 1986; Higuti *et al.*, 1988).

1.3.4 The peripheral stalk

The peripheral stalk that connects F_1 and F_o is essential for the function of the enzyme. It is thought to counter the tendency of the $\alpha_3\beta_3$ hexamer of F_1 follow the rotation of

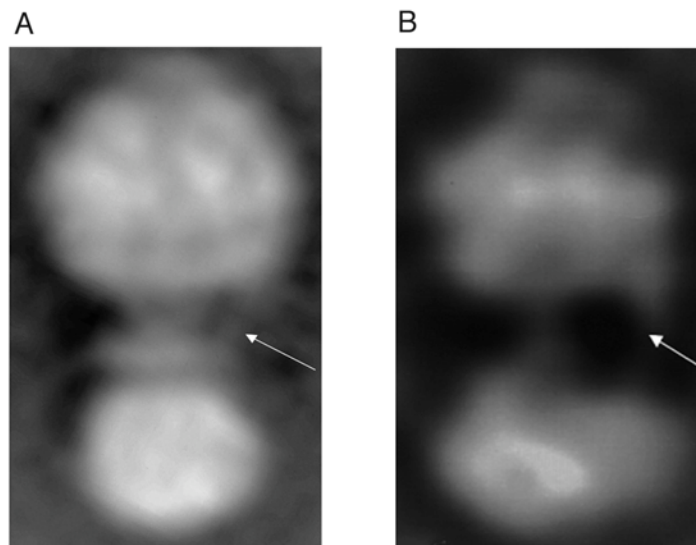


Figure 1.11 Cryo-electron microscopy of isolated ATP synthases. **A:** Negatively stained bovine ATP synthase. The peripheral stalk can be seen to the right of the complex (arrow) and additional density, probably corresponding to OSCP, is seen above F_1 . [Image from (Karrasch and Walker, 1999)]. **B:** Negatively stained ATP synthase from *E. coli*. Density for a peripheral stalk is also observed (arrow) and extra density above F_1 . [Image from (Wilkins and Capaldi, 1998)]

the rotor, (Collinson *et al.*, 1994b; Walker, 1998). It is comprised of single copies of OSCP, and subunits b, d and F₆ (Collinson *et al.*, 1994a; Collinson *et al.*, 1994b; Collinson *et al.*, 1996). The OSCP binds to the top of F₁ and extends down the side of a non-catalytic α - β interface to connect to subunit b (Collinson *et al.*, 1994b; Joshi *et al.*, 1996; Rubinstein and Walker, 2002; Rubinstein *et al.*, 2003), which is bound to the membrane and F₀ at its C-terminus (Walker *et al.*, 1987).

The OSCP and subunit b bind subunits F₆ and d (Collinson *et al.*, 1994a; Collinson *et al.*, 1994c; Rubinstein *et al.*, 2004). The peripheral stalk was first observed by electron microscopy in negative stain [(Böttcher *et al.*, 2000; Karrasch and Walker, 1999; Wilkens and Capaldi, 1998) see Figure 1.11]. A three-dimensional reconstruction of bovine ATP synthase in vitreous ice has provided the first overall glimpse of the asymmetric architecture of the peripheral stalk [(Rubinstein *et al.*, 2003) Figure 1.12]. This structure shows the peripheral stalk wrapping around the F₁-c₁₀ sub-complex in a direction opposing rotation (in this case accompanying hydrolysis). This arrangement implies a much more flexible structure than had been envisaged previously. Rather than being a rigid body, opposing rotation of $\alpha_3\beta_3$, the peripheral stalk is probably elastic and moves round with $\alpha_3\beta_3$ in the direction of the motion it opposes (Rubinstein *et al.*, 2003).

Further progress on the structure of the peripheral stalk has been made by the solution NMR study of individual subunits. The N-terminal domain of the *E. coli* δ subunit (Wilkens *et al.*, 1997), of bovine OSCP (R. J. Carbajo, F. A. Kellas, M. J. Runswick, J. E. Walker and D. Neuhaus; unpublished results) and intact bovine F₆ (Carbajo *et al.*, 2004) have been solved by NMR spectroscopy. In addition, part of the *E. coli* subunit b has been solved by X-ray crystallography as well as its membrane domain by other methods (Del Rizzo *et al.*, 2002; Dmitriev *et al.*, 1999). By fitting individual subunit structures into the EM model, it may be possible to provide a complete molecular picture of the peripheral stalk.

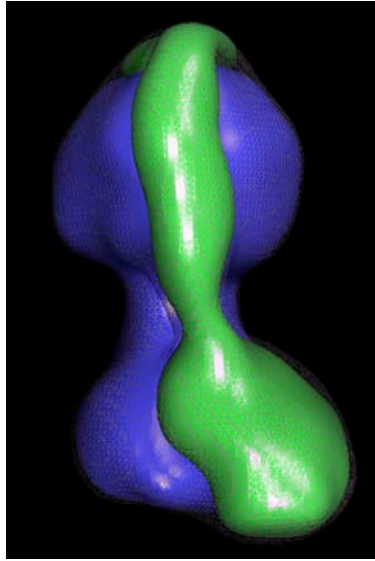


Figure 1.12 Three-dimensional model of bovine ATP synthase from analysis of single particles in ice. The model has been divided into two portions: The F₁-c₁₀ subcomplex is blue and the peripheral stalk [including subunit a and other membrane components (subunits e, f, g and A6L)] is green. The model shows the extent of the stalk and its curvature around F₁. [Image from (Rubinstein *et al.*, 2003)]

1.3.5 Proton translocation by the F_o domain

The proton channel is formed at the interface between the c ring and subunit a. The flow of protons from the intermembrane space through this interface, drives the rotation of the c ring. The a subunit probably comprises five transmembrane helices (Valiyaveetil and Fillingame, 1998; Wada *et al.*, 1999) and the c subunit of two (Hoppe *et al.*, 1984; Hoppe and Sebald, 1984). The c subunit forms a ring structure that is thought to interact intimately with the helices of subunit a forming a proton channel (Schneider and Altendorf, 1985). Exactly how protons flow through the channel and generate rotation of the c ring is still the subject of much debate.

Three models have been proposed. The two-channel model is based around a highly conserved aspartate in subunit c (Asp-61, bovine numbering) and a conserved arginine in subunit a [Arg-157 (210 in *E. coli*)], see Figure 1.13 part A. The model places the carboxylate of Asp-61 in the middle of the lipid bilayer, interacting with the positive guanidinium of Arg-157 (210 in *E. coli*). A proton is thought to enter a 'half channel' and bind to the carboxyl, removing the charged interaction with the arginine. Then the arginine is free to interact with a deprotonated carboxylate from another c subunit that had lost its proton in the second 'half channel'. This moves the subunit closer, thus driving the rotation of the c ring (Engelbrecht and Junge, 1997; Junge *et al.*, 1997; Walker, 1998).

The one channel model, based on experiments on a sodium dependent ATP synthase, places the aspartate at the surface of the membrane with a single channel between subunits a and c spanning the membrane (Figure 1.13, part B). The mechanism of rotation is proposed to be similar except the sodium ion would be released from a c subunit once the subunit no longer interacts with the a subunit (Dimroth *et al.*, 2000; Dimroth *et al.*, 1999). A third model proposes a rotation of the C-terminal helix on protonation and deprotonation of the carboxylate. The proposal is based on NMR experiments, conducted in chloroform methanol mixtures, at different pH values (Rastogi and Girvin, 1999). A 140° rotation in the C-terminal helix on protonation of the aspartate is proposed to drive rotation by a ratchet type mechanism. However, as these experiments were conducted on isolated c subunits, in chloroform:water:methanol, the biological relevance of the observed structural changes is questionable.

From the proposed models it can be seen that the number of protons translocated per complete 360° rotation depends on the number of c subunits. The number present in the *E. coli* complex has been estimated variously as between nine and eleven and eventually

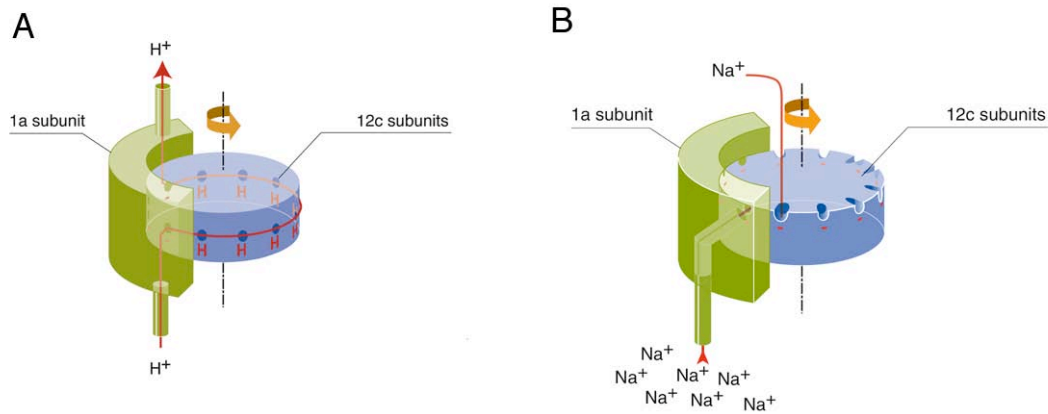


Figure 1.13 Theoretical models of the ATP synthase F₀ domain and the generation of rotation. A: The two channel model (Engelbrecht and Junge, 1997). **B:** The single channel model based on experiments performed on the sodium motive ATP synthase from *P. modestum* (Dimroth *et al.*, 1999).

twelve (Foster and Fillingame, 1982; Jones *et al.*, 2000). However, an electron density map of a sub-complex of the yeast mitochondrial ATP synthase clearly showed a ring of ten c subunits attached to F₁-ATPase (Stock *et al.*, 1999).

The presence of ten c subunits in the ATP synthase implies that 3.3 protons are translocated per ATP molecule synthesised. Previously, it had been assumed that the ATP:H⁺ ratio would be integral, and measured values were in the range of 3 and 4 (van Walraven *et al.*, 1996). The symmetry mismatch between the c ring and catalytic sites in F₁-ATPase may also be an important feature as this arrangement could avoid energy minima that may form in a symmetrical arrangement. This concept was first proposed for the rotary mechanism of the flagellum (Thomas *et al.*, 1999). As the energy of rotation from the c-ring is stored elastically within the central stalk and released in a quantised manner, the enzyme is prevented from resting at an energy minimum.

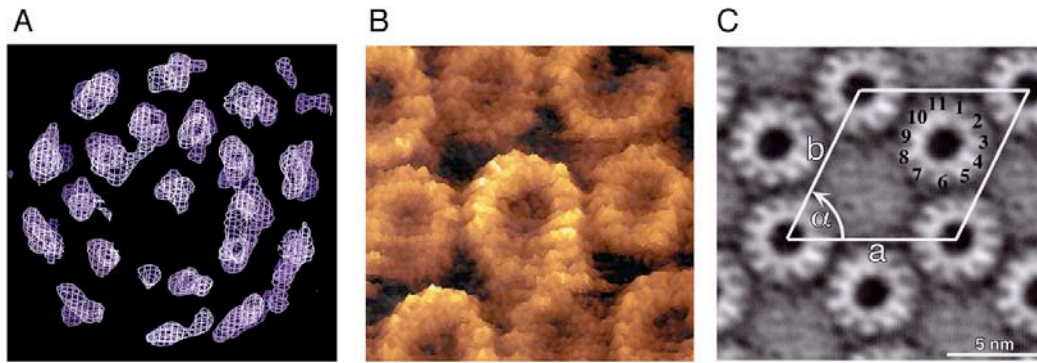


Figure 1.14 Subunit stoichiometry in the c-rings of various species. **A:** Electron density map of the yeast ATP synthase showing a ring of 10 c subunits (Stock *et al.*, 1999). **B:** An atomic force microscopy image of the 14 c-ring from chloroplast ATP synthase from spinach (Seelert *et al.*, 2000). **C:** Two-dimensional crystals of the 11 c-ring from *Ilyobacter tartaricus* (Stahlberg *et al.*, 2001).

Since the discovery of ten c subunits in the yeast enzyme, symmetry mismatch has been observed in other species (Figure 1.14). The number is different for each species but the protons translocated per ATP is always non-integral. The chloroplast ATP synthase contains a ring of 14 c subunits ($4.6 \text{ H}^+:\text{ATP}$) (Seelert *et al.*, 2000), the sodium driven ATPase from *Ilyobacter tartaricus* contains 11 c subunits ($3.6 \text{ H}^+:\text{ATP}$) (Stahlberg *et al.*, 2001; Vonck *et al.*, 2002) and the thermophilic *Bacillus* PS3 probably has 10 c subunits ($3.3 \text{ H}^+:\text{ATP}$) (Mitome *et al.*, 2004); see Figure 1.14. Recently, the structure of an isolated ring from the sodium motive V-type ATPase of *Enterococcus hirae* has been shown to contain 20 equivalents of the c subunit with 10 sodium binding sites [Murata, T, Leslie, A. G. W. and Walker, J. E.; unpublished results] and in the genome of the archaeon *Methanopyrus kandleri*, a gene for a single polypeptide containing the equivalent of 13 c subunits, fused together, has been found (Lolkema and Boekema, 2003). In the light of this evidence, and

after further experiments, the number of c subunits in the *E. coli* complex has been changed to 10 (Jiang *et al.*, 2001). It has also been suggested that *E. coli* may change the size of the ring in response to growth conditions (Schemidt *et al.*, 1998).

1.3.6 The structure of bovine mitochondrial F₁-ATPase

The best understood part of the ATP synthase is the F₁ catalytic domain, largely due to extensive structural studies of the bovine enzyme at high resolution (Abrahams *et al.*, 1996; Abrahams *et al.*, 1994; Braig *et al.*, 2000; Cabezón *et al.*, 2003; Gibbons *et al.*, 2000; Kagawa *et al.*, 2004; Menz *et al.*, 2001b; Orriss *et al.*, 1998; van Raaij *et al.*, 1996a). Treatment of SMPs with chloroform releases it in a soluble and active form (Beechey *et al.*, 1975). It is capable of ATP hydrolysis and has proved to be amenable to structural studies (Lutter *et al.*, 1993). Structural studies of the bovine heart mitochondrial F₁-ATPase have revealed the principal features of its architecture and mechanism [Figure 1.15 (Abrahams *et al.*, 1994; Braig *et al.*, 2000; Cabezón *et al.*, 2003; Gibbons *et al.*, 2000; Kagawa *et al.*, 2004; Menz *et al.*, 2001b; Orriss *et al.*, 1998)]. The three α and three β subunits surround the γ subunit in alternation and have extremely similar folds, [as expected from their related sequences with 20% identity (Walker *et al.*, 1982)]. This arrangement confers a pseudo three-fold symmetry on the complex. However the three β subunits adopt very different conformations, because of the asymmetric central stalk in the centre of the complex (Figure 1.16). The γ subunit forms an anti-parallel α -helical coiled-coil from its N and C-terminal regions. The lower end of the central stalk was disordered in the first structure, and so much of the electron density for the remaining portion of the subunit, and the δ and ϵ subunits, was missing. However, it was resolved subsequently [Section 1.3.9 (Gibbons *et al.*, 2000)]. The nucleotide binding sites are located near the interfaces of α and β subunits and there are

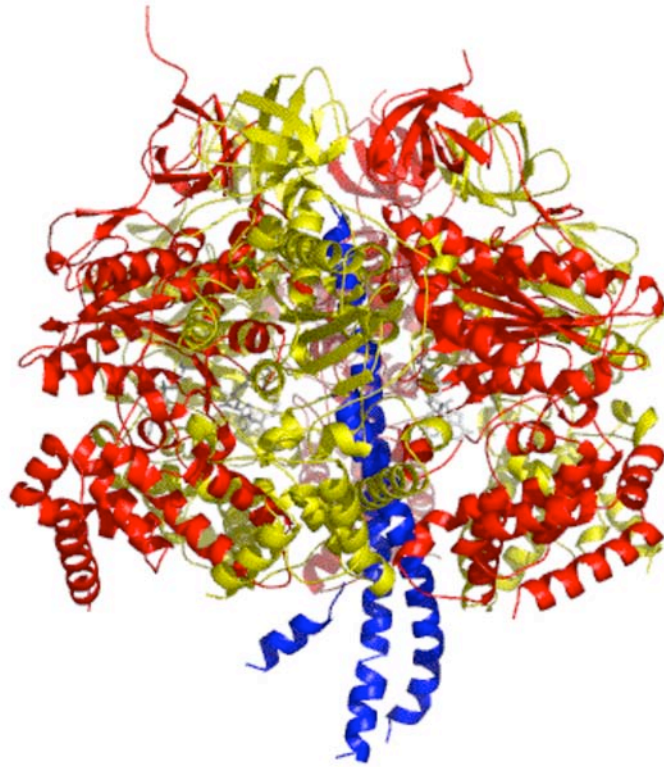


Figure 1.15 The structure of bovine heart mitochondrial F_1 -ATPase at 2.8 Å resolution. The structure is shown with α -helices as ribbons and β -sheets as arrows. The α subunits are red and the β subunits yellow. They are held together by six-stranded β -barrels located at their N-termini (top of complex). The γ subunit (blue) penetrates the $\alpha_3\beta_3$ hexamer. [Figure generated from the first F_1 -ATPase structure PDB code 1BMF (Abrahams *et al.*, 1994)]

significant differences in the bound nucleotide. The α subunits all bind the non-hydrolysable ATP analogue AMP-PNP (where the bridging oxygen between the β and γ phosphates is replaced with a nitrogen) and adopt similar ‘closed’ states binding nucleotide tightly. It is in the catalytic β chains that the significant differences lie. The three β subunits are all in different conformations: The first is in a ‘closed state’ with AMP-PNP bound tightly and is termed β_{TP} (Tri-phosphate), the second has a similar overall conformation but binds ADP and is termed β_{DP} (Di-phosphate) and the third is in an open conformation and binds no nucleotide, β_E (Empty). The three α chains are called α_{TP} , α_{DP} and α_E according to which β subunit they neighbour (Figure 1.16). The three different states of the β subunits fitted the

proposed binding change mechanism (Boyer, 1975; Boyer, 1993; Boyer *et al.*, 1975; Cross and Boyer, 1975) and they provided a molecular mechanism for rotary action (see Section 1.3.7).

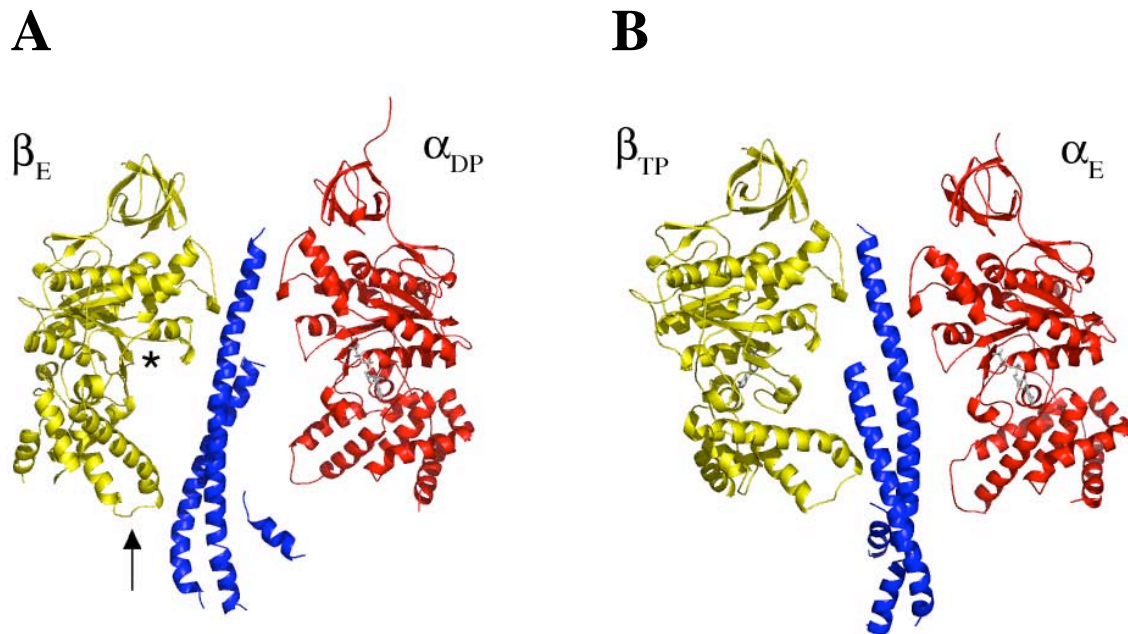


Figure 1.16 Structural differences in the β subunits of F_1 -ATPase. **A:** Cross-section of the ATPase showing subunits β_E and α_{DP} . The β chain adopts a very different conformation to the α chain. The nucleotide binding pocket (asterisk) is empty and the helix-turn-helix motif in the C-terminal region (arrow) has undergone a 37° rotation relative to the β_{TP} subunit (**B**). Two α and two β chains have been removed for clarity. **B:** The β_{TP} and α_E subunits; the complex has been rotated 120° relative to **A**. The α chain is in the same conformation as the others, the β chain is in a closed state, binding AMP-PNP. The helix-turn-helix motif is interacting closely with the γ subunit. β_{DP} (not shown) adopts a similar overall conformation as the β_{TP} subunit.

The structure of F_1 -ATPase demonstrated that the γ subunit introduced the asymmetry and caused the three β subunits to be in three different conformations. A structure of an $\alpha_3\beta_3$ hexamer, from the thermophilic *Bacillus* PS3, without the γ subunit, had exact three-fold symmetry and bound no nucleotide, demonstrating that the γ subunit confers asymmetry on

the complex (Shirakihara *et al.*, 1997). The catalytic importance of nucleotide binding pocket residues was also determined. As expected, the residues of the P-loop motif GXXXXGKT (Walker *et al.*, 1982) were found to interact with the nucleotide phosphates. Density was observed for an attacking water (or leaving water in synthesis) coordinated by β -Glu 188, the negative charge activating nucleophilic attack by the water (in the α subunits this glutamate is replaced by a glutamine residue with no charge which may explain their lack of catalytic activity). An arginine residue, contributed from a neighbouring α subunit (α Arg-373), implicated in catalysis by mutational studies (Futai *et al.*, 1989), was found to be involved in catalysis. The positively charged guanidinium group interacts closely with the γ phosphate and is thought to stabilise the negative charge that would develop on a transition state (Abrahams *et al.*, 1994).

1.3.7 The catalytic mechanism

In the intact complex, energy in the form of the pmf is converted into rotational energy which is transmitted to the catalytic sites in the F_1 domain (around 100 Å distance from F_0) via the central stalk. Exactly how this is achieved has been a focus of research since the complex was first discovered. The first mechanism to be widely accepted, and that was subsequently confirmed by X-ray crystal structures, was the binding change mechanism (Boyer, 1979; Boyer, 1993; Cross, 1981; Gresser *et al.*, 1982).

There are two main tenets of this mechanism: First, the energy required for the synthesis of ATP is used to release the product from a tightly bound pocket and second, that all three sites act cooperatively, rather than as discrete sites of catalysis. The three catalytic sites in the β subunits were proposed to adopt three conformations with three affinities for nucleotide: Open (O), loose (L) and tight (T), with low medium and high affinities for

nucleotide respectively (Figure 1.17). Energy derived from the pmf drives the conversion of one site to the next; in synthesis this would convert a tight binding site to a loose one releasing freshly synthesised ATP (T to O), the site next to this one is converted from loose, binding ADP and Pi, to a tight site causing the synthesis of ATP (L to T). The third site will be converted from an open site to a loose, binding ADP and Pi (O to L), see Figure 1.17). The sites move sequentially from one form to the next.

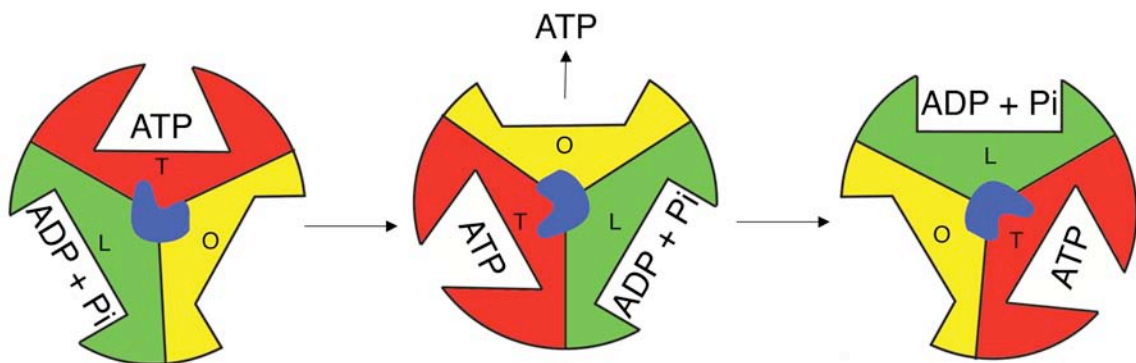


Figure 1.17 The binding change mechanism. Schematic showing the three different catalytic states of the β subunits denoted O (open), L (loose) and T (tight). As the γ subunit (blue) rotates, the tight site is converted to an open site and ATP is released, at the same time an open site is converted to a loose site binding ADP and orthophosphate. The energy put into the system by the rotation of γ is used to release tightly bound ATP. [After (Cross, 1981), the position and role of the γ subunit was not known at the time].

The crystal structure of F_1 -ATPase (Abrahams *et al.*, 1994) provided direct evidence for this catalytic mechanism (see previous section) with the three β subunits adopting the three nucleotide binding affinities (β_E , β_{TP} and β_{DP} for O, L and T) and afforded the first firm basis for a rotary mechanism. The cooperativity between the sites is caused by the asymmetric γ subunit that induces the conformational changes. The rotation of the γ subunit had been suggested as the mechanism of transfer of energy to the catalytic sites, converting them from

one form to another. This rotating mechanism was confirmed by the direct visualisation of rotation using information obtained from the structural model [see section 1.3.8 (Noji *et al.*, 1997)].

1.3.8 Direct observation of rotation

The direct observation of rotation of the γ subunit in F_1 -ATPase not only demonstrated the reality of rotary catalysis but also revealed much about the mechanism itself. Rotation was first observed in the $(\alpha\beta)_3\gamma$ subcomplex of *Bacillus* PS3; the complex has three histidine tags, on the N-termini of its β subunits, and was attached to a glass coverslip coated with Ni-NTA beads. In the first experiment, a fluorescent actin filament was connected to the γ subunit via biotin and avidin to allow inspection of rotation (Noji *et al.*, 1997).

In initial experiments rotation was seen but at much lower rates than those theoretically possible, due to the viscous drag on the actin filament. Later experiments, replacing this probe with smaller ones such as Cy3-maleimide (Adachi *et al.*, 2000) or a gold bead (Yasuda *et al.*, 2001) revealed distinct 120° substeps as postulated in the binding change mechanism but as the ATP concentration was lowered the 120° step was resolved into 90° and 30° sub-steps thought to correspond to ATP binding then subsequent hydrolysis (Yasuda *et al.*, 2001).

Rotation has also been observed in the c-ring. An actin filament attached to a c subunit showed rotation, demonstrating transmission of energy from the γ subunit to the c-ring and vice versa (Sambongi *et al.*, 1999). A later experiment linked the c subunits to Ni-NTA beads and observed rotation of the $(\alpha\beta)_3$ subcomplex or the a subunit (Nishio *et al.*, 2002) demonstrating rotation in a fully coupled complex.

These experiments all investigated the hydrolysis of ATP as opposed to synthesis. The final proof of rotary catalysis came with an experiment showing ATP synthesis during mechanical rotation of the γ subunit (Itoh *et al.*, 2004). Mechanical rotation of the γ subunit of immobilised *Bacillus* PS3 F_1 -ATPase was achieved via a linked magnetic bead. Electromagnets were rotated in the appropriate direction (clockwise in this case as the hydrolytic rotation was observed as anti-clockwise). As the magnets were rotated, synthesis of ATP from ADP and orthophosphate was measured by the luciferase assay. This experiment demonstrated for the first time that mechanical force on a protein can drive chemical synthesis in remote catalytic sites, although by the time it was demonstrated this conclusion was inescapable.

1.3.9 Structures of F_1 -ATPase

Since the first structure of bovine F_1 -ATPase was solved in 1994 nine further structures of bovine mitochondrial F_1 -ATPase have been solved (Abrahams *et al.*, 1996; Braig *et al.*, 2000; Cabezón *et al.*, 2003; Gibbons *et al.*, 2000; Kagawa *et al.*, 2004; Menz *et al.*, 2001b; Orriss *et al.*, 1998; van Raaij *et al.*, 1996a) as well as other structures from various sources (Bianchet *et al.*, 1998; Groth and Pohl, 2001; Hausrath *et al.*, 1999; Stock *et al.*, 1999). Many of the subsequent structures supported the rotary catalytic mechanism and located sites of inhibition, and helped to demonstrate that the original 1994 structure represented an intermediate in the active catalytic cycle (Abrahams *et al.*, 1996; Braig *et al.*, 2000; Kagawa *et al.*, 2004; Orriss *et al.*, 1998; van Raaij *et al.*, 1996a).

The structure of the DCCD inhibited enzyme (Gibbons *et al.*, 2000) was the first in which the entire central stalk was resolved. The γ subunit contained an unpredicted β -sheet domain and a Rossman fold which could add rigidity to the coiled-coil domain. The δ subunit consists of a ten-stranded β -sheet and two helices connected by a hairpin turn. The γ

and δ subunits are held together by the ‘pincer’ like ϵ subunit, forming two helices connected by a coiled region (Figure 1.18). The three subunits of the stalk interact extensively to form a stable shaft and a ‘foot’ that couples F_1 to the c ring in F_o .

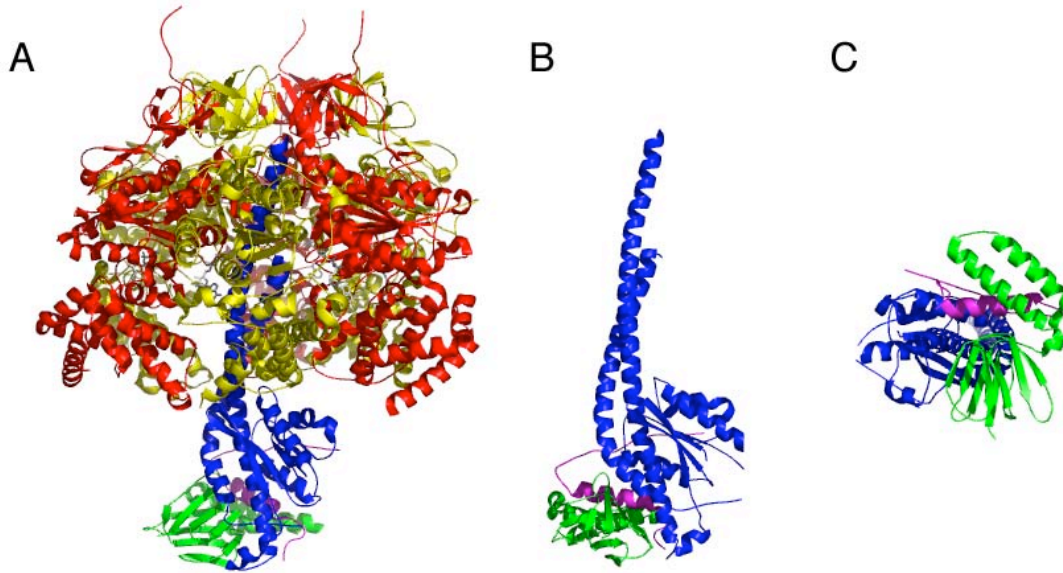


Figure 1.18 The structure of the central stalk of F_1 -ATPase at 2.4 Å resolution. **A:** The architecture of the complete F_1 -ATPase. The δ subunit is shown in green and the ϵ subunit in magenta. **B:** The central stalk. The structure contains an unpredicted Rossman fold that stabilises the coiled coil domain that penetrates the $(\alpha\beta)_3$ hexamer. **C:** The foot of the central stalk that interacts with the ring of c subunits in the F_o domain. [Figure generated from the F_1 -DCCD structure, PDB code 1E79 (Gibbons *et al.*, 2000)]

An electron density map of yeast mitochondrial ATP synthase provided the first structural glimpse of the F_o domain (Stock *et al.*, 1999). It revealed, at low resolution (3.9 Å), a ring of 10 c subunits and it showed their interaction with the central stalk of the F_1 -ATPase (Figure 1.19). The results changed the current model for coupling the pmf to ATP synthesis (Section 1.3.5). Other structures have demonstrated that the nucleotide occupancy is due to the fold the protein adopts and not the nucleotide concentration (Menz *et al.*, 2001a) or they represent

transition states in the catalytic cycle of F₁-ATPase (Kagawa *et al.*, 2004; Menz *et al.*, 2001b); the latter are discussed in Section 1.5.

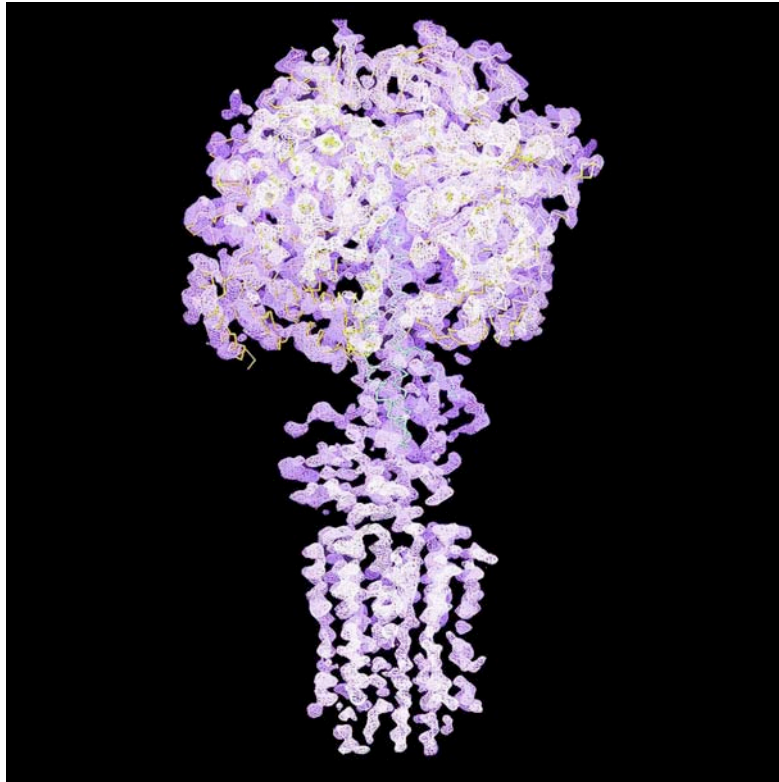


Figure 1.19 The architecture of the rotor of ATP synthase. A 3.9 Å electron density map of the yeast F₁-c₁₀ sub-complex of ATP synthase. A model was built using the α-carbon backbones of the bovine F₁-ATPase, the *E. coli* ε subunit (equivalent to the bovine δ) and ten copies of the *E. coli* c subunit. The presence of a symmetry mismatch between F₀ and F₁ (10:3) was unexpected and changed the models of F₀. [Image from (Stock *et al.*, 1999)].

1.4 The inhibitor protein of the ATP synthase

1.4.1 Regulation of the ATP synthase

The ATP synthase is regulated *in vivo* to prevent the hydrolysis of ATP under conditions where the pmf is lost, for example during anoxia (Walker, 1994). The hydrolytic activity of ATP synthase is controlled in different ways in different species. The chloroplast

ATP synthase is thought to be regulated by the γ subunit (Richter *et al.*, 2000). An insertion in the chloroplast γ subunit, not present in the mitochondrial enzyme, contains two cysteines (Arana and Vallejos, 1982). In the dark, where the pmf falls, conditions become oxidising and a disulphide bond is formed, blocking the rotation of γ and preventing hydrolysis of the ATP pool. In daylight, the pmf is restored and the disulphide bond is reduced by thioredoxin, allowing ATP synthesis to resume (Nalin and McCarty, 1984; Schwarz *et al.*, 1997).

Bacteria have no obvious physiological need to prevent ATP hydrolysis. Under anoxic conditions, ATP made by glycolysis is hydrolysed in order to generate a pmf. The addition of excesses of the ϵ subunit of the *E. coli* enzyme (homologous to bovine δ) inhibits the enzyme (Mendel-Hartvig and Capaldi, 1991; Smith and Sternweis, 1977; Weber *et al.*, 1999). It is proposed that the protein has two different conformations. In one conformation, the ϵ subunit extends towards the F_1 domain, interacting with an $\alpha\beta$ pair, preventing hydrolysis (Rodgers and Wilce, 2000). The second conformation is the down conformation observed in the bovine enzyme. It has been proposed that the up connection may be broken on the synthesis of ATP and the second conformation is assumed, regulating the enzyme like a ratchet (Tsunoda *et al.*, 2001), allowing rotation in only one direction. However, the physiological need for such a mechanism has not been explained.

Mitochondrial ATP synthase is regulated by a natural inhibitor protein, IF_1 , that is not present in either bacteria or chloroplasts. The inhibitor protein is found in all eukaryotes and has been characterised from many species (Cintron and Pedersen, 1979; Di Pancrazio *et al.*, 2004; Hashimoto *et al.*, 1981; Ichikawa and Ogura, 2003; Matsubara *et al.*, 1981; Norling *et al.*, 1990; Pullman and Monroy, 1963). The manner of regulation in mitochondria is outlined in the following sections.

1.4.2 The bovine mitochondrial IF₁

In the absence of oxygen the pmf generated by the electron transport chain will collapse. This may happen in ischemia, where blood flow to an organ is prevented, for example during a heart attack. Cellular ATP will be provided by glycolysis and the pH values of both the cytosol and matrix will drop. The loss of the pmf will lead the ATP synthase to reverse, hydrolysing ATP instead of synthesising it. The inhibitor protein is thought to prevent this detrimental activity (Rouslin, 1983). The drop in pH activates the inhibitor protein which then binds to the catalytic subunits of the ATP synthase preventing ATP hydrolysis. When the pmf is restored the matrix pH will increase and IF₁ is released from F₁ and returns to its inactive state (Walker, 1994).

The bovine protein is the best understood. It is 84 amino acids in length and forms an α -helix (Cabezón *et al.*, 2001). In the active state, formed at pH values below 7.0, it is a dimer, where the C-terminal residues 49-84 associate in an antiparallel coiled coil [Figure 1.20 (Cabezón *et al.*, 2001)]. The rest of the protein (residues 1-48) is free to bind two F₁ domains concurrently (Cabezón *et al.*, 2000a; Cabezón *et al.*, 2003). By deletion analysis, it has been demonstrated that residues 14-47 of bovine IF₁ represent the minimal inhibitory sequence (van Raaij *et al.*, 1996b). The N-terminus of the protein binds between the α_{DP} and β_{DP} subunits in each of two F₁ domains trapping an ATP molecule in the catalytic sites, preventing hydrolysis (Cabezón *et al.*, 2003). The inactive state of the protein is formed at pH values above 7.5; it is a dimer of dimers in which the inhibitory N-terminal regions are occluded in dimer-dimer contacts, preventing them from binding to the F₁ domain (Cabezón *et al.*, 2000a; Cabezón *et al.*, 2000b; Cabezón *et al.*, 2001).

The conversion between active and inactive forms is thought to involve five histidine residues that interact in the tetramer (Gordon-Smith *et al.*, 2001) and histidine 49 may be the pH sensor that prevents aggregation. Histidine 49 is located in the second of seven heptad

repeats that form the coiled coil region. Mutation of this residue to a lysine results in a protein that is an active dimer, regardless of the pH (Cabezón *et al.*, 2003; Schnizer *et al.*, 1996).

The crystal structure of bovine F₁-ATPase in complex with IF₁ revealed the mechanism of inhibition [(Cabezón *et al.*, 2003) Figure 1.21]. It contained two F₁ domains bound to an IF₁ dimer (Cabezón *et al.*, 2000a). Residues 4 to 47 were found in intimate contact with the α_{DP} β_{DP} interface and with the γ subunit. The nucleotide binding sites are in a similar conformation to the reference structure (Braig *et al.*, 2000). However, both β_{TP} and β_{DP} contain ATP or AMP-PNP (the enzyme was inhibited in the presence of ATP, but the crystallisation buffers contained AMP-PNP, and they are indistinguishable in the electron density map). ATP (or AMP-PNP) is bound in the DP site because of inhibitor protein binding preventing hydrolysis, either by locking the $\alpha\beta$ interface, preventing the interchange to a loose state, or by preventing rotation of the γ subunit, or both.

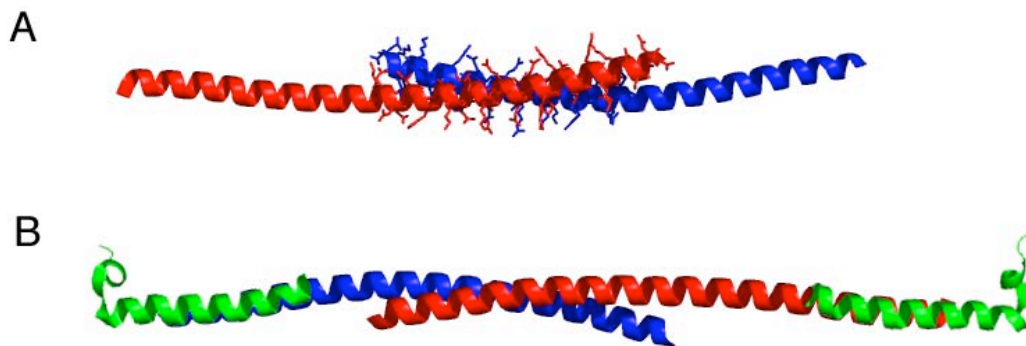


Figure 1.20 The inhibitor protein IF₁ of bovine mitochondria. **A:** The crystal structure of an IF₁ dimer. Two monomers are shown (red and blue) and residues involved in the coiled coil formation are represented as sticks. [Figure generated from PDB code 1GMJ (Cabezón *et al.*, 2001)]. **B:** The complete structure of IF₁. The crystal structure of IF₁ overlaid with the N-termini observed in the crystal structure of the F₁-IF₁ complex [PDB code 1O0H (Cabezón *et al.*, 2003)] the C-terminal region (residues 40 to 83) was disordered in the complex.

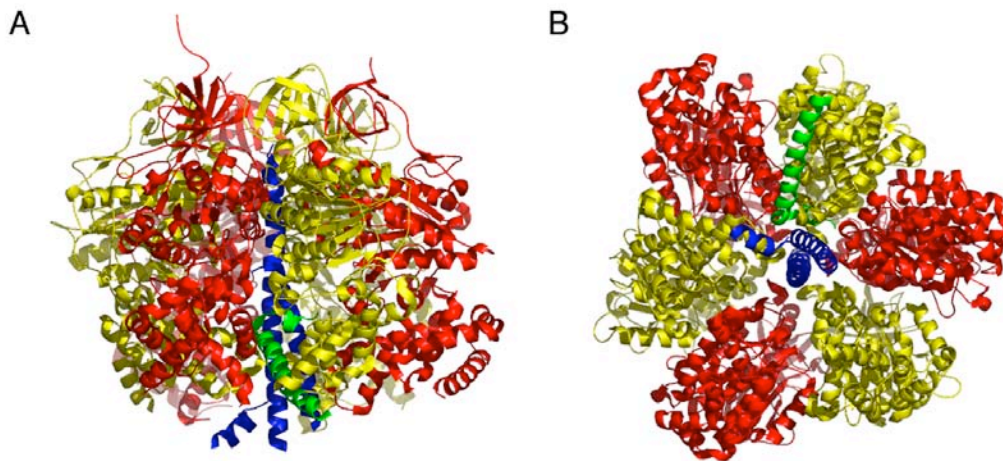


Figure 1.21 Architecture of the F₁-IF₁ complex. **A:** Side view of the complex. IF₁ (green) binds between the $\alpha_{\text{DP}}\text{-}\beta_{\text{DP}}$ interface. **B:** The complex viewed from the membrane. IF₁ extends through the $\alpha\text{-}\beta$ interface and makes contact with the γ subunit. [From PDB code 1O0H (Cabezón *et al.*, 2003)].

1.4.3 The inhibitor protein of *Saccharomyces cerevisiae*

The ATP synthase in *S. cerevisiae* is regulated by two inhibitory peptides, IF₁ (Hashimoto *et al.*, 1981; Matsubara *et al.*, 1981) and STF₁ [Stabilising Factor 1 (Akashi *et al.*, 1988)], and two other proteins, STF₂ (Okada *et al.*, 1986) and STF₃ (Hong and Pedersen, 2002), that are thought to modulate their activities, but have no intrinsic inhibitory activity. Yeast IF₁ and STF₁ are 63 amino acids in length (considerably shorter than the 83 residues of bovine IF₁) and have 49% sequence identity to each other and 30% identity to the bovine protein. Despite the sequence similarity of IF₁ and STF₁ their inhibitory potencies differ. Below pH values of 7.0, IF₁ is much more active than STF₁, but it is still able to inhibit ATP hydrolysis completely at high concentrations. It has been suggested that the role of STF₁ is to assist in the binding of IF₁ to the F₁ domain (Akashi *et al.*, 1988). However, removal of the *stf1* gene has no effect on the inhibition of hydrolysis in the absence of a pmf (Venard *et al.*, 2003). Another proposed role is that STF₁, having a lower tendency to aggregate than IF₁,

can act as an inhibitor at higher pH values (Cabezón *et al.*, 2002). As it has a lower binding constant (Venard *et al.*, 2003), it should not prevent ATP synthesis on the restoration of the pmf. The mechanism of activation of the yeast proteins seems to be based on the same principle as the bovine protein but via a different mechanism. The yeast proteins have no equivalent to H49 and their C-termini are truncated with respect to the bovine protein. Two residues, histidine-39 and glutamate-21 have been shown to confer pH sensitivity on the proteins (Ichikawa *et al.*, 2001). However, how these residues affect oligomer formation has yet to be discovered.

1.5 Metallofluorides as analogues of nucleotides and of the transition state of phosphoryl transfer

The transfer of phosphate groups is central to organisms as it is the primary way of transducing energy and is a major component of cell signalling and its regulation. A vast number of protein families exist that hydrolyse nucleotide triphosphates, and their mode of action is an area that has been studied extensively. Biological systems maintain the ATP to ADP ratio far from equilibrium, allowing a large amount of free energy to be generated by the hydrolysis of ATP to ADP and phosphate (typically -57 kJ M^{-1} , in the cytoplasm, where the ATP:ADP ratio can be maintained at 1000:1).

While the hydrolysis of ATP is a thermodynamically favourable reaction, it will not occur spontaneously as the activation energy is too high. This barrier makes ATP an ideal molecule for storage of energy, allowing organisms to develop a large number of proteins able to hydrolyse ATP, and to utilise the energy released. Many of these enzymes contain a common motif where the transition state intermediate of hydrolysis is surrounded by positive charges, thereby stabilising it and decreasing the activation energy required. The common motif for phosphate binding is referred to as the P-loop or Walker A motif [(Walker *et al.*,

1982) Figure 1.22]. A vast number of proteins contain this motif including kinases, ion motive ATPases (F, V and P-types) and ATP binding cassette (ABC) transporter superfamilies (Higgins *et al.*, 1986). Metallofluorides have been used extensively in the study of protein mediated phosphoryl transfer reactions. In the presence of ADP (or GDP), metallofluorides bind in the position occupied by the γ phosphate mimicking either the terminal phosphate or a transition state intermediate, depending on the metal. The chemistry of phosphoryl transfer and the use of metallofluorides in the study of the catalytic mechanism of bovine F_1 -ATPase, and other enzymes, is discussed below.

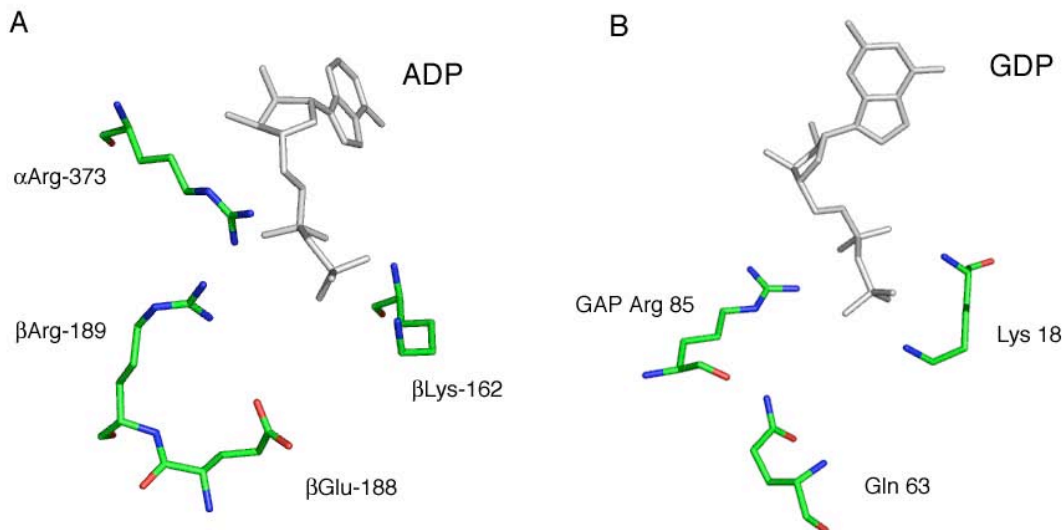


Figure 1.22 Comparison of some P-loop residues from different enzymes. A: The ATP binding pocket of the β_{DP} subunit of F_1 -ATPase. The negative charge that develops on the phosphoryl intermediate is stabilised by the positive side chains of β Arg-189 and β Lys-162 and α Arg-373. β Glu -88 activates the attacking water. **B:** The nucleotide binding pocket of the RAS GTPase. The phosphoryl intermediate is stabilised by similar residues to the ATPase and an arginine is contributed from the GTPase activating protein (GAP). Gln-63 activates the attacking water performing the same role as Glu-188 in the ATPase. [Figure generated from bovine F_1 -ATPase (Abrahams *et al.*, 1994), PDB 1BMF and RhoA.GTPase RhoGAP complex (Graham *et al.*, 2002), PDB 1OW3].

1.5.1 The chemistry of phosphoryl transfer

The transfer of phosphoryl groups may take place via either of two proposed mechanisms; dissociative (S_N1) and associative (S_N2) [Figure 1.23 A and B respectively (Knowles, 1980)]. In the dissociative mechanism, the bridging oxygen bond between the β and γ phosphates is broken as the nucleophile approaches, but before a new bond is formed with the nucleophile. The reaction intermediate formed is a metaphosphate, which then forms a bond with the nucleophile, transferring the phosphate group. In an associative reaction, nucleophilic attack takes place on the phosphorous without bond breakage, forming a trigonal bipyramidal penta-coordinated phosphorane. The metaphosphate intermediate contains only one negative charge as opposed to three in the phosphorane; the charge is compensated in enzyme mediated hydrolysis by positively charged side chains and divalent metal ions.

In the F_1 -ATPase, hydrolysis of ATP begins with an 'in-line' nucleophilic attack, from a water polarised by β Glu-188, on the γ phosphate. The transition state is a trigonal bipyramid, with the apical positions occupied by the oxygen of the β phosphate and the attacking water. Hydrolysis leads to an inversion of the phosphate stereochemistry (Webb *et al.*, 1980). Evidence that NTP hydrolysis proceeds via a dissociative mechanism is provided by experiments based on kinetic analysis, which show that the rate limiting step of the reaction is bond cleavage of the leaving group, before bond formation with the nucleophile (Admiraal and Herschlag, 1995; Westheimer, 1981). However, it has been suggested that the same data could be interpreted equally well as supporting an associative mechanism (Aqvist *et al.*, 1999). In the dissociative mechanism, the role of the nucleophile is less than in the associative mechanism. Using this premise, tyrosine kinases were studied where the

nucleophilicity of the attacking group (the tyrosine oxygen) was varied (Ablooglu *et al.*, 2000). The results indicated strongly a dissociative mechanism.

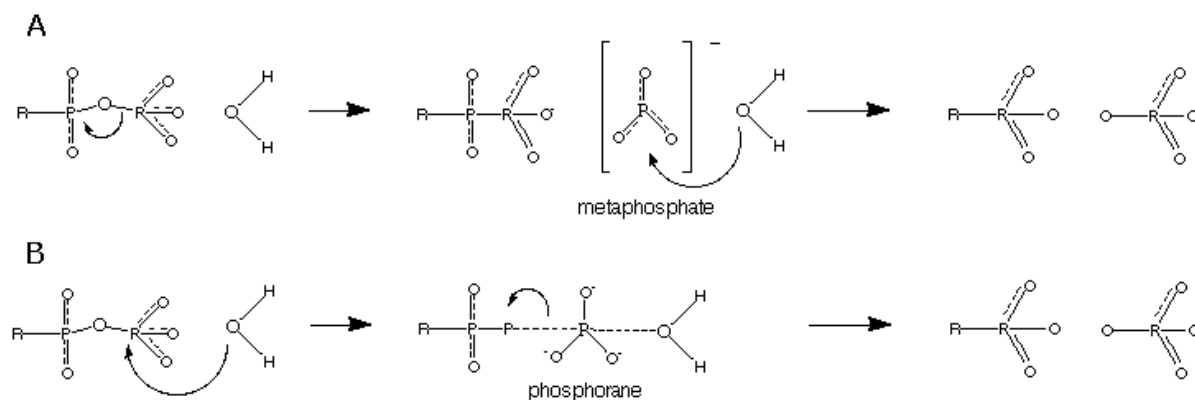


Figure 1.23 Reaction mechanisms of phosphoryl transfer. A: The dissociative mechanism. The covalent β - γ phosphonate ester bond is broken before the nucleophile bond is formed, the reaction proceeds with a metaphosphate intermediate. **B:** The associative mechanism. Nucleophilic attack forms a new bond before the phosphonate ester bond is broken. The reaction proceeds via a trigonal bipyramidal pentavalent phosphorane intermediate.

Transfer intermediates are extremely short lived (around 10^{-3} sec) making their study by X-ray crystallography difficult. However, there is some crystallographic evidence about transition states. Two crystal structures have been solved that have been interpreted as containing a true phosphoryl transfer transition state. First, the crystal structure of β -phosphoglucomutase may contain a stabilized penta-coordinated phosphorane intermediate [Figure 1.24 A (Lahiri *et al.*, 2003)], but this interpretation has been disputed (Blackburn *et al.*, 2003; Webster, 2004). Second, the structure of fructose-1,6-bisphosphatase, inhibited by high concentrations of potassium, contains a stabilized metaphosphate intermediate, perhaps demonstrating a dissociative mechanism [Figure 1.24 B (Choe *et al.*, 2003)].

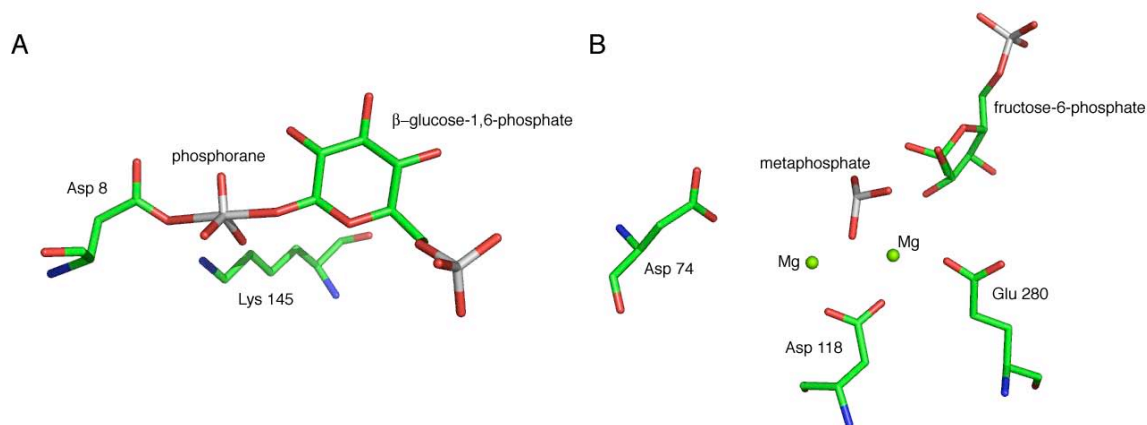


Figure 1.24 Crystallographically observed transition states of phosphoryl transfer. A: The possible pentavalent phosphorane observed in β -phosphoglucomutase. However, the observed transition state may be MgF_3^- rather than a phosphorane (Blackburn *et al.*, 2003). [Figure created from PDB 1O03 (Lahiri *et al.*, 2003)]. **B:** The metaphosphate intermediate observed in fructose-1,6-bisphosphatase, an equilibrium between metaphosphate and orthophosphate. [Figure created from PDB code 1NUW (Choe *et al.*, 2003)].

Transition states are usually studied using non-reactive analogues that mimic the geometry, size and charge distribution of phosphoryl transfer. Many crystal structures containing analogues have been interpreted as indicating an associative mechanism (Klabunde *et al.*, 1996; Lindqvist *et al.*, 1994; Sondek *et al.*, 1994). However, the analogue may be forcing the geometry of a phosphorane intermediate on the protein and may not represent an actual reaction intermediate. Another crystal structure, of a cyclin dependent kinase, solved with a metaphosphate analogue (NO_3^-) suggests a dissociative mechanism (Cook *et al.*, 2002), but again this may be influenced by the analogue. The most commonly used transition state analogues in nucleotide hydrolysis are complexes between ADP (or GDP) and aluminium fluoride and beryllium fluoride as described in the next section.

1.5.2 Aluminium and beryllium fluoride

In solution, aluminium and beryllium fluoride form mixtures of species. The distribution depends on the fluorine concentration and the pH value of the solution (Martin, 1988). Many crystal structures of NTPases containing aluminium fluoride as either AlF_3 or AlF_4^- have been solved. In all cases, both species are planar and mimic the transition state of phosphoryl transfer. Beryllium fluoride is usually found as BeF_3^- [one structure, a UMP/CMP kinase, has been solved that contained BeF_2 , forming a bridge between the terminal oxygens of the nucleotides (Schlichting and Reinstein, 1997)]. Beryllium fluoride adopts tetrahedral geometry regardless of valency, mimicking a ‘ground state’ phosphate group. Fluorine is one atomic number greater than oxygen and is highly electronegative, giving it a strong propensity to form hydrogen bonds. The lengths of aluminium-fluorine and beryllium-fluorine bonds are very close in length to phosphorous-oxygen bonds (Table 1.2).

Table 1.2 Comparison of lengths of the phosphorous-oxygen bond compared to metal-fluorine bonds.

Bond	Length (Å)
P-O	1.55 (1.67 in phosphorane)
Al-F	1.61
Be-F	1.48

As the bonds in metallofluorides are ionic, the fluorides are freely exchangeable with those in solution, and a high concentration is needed to inhibit nucleotide hydrolases fully. The metallofluoride is thought to bind quickly, via hydrogen bonds, to the site in the protein normally occupied by the γ phosphate of ATP. Then the metal forms an ionic bond with the β phosphate oxygen of ADP. As the geometry of the analogues is fixed the conformation of the protein is locked by coordinating to it and the protein is inhibited. Aluminium and

beryllium fluoride have been used to study the catalytic mechanism of F₁-ATPases by both biochemical (Issartel *et al.*, 1991; Lunardi *et al.*, 1988) and structural methods (Braig *et al.*, 2000; Kagawa *et al.*, 2004; Menz *et al.*, 2001b).

1.5.3 Transition states in the catalytic cycle of F₁-ATPase

While the majority of structures of bovine F₁-ATPase have been found to be very similar, three structures differ. They are the ATPase in complex with IF₁ which contains ATP in both the β_{TP} and β_{DP} catalytic sites [(Cabezón *et al.*, 2003), discussed in Section 1.4.2] and two structures inhibited with metallofluorides also have different nucleotide occupancies (Kagawa *et al.*, 2004; Menz *et al.*, 2001b), these are described in the following sections.

1.5.3.1 The structure of bovine F₁-ATPase with all three catalytic sites occupied

The first structure of bovine F₁-ATPase inhibited with aluminium fluoride was determined with crystals where the aluminium fluoride was not maintained in the mother liquor during crystallisation. It contained an AlF₃ in the β_{DP} subunit and was similar to the reference structure [the first crystal structure, solved from a single crystal cooled to 100K (Braig *et al.*, 2000)]. However, when AlCl₃ and NaF were maintained in the crystallisation buffers, the protein structure, solved to 2.0 Å, contained nucleotide in all three catalytic sites (Menz *et al.*, 2001b). It provided the first direct evidence that three sites could be occupied concurrently during hydrolysis. In this structure the β_E site adopted a 'half-closed' conformation binding ADP and a sulphate ion mimicking orthophosphate (Figures 1.25 and 1.26). This structure probably represents a post hydrolysis step before the release of products.

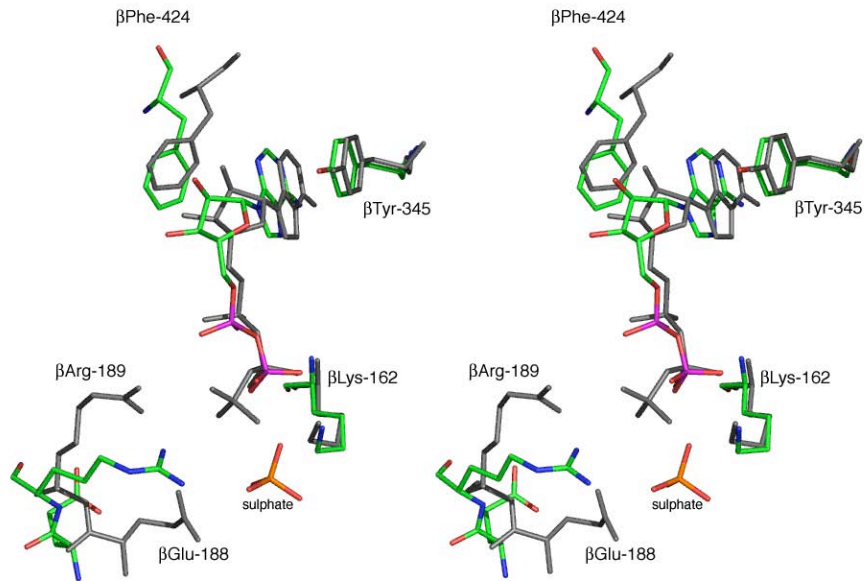


Figure 1.25 Stereo image of the superimposed half closed site in the $(\text{ADP AlF}_4^-)_2\text{-F}_1$ structure and the β_{TP} of the reference structure. The ‘half closed’ site (coloured) is superimposed on the β_{TP} site (grey). The adenine ring binding residues ($\beta\text{Phe-424}$ and $\beta\text{Tyr-345}$) adopt a similar conformation. $\beta\text{Glu-188}$ activates the attacking water in the TP site but has moved out of the way in the half closed site. $\beta\text{Arg-189}$ coordinates the γ phosphate in the TP site and moves with the sulphate.

The other two catalytic sites contain ADP-AlF_4^- , whereas the first aluminium structure contained ADP-AlF_3 in the β_{DP} site only (Braig *et al.*, 2000). Both species are planar, the first mimics the shape of a phosphoryl transfer analogue, the second mimics the equivalent charge. Also, the γ subunit was observed in a different position to other structures. It was twisted by around 20° in its C-terminal region. This rotation may be equivalent to the 30° substep observed in rotational experiments (Yasuda *et al.*, 2001). This structure implied that in the catalytic cycle the enzyme alternates between states where two and three sites are occupied.

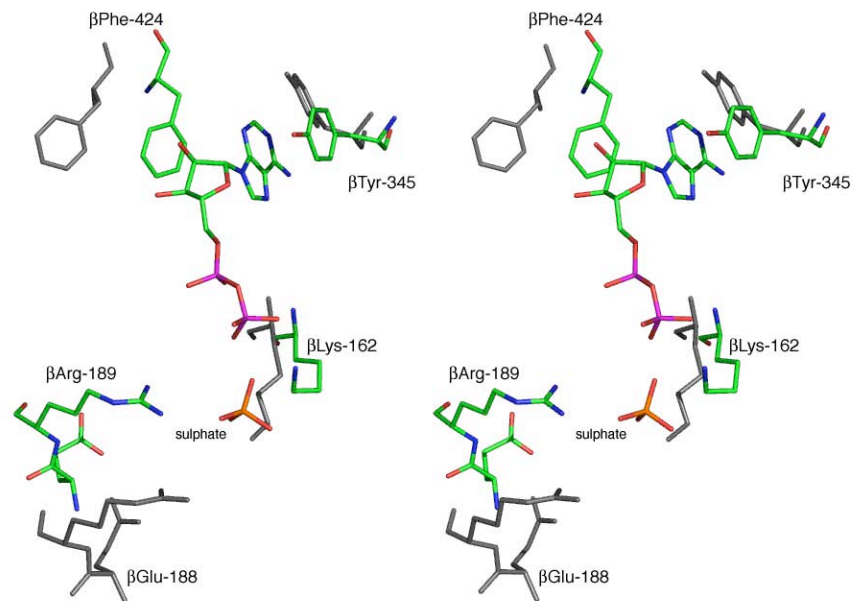


Figure 1.26 Stereo image of the superimposed half closed site in the $(\text{ADP-AlF}_4^-)_2\text{-F}_1$ structure and the β_E of the reference structure. The ‘half closed’ site is coloured and the β_E site is grey. The adenine ring binding residues have opened to release nucleotide and β Arg-189 and β Glu-188 adopt a different conformation no longer coordinating the sulphate.

This was confirmed by the results of tryptophan fluorescence experiments (Weber and Senior, 2000) and studies of fluorescent ATP analogues (Nishizaka *et al.*, 2004). A new catalytic scheme was proposed based on the structural information. Binding of ATP to an open site causes a rotation in the γ subunit causing ATP bound in a tight site to be committed to hydrolysis (T') and a loose site to ‘half-close’ around an ATP (L'). The next step is the hydrolysis of ATP in the site committed to it and its conversion to a half-open site corresponding to the β_E in the $(\text{ADP-AlF}_4^-)_2\text{-F}_1$ structure (L''). The release of ADP and Pi from this site converts it to an open site and the ‘ground state’ (equivalent to the reference structure) is returned to (Figure 1.27).

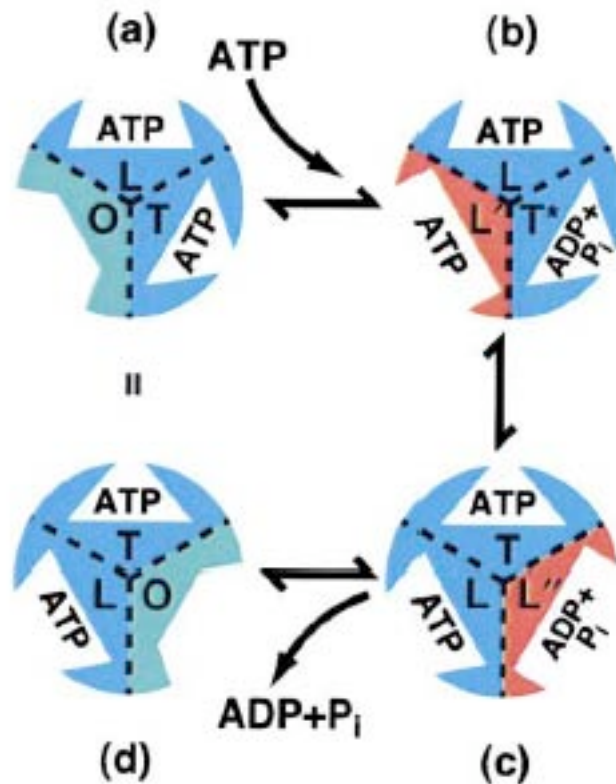


Figure 1.27 Schematic of the binding change mechanism based on structures of bovine F_1 -ATPase. The binding of ATP changes an open site (O) to a half-closed site (L') causing rotation of the γ subunit and the commitment of ATP in T to hydrolysis [(T^*), b]. Hydrolysis in T^* converts it to a half-closed state (L'') and the loose to a tight [(L to T), c]. Release of ADP and phosphate returns the enzyme to the ground state (d). [Figure from (Menz *et al.*, 2001b)]

1.5.3.2 The structure of bovine F_1 -ATPase with two sites occupied by ATP

The structure of bovine F_1 -ATPase inhibited with ADP and beryllium fluoride was the first to be solved with a truly non-hydrolysable ATP analogue bound to the active sites (Kagawa *et al.*, 2004). Although in many respects it is similar to the reference structure it differs significantly that ATP analogues are bound in both the β_{DP} and β_{TP} subunits. Beryllium fluoride mimics the γ phosphate of ATP. It binds at nearly covalent distance to the

bridging oxygen of the β phosphate of ADP and adopts a tetrahedral atomic arrangement closely imitating the terminal phosphate of ATP.

The hydrolysis of ATP involves the terminal phosphate undergoing a series of coordination states (see Section 1.5.1), as beryllium fluoride can only be tetrahedral, the enzyme is inhibited in this state. The structure contained two ATP analogues in the β_{TP} and β_{DP} sites; and was the first structure to contain an ATP in the catalytically active DP site [the tight site in the binding change mechanism (see Section 1.3.7)]. As in earlier structures the empty site contained no nucleotide. The DP site had been designated as the catalytically active site from the original structure (Abrahams *et al.*, 1994) and other experiments (Gao *et al.*, 2003), as the nucleotide binding pocket was more tightly closed than the TP site. This was confirmed by the beryllium fluoride structure.

In this structure the nucleophilic water molecule in the β_{DP} site is 2.6 Å from the beryllium, over 1 Å closer than the equivalent water molecule in β_{TP} subunit (3.6 Å from beryllium). The high resolution of the structure (2.2 Å) allowed these water molecules to be confidently modelled into the density. Alignment of the two binding pockets revealed the reason for the catalytic differences. The arginine finger that stabilises the phosphoryl transition state is 1 Å further away from the nucleotide binding pocket in the TP site. This arrangement moves the beryllium away from the attacking water molecule and changes the geometry of the interaction, making nucleophilic attack less likely (Figure 1.28).

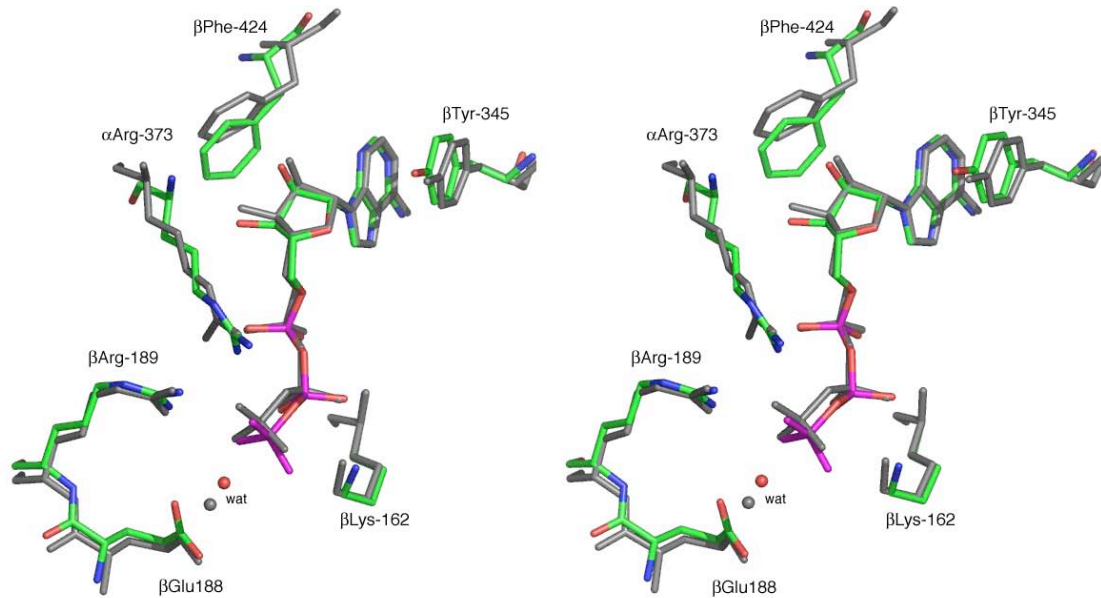


Figure 1.28 Stereo image of the superimposition of the β_{TP} and β_{DP} catalytic sites of the beryllium fluoride inhibited bovine F_1 -ATPase. The β_{DP} site is coloured and the β_{TP} site is grey. The major shifts are seen in the attacking water molecule (wat), the γ phosphate (in this case beryllium fluoride) and α Arg-373.

1.5.4 Magnesium fluoride

The activating effect of aluminium fluoride on GTPases has been investigated for many years (Sternweis and Gilman, 1982) and later it was found that fluoride has a similar effect in the absence of aluminium but in the presence of magnesium (Higashijima *et al.*, 1987). This effect is due to magnesium binding three fluorines and mimicking the γ phosphate in a similar manner to aluminium fluoride. The crystal structure of RhoA.GDP bound to RhoGAP (GTPase activating protein) with magnesium and fluoride present showed that an MgF_3^- was bound in the active site, replacing the γ phosphate of GTP (Graham *et al.*, 2002). The MgF_3^- species was planar and mimicked the charge and geometry of a phosphoryl transfer intermediate (Figure 1.29 B). As the coordination and charge of this

species matches a phosphoryl intermediate so well, magnesium fluoride was suggested as the best analogue to study these reactions (Graham *et al.*, 2002). It has been suggested that the crystal structure of β -phosphoglucomutase containing the pentavalent phosphorane really contains MgF_3^- (Blackburn *et al.*, 2003). The crystals were grown in the presence of 100 mM fluoride and magnesium and it has been proposed that as magnesium fluoride mimics this state so closely it has been mistaken for phosphorane. However, this interpretation has been refuted by the original authors (Blackburn *et al.*, 2003).

To date only two other structures containing magnesium fluoride have been solved, these are an NMR solution structure of Ap_4A hydrolase (Fletcher *et al.*, 2002) and the crystal structure of the sarcoplasmic calcium ATPase (Toyoshima *et al.*, 2004). The latter appears to contain MgF_4^{2-} representing the post hydrolytic release of phosphate from phosphorylated Asp351 and is not associated with nucleotide (Figure 1.29 A). Therefore, it does not represent a transition state. However, the electron density could also be interpreted as a planar MgF_3^- species with the 'top' fluorine actually being a nucleophilic water molecule. If this is the case, the structure represents a transition state of phosphorous release from Asp-351. The catalytic mechanism of this protein has been revealed almost entirely by X-ray crystallography experiments using reaction intermediate analogues and non-hydrolysable ATP analogues (Sorensen *et al.*, 2004; Toyoshima and Mizutani, 2004; Toyoshima *et al.*, 2000; Toyoshima and Nomura, 2002; Zhang *et al.*, 1998).

In this thesis, the structure of bovine mitochondrial $\text{F}_1\text{-ATPase}$ inhibited with ADP and MgF_3^- is presented. Magnesium fluoride is bound in both the β_{DP} and β_{TP} sites and the β_{E} site binds ADP. The structure represents a new step in the catalytic cycle.

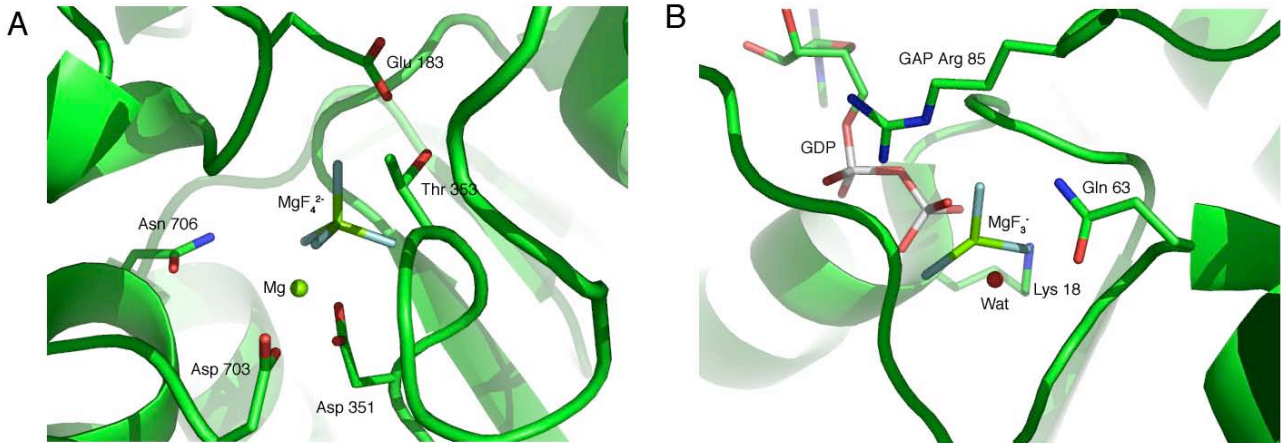


Figure 1.29 The magnesium fluoride found in the structures of sarcoplasmic Ca^{2+} ATPase and the RhoA.GDP GAP complex. **A:** The MgF_4^{2-} in the Ca^{2+} -ATPase. The magnesium fluoride is thought to represent the released phosphate from Asp 351 that is phosphorylated during the catalytic cycle. **B:** The nucleotide binding pocket of RhoA GTPase. The MgF_3^- is in the position of the γ phosphate of GTP and mimics the planar transition state. The attacking water is polarised by Gln 63 and the negative charge on the transition state is stabilised by the positively charged side chains of Lys 18 and Arg 85 [contributed from the GTPase activating protein (GAP)]. [Figures generated from PDB files 1WPG for part A (Toyoshima and Mizutani, 2004) and 1OW3 for part B (Graham *et al.*, 2002)]

1.6 Aims of this work

The aims of this study were two fold: First, to investigate the mechanism of pH sensitivity of the yeast inhibitor proteins IF_1 and STF_1 . The present investigation built on previous work on the aggregation states of bovine IF_1 in response to differing pH values (Cabezón *et al.*, 2002). Their properties both in solution and bound to the *S. cerevisiae* F_1 -ATPase have been studied. In contrast to bovine IF_1 , the yeast inhibitors are active as monomers. Like the bovine protein they form inactive higher oligomers above pH 7.0.

Second, the catalytic cycle of bovine F_1 -ATPase was investigated by crystallisation with a novel analogue of phosphoryl transfer, magnesium fluoride. While many of features of the mechanism of catalysis of the ATP synthase are well understood, it is now clear that there are many sub-steps within the cycle. Revealing and understanding these steps will provide a clearer understanding of how ATP is made and how rotation is generated. An important method for understanding these steps is to crystallise the protein in a sub-step that is also accessible by biochemical or biophysical means. This approach had previously revealed new steps in the catalytic mechanism of F_1 -ATPase (Kagawa *et al.*, 2004; Menz *et al.*, 2001b) and the P-type Ca^{2+} -ATPase (Sorensen *et al.*, 2004; Toyoshima and Mizutani, 2004; Toyoshima *et al.*, 2000; Toyoshima and Nomura, 2002; Toyoshima *et al.*, 2004). It was hoped that a new crystal structure would reveal a new state in the catalytic mechanism.

CHAPTER 2: MATERIALS AND METHODS

2.1 Materials

2.1.1 Chemicals

All chemicals, biochemicals and enzymes were purchased from Sigma-Aldrich Chemicals (St. Louis, MO, USA), Fluka Chemicals (Gillingham, UK), VWR International (Merck House, Poole, Dorset, BH15 1TD) and New England Biolabs (73 Knowl Piece, Wilbury Way, Hitchin, Herts, SG4 0TY, UK), except for the following:

Acrylamide/bis acrylamide 37.5:1 30% (w/v) stock solution was purchased from Severn Biotech Ltd (Unit 2, Park Lane, Kidderminster, DY11 6TJ, UK), DTT, ampicillin and IPTG were obtained from Melford Laboratories (Bildeston Rd, Chelsworth, Ipswich IP7 7LE, UK) and dimethyl suberimidate was acquired from Perbio Science (Unit 9, North Nelson Industrial Estate, Cramlington, Northumberland, NE23 1WA, UK). Complete protease inhibitor tablets were bought from Roche Biochemicals (Lewes, UK). Agarose (electrophoresis grade) was procured from BioGene Ltd (Kimbolton, UK). Crystallisation screens were purchased from Hampton Research (Laguna Niguel, CA, USA), Emerald Biostructures (7869 NE Day Road Bainbridge Island, WA 98110 USA) and Molecular Dimensions (61-63 Dudley St, Luton, LU2 0NP, UK).

Deionised water was purified using a Milli-Q academic purification system (Millipore Ltd, Herts, UK) by reverse osmosis and microfiltration to produce ultra-pure water. This water was used to prepare all aqueous solutions where deuterium oxide was not used.

2.1.2 Chromatography

Chromatographic columns were obtained pre-packed or they were packed 'in-house'. Ion exchange chromatography was performed using CM-sepharose packed in a XK 26 column (Amersham Biosciences, Amersham Place, Little Chalfont, Buckinghamshire, HP7 9NA). Gel filtration chromatography was conducted using a Superdex 200 XK16/60 column or a Superose 6 HR 10/30 column (Amersham Biosciences, Amersham Place, Little Chalfont, Buckinghamshire, HP7 9NA, UK). Nickel affinity chromatography was carried out using either Ni-NTA superflow (Qiagen Ltd. Qiagen House, Fleming Way, Crawley, West Sussex, RH10 9NQ, UK) packed in a XK50 column or a 1 mL HisTrap HP column (Amersham Biosciences, Amersham Place, Little Chalfont, Buckinghamshire, HP7 9NA, UK).

2.1.3 Bacterial strains and growth media

The *Escherichia coli* strain XL1-Blue (Stratagene, 11011 N. Torrey Pines Road La Jolla, CA 92037, USA) was used for propagation and production of plasmid DNA. For protein expression, the strain C41 (DE3) (Miroux and Walker, 1996) was used. It is a derivative of BL21 (DE3) selected for high level expression of globular and membrane proteins.

Agar plates were made with TYE medium [tryptone 0.16% (w/v), yeast extract 0.1% (w/v) and NaCl 0.5% (w/v) pH 7.4] supplemented with 1.5% (w/v) Bacto agar and the appropriate antibiotic. The liquid growth medium contained 2xTY [tryptone 0.16% (w/v), yeast extract 0.1% (w/v) and NaCl 0.5% (w/v) pH 7.4].

2.1.4 *Saccharomyces cerevisiae* strains and growth medium

S. cerevisiae strain DMV301ATP2HIS, a variant of strain W303-1A lacking the β -subunit of the ATP synthase, but bearing the plasmid pRSATP2HIS expressing the β -subunit with an N-terminal hexa-histidine tag (his tag) (Mueller *et al.*, 2004), was a gift from Prof. D. Mueller, The Department of Biochemistry and Molecular Biology, Rosalind Franklin University of Medicine & Science, 3333 Green Bay Road, North Chicago, IL 60064, U. S. A.

Yeast was grown in YPEG medium which consists of 1% (w/v) yeast extract, 2% (w/v) peptone, 3% (w/v) glycerol, 2% (v/v) ethanol and 1.5% (v/v) antifoam 204.

2.1.5 Synthetic oligonucleotides

Oligonucleotide primers were made by Sigma-Genosys (London Road, Pampisford, Cambridgeshire, CB2 4EF, UK). They were desalted before use.

2.2 Biochemical Methods

2.2.1 Agarose gel electrophoresis

Agarose gels were prepared in TBE buffer (90 mM Tris-boric acid pH 8.3 and 1 mM EDTA) containing 1% (w/v) agarose. They were cast as slabs. Ethidium bromide (1 μ g/mL) was added to both the gel and the running buffer to allow visualisation of DNA under UV light. Samples were mixed with a one-quarter volume of sample buffer [50% (w/v) sucrose, 0.3% (w/v) bromophenol blue and 0.3% (w/v) xylene cyanol FF in TBE] and then loaded into the wells. Electrophoresis was performed in TBE buffer at a constant current of 100 mA until the dye front had reached the end of the gel.

2.2.2 SDS-PAGE

SDS-PAGE was used to analyse the protein content of samples. They were run according to the conditions of Laemmli (Laemmli, 1970). Mini-gels (10 cm x 10 cm) were prepared with a 12 to 22% (w/v) acrylamide gradient separating gel and a 4% (w/v) stacking gel. The separating gel was prepared in Anderson's buffer [375 mM Tris-HCl pH 8.8, 0.1% (w/v) SDS] and the stacking gel was prepared in stacking buffer [125 mM Tris-HCl pH 6.8 and 0.1% (w/v) SDS]. Gels were run in a protein gel electrophoresis unit (Cambridge Electrophoresis Ltd, Cambridge, UK). The running buffer contained 0.25 M glycine, 25 mM Tris-HCl pH 6.8, 10% (w/v) SDS. It was poured into top and bottom reservoirs. Samples were mixed with 3 μ L loading buffer [0.3 M Tris-HCl pH 6.8, 10% (w/v) SDS, 25% (v/v) glycerol, 5 mM β -mercaptoethanol and 0.015% (w/v) bromophenol blue] and loaded into wells. Electrophoresis was performed at a constant current of 42 mA until the dye front had reached the end of the gel.

Proteins were visualised by soaking gels in staining solution [50% (v/v) methanol, 7% (v/v) acetic acid and 0.2% coomassie blue] for 15 min and by then transferring them to destaining solution [20% (v/v) methanol and 7% (v/v) acetic acid]. If samples contained low concentrations of protein, gels were silver stained according to the following protocol (Ansoerge, 1985):

Gels were soaked for 5 min in each of the following solutions: 50% methanol (v/v), 12% TCA (w/v) and 2% CuCl_2 (w/v); 10% ethanol (v/v), 5% (v/v) acetic acid; 0.01% (w/v) KMnO_4 ; 10% ethanol (v/v), 5% (v/v) acetic acid; 10% (v/v) ethanol; water; 0.1% (w/v) AgNO_3 . Then they were soaked in developing solution [2% (w/v) K_2CO_3 and 0.04% (v/v) formaldehyde] until protein bands appeared. Once bands were clearly visible, the reaction was stopped by placing the gels in water.

2.2.3 Western Blotting

2.2.3.1 Protein transfer

After SDS-PAGE unstained gels were placed in transfer buffer [10 mM NaHCO₃, 3 mM Na₂CO₃ and 0.05 (w/v) SDS]. PVDF membranes (Immobilon P, Millipore, Watford, UK) were placed in methanol then wetted in transfer buffer. Six pieces of blotting paper, soaked in transfer buffer, were placed on the anode of a BioRad Trans-blot semi-dry transfer cell (BioRad Laboratories, Hercules, CA, 94547, USA). The PVDF membrane was placed on top of the blotting paper and the gel on top of the membrane. Then the gel was covered with four pieces of blotting paper and the cathode placed over the sandwich. The transfer of proteins was carried out at 10 V for 30 min.

2.2.3.2 Immuno-detection of proteins

After transfer of proteins, the membrane was incubated in blocking buffer [4.3 mM Na₂HPO₄, 1.4 mM KH₂PO₄, 137 mM NaCl, 2.7 mM KCl, 5% (w/v) BSA and 1% (w/v) Marvel milk powder] for 1 hr at room temperature. Then membranes were incubated in blocking buffer containing the appropriate primary antibody at a dilution of 1/10,000 for 2 hr at room temperature. Membranes were washed extensively in blocking buffer before incubation with the secondary antibody (goat anti-chicken or rabbit IgG-alkaline phosphatase conjugate, at a dilution of 1/1000, in blocking buffer for 1 hr at room temperature. Then the membrane was exhaustively washed in PBS (4.3 mM Na₂HPO₄, 1.4 mM KH₂PO₄, 137 mM NaCl and 2.7 mM KCl) and proteins were detected using the ECL GST Western Blotting Detection Kit (Amersham Biosciences).

2.2.4 Measurement of protein concentration

Protein concentrations were determined by the bicinchoninic acid (BCA) assay (Smith *et al.*, 1985) the reagents were purchased from PerBio Science (Unit 9, North Nelson Industrial Estate, Cramlington, Northumberland, NE23 1WA, UK). When sample conditions were incompatible with the BCA assay the Bradford assay (Bradford, 1976) was used, reagents were purchased from BioRad Laboratories (BioRad Laboratories, Hercules, CA, 94547, USA). Assays were performed according to the manufacturers' instructions.

2.2.5 Preparation of competent cells

2.2.5.1 Electro-competent cells

A single colony of XL1-Blue cells (Stratagene, 11011 N. Torrey Pines Road La Jolla, CA 92037) was picked and used to inoculate 1 L of 2xTY broth. The culture was incubated at 37°C until the optical density at 600 nm (OD_{600}) had reached 0.5, then the culture was placed on ice for 30 min. Cells were harvested by centrifugation (10,000 g, 10 min) and resuspended in 1 L of sterile water at 4°C. Then cells were re-centrifuged and resuspended in 500 mL of sterile water at 4°C. The cells were centrifuged once more and then resuspended in 40 mL of 10% (v/v) glycerol. The suspension was centrifuged at 8,000 g for 10 min and resuspended in 6 mL 10% (v/v) glycerol. Then resuspended cells were divided into 100 μ L portions and stored at -80°C until required.

2.2.5.2 Chemically competent cells

A single colony of *E. coli* C41 (DE3) cells was used to inoculate a 50 mL culture in 2xTY medium. The culture was placed in a shaker incubator at 37°C until the OD_{600} had reached 0.4. Cells were harvested immediately by centrifugation (10,000 g, 5 min) and

resuspended in 20 mL of a sterile solution of 0.1 M calcium chloride at 4°C. The cells were kept at 4°C and then centrifuged as before. They were resuspended in 4 mL of 0.1 M calcium chloride and the suspension was stored at 4°C. They remained competent for 10 days.

2.2.6 Transformation of bacteria

2.2.6.1 Electroporation

Electro-competent cells (80 µL) were added to 10 µL of ligation reaction product and transferred to an electroporation cuvette with an electrode gap of 2 mm at 4°C. Electroporation was performed with a Gene Pulser (BioRad Laboratories, Hercules, CA, 94547, USA). The pulse was set to 2.5 kV, the resistance to 200 Ω and the capacitance to 25 µF with a pulse time of 4.6 msec. Then the cells were added to 100 µL of 2xTY buffer and incubated at 37 °C for 1 hour to allow the cells to recover. The cells were plated onto TYE plates and incubated overnight at 37°C.

2.2.6.2 Heat shock transformation

A 50 µL portion of chemically competent cells was added to 1 µL of plasmid DNA and the mixture was kept on ice for 30 min. The cells were first heat shocked for 2 min at 42°C to allow uptake of DNA and then kept on ice for a further 2 min. Then the cells were added to 50 µL of 2xTY medium and incubated at 37°C in a shaker incubator for 30 min to allow cells to recover. The cells were spread onto a TYE plate, containing ampicillin (100 µg/mL) to select for successful transformants, and incubated at 37°C overnight.

2.2.7 Calibration of gel filtration columns

A Superose 6 HR 10/30 column (Amersham Biosciences, Amersham Place, Little Chalfont, Buckinghamshire, HP7 9NA) was calibrated with the following proteins: thyroglobulin (669 kDa), ferritin (440 kDa), catalase (232 kDa) and aldolase (158 kDa). The void volume was measured with blue dextran 2000. The K_{av} of each protein was calculated from Equation 2.1:

$$K_{av} = (V_e - V_0) / (V_t - V_0) \quad (2.1)$$

Where V_e is the elution volume, V_t is the total bed volume and V_0 is the void volume. By plotting K_{av} against $\log(\text{molecular weight})$ a straight line with a correlation coefficient of 0.99 was obtained. The graph was used to estimate apparent molecular weights.

2.2.8 Activity assays

The ability of *S. cerevisiae* and bovine F_1 -ATPases to hydrolyse ATP was determined by an assay that couples ATP hydrolysis to oxidation of NADH (Pullman *et al.*, 1960). The rate of hydrolysis was measured from the decrease in absorption at 340 nm corresponding to decreasing NADH. ATP consumed by F_1 is regenerated by pyruvate kinase which transfers a phosphate group from phosphoenolpyruvate to ADP producing pyruvate. The pyruvate is reduced to lactate by lactate dehydrogenase, a reaction that reduces NADH to NAD^+ causing a decrease in absorption at 340 nm proportional to ATP hydrolysis.

Reactions were carried out in a solution containing 83mM sucrose, 33 mM Tris pH 8.0, 10 mM KHCO_3 , 12 mM MgCl_2 , 3 U pyruvate kinase and 3 U lactate dehydrogenase. ATP (5 mM), 5 mM phosphoenol pyruvate and 0.25 mM NADH were added before the assay. The reactions were carried out at 37 °C over 30 seconds.

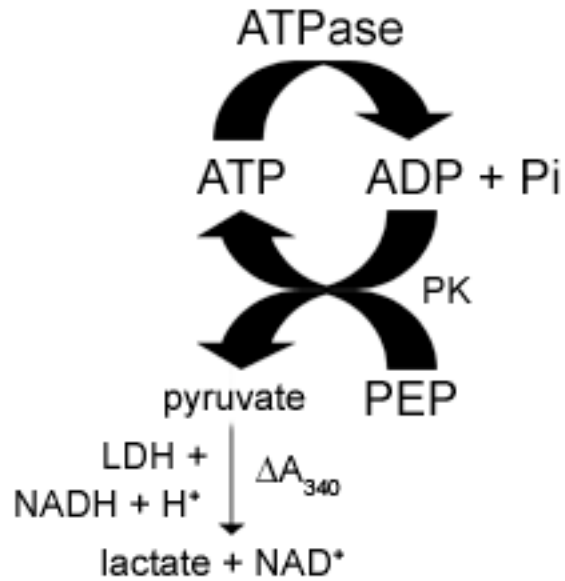


Fig. 2.1 The ATP regenerating assay system. The rate of hydrolysis of ATP is coupled directly to the reduction of NADH. The accompanying drop in the absorbance at 340 nm is proportional to the rate of ATP hydrolysis. Hydrolysed ATP is converted back to ATP by pyruvate kinase (PK) transferring a phosphate from phosphoenol pyruvate (PEP). The pyruvate produced in this reaction is reduced to lactate by lactate dehydrogenase (LDH), NADH is reduced to NAD⁺ during this reaction and the resulting drop in absorbance by 340 nm is used to estimate the rate of ATP hydrolysis (Pullman *et al.*, 1960).

2.2.9 Construction of expression plasmids bearing wild type and mutant IF₁

Construction of expression plasmids bearing the coding sequence for the mature (i.e. lacking presequence) inhibitor proteins IF₁ from *Bos taurus* and IF₁ and STF₁ from *Saccharomyces cerevisiae* has been described previously (Cabezón *et al.*, 2000a; Cabezón *et*

al., 2002; Cabezón *et al.*, 2000b; van Raaij *et al.*, 1996b). The plasmid expressing *S. cerevisiae* YIF₁ containing the mutation E21A was generated by PCR using the plasmid bearing the wild type sequence as template.

2.2.9.1 Polymerase chain reaction (PCR)

PCR reactions (Saiki *et al.*, 1985) were used to amplify DNA for cloning and to introduce specific mutations into genes. Oligomeric primers were designed to anneal in the 5' to 3' direction (forward primer) and in the 3' to 5' direction (reverse primer) of the gene of interest. They also contained a specific site for a restriction endonuclease. Alternatively they were annealed to an area within the gene but introduce a mutation (see Table 2.1). Primers were made by Sigma-Genosys (London Road, Pampisford, Cambridgeshire, CB2 4EF, UK). They were desalted before use. Lyophilized primers were diluted in 200 µL of water and a stock solution was made at 1 in 10 dilution, and stored at -20°C.

PCRs were performed in a Techne Touchgene thermal cycler (Techne, Duxford, Cambridge, CB2 4DZ, UK). The reaction mixture (100 µL) contained template DNA, 200 µM of each deoxyribonucleic acid triphosphate (dNTPs), 1 µM of each primer, DNA polymerase and 10x reaction buffer supplied with the polymerase. The choice of polymerase depended on the task required. For amplification of DNA fragments, where fidelity was important, the Expand high fidelity PCR system (Roche Biochemicals, Lewes, UK) was used. It contains a mixture of two thermostable polymerases: *Taq* polymerase from *Thermus aquaticus* and *Pwo* polymerase from *Pyrococcus woesei*. The latter has 3' to 5' exonuclease activity (proof-reading) and so introduces fewer mutations into DNA sequences. As this activity would also correct any mutations deliberately inserted on primers, only *Taq* polymerase was used in these cases.

Samples were heated initially to 90°C, without DNA polymerase, for 5 min to reduce any secondary structure within primers and template DNA. After the initial denaturing step, reaction mixes were subjected to the following cycle: 1 min at 94°C denaturing, 2 min at 55°C annealing and 2 min at 72 °C extension, for 30 cycles. After these cycles the reaction mixtures were maintained at 72°C for a final 7 min extension. Once the cycle had been completed, the mixtures were cooled to 4°C. The presence and correct size of reaction products was assessed by agarose gel electrophoresis. PCR products were purified to remove primers and enzymes using the QiaQuick nucleotide removal kit (Qiagen Ltd. Qiagen House, Fleming Way, Crawley, West Sussex, RH10 9NQ) and stored at –20°C until required.

Table 2.1 Oligonucleotide primers used to produce plasmids expressing mutants of the yeast inhibitor protein YIF₁. Codons that introduce mutations are underlined. Forward and reverse primers are indicated by F or R respectively.

Primer	Sequence
YIF1E21AF	TTT GTT AAA AGG <u>GCT</u> AGG GCC ACG
YIF1E21AR	GCT GGC CCT AGC <u>CCT</u> TTT AAC AAA
YIF1H39RF	GAA CAA CTA CGC <u>CGT</u> TTG AAA GAA CAA
YIF1H39RR	TTG TTC TTT CAA <u>ACG</u> GCG TAG TTG TTC

2.2.9.2 Restriction digestions

Restriction endonucleases were used to create ‘sticky’ ends that were compatible to those of an expression plasmid. Recognition sequences for the restriction endonucleases *HinD* III and *Nde* I were included in the primers for PCR. Reaction products were incubated for 1.3 hours at 37°C with both enzymes at the same time in Carlos buffer (33 mM Tris-

acetate pH 7.5, 66 mM potassium acetate, 10 mM magnesium acetate, 3 mM spermidine, 0.1 mg/mL BSA fraction V and 1 mM DTT). As the cutting efficiency of *Nde* I is greatly reduced after 20 min at 37°C, the enzyme was added in 4 portions every 20 min. After digestion, the reaction products were purified to remove the enzymes using the QiaQuick nucleotide removal kit (and stored at –20°C until required).

2.2.9.3 Vector preparation

The digested PCR fragments were ligated into an expression plasmid (pRun) with compatible ‘sticky ends’. The plasmid pRun is a construction, made by M. J. Runswick, derived from the pET series of vectors where expression is controlled by the T7 promoter (Studier and Moffatt, 1986). The T7 promoter allows high-level expression of recombinant proteins in *E. coli*. Ligation reactions were performed in 10 µL of ligase buffer [50 mM Tris-HCl pH 7.5, 5% (w/v) PEG 8000, 10 mM MgCl₂ and 1 mM DTT] with a five-fold excess of insert over plasmid and 16 units of T4 DNA ligase. The reactions were kept at room temperature for 2 hours.

2.2.9.4 Vector screening and preparation

The reaction mixtures were diluted to 100 µL with water and the DNA was precipitated by the addition of 260 µL of ethanol:3 M sodium acetate (25:1, v/v) and by cooling to –70°C for 30 min. Precipitated DNA was pelleted by centrifugation (7,500 g, 10 min), washed in 70% (v/v) ethanol and dried under vacuum. Dried DNA was resuspended in 10 µL water and used to transform XL1-Blue cells by electroporation (see Section 2.2.6.1).

Colonies from the transformation were screened by PCR for the presence of the inserted gene. Typically, 10 colonies were picked and added to a PCR reaction mix. The remainder of the colony was placed in 2 mL of 2xTY medium supplemented with ampicillin

(100 µg/mL) and grown at 37°C in a shaker incubator. The PCR reaction mixtures contained a forward primer specific to the T7 promoter region of pRUN (T7FOR) and a reverse primer complementary to the insert. Reactions were analysed by agarose gel electrophoresis (section 2.2.1). Those reactions that contained a product with the correct size of insert should come from colonies containing both the plasmid and insert. Cultures grown from positive clones were transferred to 10 mL of 2xTY broth supplemented with ampicillin (100 µg/mL) and grown overnight at 37°C in a shaker incubator. The cells were harvested by centrifugation (8000 g, 5 min) and the plasmid DNA was purified using the QiaPrep spin miniprep kit. Plasmid DNA was eluted in 100 µL of water and stored at –20°C until required.

2.2.9.5 DNA sequence analysis

Clones were sequenced by the MRC Geneservice (Babraham Bioincubator, Babraham, Cambridge, CB2 4AT) in order to verify the presence of correct DNA sequences.

2.2.10 Purification of inhibitor proteins

2.2.10.1 Overexpression

The bacterial expression of yeast inhibitor proteins and mutants was performed as described previously (Cabezón *et al.*, 2002).

Competent cells of *E. coli* C41 (DE3) were transformed with the appropriate plasmid and plated out onto TYE plates. Single colonies were picked and transferred to 2 L flasks containing 1 L of 2xTY broth supplemented with ampicillin (100 µg/mL). Flasks were incubated at 37°C in a shaker incubator. When the culture had reached an OD₆₀₀ of 0.6,

expression was induced by addition of 600 μ M IPTG. The culture was incubated at 25 °C overnight.

2.2.10.2 Purification of yeast IF₁

Cells were harvested by centrifugation (5,000 g, 10 min, 4 °C) and resuspended in 30 mL of TEP buffer [50 mM Tris-HCl pH 7.0, 1 mM EDTA, 0.001% (w/v) PMSF] containing a complete protease inhibitor tablet (Roche Biochemicals, Lewes, UK). The cells were passed through a French Pressure Cell (SLM Instruments, Urbana, IL, USA) three times to lyse the cells and to shear the DNA. Then samples were centrifuged (180,000 g, 2 hr, 4 °C) to remove cell debris. The supernatant was dialysed twice against 4 L of TEP buffer for 4 hours and applied to a column of CM-sepharose (XK 26) pre-equilibrated in TEP buffer. The column was washed with TEP buffer until the eluate absorption (monitored at 280 nm) was stable. A gradient of 0 to 1M NaCl was run over the column. The yeast inhibitor proteins eluted at 0.4 M NaCl. Fractions containing the inhibitor protein were identified by SDS-PAGE. They were pooled and concentrated to 10 mg/mL using a stirred cell (Millipore, Watford, U.K.). The concentrated protein was dialysed twice against 4 L TEP and stored at -20°C until required.

2.2.11 Purification of F₁-ATPase from *Saccharomyces cerevisiae*

2.2.11.1 Cell growth and purification of mitochondria from *S. cerevisiae*

S. cerevisiae strain DMV301ATP2HIS, was used for all experiments. A preculture of this strain (500 ml) was used to inoculate 30 L of YPG medium containing 3% (v/v) ethanol as an additional carbon source in a 40 L fermentor (FT Applikon, Gloucestershire, U.K.). Cells were grown for 48 h at 30 °C. They were harvested by centrifugation at 3000 g for 15

min and washed three times in chilled water. Cells were resuspended in breaking buffer [0.65 M sorbitol, 0.1 M Tris-HCl pH 8.0, 10 mM EDTA, 5 mM ϵ ACA, 5 mM PAB, 2% bovine serum albumin and 0.001% PMSF], (v/w), 2:1 and disrupted either in a cell disruptor (Constant Systems, Daventry, UK) or in a cooled bead beater (Biospec Products, Bartlesville, OK, USA). Cellular debris was removed by centrifugation at 2000 g for 15 min. Then the supernatant was centrifuged at 53000 g for 20 min. The mitochondrial pellets were washed in buffer WB [0.65 M sorbitol, 0.02 M Tris-HCl pH 7.5, 1 mM EDTA, 5 mM ϵ ACA, 5 mM PAB and 0.001% PMSF] by resuspension and centrifugation, and stored at -20°C . All steps were performed at 4°C .

2.2.11.2 Preparation of submitochondrial particles

Thawed mitochondria were suspended in SBE buffer (0.25 M sucrose, 8 mM NaH_2PO_4 , 42 mM Na_2HPO_4 pH 7.5, 1 mM EDTA, 5 mM ϵ ACA, 5 mM PAB) to a protein concentration of 10 mg/ml and sonicated (Misonix Inc., Farmingdale, NY, USA.) twice in 70 ml portions at power 6. Then the solution was centrifuged at 3000 g for 10 min to remove unbroken mitochondria. The supernatant was centrifuged for 1 hour at 160000 g to pellet the SMPs.

2.2.11.3 Purification of *S. cerevisiae* F_1 -ATPase

The pellets of SMPs were resuspended in SB buffer [0.25 M sucrose, 12 mM NaH_2PO_4 , 38 mM Na_2HPO_4 pH 7.3, 5 mM ϵ ACA, 5 mM PAB] at a protein concentration of 20 mg/ml and Tris-HCl buffered chloroform was added [0.5:1 (v/v)]. The mixture was shaken vigorously for 30 seconds to release F_1 -ATPase from the SMPs and then centrifuged for 5 min at 4500 g to break the emulsion. The supernatant was removed and centrifuged at 96000 g to remove residual chloroform. Methanol was added to the supernatant to 10% (v/v)

to prevent cold sensitivity of F_1 -ATPase and applied to a column of Ni-NTA superflow (Qiagen, Crawley, UK) at a flow rate 2 mL/min. Then the column was washed extensively with buffer A (10% methanol, 0.25 mM sucrose, 0.3 M NaCl, 50 mM Tris-HCl pH 7.5, 5 mM $MgCl_2$, 5 mM ϵ ACA, 5 mM PAB and 1mM ADP) supplemented with 15 mM imidazole. The protein was eluted from the column with buffer A containing 200 mM imidazole and concentrated immediately to approximately 10 mg/ml in a stirred cell (Millipore, Watford, U.K.). Then the protein was applied to a column of Superdex 200 (XK16/60) (Amersham Biosciences, Amersham, U.K.) pre-equilibrated in SDX buffer [10% methanol, 0.25 M sucrose, 0.2 M NaCl, 50 mM Tris-HCl pH 8.0, 1 mM EDTA, 5 mM $MgCl_2$ and 1 mM ADP]. Fractions containing pure F_1 -ATPase were identified by SDS-PAGE. They were pooled and the protein was precipitated with 70% saturated ammonium sulphate. All steps (except preparation of SMPs) were performed at 4°C.

2.2.12 Purification of bovine mitochondrial F_1 -ATPase

2.2.12.1 Purification of bovine heart mitochondria

Bovine hearts were collected from an abattoir (Dawn Cardington, Bedford, UK) and immediately packed in ice. Fat and connective tissue were removed from the hearts and diced. The meat was minced and suspended in 1 kg portions of 1.4 L buffer A (10 mM Tris-HCl pH 7.8, 0.25 M sucrose and 5 mM β -mercaptoethanol) and then filtered through muslin. The filtered minced meat was added to 1.6 L of buffer B [10 mM Tris-HCl pH 7.8, 0.25 M sucrose, 5 mM β -mercaptoethanol, 0.2 mM EDTA and 1 mM Tris-succinate pH 7.8], with 25 mL 2M Tris to maintain the pH at 7.8, and homogenised in a blender (Waring Products Division, New Hertford, CT, USA) for 30 sec. Cellular debris was pelleted by centrifugation at 2700 rpm for 15 min in a Sorvall RC12 centrifuge. The supernatant was decanted through a single layer of muslin and centrifuged at 11,000 rpm for 27 min in a Sorvall centrifuge.

The pellets were resuspended and combined in a total volume of 3.6 L of buffer B and centrifuged for 42 min at 11,000 rpm. The supernatant was discarded and the pellets were stored at -20°C. All steps were performed at 4°C.

2.2.12.2 Purification of bovine F₁-ATPase

Mitochondria from 2 hearts were thawed and resuspended in 210 mL of buffer A (20 mM Tris-HCl pH 7.5, 0.25 M sucrose, 1 mM DTT and 0.002% PMSF) using a Potter homogeniser. The sample was divided into three portions of 70 mL and sonicated (Misonix Inc., Farmingdale, NY, USA) for 3 x 40 sec at power 10 with rest periods of 2 min between sonicating. Unbroken mitochondria were removed by centrifugation for 10 min at 12,000 rpm in an SS34 rotor. SMPs were pelleted by centrifugation overnight in an SW28 rotor at 27,000 rpm.

Pelleted SMPs were resuspended to a total volume of 120 mL in buffer B (50 mM Tris-HCl pH 8.0, 0.25 M sucrose, 1 mM DTT, 4 mM EDTA, 2 mM ADP, 0.002% PMSF and 10 µM amastatin), at room temperature, using a Potter homogeniser. The solution was added to 60 mL of chloroform saturated with 1 M Tris-HCl pH 8.2 and shaken vigorously for 20 sec. The emulsion was broken by centrifugation at 4000 rpm in a benchtop centrifuge (Biofuge Primo, Heraeus Instruments Ltd.) for 5 min. The supernatant was centrifuged at 27,000 rpm in an SW28 rotor for 30 min to remove F₁-ATPase depleted SMPs and any remaining chloroform. The supernatant was removed and nitrogen blown over the surface for 15 min to ensure that no chloroform remained. The supernatant was concentrated to 4-7 mL in an Amicon Ultra-Filtration cell using a XM300 membrane (Millipore), filtered (0.22 µM) and applied to an XK26/60 Superdex 200 gel filtration column (Amersham Biosciences, Amersham Place, Little Chalfont, Buckinghamshire, HP7 9NA) pre-equilibrated in F₁-column buffer (20 mM Tris-HCl pH 8.5, 200 mM NaCl, 1 mM DTT, 4 mM EDTA, 1

mM ADP, 0.002% PMSF and 0.02% NaN₃). The eluate was monitored from its absorption at 280 nm, and the fractions containing F₁-ATPase were identified by SDS-PAGE. The purest fractions were pooled and loaded onto a Matrix Gel Blue A column pre-equilibrated in F₁-column buffer. Fractions of 4 mL were collected by gravity flow. F₁-ATPase does not bind to this column, whereas creatine kinase and any endogenous inhibitor protein IF₁ bound to F₁-ATPase are removed. Fractions containing F₁-ATPase were identified by the Bradford assay and the purity of the enzyme analysed by SDS-PAGE. The purest fractions were pooled and precipitated with 50% saturated ammonium sulphate and stored at 4°C.

2.2.13 Inhibition of F₁-ATPases by inhibitor proteins

Assay of the inhibition of the ATPase activity of bovine and *S. cerevisiae* F₁-ATPase by YIF₁, STF₁ and mutants was performed as described previously (Cabezón *et al.*, 2002; Cabezón *et al.*, 2000b). The activities of YIF₁ and YIF₁-E21A were assayed at various pH values with purified yeast F₁-ATPase. YIF₁ or YIF₁-E21A (1 µg) were mixed with 12 µg F₁-ATPase in a volume of 100 µl in 10 mM 4-morpholinepropanesulphonic acid for pH 6.1-7.1, 10 mM Tris-HCl for pH 7.4-8.0 and 10 mM 3-[1,1-dimethyl-2-hydroxyethylamino]-2-hydroxypropanesulfonic acid for pH 9.1. Then the samples were incubated at 37°C for 5 min with 1 mM MgATP. ATPase activity was measured by transferring 10 µl of the mixture to 1 ml of ATPase assay mixture at 37°C and measuring the decrease in absorbance of NADH at 340 nm for 5 min. Control activities were measured using yeast F₁-ATPase, incubated at 37°C for 5 min at each pH value, in the absence of any inhibitor.

2.2.14 Analysis of the oligomeric state of *S. cerevisiae* IF₁

2.2.14.1 Gel filtration chromatography

Precipitated yeast F₁-ATPase was redissolved in minimal buffer (50 mM 4-morpholinepropanesulphonic acid, pH 6.6, 1 mM EDTA, 10 % (v/v) glycerol and 0.001% PMSF) and desalted on a Micro Bio-Spin 6 column (BioRad Laboratories, Hercules, CA, 94547, U. S. A.). The enzyme was mixed with a seven-fold molar excess of inhibitor protein, and incubated at 37°C for 20 min with 1 mM MgATP. Samples were applied to a Superose 6 HR 10/30 column (Amersham Biosciences) pre-equilibrated in minimal buffer, and run at a flow rate of 0.5 ml/min. The absorbance of the eluant was monitored at 280 nm

2.2.14.2 Covalent cross-linking

Cross-linking of primary amines in the inhibitor proteins with dimethyl suberimidate was performed at pH 9.1. Samples (0.5 mg/ml) were dialysed overnight in 100 mM 3-[1,1-dimethyl-2-hydroxyethylamino]-2-hydroxypropanesulphonic acid, pH 9.1. Dimethyl suberimidate was added to a final concentration of 1 mg/ml from a freshly prepared stock solution (20 mg/ml) and kept for 2 h at room temperature. Samples were removed at various times, and the reaction was quenched with Tris-HCl buffer, pH 8.0. The degree of cross-linking was assessed by SDS-PAGE.

2.2.14.3 Analytical ultracentrifugation

Sedimentation velocity measurements were made with a Beckman Optima XL-A analytical ultracentrifuge and an An60-Ti rotor, using double-sector cells with a 12 mm pathlength. Samples were prepared as described in Section 2.2.14.1, but in a different buffer (10 mM 4-morpholinepropanesulfonic acid, pH 6.6, 100 mM NaCl and 1 mM MgATP) and

incubated for 20 min with a seven fold molar excess of YIF_1 . After inhibition, the sample was diluted with the same buffer, but lacking MgATP, to a protein concentration of 1.5 mg/ml and a MgATP concentration of 0.1 mM to lower the background absorbance at 280 nm. The enzyme remained inhibited after dilution and throughout the course of the experiment. Measurements were made at 32,500 rpm and 20.0 °C, scanning at 280 nm and with a 0 min interval (i.e. to give repetitive scans as quickly as possible). Adjacent sets of scans (up to 12, but fewer when band broadening would not permit this many for the molecular mass of a monomer) were analysed using the programme DcDt+ version 1.16 (Philo, 2000) and taking the partial specific volume as 0.73 ml/g and the solvent density as 1.005 g/ml. The molecular mass of the complex was calculated taking values of 0.7418 ml/g for the partial specific volume, 1.00265 g/ml for the solvent density and 1.0137 (cpoise) for the viscosity, calculated with SENTERP (Laue, 1992). This programme was also used to fit the dc/dt data for each set of scans, optimising the initial concentration, the sedimentation coefficient and the molecular mass, using a model with only a single component. Plots of the residuals from the fitting, and the standard deviations for the fitted parameters, showed that this model fitted the data well. Therefore, no attempt was made to fit a model with two, or more, components.

2.2.15 Inhibition of bovine F_1 -ATPase with ADP and magnesium fluoride

Precipitated bovine F_1 -ATPase was redissolved in MgF buffer (200 mM Tris-DCl pH 7.2, 400 mM NaCl, 1 mM ADP and 0.04% (w/v) NaN_3 in D_2O) and desalted on a Micro Bio-Spin 6 column (BioRad Laboratories, Hercules, CA, 94547, U. S. A.). Then the protein was incubated for 20 min with 10 mM $MgCl_2$. After this incubation 10 mM NH_4F was added and the protein was kept at room temperature until inhibition was complete (typically 2 hrs). The

enzyme inhibited in this way was immediately used in crystallisation experiments described below in Section 2.2.16.

2.2.16 Protein Crystallisation

Three-dimensional protein crystals are grown by forming a super-saturated solution and causing precipitation sufficiently slowly, and in such a manner, that ordered arrays of the protein are formed. Reagents, such as salts or polyethylene glycols (PEGs), that ‘compete’ for the water in the protein solution, bring the protein out of solution. Changing the pH of the solution, the length of equilibration or changing the temperature can alter the way the protein molecules interact with each other leading to crystallisation.

2.2.16.1 Crystallisation of bovine F₁-ATPase inhibited with ADP and magnesium fluoride

The crystallisation of bovine F₁-ATPase inhibited with magnesium fluoride was carried out as in (Lutter *et al.*, 1993) but with several modifications. Purified F₁-ATPase was desalted and inhibited as described in Section 2.2.15 and the concentration of the protein was adjusted to 10 mg/mL. An equal volume of inside buffer [100 mM Tris-DCI pH 7.2, 400 mM NaCl, 10 mM MgCl₂, 0.05 mM ADP, 0.04% (w/v) NaN₃, 0.004% (w/v) PMSF and 14% (w/v) PEG 6000 in D₂O] was added slowly to the protein and the solution mixed gently. Then the sample was centrifuged (33,000 g, 10 min) to remove any particulate matter. Microdialysis buttons (50 µL, Cambridge Repetition Engineers, Cambridge, UK) were filled with 55 µL protein solution and covered with dialysis membrane (SpecraPor, 3,500 molecular weight cut-off, Spectrum Medical Industries, Houston, TX, USA), taking care to exclude bubbles, and sealed with a rubber O-ring. The button was placed in a vial and dialysed against 3 mL of outside buffer [50 mM Tris-DCI pH 8.2, 200 mM NaCl, 10 mM

MgCl₂, 10 mM NH₄F, 0.05 mM ADP, 0.02% (w/v) NaN₃, 0.004% (w/v) PMSF and 9% (w/v) PEG 6000]. After 48 hr, this buffer was removed and replaced with the same buffer containing concentrations of PEG 6000 from 10 to 14% (w/v) in 0.25% steps. Crystals appeared after 1 week and were fully grown after 6 weeks.

2.2.16.2 Harvesting and cryoprotection

In order to assess the diffraction quality of crystals, they must be removed from the mother liquor and mounted in an X-ray beam. Protein crystals are extremely sensitive to damage by X-radiation caused by free radicals which can seriously compromise the quality of the data collected. Cooling the crystals to 100 K dramatically reduces the damage to the crystals by preventing the chain reaction of radical damage (Garman, 1999). However, cooling crystals to these temperatures can also cause damage to the crystals by the formation of ordered ice disrupting the order of the crystals and itself diffracting X-rays, thereby compromising data collection. This latter damage can be prevented in two ways. First, the crystal must be frozen extremely quickly to reduce the time available for ordered ice to form. Second, the crystal can be transferred to a mother liquor solution containing a known cryoprotectant (Garman and Schneider, 1997). The cryoprotection agent changes the freezing point and kinetics of the mother liquor allowing sufficient time for the formation of vitrified water (an amorphous state without ice crystals). Cryoprotection has several advantages: The crystal is mounted in a thin film held by surface tension in a loop. This technique (Teng, 1990) involves less handling of the crystal, and therefore less mechanical damage; cryocooled crystals can be stored for long periods, and as there is less radiation damage, usually a complete data set can be taken from a single crystal increasing the quality of the data. Cryocooling of crystals can increase the mosaic spread; however, careful selection of cryoprotectant and cryoprotection protocol can minimise this effect.

As crystals of bovine F₁-ATPase are grown in microdialysis buttons, the transfer of crystals to a cryoprotection buffer is relatively simple and avoids extensive handling of the crystals. The outside buffer was removed from the vial and replaced with buffer containing 5% (v/v) glycerol and a PEG 6000 concentration of 15% (w/v). The solution was left for 15 min and then replaced with a solution containing 10% (v/v) glycerol. The concentration of glycerol was increased to 20% in 5% steps with 15 min at each concentration. At the end of the final soak, the dialysis membrane was removed from the button with a razor blade. Crystals were harvested using a mounted cryo-loop (Hampton Research, Laguna Niguel, CA, USA) of appropriate size and immediately plunged into liquid nitrogen. The cryo-loop was transferred to a vial, placed in a cryo-cane and stored at 100 K until required.

2.2.17 X-ray crystallography analysis

2.2.17.1 Crystal screening

The diffraction quality of the crystals was assessed using CuK_α radiation from a laboratory X-ray source (RuH3R rotating anode generator, Rigaku MSC, The Woodlands, TX USA) and a MAR345 image plate detector (Mar Research, Hans-Böckler-Ring, 1722851, Norderstedt, Germany) at a crystal to detector distance of 300 mm (resolution limit 3 Å). Crystals were mounted in cryo-loops, using cryotongs, and maintained at 100 K by a stream of dry nitrogen gas at 100 K from a cryo-stream (Oxford Cryosystems Ltd, 3 Blenheim Office Park, Lower Road, Long Hanborough, Oxford OX29 8LN). Two diffraction images (oscillation angle 0.5°) were taken at ϕ 0° and 90° with an exposure time of 10 min, and the quality of the diffraction inspected visually. Crystals that diffracted to between 3–4 Å and had low mosaic spread were recovered and stored for data collection at a synchrotron radiation source.

2.2.17.2 Data Collection

Crystals showing good quality diffraction patterns were taken to the European Synchrotron Radiation Facility (ESRF, 6 Rue Jules Horowitz, Grenoble, France) beamline ID29 for data collection. The quality of the diffraction was assessed in the same manner as Section 2.2.17.1 with careful inspection for split spots and the resolution limit and a decision made on whether to take a data set. Diffraction data were collected on an ADSC Q210 2D CCD detector (Area Detector Systems Corporation, 12550 Stowe Drive, Poway, California 92064, USA) at a crystal to detector distance of 245 mm. Initial diffraction images were inspected with MOSFLM (Leslie, 1992) and the crystal orientation, probable space group and unit cell parameters were determined by the autoindexing function. MOSFLM produces a list of possible space groups and unit cell parameters; generally, the option with the lowest penalty and highest symmetry space group is correct. The accuracy of the choice of unit cell is verified by MOSFLM placing boxes where spots are predicted from the selected space group: If the boxes overlay all observed reflections, the unit cell is correct. Once the orientation of the crystal was determined, the strategy function was used to calculate the starting angle and minimum ϕ range needed to collect a complete data set; for the orthorhombic space group this was 60° .

2.2.17.3 Data processing

Once a complete data set had been collected, the unit cell parameters were refined. The initial measurements from autoindexing were calculated from the position of the spots; the cell is refined accurately by measuring observed reflections. Two wedges of data (typically 2 degrees) at a large distance apart in ϕ were used for the measurement using the refine cell function in MOSFLM. After refinement the data were integrated. MOSFLM

places a rectangle over the predicted spot position and measures the peak intensity and background within the rectangle. This was performed for the entire data set and the intensities written out to an 'mtz' file.

Once the data had been integrated they were scaled and merged. The intensities recorded will vary over time and place due to a number of factors: The intensity of the beam may change over time and differences in the size of the crystal will affect measured intensities and radiation damage to the crystal will also influence the scale of the data. The program SCALA (Evans, 1997) compares symmetry related reflections and models the scale factor to achieve a data set with overall consistency of intensities. This step in data processing provides the best measure of the quality of the data. The integrated and scaled data were then merged to form a single mtz containing the intensities for a complete data set.

The scaled and merged intensities were converted to amplitudes by TRUNCATE (French and Wilson, 1978). The intensity of reflections is directly proportional to the square of the amplitude of the incident X-rays. Therefore, the amplitude is the square root of the intensity. However, by taking the square root of the intensity, the negative intensities are set to zero and the contribution from weak reflections is underestimated. TRUNCATE calculates amplitudes by comparing intensities and their standard deviations and the intensities to the resolution shell. This gives better estimates of the data as negative intensities become positive. TRUNCATE outputs an mtz file containing the observed amplitudes and a Wilson B factor, reflecting how the intensities fall off with resolution. At this stage a random 5% of the data were 'flagged' to be used in the Free R-factor calculation (see appendix A: Crystallographic Theory) using the program FreeRFlag.

2.2.17.4 Molecular replacement

The structure factor amplitudes contain half the structural information, but the phases are also required to calculate an electron density map. The phases can be estimated by several techniques (see Appendix A: Crystallographic Theory). In the case of F₁-ATPase, the overall architecture of the protein is well known so the phases can be estimated from the structural model; this procedure is referred to as molecular replacement (Rossmann and Blow, 1962). Molecular replacement was performed using the program AMoRe [Automated Molecular Replacement (Navaza, 1994)] using the beryllium fluoride inhibited structure [PDB accession code 1WOJ (Kagawa *et al.*, 2004)], with the beryllium fluoride and waters removed, as a search model. There are several programs that run within AMoRe. The first is SORTING, which reads in the amplitudes from the mtz file and converts them to an AMoRe format. In the next step, TABLING, calculates the amplitudes from the search model by performing a Fourier transform on the electron density predicted from the atomic coordinates. Then data are compared to the observed amplitudes of the new structure.

The first stage of molecular replacement is the rotation search performed by ROTING. This program compares the Patterson maps [the Fourier transform of the intensities (see Appendix A: Crystallographic Theory)] from the model and new structure; peaks within the Patterson maps from intramolecular vectors only depend on the orientation of the structure in the unit cell. Therefore, peaks for approximately $2/3$ of the volume of the molecule are looked at and matching the peaks from the Patterson maps will find the orientation of the new structure within the unit cell. ROTING produces a list of the possible Euler (rotation) angles listed in order of peak height; generally, the first option is correct, but all solutions (above a threshold) are used in the translation search.

Once the orientation of the structure has been found, its position within the unit cell can be calculated. This calculation is performed by TRAINING. This search looks at the

intermolecular vector peaks that are in the Patterson map. The intramolecular peaks found in ROTING are subtracted from the Patterson and only these peaks are matched. These peaks arise from any pair of atoms in different molecules related by crystal symmetry. This places the molecule within the unit cell. Then AMoRe compares calculated structure factors from various orientations of the model to the observed data, and for each solution calculates the correlation coefficient between the data and the R-factor (the measure of agreement between observed structure factors and those calculated from the model: see Appendix A: Crystallographic Theory). The solution with the highest correlation coefficient and the lowest R-factor is generally the correct one.

The chosen rotation and translation parameters are refined by rigid body refinement performed by FITING. This procedure will indicate if the solution choices were correct, as the R-factor should decrease and the correlation coefficient increase if the solutions are correct. The final output from AMoRe is a coordinate file which can be refined against the observed data.

2.2.17.5 Model refinement

2.2.17.5.1 Refinement using REFMAC5

The model produced by AMoRE was refined against the observed data using the program REFMAC (Murshudov *et al.*, 1997). This program refines the data using maximum likelihood methods and contains a dictionary of bond angles, lengths and other restraints for polypeptides and ligands to maintain correct stereochemistry within the model during refinement. The matrix weighting term (the weight given to the observed data against the stereochemistry of the model) was varied. The value that gave the lowest Free R-factor and best stereochemistry was chosen. The quality of the refinement was assessed by the values of the Free R-factor and RMS deviations in bond angle and chirality.

2.2.17.5.2 Manual rebuilding

After the first round of refinement with REFMAC, electron density and difference maps (showing densities for regions that are either missing or misplaced in the model) were calculated from the Fourier transform of observed amplitudes and phases calculated from the refined model using the program FFT. Then the maps and model were read into the program 'O' (Jones *et al.*, 1991) a molecular modelling program. 'O' allows the maps and model to be displayed in three-dimensions and the rebuilding of the model to match the observed electron density. The maps were inspected initially for their quality and for novel features. The first stage of manual rebuilding was to search for the highest density peaks (either positive or negative). This procedure was performed using PEAKMAX, a program that searches for peaks above a certain value and ranks them in order of height and writes out their coordinates. Then the peaks are displayed in 'O' and interpreted. The largest features in the difference maps were due to side-chains that had moved as a result of different lattice contacts in the crystal and ordered water molecules. Large novel features (for example the magnesium fluoride) were not included in the model until further refinement had been performed, so as not to bias the maps. Waters were inserted where the stereochemistry was correct. After manual rebuilding, the coordinates were written out and refined against the observed X-ray data in REFMAC. This process was repeated until the density peaks remaining could not be interpreted.

2.2.17.6 Structure validation

The final model was analysed for gross structural errors using the program PROCHECK (Laskowski *et al.*, 1992). The ϕ and ψ bond torsion angles of the α -carbon backbone of proteins adopt preferred combinations due to steric hindrance (Ramakrishnan and Ramachandran, 1965). PROCHECK analyses the model for the ϕ and ψ angles for any

deviation from the preferred conformations. A Ramachandran plot of the ϕ versus ψ angles is output that will show any residues that deviate from ideality (Ramachandran *et al.*, 1963).

2.2.17.7 Figure preparation

All images of the F_1 -ATPase models, electron density maps and other structures were produced using the molecular graphics program PyMOL (DeLano, 2002). The coordinates for solved structures, used to prepare figures, were downloaded from the Protein Data Bank [<http://pdb.ccdc.cam.ac.uk/pdb/>, (Berman *et al.*, 2000)].

CHAPTER 3: MECHANISM OF ACTION OF THE F-ATPase INHIBITOR PROTEIN IF₁ FROM *Saccharomyces cerevisiae*

3.1 Results

The ATP synthase in mitochondria of *Saccharomyces cerevisiae* is regulated by two inhibitory proteins YIF₁ and STF₁ and one, or possibly two, other proteins STF₂ and STF₃. The bovine inhibitor protein is active as a dimer at pH values below 7.0, as the pH increases above this value, tetramers and higher oligomers form that occlude the inhibitory regions. As the yeast proteins are considerably shorter than the bovine, their physical properties at various pH values were investigated. In this chapter the mechanism of activation and oligomeric states of the yeast inhibitory proteins are discussed and compared to the bovine inhibitor protein, IF₁, throughout.

3.1.1 Purification of recombinant inhibitor proteins

The inhibitor proteins from *Sacharomyces cerevisiae* YIF₁ and STF₁ and mutants of YIF₁ E21A and H39R were cloned and expressed in *E. coli* to high levels [typically 10-20 mg protein per litre culture (see Section 2.2.9)]. All of the proteins were expressed in the cytoplasm as soluble, folded protein. After overexpression and cell lysis the proteins were purified by ion exchange chromatography (see Section 2.2.10 and Figures 3.1, 3.2, 3.3 and 3.4). There was no difference in the chromatographic behaviour of YIF₁, STF₁ or YIF₁ mutants.

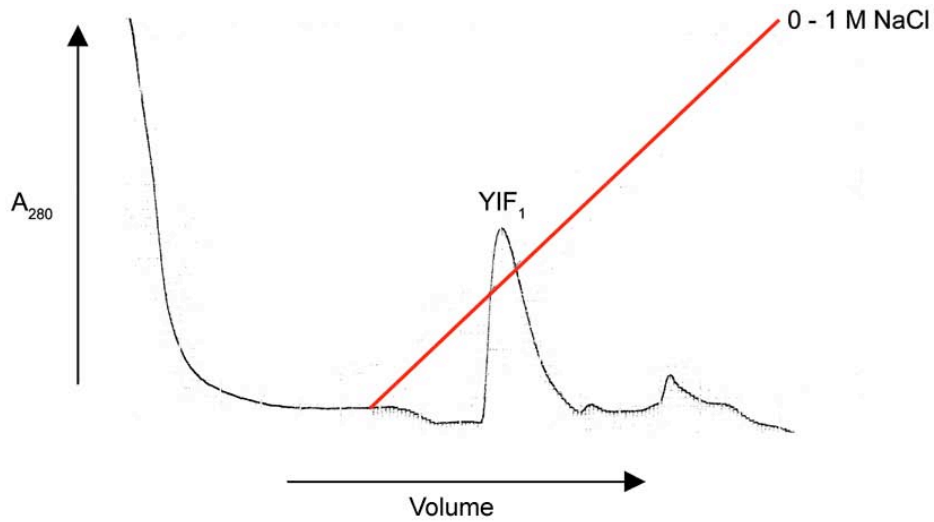


Figure 3.1 Purification of YIF_1 by ion exchange chromatography (CM-Sephacrose). The elution profile of the purification is shown. Cell lysate was loaded and the column washed until the baseline stabilised. A 0 to 1 M NaCl gradient (red line) was passed over the column to elute YIF_1 .

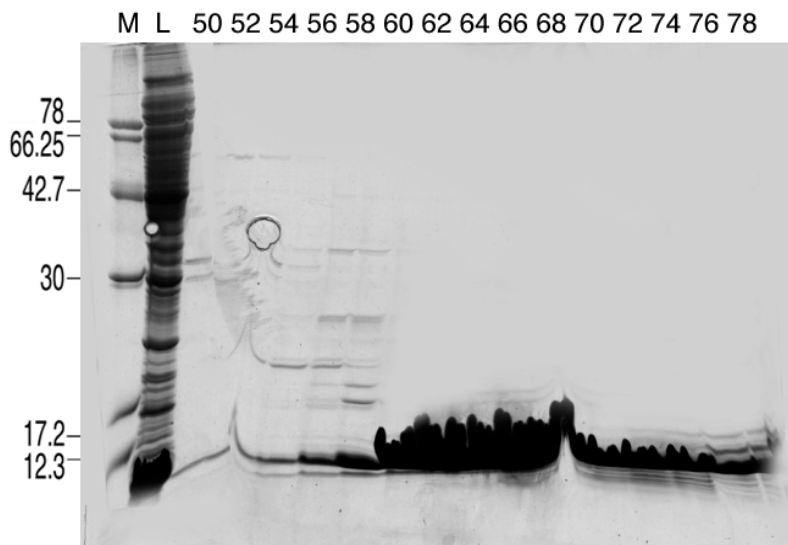


Figure 3.2 SDS-PAGE analysis of column fractions from ion-exchange chromatography. Fractions corresponding to the peak seen in Figure 3.1 were analysed. The protein was present at high levels and no further purification was required. The positions of molecular weights (M) are shown on the left hand side and L is the cell lysate loaded onto the column.

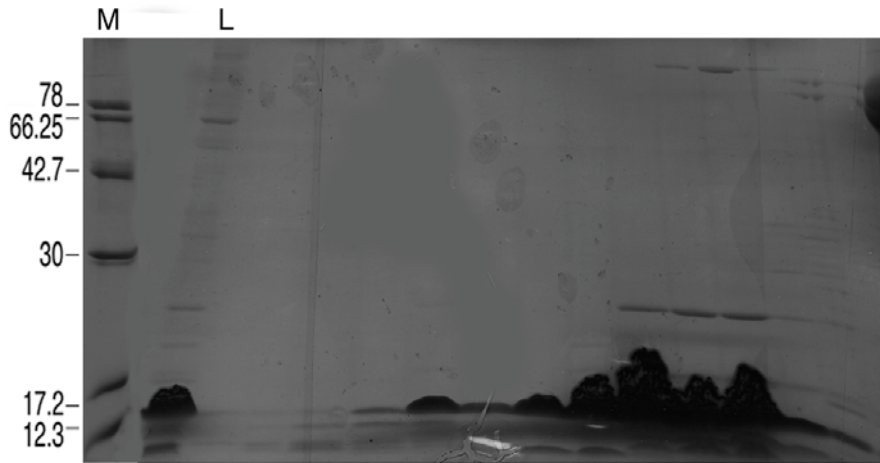


Figure 3.3 SDS-PAGE analysis of column fractions from ion-exchange chromatography of YIF₁-E21A. The protein was present at high levels and no further purification was required. The positions of molecular weights (M) are shown on the left hand side and L is the cell lysate loaded onto the column.

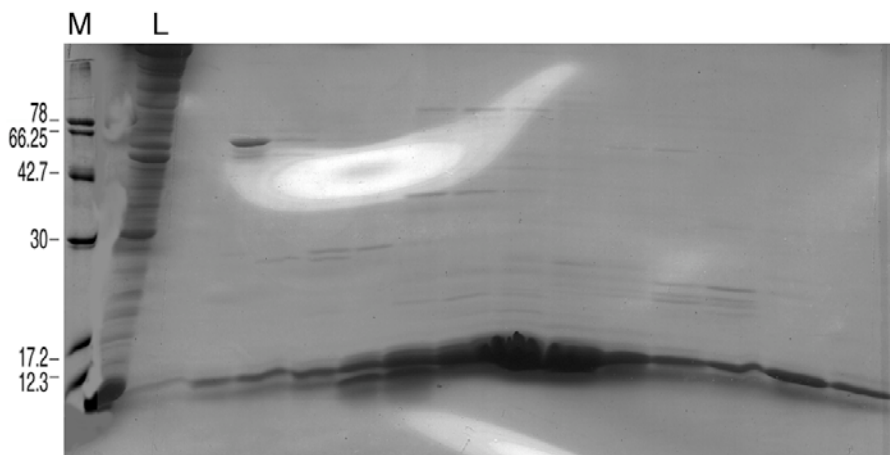


Figure 3.4 SDS-PAGE analysis of column fractions from ion-exchange chromatography of STF₁. The protein was present at high levels and no further purification was required. The positions of molecular weights (M) are shown on the left hand side and L is the cell lysate loaded onto the column.

3.1.2 Inhibitory activity of *S. cerevisiae* inhibitor proteins

The inhibitory potency of the recombinant proteins was measured by the degree to which they inhibited the activity of purified F₁-ATPase from *S. cerevisiae*. The ATP hydrolase activity of the F₁-ATPase was found to be inhibited by 94% by a seven fold molar excess of YIF₁ and by 96% by a twenty-seven fold molar excess of STF₁ (Figure 3.5). The IC₅₀ of the inhibitor proteins was estimated from the inhibition curves. The IC₅₀ was taken to be the concentration of inhibitor protein which inhibited 50% of the control ATPase activity. The values were found to be 1.3 for YIF₁ and 6.4 for STF₁. This correlates well to the differences in the dissociation constant (K_D) found in another study (Venard *et al.*, 2003). This established the activity and correct folding of the recombinant proteins.

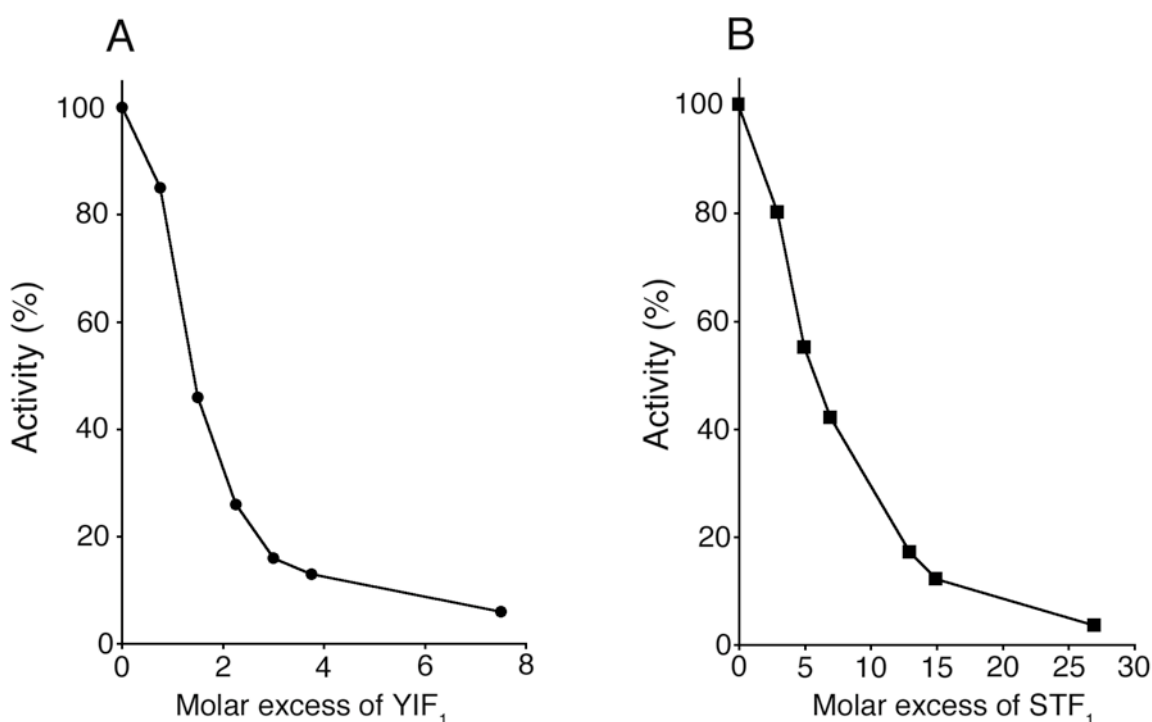


Figure 3.5 Inhibition of F₁-ATPase from *S. cerevisiae* by the YIF₁ and STF₁ inhibitor proteins. Parts (A) and (B), inhibition of the activity of F₁-ATPase by YIF₁ and STF₁, respectively.

Chapter 3: Mechanism of action of the F-ATPase inhibitor protein IF₁ from S. cerevisiae

The YIF₁ mutant E21A has been shown to be active at all pH values (Ichikawa *et al.*, 2001). This activity was investigated, at a range of pH values, for the mutant produced in this work. YIF₁ or YIF₁-E21A (1 µg) were mixed with 12 µg yeast F₁-ATPase in a volume of 100 µl in 10 mM 4-morpholinepropanesulfonic acid for pH 6.1-7.1, 10 mM Tris-HCl for pH 7.4-8.0 and 10 mM 3-[1,1-dimethyl-2-hydroxyethylamino]-2-hydroxypropanesulfonic acid for pH 9.1. The samples were then incubated at 37°C for 5 min with 1 mM MgATP. ATPase activity was measured by transferring 10 µl of the mixture to 1 ml ATPase assay mixture at 37°C and measuring the decrease in absorbance of NADH at 340 nm for 5 min. Control activities were measured using yeast F₁-ATPase, incubated at 37°C for 5 min at each pH value, in the absence of any inhibitor. The results show that the mutant E21A is fully active above pH 7.0 (Figure 3.6)

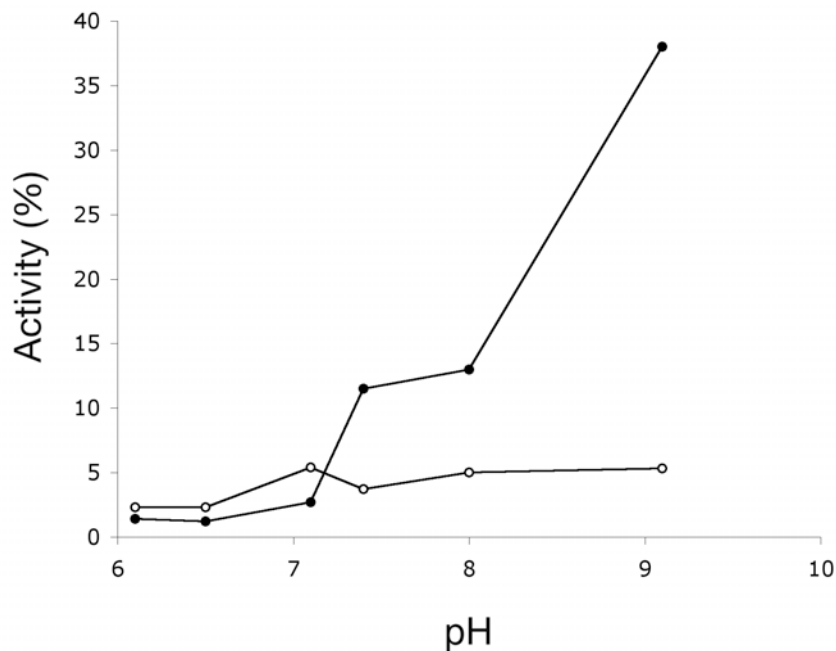


Figure 3.6 The effect of pH on the inhibitory activities of the YIF₁ and YIF₁-E21A proteins. The ATPase activity increases steeply above pH values of 7 for the wild type YIF₁ but remains below 6% for the mutant E21A. ●, YIF₁; ○, YIF₁-E21A

3.1.3 Covalent crosslinking of inhibitor proteins

By creating covalent bonds between near-neighbour proteins the oligomeric nature of the inhibitor proteins at different pH values could be probed. The crosslinking reagent dimethyl suberimidate (DMS) was used to covalently link protein oligomers by crosslinking amine groups on lysine residues. The extent of oligomer formation was monitored by observing the pattern of oligomers seen by SDS-PAGE. During all crosslinking experiments results were compared to the bovine IF₁ as a control. The bovine protein is well characterised in vitro and its structure is known in both an F₁-ATPase bound and free form (Cabezón *et al.*, 2003; Cabezón *et al.*, 2001). Samples of inhibitor proteins were dialysed into buffers at pH values of either 7.1 or 9.1 overnight and crosslinking experiments were performed as described in Chapter 2. The results are shown in Figures 3.7 and 3.8.

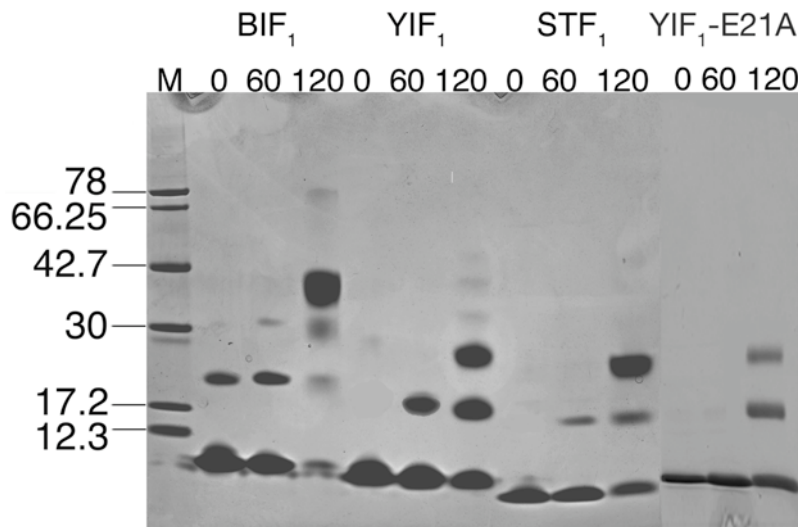


Figure 3.7 Covalent crosslinking of wild type and mutant inhibitor proteins at pH 9.1. The durations of cross-linking of quenched samples of bovine IF₁ (BIF₁), YIF₁, STF₁ and YIF₁ containing the mutation E21A (denoted YIF₁-E21A) analyzed by SDS-PAGE are indicated above the lanes of the stained gel. The positions of molecular weights (M) are shown on the left hand side.

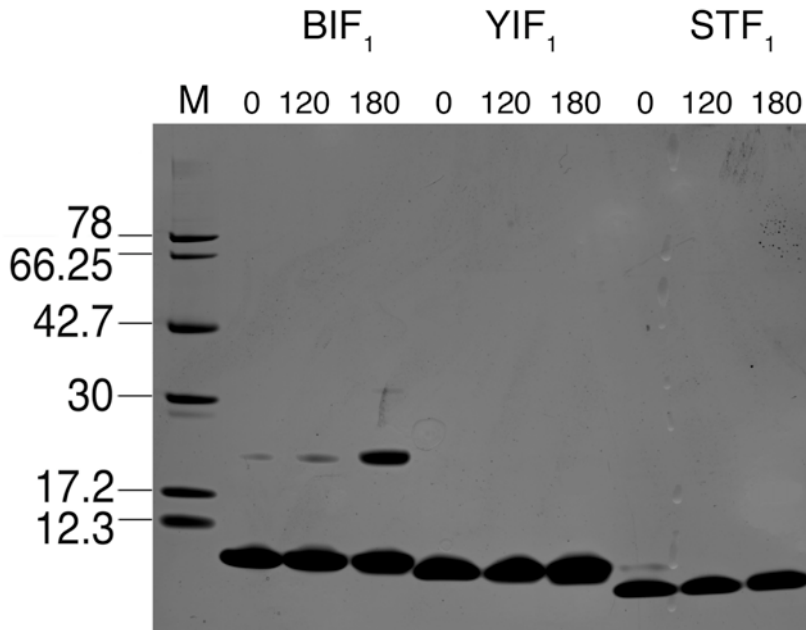


Figure 3.8 Covalent crosslinking of inhibitor proteins at pH 7.0. The durations of crosslinking of quenched samples of bovine IF₁ (BIF₁), YIF₁ and STF₁ by SDS-PAGE are indicated above the lanes of the stained gel. The positions of molecular weights (M) are shown on the left hand side.

The bovine protein shows clear tetramer formation after 120 minutes and by this time almost all of the protein has been converted to this form. In contrast the yeast proteins show clear trimer formation and at 120 minutes around half of the protein has been converted to this form. The first three lanes in Figures 3.7 and 3.8 show the crosslinking of bovine IF₁, the interaction to form dimers is sufficiently strong to be seen even before crosslinking has taken place (0 minutes), this is not evident in the yeast proteins. The bovine protein shows a clear pattern of crosslinking progressing from monomer to tetramer with some higher oligomer formation at pH 9.1 but only dimers at pH 7.0. The yeast proteins show clear trimer formation and again higher oligomer formation at pH 9.1 but no oligomer formation at pH 7.0. The crosslinking of the mutant YIF₁-E21A shows a lower tendency to form oligomers

Chapter 3: Mechanism of action of the F-ATPase inhibitor protein IF₁ from *S. cerevisiae*

(Figure 3.7) consistent with previous experiments showing that this mutant is able to inhibit F₁-ATPase at all pH values [Figure 3.6 and (Ichikawa *et al.*, 2001)].

3.1.4 Oligomeric state of the *S. cerevisiae* F₁-YIF₁ complex

It has been shown, by hydrodynamic and X-ray crystallographic experiments (Cabezón *et al.*, 2000a; Cabezón *et al.*, 2003), that the bovine F₁-IF₁ complex is a dimer. This dimeric state depends on the dimeric nature of the active inhibitor protein. To investigate the oligomeric nature of the active *S. cerevisiae* inhibitor protein, its state in complex with F₁-ATPase was studied. The oligomeric state of the *S. cerevisiae* F₁-YIF₁ complex was investigated by gel filtration chromatography and sedimentation velocity analytical centrifugation.

3.1.4.1 Gel filtration analysis

A Superose 6 HR 10/30 column was calibrated (Figure 3.9 and Section 2.2.7) and the *S. cerevisiae* F₁-YIF₁ complex and uninhibited F₁-ATPase applied to the column. The complex and inhibitor free F₁-ATPase eluted at the same position with an apparent molecular weight of 306 kDa. This confirmed that the *S. cerevisiae* complex is monomeric and consists of one copy each of YIF₁ and F₁-ATPase (Figure 3.10). Analysis of the peak fractions, by SDS-PAGE, confirmed the presence of both YIF₁ (7.3 kDa) and F₁-ATPase in the complex in approximately equivalent amounts (Figure 3.11). In contrast, as expected, the bovine F₁-IF₁ complex eluted from the same column with an apparent molecular mass of 620 kDa (Figure 3.10) consistent with its known structure as a dimeric complex composed of dimeric IF₁ attached to two F₁-ATPase assemblies (Cabezón *et al.*, 2003).

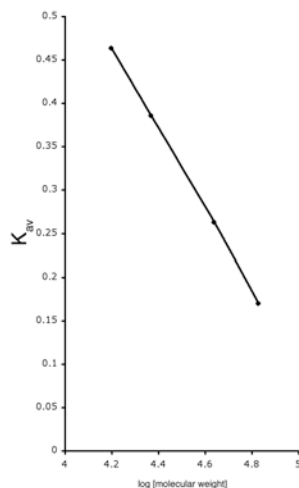


Figure 3.9 Calibration of the Sepharose 6 column. The column was calibrated with the following proteins: thyroglobulin (669 kDa), ferritin (440 kDa), catalase (232 kDa) and aldolase (158 kDa). The void volume was measured with blue dextran 2000. The plot of K_{av} against $\log[\text{molecular weight}]$ gives a straight line and enables the apparent molecular weight of unknowns to be estimated. See Section 2.2.7 for experimental details.

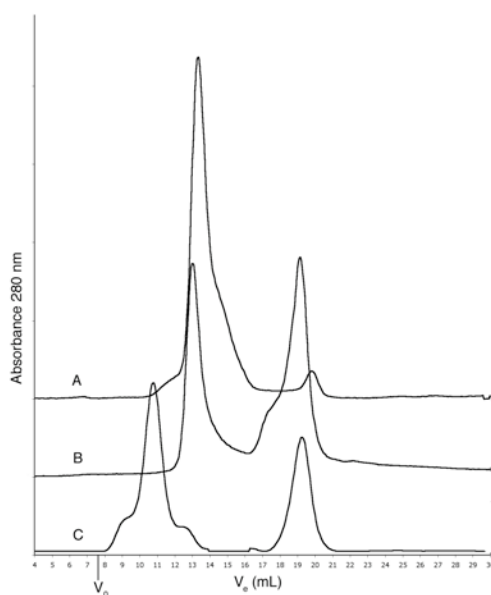


Figure 3.10 Estimation of molecular weights of complexes by size exclusion chromatography. Elution profiles of the yeast F_1 -ATPase, the YIF_1 - F_1 complex and the bovine IF_1 - F_1 complex, denoted by traces A, B and C, respectively. The peaks that elute second in traces B and C are excesses of unbound inhibitor proteins. The excluded volume of the column, V_0 , is indicated.

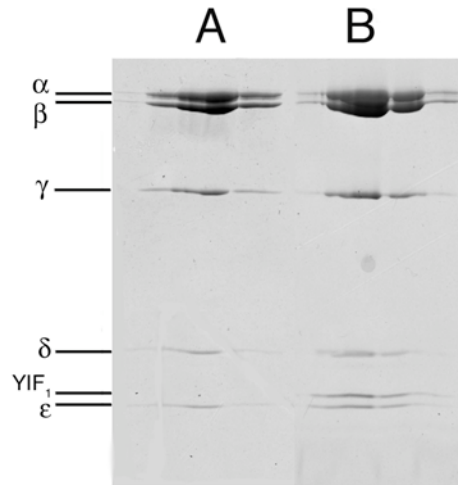


Figure 3.11 Analyses by SDS-PAGE of the main peaks in traces A and B from Figure 3.10 (denoted by A and B above the gel). The positions of the five subunits α , β , γ , δ and ϵ of the *S. cerevisiae* F_1 -ATPase and of the inhibitor protein, YIF_1 , detected by staining with Coomassie blue dye, are indicated on the left.

3.1.4.2 Analytical ultracentrifugation

To confirm the conclusion that the F_1 - YIF_1 complex is monomeric, it was analysed by sedimentation velocity ultracentrifugation (Figure 3.12). The F_1 - YIF_1 complex gave a mean $s_{20,w}$ value of 12.84 S and a mean molecular mass of 338 kDa, consistent with monomeric F_1 -ATPase bound to monomeric YIF_1 . The values obtained with bovine F_1 -ATPase and the bovine F_1 - IF_1 complex were 12.1 ± 0.7 S and 17.0 ± 0.1 S, respectively, with corresponding molecular masses of 330 kDa and 521 kDa. This latter value is somewhat low for the dimer, but this could well be due to some non-homogeneity in the boundary (which is rather broad, although still well fitted as a single component), possibly due to different conformations of how the IF_1 can bind two F_1 -ATPases together.

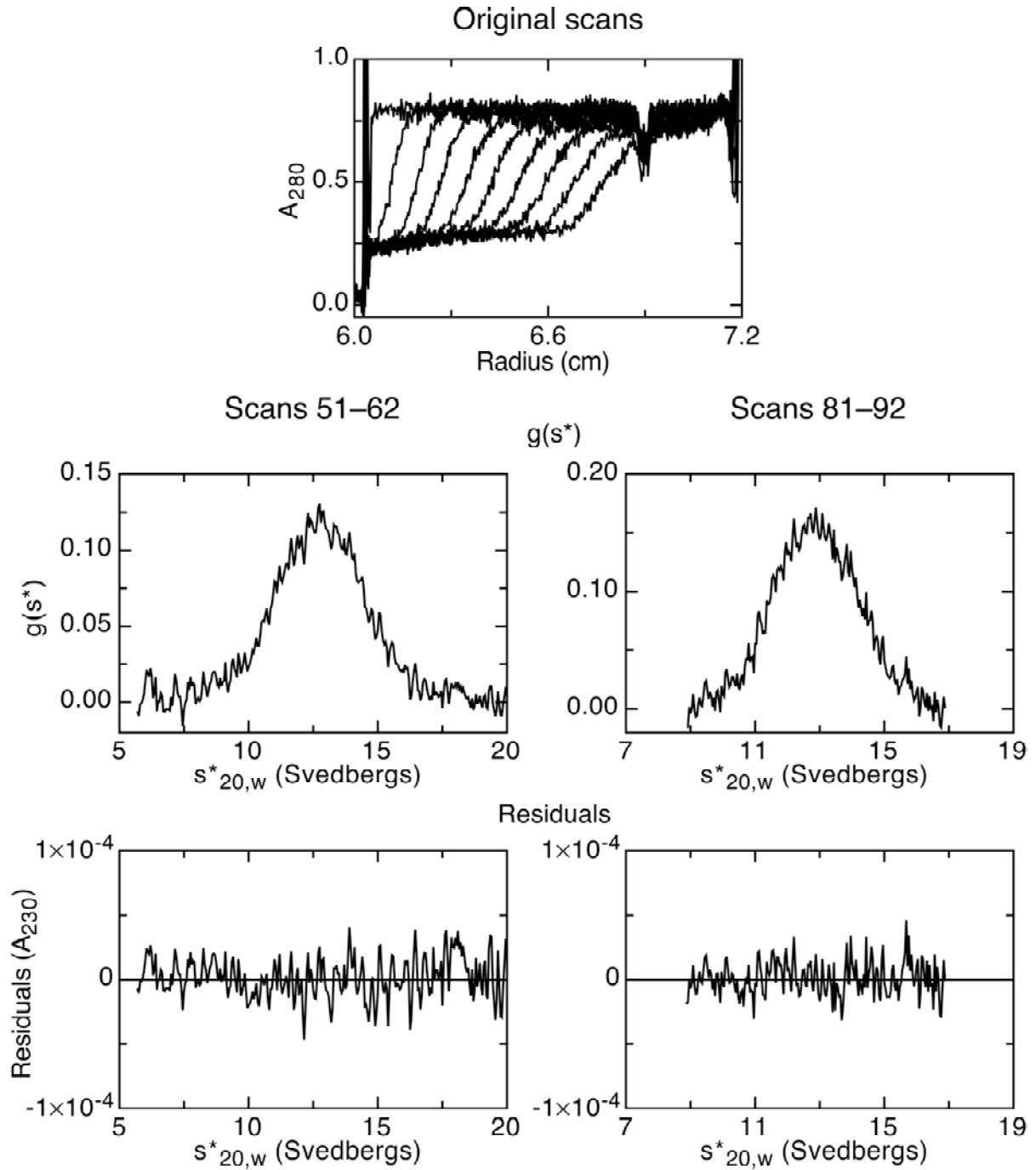


Figure 3.12 Sedimentation velocity analysis of the yeast F_1 -ATPase-YIF₁ complex. Original scans taken at intervals of 15 min are shown, together with plots of $g(s^*_{20,w})$ against $s^*_{20,w}$ and of the residuals from the model fitting against $s^*_{20,w}$ for sets of scans from 51–62 and from 81–92.

3.2 Discussion

3.2.1 Active and inactive states of the *S. cerevisiae* inhibitor proteins

The results from crosslinking experiments show that at pH values above 7.0 the *S. cerevisiae* inhibitor proteins forms trimers, in contrast to the tetramer formation observed in the bovine inhibitor protein (Figure 3.7). The patterns obtained with YIF₁ and STF₁ differ. STF₁ shows a weaker tendency to aggregate at pH values of 9.1. This is consistent with analytical ultracentrifugation experiments in a previous study (Cabezón *et al.*, 2000a; Cabezón *et al.*, 2002). STF₁ contained less dimer and more trimer indicating a stronger equilibrium between monomeric and trimeric states than in YIF₁ where monomer, dimer and trimer coexisted in equilibrium. The crosslinking results also demonstrate that the bovine protein is more stringently controlled than the *S. cerevisiae* proteins. After 120 minutes the bovine protein is almost entirely converted to the tetrameric form. In contrast, the *S. cerevisiae* proteins remain as an equal mixture of oligomers after the same time (Figure 3.7).

The crosslinking experiments at pH 7.0 show the active state of the proteins (Figure 3.8). The bovine protein shows monomer and dimer even at 0 min, indicating that the dimer interaction is sufficiently strong to withstand a denaturing gel to some extent. The *S. cerevisiae* proteins only show monomer, even after 180 min. The crosslinking experiments at this pH value were left for a longer period, as DMS is much less active at this value. However, as crosslinking is observed in the bovine protein, oligomers of the *S. cerevisiae* proteins, if present, should be observed.

These experiments investigate the properties of the free inhibitor proteins, but how do they behave when interacting with F₁-ATPase? The gel filtration and analytical ultracentrifugation experiments show that the complex is monomeric (Figures 3.10 and 3.12).

Chapter 3: Mechanism of action of the F-ATPase inhibitor protein IF₁ from *S. cerevisiae*

Analysis of the fractions containing F₁-YIF₁ eluted from the gel filtration column show that the F₁-ATPase and YIF₁ are present in approximately equivalent amounts (Figure 3.11). The exact stoichiometry of the complex cannot be determined from the SDS-PAGE gel and it may be possible that a dimeric YIF₁ binds to the F₁-ATPase. This may be possible as the shorter length of YIF₁ compared to bovine IF₁ (63 amino acids and 84 amino acids respectively) may not enable the second C-terminus to reach another F₁-ATPase. However, coupled with the crosslinking results it seems likely that a monomeric YIF₁ binds one F₁-ATPase. The length of the *S. cerevisiae* proteins also indicates a monomeric active state. Truncating the bovine IF₁ to the first 64 amino acids renders the protein monomeric (Gledhill, J. G., personal communication) probably because the α -helical coiled coil forming regions are removed. The mechanism of oligomerisation of the *S. cerevisiae* inhibitor proteins is discussed in the following section.

3.2.2 Structure and mechanism of action of the inhibitor proteins

By deletion analysis, it has been demonstrated that residues 14-47 of bovine IF₁ represent the minimal inhibitory sequence (van Raaij *et al.*, 1996b), and the structure of the bovine F₁-IF₁ complex has shown that residues 1-37 are in intimate contact with the β_{DP} - α_{DP} catalytic interface of F₁-ATPase (Cabezón *et al.*, 2003). The bovine and yeast proteins are most strongly conserved in this N-terminal inhibitory region (Figure 3.13). Their sequences are more divergent in the C-terminal regions, which are involved in the modulation of active and inactive states of the protein by pH. The major difference between the bovine and yeast proteins is that the C-terminal regions of the yeast proteins are truncated by 21 amino acids relative to the bovine sequence. Residues 39-80 of bovine IF₁ contain seven consecutive heptad repeats that are involved in dimer formation by formation of an anti-parallel coiled-coil of α -helices. The critical role of histidine-49 in heptad-2 in the formation of tetramers

Chapter 3: Mechanism of action of the F-ATPase inhibitor protein IF₁ from *S. cerevisiae*

was demonstrated by the mutation H49K which led to the bovine IF₁ being maintained in an active dimeric state independent of pH (Cabezón *et al.*, 2003; Schnizer *et al.*, 1996).

```

BIF1  GSESGDNVRSSAGAVRDAGGAFGKREQAEEERYFRARAKEQLAALKKHHEENEISHHAKE 59
YIF1  --SEGSTGTPRGSGSEDS---FVKRERATEDFFVRQREKEQLRHLKEQLE----KQRKK 50
STF1  --SDGPLGGAGPGNPQDI---FIKRERAKEDYYARQQEREQLA VKEQLK----EHKKK 50
      ..*      . . . *      * **:* * *: * : :*** :*::: : .: *:

BIF1  IERLQKEIERHKQSIKKLKQSEDDD 84
YIF1  IDSLENKID----SMTK----- 63
STF1  LENLENKIN----NLSK----- 63
      :: *:::*:      ...*

```

Figure 3.13 Sequence alignment of inhibitor proteins. Alignment of the sequences of bovine IF₁ (BIF₁) with those of YIF₁ and STF₁ from *S. cerevisiae* with the program ClustalW (Thompson *et al.*, 1994). Residues that have been found to be important in oligomer formation are shown in bold. Identical residues are indicated by an asterisk, highly conserved residues by a colon and weakly conserved residues by a full stop.

By analysis of the sequences of the yeast proteins for heptad repeats with the program MultiCoil (Wolf *et al.*, 1997), four or five repeats were predicted to be present in their C-terminal regions (Figure 3.14). The yeast proteins do not contain a residue equivalent to histidine-49, but two residues, histidine-39 and glutamate-21, appear to influence the pH regulation of their activities (Ichikawa *et al.*, 2001). The former is in the coiled-coil forming region (Figure 3.14), and mutation of this residue could interfere directly with coiled-coil formation. One striking difference between the bovine and yeast proteins is the formation of dimers and of dimers-of-dimers by the former, and of dimers and trimers (and no dimers-of-dimers) by the latter, implying that the aggregation process involves coiled-coil formation by two and three α -helices in dimers and trimers, respectively. A leucine zipper sequence provides an example of how one sequence can form both dimeric and trimeric parallel coiled-coils under slightly different conditions (Gonzalez *et al.*, 1996). In the case of the yeast

Chapter 3: Mechanism of action of the F-ATPase inhibitor protein IF₁ from *S. cerevisiae*

inhibitor proteins, it is not known whether the coiled-coils are parallel or antiparallel. Further mutational and structural analyses will be required to elucidate how their coiled-coils are formed.

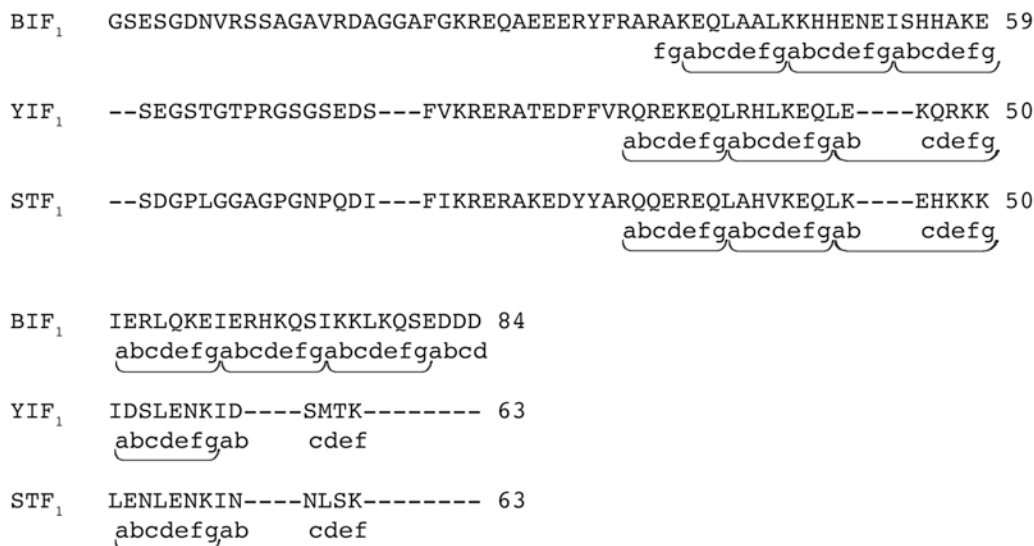


Figure 3.14 Positions of heptad repeats in inhibitor proteins. The positions of heptad repeats, a-g, predicted by the program MULTICOIL (Wolf *et al.*, 1997) to be involved in the formation of α -helical coiled-coils in bovine IF₁ (BIF₁) and YIF₁ and STF₁ from *S. cerevisiae*.

Glutamate-21, a second residue in the yeast protein that has been identified as influencing oligomer formation (Ichikawa *et al.*, 2001), is in the inhibitory region, and, by comparison with the bovine F₁-IF₁ structure, it would be expected to be in contact with F₁-ATPase and not to influence coiled-coil formation directly. However, the mutation E21A causes YIF₁ to become fully active at pH 8.0. By cross-linking (Figure 3.7), it was shown that the mutation suppresses the formation of dimers and trimers, and the inhibitory activity of the mutant protein becomes independent of pH (Figure 3.6), suggesting that the negative

charge at residue-21 in the wild-type protein helps to promote higher oligomer formation and aggregation.

Further structural analysis will also be required to understand the precise mechanism of inhibition of yeast F₁-ATPase by YIF₁ and STF₁, although it is likely that the general modes of interaction and inhibition will be similar to the bovine proteins. However, it is already clear that the YIF₁ and STF₁ proteins are less potent than bovine IF₁, and the activity of the bovine protein is more stringently regulated since more yeast inhibitor protein remains active at elevated pH than does the bovine protein (Figure 3.7).

3.2.3 Dimerisation of F-ATPases

Dimeric forms of both the bovine and yeast F₁F₀-ATPases have been observed by blue native PAGE (Arnold *et al.*, 1998; Schagger and Pfeiffer, 2000). Dimerisation of bovine F₁-ATPase, but not as yet of the intact F₁F₀-ATPase, by the inhibitor protein has been demonstrated by a range of independent methods, including X-ray crystallography (Cabezón *et al.*, 2000a; Cabezón *et al.*, 2003). Therefore, the dimers of the bovine F₁F₀-ATPase observed by gel analysis could be mediated by IF₁. However, dimerisation of the F₁F₀-ATPase in *S. cerevisiae* is mediated by other subunits, namely subunits e and f, which appear to make homodimeric parallel α -helical coiled-coils (Arnold *et al.*, 1998). It has also been shown that an *Inh1* null strain of *S. cerevisiae* still contains ATP synthase dimers (Dienhart *et al.*, 2002). The present results, which show that monomeric YIF₁ and STF₁ are the active forms of these inhibitors, effectively eliminates their participation in the dimerisation of the yeast F₁F₀-ATPase.

CHAPTER 4: THE STRUCTURE OF BOVINE MITOCHONDRIAL F_1 -ATPase INHIBITED WITH ADP AND MAGNESIUM FLUORIDE

4.1 Results

4.1.1 Introduction

Metallofluorides, together with ADP, inhibit F_1 -ATPase by replacing the γ phosphate of ATP. As they have fixed geometric arrangements (either as a phosphate analogue or a transition state analogue), the protein is stabilised in this conformation. Crystallographic studies of F_1 -ATPase with metallofluorides have revealed new substeps in the catalytic mechanism (Kagawa *et al.*, 2004; Menz *et al.*, 2001b) and as described below, crystallisation with a novel metallofluoride, magnesium fluoride, has shown a new step in the catalytic pathway. Bovine F_1 -ATPase was inhibited with ADP and magnesium fluoride as described in Section 2.2.15, and crystallised in their presence. The structure was solved to high resolution revealing a new step in the catalytic cycle in which nucleotide is bound to the β_E subunit with the subunit in an essentially open conformation. The β_{TP} and β_{DP} sites contain ADP-MgF₃⁻ complexes. This structure probably represents a stage in the catalytic cycle of ATP hydrolysis just before release of the products of ATP hydrolysis.

4.1.2 Inhibition of bovine F_1 -ATPase with ADP and magnesium fluoride

The inhibition of F_1 -ATPase by ADP and magnesium fluoride was examined under various conditions. The progress of inhibition was monitored at 20 min intervals by measuring the hydrolytic activity of the enzyme. Several conditions were tried so as to attain maximum inhibition of the enzyme. Initial trials using MgSO₄ as the magnesium salt failed

Chapter 4: *The structure of bovine F_1 -ATPase inhibited with ADP and magnesium fluoride*

to inhibit the enzyme sufficiently for crystallisation experiments. Changing the salt to $MgCl_2$ rectified this problem. In the final protocol, the enzyme was incubated first with 10 mM $MgCl_2$ for 20 min. Then 10 mM NH_4F was added. After approximately 2 hours the enzyme was 94% inhibited (Figure 4.1).

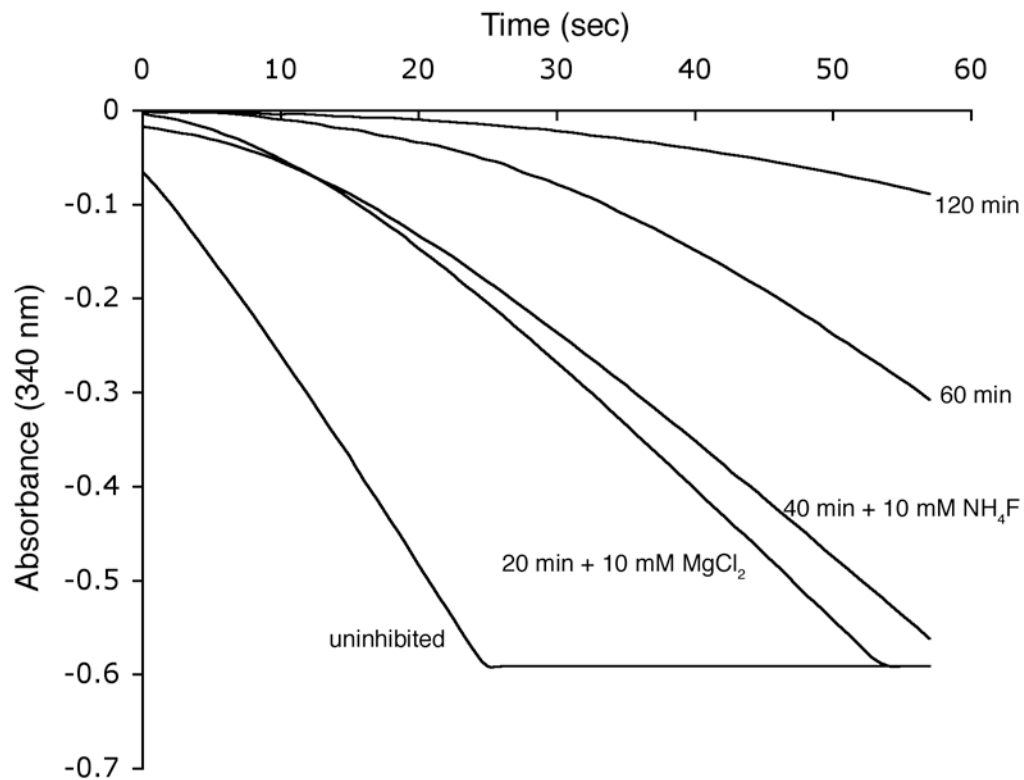


Figure 4.1 The inhibition of bovine mitochondrial F_1 -ATPase by ADP and magnesium fluoride. The protein was incubated in 10 mM magnesium chloride and 1 mM ADP. After 20 min 10 mM ammonium fluoride was added. The inhibition of the enzyme was monitored, by measuring ATP hydrolysis at intervals, until the sample approached complete inhibition. After 2 hours, 94% inhibition had been achieved.

4.1.3 Crystallisation of bovine F₁-ATPase inhibited with ADP and magnesium fluoride

Crystallisation experiments were set up with the inhibited enzyme using the microdialysis method (see Section 2.2.16.1) using conditions similar to standard conditions for producing reference state crystals (Lutter *et al.*, 1993). Experiments were conducted with a range of concentrations of PEG 6000. The first crystals appeared after one week with 13-14% PEG 6000. However, these experiments produced a large number of badly formed crystals. Experiments with PEG 6000 concentrations from 11.75-13% produced a small number of well formed crystals after two weeks (Figure 4.2). The crystals were fully grown after a month and their dimensions were typically 250 x 50 x 50 μm^3 .

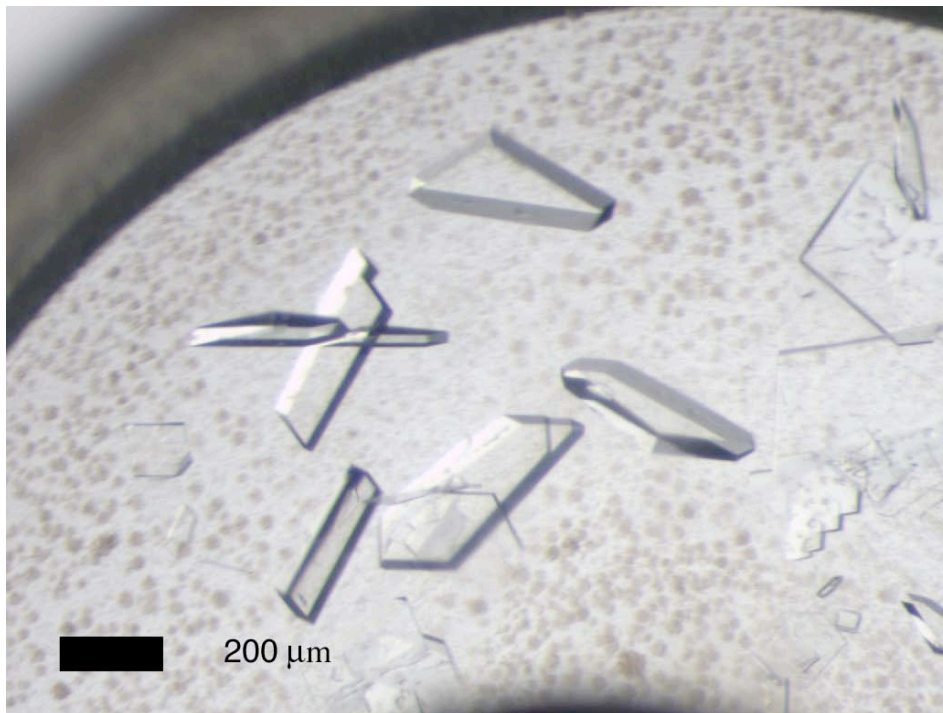


Figure 4.2 Crystals of bovine F₁-ATPase inhibited with ADP and magnesium fluoride. Crystals were grown from 50 mM Tris-DCI pH 8.2, 200 mM NaCl, 10 mM MgCl₂, 10 mM NH₄F, 0.05 mM ADP, 0.02% (w/v) NaN₃, 0.004% (w/v) PMSF and 12.5% (w/v) PEG 6000.

4.1.4 Cryoprotection of crystals

4.1.4.1 Harvesting solution

Previous crystallographic studies of the F_1 -ATPase have shown that a shorter crystallographic cell edge in the a dimension correlates with an increase in the order of the molecules within the crystal (see Appendix B for a figure of the unit cell). Such crystals have produced more complete data sets with higher resolution limits (Gibbons *et al.*, 2000; Menz *et al.*, 2001b). The shrinkage in the a dimension was probably due to higher concentrations of PEG 6000 in the harvesting solution, which dehydrated the crystals and reduced the unit cell a dimension by up to 16 Å (the range of values is 267-283 Å). Similar effects have been observed in crystals of a number of other proteins (Cramer *et al.*, 2000; Esnouf *et al.*, 1998; Haebel *et al.*, 2001; Kuo *et al.*, 2003). Therefore, the higher limit of PEG 6000 concentration was investigated. The concentration of PEG 6000 was increased stepwise by dialysis until deleterious effects were observed (usually cracking of the crystals). From these studies, the upper limit for PEG 6000 concentration, for harvesting the magnesium fluoride inhibited crystals, was judged to be 15%.

4.1.4.2 Cryoprotectant

In previous studies, glycerol and ethylene glycol have been used successfully to cryoprotect crystals of F_1 -ATPase. In the present study glycerol was used and the concentration and time course of soaks investigated. Glycerol was introduced to the mother liquor by dialysis (the concentration of PEG 6000 was increased at the same time). The concentration was increased in 5% steps with a soaking time of 15 min. The success of cryoprotection was judged by analysing the crystals using the laboratory X-ray source and inspecting the diffraction pattern for ice rings and mosaic spread of the crystals. Previous cryoprotection protocols have used soaking times between 30 min and 12 hours. By

Chapter 4: The structure of bovine F_1 -ATPase inhibited with ADP and magnesium fluoride

decreasing the time to 15 min, no decrease in the quality of diffraction from crystals was observed and the process of cryoprotection was considerably faster. A final concentration of 20% (v/v) glycerol (in combination with 15% (w/v) PEG 6000) led to diffraction patterns with no ice rings and a typical mosaic spread of 0.4-0.6°. Figure 4.3 shows a typical 'in house' diffraction pattern from a 'good' crystal.

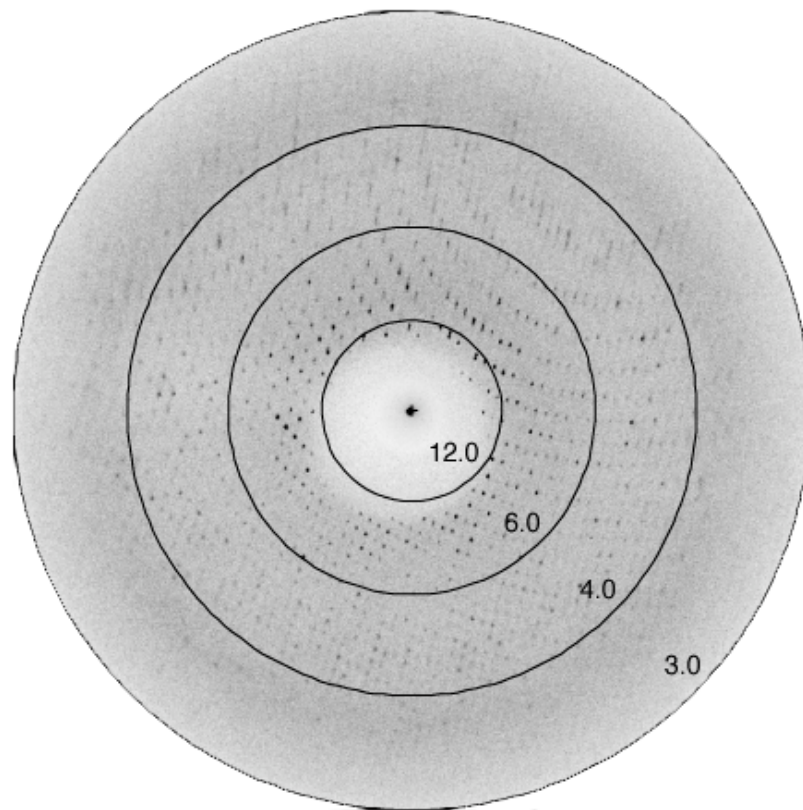


Figure 4.3 Diffraction pattern of F_1 - MgF_3^- crystals using the laboratory X-ray source.

The rings show the resolution in Ångströms. The crystals diffract to approximately 3.5 Å. No ice rings were observed and the mosaic spread was estimated to be 0.5°.

4.1.4.3 Screening of crystals

Approximately 100 crystals were cryoprotected and stored at 100 K. These crystals were screened with a laboratory X-ray source. Diffraction patterns were assessed for the resolution limit and mosaic spread with MOSFLM (Leslie, 1992). Crystals that diffracted to at least 4 Å and had a mosaicity of less than 0.6° were recovered and stored for data collection at a synchrotron radiation source.

4.1.5 Structure determination

4.1.5.1 Data collection

Selected crystals were taken to the European Synchrotron Radiation Source (ESRF, Grenoble, France) where data were collected at beamline ID29. Out of 30 crystals that were examined, 3 of them were of sufficient quality to collect data sets. The details of collection of the data sets are summarised in Table 2.1.

Table 2.1 Data sets of bovine F₁-ATPase inhibited with ADP and magnesium fluoride.

Crystal	ϕ range	Exposure time	Oscillation angle	X-ray λ (Å)
X2	267 to 297 and 317 to 347	1 s	0.2°	0.976
X22	251 to 281 and 301 to 331	1 s	0.3°	0.976
X25	196 to 226 and 246 to 276	1 s	0.2°	0.976

For 3 crystals, complete data sets were taken to 2.5 Å resolution. All of the crystals belonged to the orthorhombic space group P2₁2₁2₁, but they had different unit cell dimensions (Table 2.2) with an a axis varying from 270 to 279 Å. These values are intermediate between the

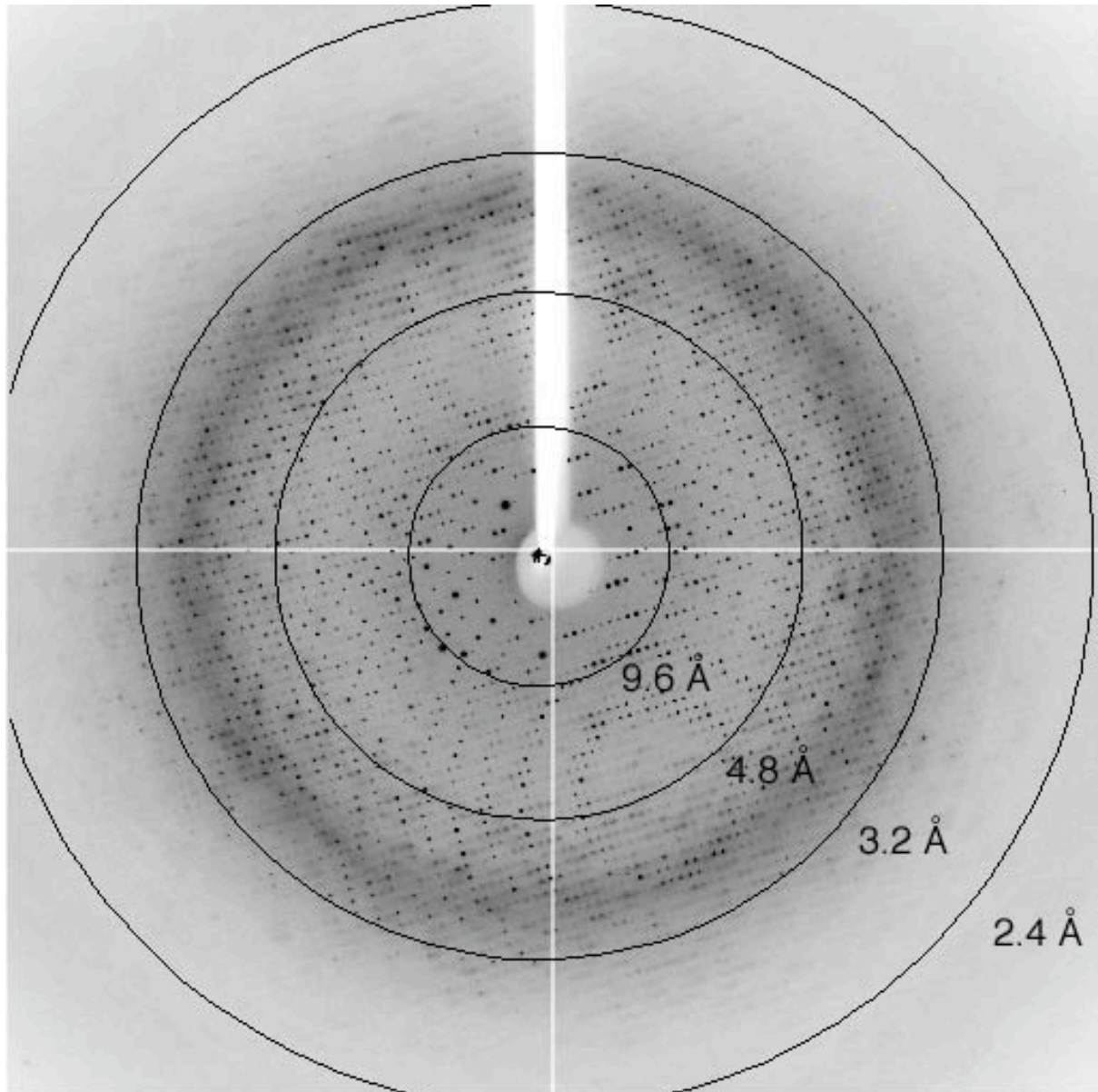


Figure 4.4 Diffraction by crystals of F₁-ATPase inhibited by magnesium fluoride and ADP. The image was recorded on an ADSC Q210 2D CCD detector at beamline ID29, ESRF, Grenoble. Circles mark resolution shells. Diffraction was observed to 2.4 Å.

fully ‘shrunk cell’ (ca 267 Å) and the standard cryo-cooled cell (ca 280 Å). An example of the diffraction pattern from crystal 2 is shown in Figure 4.4.

4.1.5.2 Structure solution

Data were processed and the model refined using programs from the CCP4 suite (Collaborative Computational Project Number 4, 1994). The methods used to process the data and solve the structure of the magnesium fluoride inhibited F_1 -ATPase are described in Section 2.2.17.

Table 2.2 Unit cell dimensions of crystals

Crystal	Unit cell dimensions (Å)
X2	a= 270.5, b=107.4, c=134.6
X22	a= 278.6, b=106.8, c=134.2
X25	a= 274.5, b=107.2, c=133.5

Initial inspection of the data sets showed that only the data set from crystal 2 (X2) could be processed to give a data set with high completeness due to problems in resolving diffraction spots that were too close to permit their intensities to be measured accurately. This dataset was used for structure solution.

The structure was solved by molecular replacement using the beryllium fluoride inhibited structure [PDB accession code 10WJ (Kagawa *et al.*, 2004)] as the search model. So as not to bias the density map calculations, the beryllium fluoride and water molecules were removed. After molecular replacement, the model was refined against the data using REFMAC5 (Murshudov *et al.*, 1997). During refinement, the R-factor and Free R-factor dropped from 31.5%, for both, to 22.1% and 29.4%, respectively. At this stage, ($2F_o - F_c$) and ($F_o - F_c$) electron density maps were calculated and inspected for novel features. The catalytic sites in the β_{DP} and β_{TP} subunits were found to contain density for ADP and additional

Chapter 4: The structure of bovine F_1 -ATPase inhibited with ADP and magnesium fluoride

trigonal planar density in the position normally occupied by the γ phosphate of ATP. In the β_E subunit, strong positive density peaks for the adenine ring and phosphates of ADP were detected. Surprisingly, the β_E subunit was in the open conformation found in the reference structure, rather than being in the ‘half-closed’ conformation seen in the $(ADP-AlF_4^-)_2-F_1$ structure. Altered side chain conformations, due to lattice contacts, and ordered water molecules, were built using the program ‘O’ (Jones *et al.*, 1991).

The coordinates of magnesium trifluoride were taken from the structure of Rho GTPase in complex with the GTPase activating protein [PDB accession code 1OW3, (Graham *et al.*, 2002)]. They were modelled into the density in the β_{TP} catalytic site (Figure 4.5). The additional density present in the β_{DP} catalytic site resembled divalent magnesium.

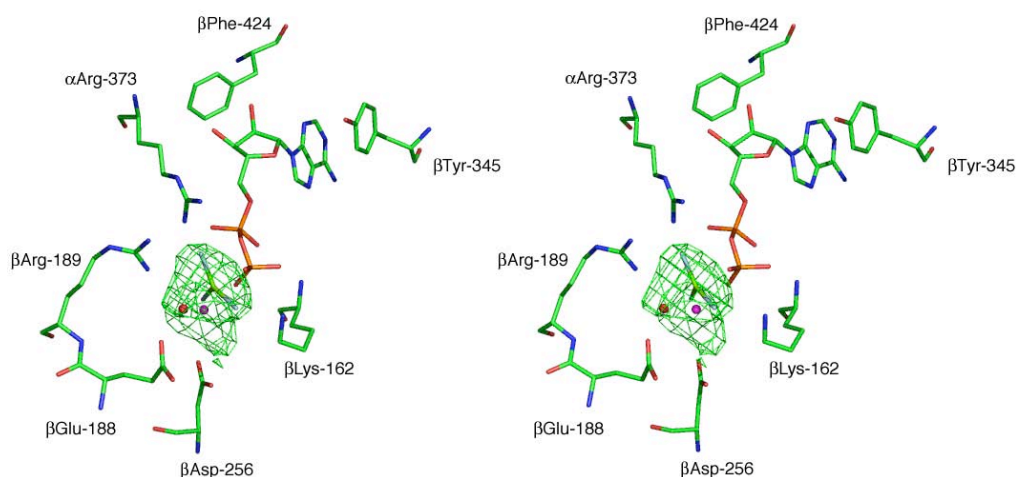


Figure 4.5 Stereo image of the β_{TP} catalytic site in the F_1 - MgF_3^- structure. Density from initial F_O - F_C difference map for the magnesium fluoride is shown (green mesh) before it was included in the model. The density is contoured at 2σ . The orientation of the model in this and subsequent figures is chosen to illustrate amino acid side chains and ligands clearly. The orientation is different to that shown in Figure 4.10. See Appendix B for the orientation of catalytic sites relative to the ‘standard’ orientation seen in Figure 4.10.

Chapter 4: The structure of bovine F_1 -ATPase inhibited with ADP and magnesium fluoride

Therefore, initially MgF_3^- was not modelled into this subunit. After subsequent rounds of refinement, the density in the β_{DP} subunit became trigonal in appearance and MgF_3^- was modelled in [Similar observations were made during refinement of the $(\text{ADP-AlF}_4^-)_2\text{-F}_1$ structure, where density in one of the catalytic sites initially looked like a combination of AlF_3 and AlF_4^- , but the morphology changed to square planar AlF_4^- during refinement (Leslie, A. G. W., personal communication)]. To avoid introducing model bias to the density, ADP was not placed in the density present in the β_{E} subunit until the last stage of refinement.

Crystals with a shorter a axis have often been found to have greater order in the region of the γ subunit most remote from the $\alpha_3\beta_3$ hexamer. However, in the case of $\text{F}_1\text{-MgF}_3^-$, there was no clear density corresponding to this region in the calculated maps. The density around the N and C-termini of the γ subunit, the part that penetrates the $\alpha_3\beta_3$ hexamer



Figure 4.6 Difference density map for the γ subunit. Refinement was carried out against a model of F_1 -ATPase with the γ subunit removed. The resulting difference maps showed strong peaks for the α -helical coiled coil region of the γ subunit and gave its position unambiguously.

showed a higher level of noise than was expected, possibly because of the presence of an alternative conformation. To test the location of the central stalk, refinement was carried out after excluding the γ subunit from the model. The difference maps, following refinement, had very strong positive peaks for the α -helical coiled coil regions of the γ subunit, indicating that there was no significantly occupied alternative conformation for the γ subunit (Figure 4.6). The additional features may be due to the relatively low quality of the data set or high mobility of the exposed part of the γ subunit.

After several rounds of refinement, the model contained 261 ordered water molecules and as much of the difference density as was possible had been interpreted. The R factor had dropped to 22.7% and the free R factor to 27.8%. At this stage, the remaining novel features

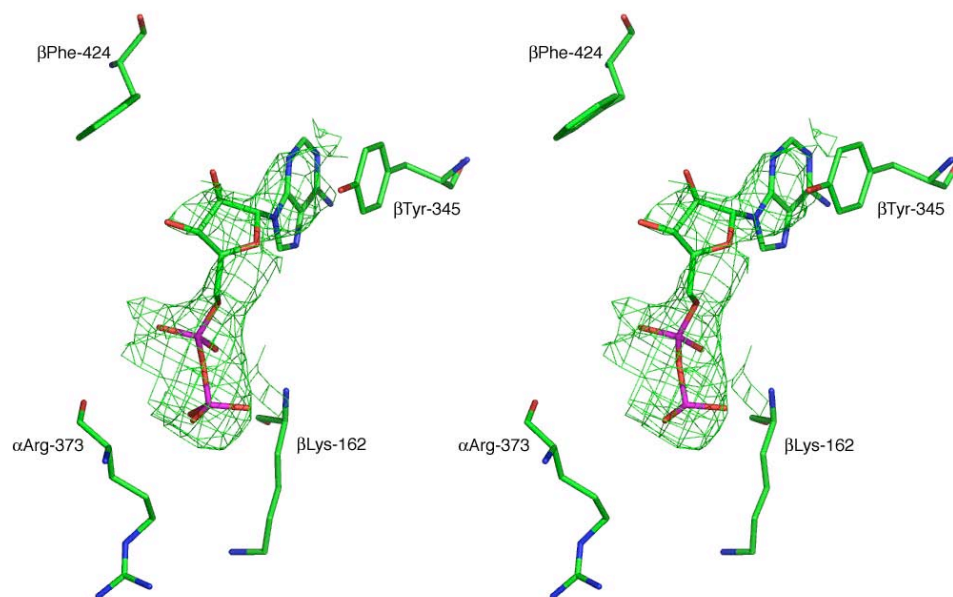


Figure 4.7 Stereo image of the difference density for nucleotide in the β_E catalytic site. The green mesh shows the initial $F_o - F_c$ difference map contoured at 3σ . The final refined coordinates for the nucleotide are superimposed and show the correspondence between the density and model.

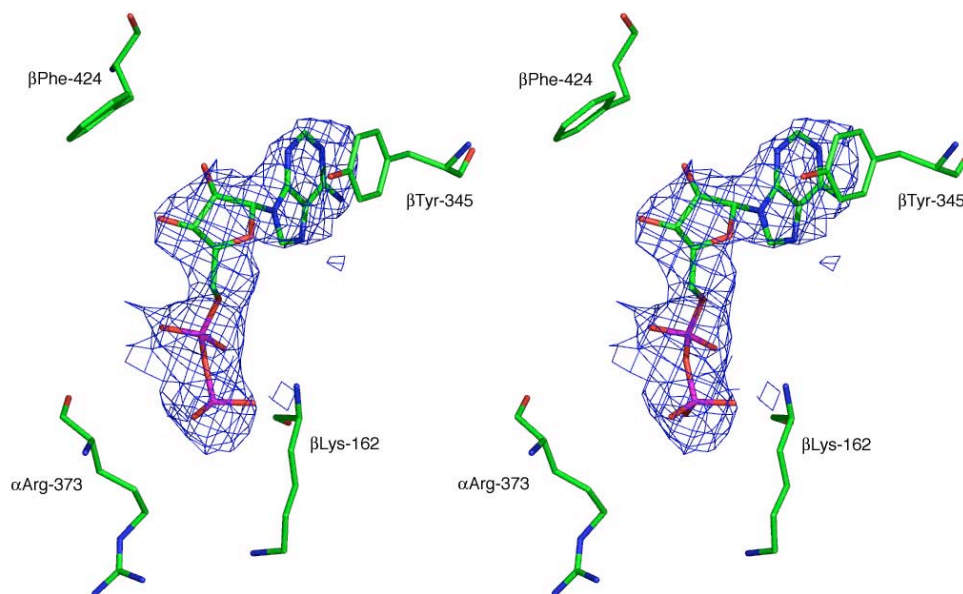


Figure 4.8 Stereo image of the refined $2F_o-F_c$ density for nucleotide in the β_E catalytic site. Density is clear for the entire nucleotide molecule and the B factors are sufficiently low to place the occupancy at 100%. The density is contoured at 1σ .

were modelled into the density. Coordinates for ADP from the β_{TP} catalytic site were aligned onto the P-loop of the β_E subunit and then moved into the density (Figures 4.7 and 4.8). Then the new coordinates were refined against the data and the temperature factors (B factors) for the nucleotide inspected. As the density for nucleotide was of low quality, the occupancy may be less than 100%. However, the average B factors were 72 \AA^2 for the nucleotide and the surrounding residues had similar B factors, so the occupancy was placed at 100%.

4.1.5.3 Structure validation

After a final round of refinement, the R factor was 20.4% and the free R factor was 26.8%. The statistics for data processing and refinement are shown in Table 4.3. The

Chapter 4: The structure of bovine F_1 -ATPase inhibited with ADP and magnesium fluoride

stereochemistry of the model was checked with the program PROCHECK (Laskowski *et al.*, 1992).

Table 4.3 Data collection and refinement statistics

Space group	P2 ₁ 2 ₁ 2 ₁
Unit cell dimensions (Å) a, b, c	270.5, 107.4, 134.6
Resolution range (Å)	20.0-2.53
Number of unique reflections	126,279
Multiplicity ¹	2.5 (2.5)
Completeness ¹ (%)	97.4 (98.7)
R _{merge} ^{1,2}	0.135 (0.596)
<I/σ(I)> ¹	5.8 (1.6)
Average B factor (from Wilson)	52.8 Å ²
Water molecules	261
R-factor ³ (%)	20.4
Free R-factor ⁴ (%)	26.8
RMS deviations:	
Bonds (Å)	0.007
Angles (°)	0.952

¹ Statistics for the highest resolution bin (2.67 - 2.53 Å) are shown in parenthesis

$$^2 R_{\text{merge}} = \frac{\sum_h \sum_i |I(h) - I(h)_i|}{\sum_h \sum_i I(h)_i}, \text{ where } I(h) \text{ is the mean weighted intensity after rejection of outliers.}$$

$$^3 R = \frac{\sum_{hkl} \|F_{\text{obs}} - k|F_{\text{calc}}\|}{\sum_{hkl} |F_{\text{obs}}|}, \text{ where } F_{\text{obs}} \text{ and } F_{\text{calc}} \text{ are the observed and calculated structure factor amplitudes.}$$

$$^4 R_{\text{free}} = \frac{\sum_{hkl \subset T} \|F_{\text{obs}} - k|F_{\text{calc}}\|}{\sum_{hkl \subset T} |F_{\text{obs}}|}, \text{ where } F_{\text{obs}} \text{ and } F_{\text{calc}} \text{ are the observed and calculated structure factor amplitudes}$$

and T is the test set of data omitted from refinement (5% in this case)

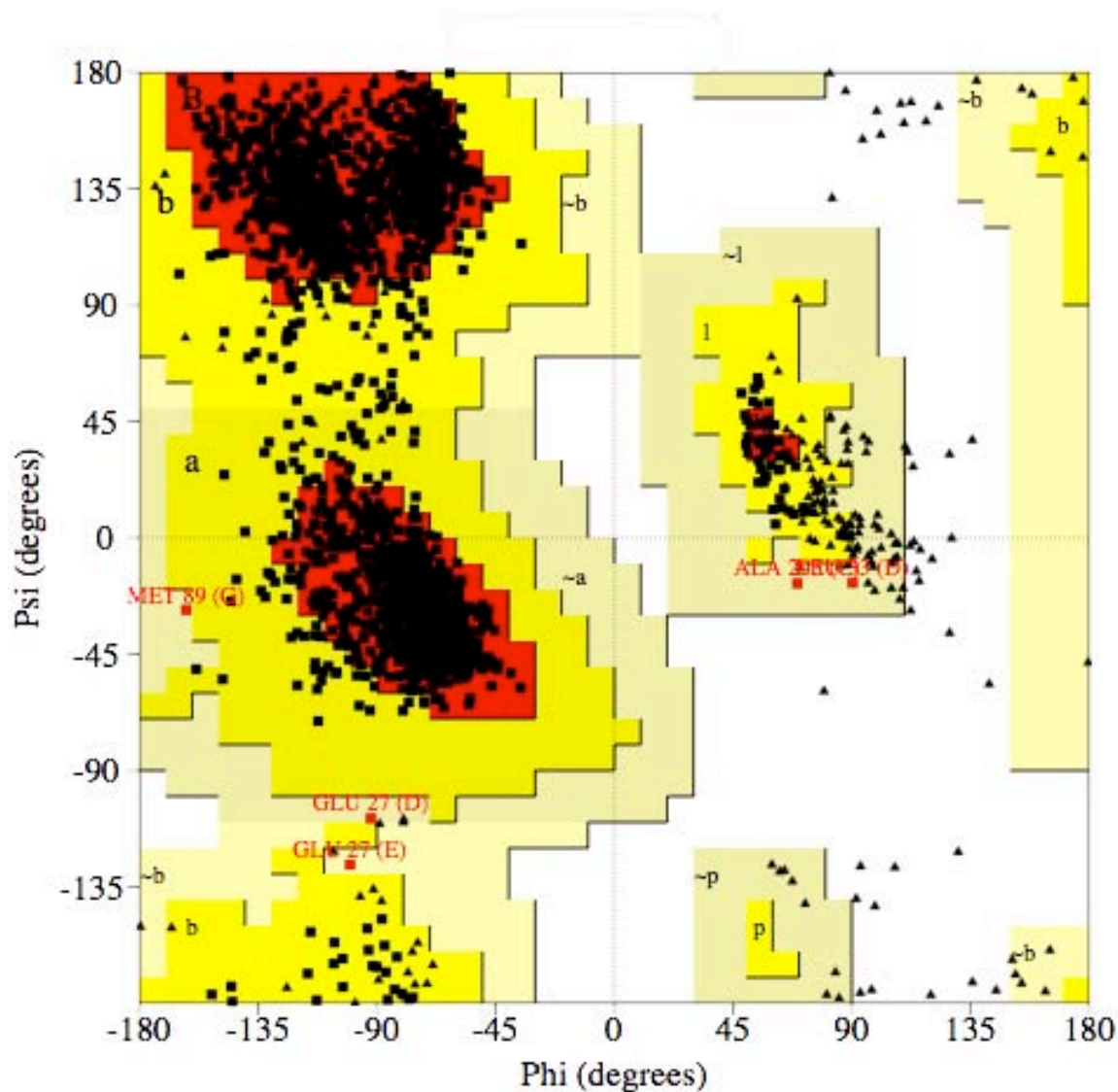


Figure 4.9 Ramachandran plot for the model of F₁-MgF₃. Main chain torsion angles ϕ and ψ are plotted against each other. The most favoured regions are shown in red, additionally allowed regions in yellow, and generously allowed regions in cream. The triangles represent glycine residues, which have no restrictions on the ϕ and ψ angles. All other residues are marked by a black square (red squares for residues in generously allowed regions).

Chapter 4: The structure of bovine F_1 -ATPase inhibited with ADP and magnesium fluoride

The ϕ and ψ bond torsion angles of the α -carbon backbone of proteins adopt preferred combinations due to steric hindrance (Ramachandran *et al.*, 1963; Ramakrishnan and Ramachandran, 1965). A Ramachandran plot of the ϕ and ψ angles of the carbon backbone placed 91.6% of residues in the most favoured regions, 8.2% in additionally allowed regions and 0.2% in generously allowed regions (Figure 4.9). No residues were found in disallowed regions.

4.1.6 Molecular architecture of the ADP and magnesium fluoride inhibited bovine F_1 -ATPase

The final model contains 3235 amino acid residues and 261 water molecules, and the overall architecture is very similar to the reference structure (Figure 4.10). The overall B

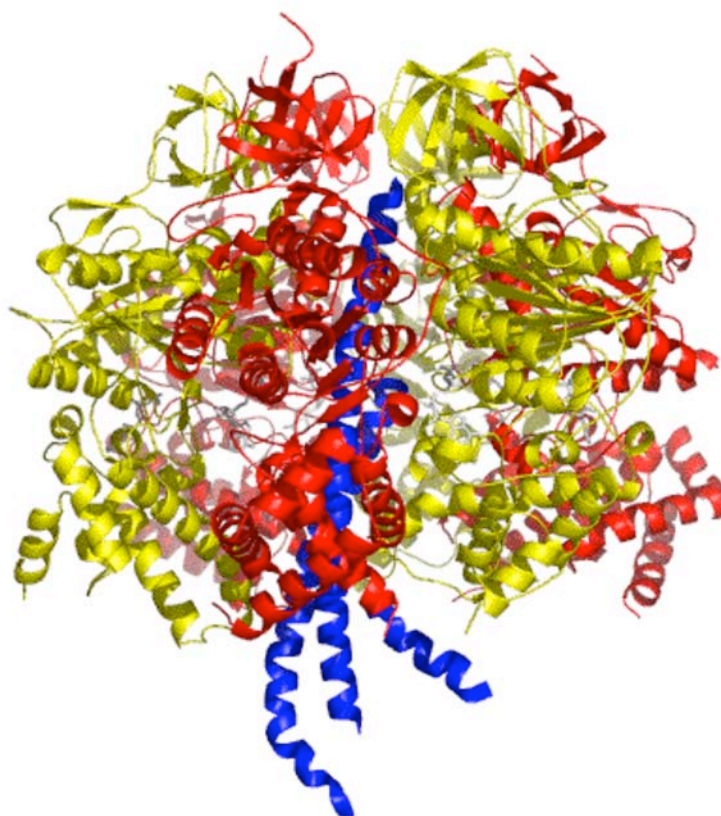


Figure 4.10 Structure of the F_1 - MgF_3^- structure. A ribbon representation of the structure is shown where α subunits are in red, β subunits in yellow and the γ subunit in blue.

Chapter 4: The structure of bovine F_1 -ATPase inhibited with ADP and magnesium fluoride

factor for the structure is 49 \AA^2 . Superimposition of the F_1 - MgF_3^- and reference structures gave an rms deviation of 0.56 \AA for the $C\alpha$ atoms. Superimposition of the $C\alpha$ atoms of P-loop residues of individual subunits (residues 155-165), gave rms deviations of approximately 0.15 \AA for the α subunits and for the β_{DP} and β_{TP} subunits. Comparison of the P-loops of the β_{E} subunits gave an rmsd of 0.34 \AA , the increase due to binding ADP. The average B factor of the F_1 - MgF_3^- β_{E} subunit was also much lower than the reference structure β_{E} subunit's average B factor (Table 4.4). The γ subunit gave an rmsd of 0.62 \AA . None of these values correspond to major structural differences in the subunits.

Table 4.4 Average B (temperature) factors for all atoms of the β_{DP} , β_{E} and γ subunits and β_{DP} and β_{E} bound ligands of the reference, $(\text{ADP-AlF}_4^-)_2$ - F_1 and F_1 - MgF_3^- structures.¹

Domain	Structure		
	Reference	$(\text{ADP-AlF}_4^-)_2$ - F_1	F_1 - MgF_3^-
β_{DP} subunit	61 \AA^2	37 \AA^2	45 \AA^2
β_{DP} bound ADP	43 \AA^2	28 \AA^2	28 \AA^2
β_{E} subunit	73 \AA^2	55 \AA^2	54 \AA^2
β_{E} bound ADP	None	42 \AA^2	73 \AA^2
γ subunit	84 \AA^2	62 \AA^2	77 \AA^2

In general, the nucleotide binding sites of F_1 - MgF_3^- are similar to those is a number of previously solved structures (Abrahams *et al.*, 1996; Abrahams *et al.*, 1994; Braig *et al.*, 2000; Orriss *et al.*, 1998; van Raaij *et al.*, 1996a). The α subunits all contained MgADP as in the beryllium fluoride inhibited and F_1 -ADP structures (Kagawa *et al.*, 2004). The β_{DP} and

¹ The average B factor is also dependent on the resolution to which the structure is solved. As a control the average B factor of the β_{DP} subunit is included. The resolutions are as follows: Reference: 2.8 \AA ; $(\text{ADP-AlF}_4^-)_2$ - F_1 : 2.0 \AA and F_1 - MgF_3^- 2.53 \AA .

Chapter 4: The structure of bovine F_1 -ATPase inhibited with ADP and magnesium fluoride

β_{TP} nucleotide binding sites both contained MgADP and MgF_3^- . The most unusual feature of the structure is found in the β_E subunit, which despite being in the open conformation contains ADP, but no magnesium, in its nucleotide binding site (Figure 4.8). Also, although the length of the a axis of the unit cell was reduced, the γ subunit was considerably disordered and only residues 1-47, 77-90 and 216-272 could be modelled into the density. There was no density corresponding to the δ and ϵ subunits. The residues of the subunits that have been built into the model are summarised in Table 4.5

Table 4.5 Summary of the residues of the subunits of F_1 -ATPase that are present in the F_1 - MgF_3^- model and of the bound substrates.

Subunit	Residues	Bound substrate
α_{TP}	23-401 and 413-510	ADP, Mg^{2+}
α_{DP}	25-510	ADP, Mg^{2+}
α_E	24-510	ADP, Mg^{2+}
β_{TP}	9-474	ADP- MgF_3^- , Mg^{2+}
β_{DP}	9-475	ADP- MgF_3^- , Mg^{2+}
β_E	9-474	ADP
γ	1-47, 77-90 and 216-272	None

4.1.7 The nucleotide binding sites

The nucleotide binding sites of β_{DP} and β_{TP} have adopted a very similar conformation. The rmsd for their P-loops is 0.16 Å compared with an rmsd of 0.33 Å for the β_{DP} and β_{TP} subunits in the reference structure. The P-loops in the reference structure adopt slightly different conformations as the nucleotide content is different (AMP-PNP in β_{TP} and ADP in

Chapter 4: The structure of bovine F_1 -ATPase inhibited with ADP and magnesium fluoride

β_{DP}). When the nucleotide content is the same, the two P-loops align more closely. The rms deviations for the β_{TP} and β_{DP} subunits for the $(ADP-AlF_4^-)_2-F_1$ and $BeF_3^-F_1$ structures are 0.14 Å and 0.09 Å, respectively. The MgF_3^- occupies the site where a proposed metaphosphate or phosphorane reaction intermediate would form during hydrolysis (Figure 4.11). This is the first structure of F_1 -ATPase to contain an accurate mimic of phosphoryl transfer, as MgF_3^- adopts the bond lengths and charge of a phosphorane intermediate (Graham *et al.*, 2002).

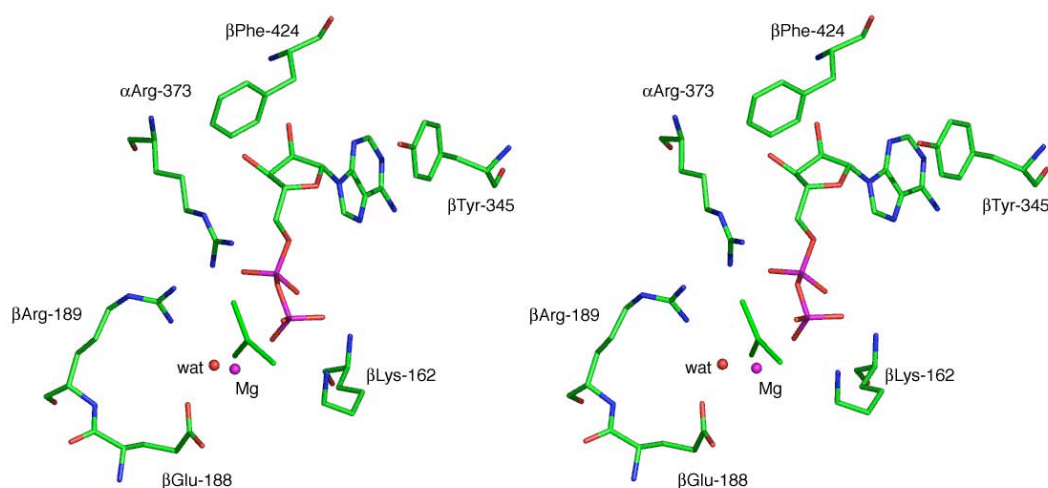


Figure 4.11 Stereo image of the catalytic site in the β_{TP} subunit. The catalytic and adenine binding residues are shown. The negatively charged magnesium fluoride is coordinated by the positively charged side chains of β Arg 189, β Lys 162 and α Arg 373. The attacking water molecule (wat) is coordinated by β Glu 188 and the magnesium of MgF_3^- . The adenine is held in place by β Phe 424 and β Tyr 345.

Chapter 4: The structure of bovine F_1 -ATPase inhibited with ADP and magnesium fluoride

The only major difference between the β_{DP} and β_{TP} catalytic sites is the absence of an attacking water in the β_{DP} site. The attacking water in the β_{TP} catalytic site has a peak of 3.5 σ in the initial difference (F_O-F_C) maps. Close inspection of the electron density at this level in the β_{DP} catalytic site gives no indication of an ordered water molecule coordinated between the magnesium of MgF_3^- and the β Glu-188. Water has not always been observed in the catalytic sites of previous structures. In the $F_1-MgF_3^-$ structure it is either present but disordered, so no density is calculated for it, or it may just not be present in the crystal.

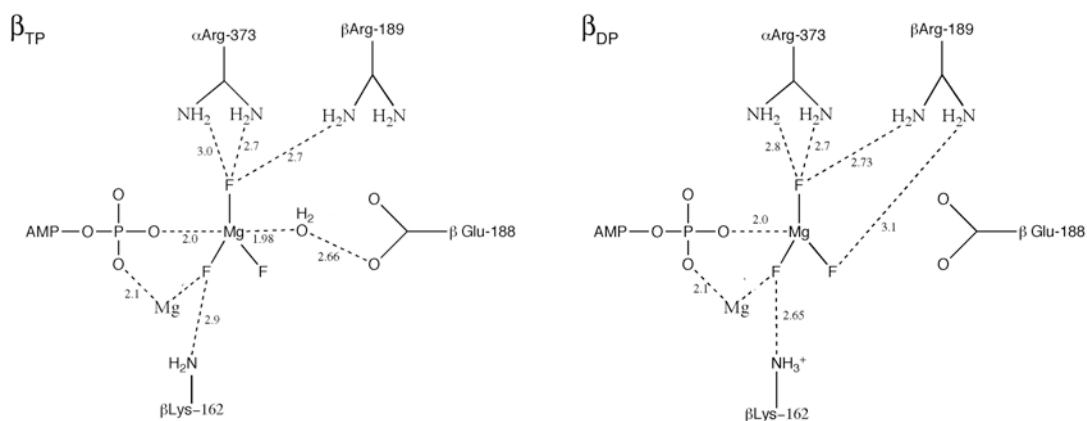


Figure 4.12 Schematic of the nucleotide binding sites of the β_{TP} and β_{DP} subunits. The two catalytic sites have very similar conformations and intermolecular distances are closely matched. Distances are shown in Ångstroms. Possible hydrogen bonds are shown as dotted lines.

The $F_1-MgF_3^-$ structure contains ADP in the β_E subunit nucleotide binding site, despite the open conformation that it adopts (Figure 4.13). There are very few structural differences between the $F_1-MgF_3^-$ structure β_E subunit and the β_E subunit in the reference structure. The most obvious difference is the conformation of β_E Phe-424, where the aromatic ring of the

side chain is positioned half way between the conformations observed in the β_{DP} (and β_{TP}) sites and in the β_E site of the reference structure, coordinating the adenine ring.

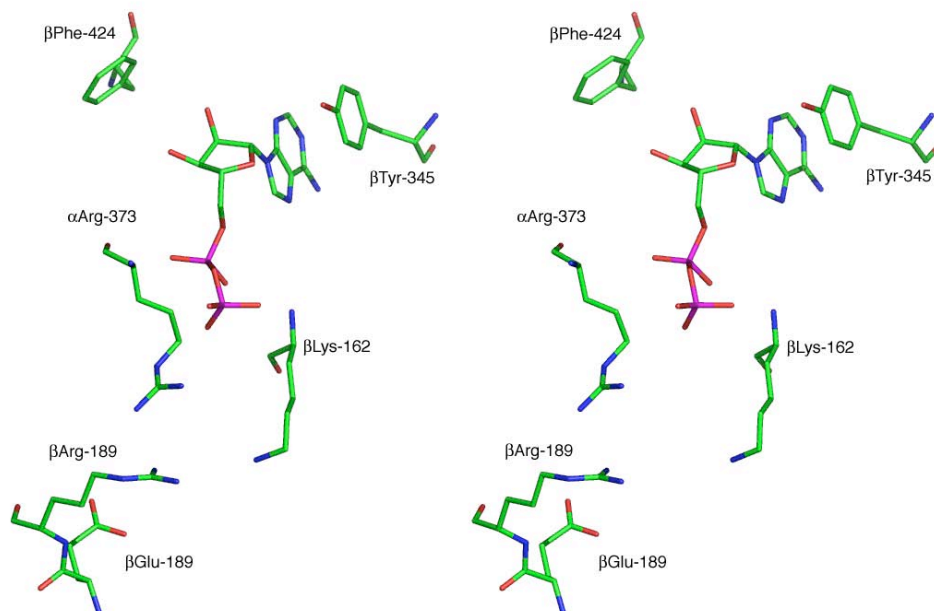


Figure 4.13 Stereo image of the β_E subunit in the F_1 - MgF_3^- structure. The β_E Phe-424 and β_E Tyr-345 side chains are in a similar position to the other catalytic sites. They form a hydrophobic binding pocket for the adenine ring. The side chains of β_E Arg-189, β_E Glu-188, β_E Lys-162 and α_E Arg-373 adopt dramatically different conformations, where the nucleotide phosphates are no longer coordinated (see Figure 4.11).

4.1.8 The nucleotide occupancy of F_1 -ATPase in crystal 22

The only other structure of bovine F_1 -ATPase determined so far that contains nucleotide in all three catalytic sites is the $(ADP-AlF_4^-)_2$ - F_1 structure (Menz *et al.*, 2001b). Exactly why the nucleotide is bound to the β_E subunit in the F_1 - MgF_3^- structure is unclear. The smaller a axis of the unit cell could lead to increased lattice contacts, which may

Chapter 4: The structure of bovine F_1 -ATPase inhibited with ADP and magnesium fluoride

influence the nucleotide binding pocket. To test this theory, the data set taken from crystal 22 (X22) was processed and the structure was solved. This crystal had an a axis dimension of 278 Å (7 Å longer than in X2) and contained magnesium fluoride. The data were of low quality, but if the β_E subunit contained nucleotide, then positive density should be observed.

After processing, the data were 60% complete. The structure was solved by molecular replacement as before, but using the refined F_1 - MgF_3^- coordinates (with MgF_3^- and the β_E nucleotide removed) as a search model. After one round of refinement, the R factor was 29% and the free R factor was 37%. Electron density maps were calculated and inspected for positive density in the β_E subunit.

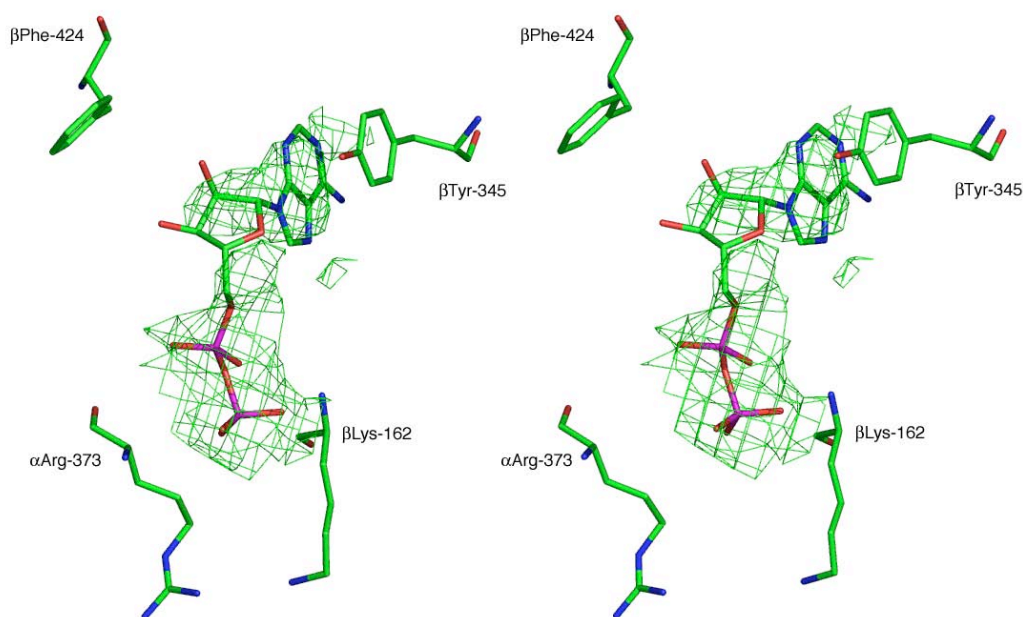


Figure 4.14 Stereo image of the difference electron density found in the β_E subunit of crystal 22. The β_E nucleotide from the F_1 - MgF_3^- structure (crystal 2) was aligned with the X22 structure and fitted the density well. The F_O - F_C map is shown contoured at 2σ .

Chapter 4: The structure of bovine F_1 -ATPase inhibited with ADP and magnesium fluoride

The difference density clearly showed positive peaks for nucleotide (Figure 4.14). The β_{TP} and β_{DP} subunits both contain MgADP-MgF₃⁻ and the structure is very similar to the X2 crystal structure. This result indicates that nucleotide binding to the β_E subunit is a function of the inhibitor rather than being influenced by crystal contacts. This aspect is discussed further in the following section.

4.2 Discussion

4.2.1 Comparison of the F_1 - MgF_3^- structure with previously solved structures.

In some respects the F_1 - MgF_3^- structure is similar to the reference structure and many of the other solved structures of bovine F_1 -ATPase (Abrahams *et al.*, 1996; Abrahams *et al.*, 1994; Braig *et al.*, 2000; Gibbons *et al.*, 2000; Orriss *et al.*, 1998; van Raaij *et al.*, 1996a). The individual subunits adopt similar conformations and the overall structures superimpose with small deviations. However, the catalytic sites in the β_{TP} and β_{DP} subunits are more closely matched to the $(ADP-AlF_4^-)_2-F_1$ structure (Figure 4.15). This structure contained a square planar AlF_4^- in the catalytic sites in the β_{TP} and β_{DP} subunits, mimicking the transition state of hydrolysis of the γ phosphate.

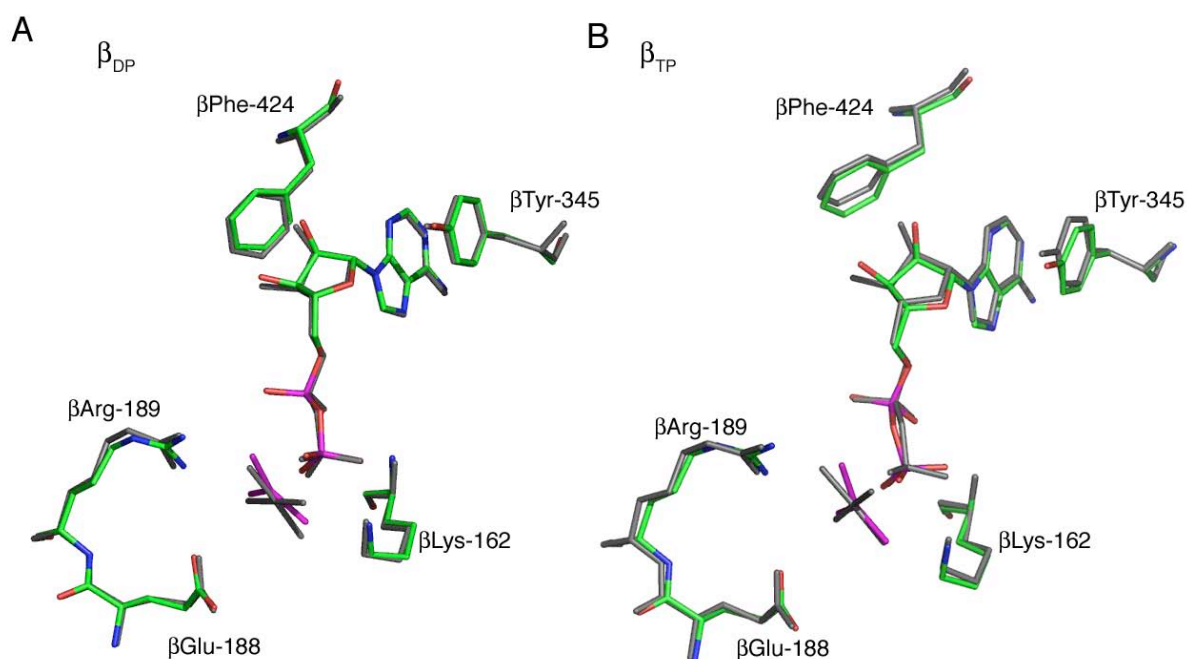


Figure 4.15 Superimposition of the nucleotide binding sites of the β_{DP} and β_{TP} subunits from the F_1 - MgF_3^- and $(ADP-AlF_4^-)_2-F_1$ structures. **A:** Superimposition of the β_{DP} sites of the F_1 - MgF_3^- (coloured) and $(ADP-AlF_4^-)_2-F_1$ (grey) structures. **B:** Superimposition of the β_{TP} sites of the F_1 - MgF_3^- (coloured) and $(ADP-AlF_4^-)_2-F_1$ (grey) structures. Very little deviation is observed in the positions of nucleotides, side chains or metallofluorides.

Chapter 4: The structure of bovine F_1 -ATPase inhibited with ADP and magnesium fluoride

The C α atoms of the P-loops of these subunits in the two structures superimpose with rms deviations of 0.16 Å (β_{TP}) and 0.15 Å (β_{DP}). The positions of the metallofluorides and coordinating residues also correspond closely (Figure 4.15). Both the ADP-AlF $_4^-$ and ADP-MgF $_3^-$ species mimic the reaction intermediate of phosphoryl transfer. It is largely unknown whether this is an associative, a dissociative or a mixed reaction (see Section 1.5.1), but in both cases the transition state will be trigonal bipyramidal; ADP-AlF $_4^-$ and ADP-MgF $_3^-$ mimic this state. However, ADP-MgF $_3^-$ is a much more accurate analogue than AlF $_4^-$, as it has both the geometry and charge of a phosphoryl transfer intermediate (Graham *et al.*, 2002). The distances between the magnesium of MgF $_3^-$ and the bridging oxygen of ADP and the attacking water are similar to those that would be found in an associative mechanism. However, by placing a phosphorane analogue in the active site, the distances will, to some extent, be forced into these values.

The catalytic sites containing AlF $_4^-$, AlF $_3$, BeF $_3^-$ and MgF $_3^-$ all superimpose well. This similarity is despite significant differences in shape, size and distances in the apical atoms between the metallofluorides. The active site seems to be able to accommodate all of these species, with very little energetic cost, facilitating the hydrolytic, or synthetic, reaction stages.

The β_{DP} catalytic site has been characterised as the catalytically active site by the tighter binding of nucleotide (Abrahams *et al.*, 1994), the binding of AlF $_3$ in the β_{DP} site alone (Braig *et al.*, 2000), and the position of the attacking water in the BeF $_3^-$ -F $_1$ structure (Kagawa *et al.*, 2004). This interpretation is also supported by molecular dynamics simulations (Gao *et al.*, 2003). Thus, it is odd that there is no ordered attacking water in this site in the F $_1$ -MgF $_3^-$ structure.

Although there is a close correspondence between the β_{TP} and β_{DP} subunits in the (ADP-AlF $_4^-$) $_2$ -F $_1$ and F $_1$ -MgF $_3^-$ structures, they differ significantly in the conformation of the β_E subunits (Figure 4.16). In the (ADP-AlF $_4^-$) $_2$ -F $_1$ structure, the β_E subunit adopts a

Chapter 4: The structure of bovine F_1 -ATPase inhibited with ADP and magnesium fluoride

half-closed conformation and binds MgADP and sulphate (the latter mimicking orthophosphate). In the F_1 -MgF₃⁻ structure, the β_E subunit is in the open conformation and it binds ADP only. The rmsd between these β_E subunits is 0.9 Å. This value is less than the value of 1.44 Å for the reference structure and the (ADP-AlF₄⁻)₂-F₁, suggesting that the β_E subunit in the F_1 -MgF₃⁻ structure is intermediate between them. No sulphate or phosphate was present in the crystallisation buffers; therefore, it is not known whether phosphate can bind to the P-loop region of the β_E subunit in this state. It is possible that the binding of phosphate, or an analogue, will cause the half-closed conformation to form in ADP-MgF₃⁻ inhibited F_1 -ATPase.

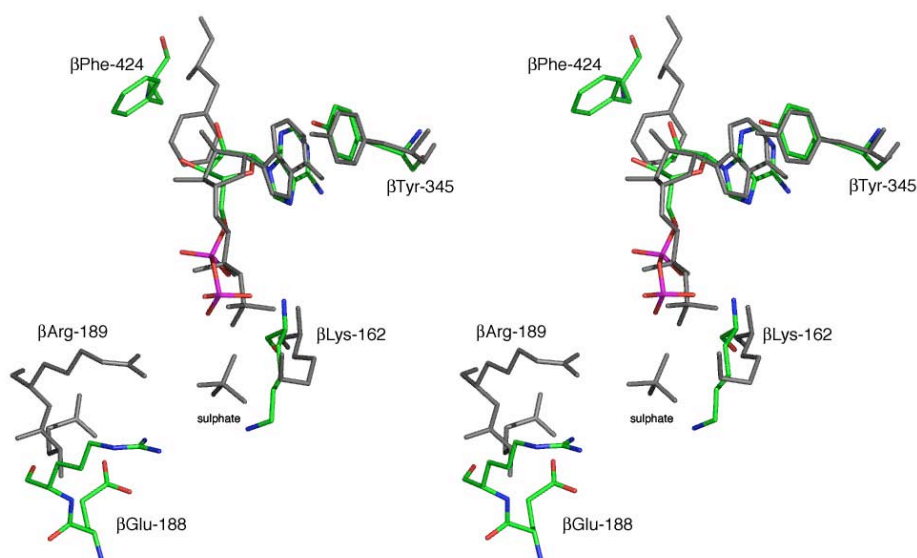


Figure 4.16 Stereo image of the superimposed β_E subunits of F_1 -MgF₃⁻ (coloured) and (ADP AlF₄⁻)₂-F₁ (grey) structures. The nucleotide and β Tyr-345 align well. The β Phe-424 side chain in the F_1 -MgF₃⁻ subunit is much further away from the adenine ring and the β Glu-188 and β Arg-189 side chain are in a similar conformation to the β_E subunit of the reference structure. Subunits were aligned on C α atoms of the P-loop residues (155 to 165).

4.2.2 The catalytic sites

While the rms deviations for the β_{DP} and β_{TP} catalytic sites are low, there are subtle differences in the positions of side chains in the site (Figure 4.17). The ADP and MgF_3^- molecules align well, as do most of the side chains of catalytic residues. However, the guanidinium group of the α Arg-373 in the β_{DP} site is about 1 Å closer to the MgF_3^- than in the β_{TP} subunit (Figure 4.17).

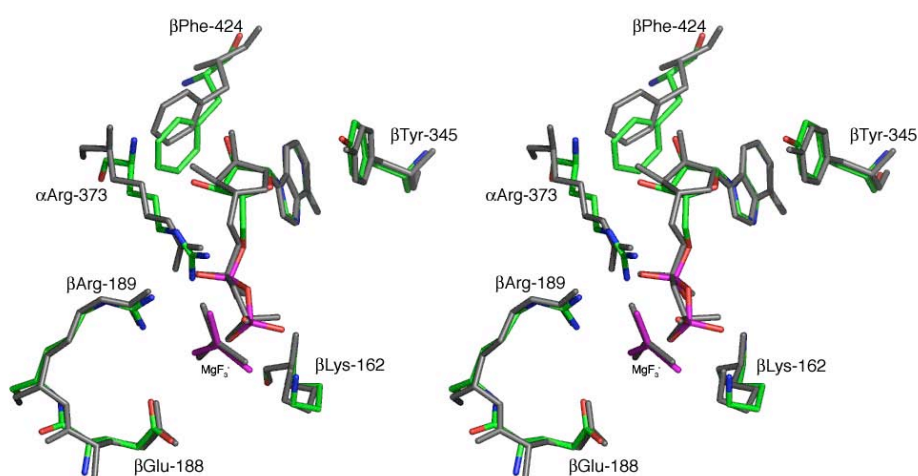


Figure 4.17 Stereo image of the superimposed β_{TP} (grey) and β_{DP} (coloured) catalytic sites from the F_1 - MgF_3^- structure. The α Arg-373 side chain of α_{DP} is about 1 Å closer to the MgF_3^- than the α Arg-373 side chain of α_{TP} .

Such a shift in the position of the guanidinium group of the α Arg-373 has been noted in the previously solved structures of $(ADP AlF_4^-)_2$ - F_1 and BeF_3^- - F_1 . This arrangement indicates that the β_{DP} site is catalytically active. It is interesting to note that only very small changes are required in the arrangement of side chains to effect large changes to the activity of the catalytic site. This was best illustrated by the BeF_3^- - F_1 structure. The only significant

difference between the β_{TP} and β_{DP} subunits was the shift in the α Arg-373 side chain. This shift caused a dramatic change in the position of the attacking water, the β_{DP} water being over 1 Å closer to the γ phosphate site than in the β_{TP} subunit (Kagawa *et al.*, 2004). It is unfortunate that the attacking water is not resolved in the β_{DP} subunit of the F_1 -MgF₃⁻ structure, enabling any differences in the positions to be resolved. This is the first structure of bovine F_1 -ATPase to contain a true analogue of phosphoryl transfer and enables the coordination of a negatively charged trigonal planar species to be observed in the catalytic sites.

4.2.3 Why does the β_E subunit bind nucleotide?

The β_E subunit in the F_1 -MgF₃⁻ structure binds ADP, but not magnesium. The conformation of this subunit is essentially the same as the in the reference structure (Abrahams *et al.*, 1994) which is in the ‘open’ state with an apparent low affinity for nucleotide. Could the concentration of nucleotide affect the occupancy in the crystals? The concentration of ADP in the crystallisation buffers was 50 μ M. This is 100 fold lower than the physiological concentration of nucleotide in the mitochondrial matrix and cannot be considered to be a ‘high’ concentration. Many other structures of the bovine F_1 -ATPase have been solved in similar concentrations of nucleotide without any observed binding of nucleotide to the β_E subunit. It has also been shown that raising the concentration of AMP-PNP to 5 mM does not affect the nucleotide occupancy of the enzyme and the β_E subunit remained unoccupied (Menz *et al.*, 2001a). The crystals of F_1 -ADP were grown in the presence of 2 mM ADP; again, the β_E subunit in this structure remained unoccupied by nucleotide (Kagawa *et al.*, 2004). Therefore, it is unlikely that the concentration of nucleotide affects the occupancy of the β_E subunit.

Chapter 4: The structure of bovine F_1 -ATPase inhibited with ADP and magnesium fluoride

Another factor to be considered is the smaller a axis of the unit cell which could lead to increased lattice contacts and thus influence the affinity of the β_E subunit for nucleotide. The $(ADP AlF_4^-)_2$ - F_1 structure contains nucleotide in the β_E subunit and has an a axis of 267.7 Å, compared to previously solved structures that have values of ca 280 Å (Braig *et al.*, 2000; Kagawa *et al.*, 2004; Menz *et al.*, 2001a; Orriss *et al.*, 1998). However, the F_1 -DCCD crystal (Gibbons *et al.*, 2000) had an a axis of 267.2 Å and no nucleotide was bound to the β_E subunit. The absence of nucleotide from the β_E subunit could have been influenced by the inhibitor (DCCD) or by different lattice contacts in the crystals. The presence of ADP in the β_E subunit of crystal 22 (X22) (see Section 4.1.8) does not support the suggestion that lattice contacts influence the nucleotide occupancy of the β_E subunit. This crystal had a crystallographic a axis of 278.6 Å, sufficiently similar to the 'normal' a dimension to distinguish whether nucleotide binding is influenced by lattice contacts.

One remaining possible explanation of nucleotide binding to the β_E subunit is that it is connected to the presence of transition state analogues in the β_{DP} and β_{TP} catalytic sites. The only structures that bind nucleotide in the β_E subunit contain either AlF_4^- or MgF_3^- in both the β_{TP} and β_{DP} subunits. The ADP beryllium fluoride inhibited structure has BeF_3^- in these subunits but no nucleotide in the β_E subunit. However, ADP BeF_3^- mimics the 'ground-state' of the γ phosphate, it is not a transition state analogue. The corollary is that the transition state analogues fix the β_{TP} and β_{DP} subunits into a conformation that somehow transmits structural changes to the β_E subunit causing it to bind nucleotide.

How this communication could be achieved is unclear. The γ subunit provides the means of interconverting the binding affinities of the β -subunits. In the $(ADP AlF_4^-)_2$ - F_1 structure, the γ subunit has rotated by 1° at its C-terminus and by 30° in the α -helical coiled coil region. This rotation results in a greater extent of twisting of the subunit than in the reference structure. This twisting accompanies the change in the β_E from the open to the

Chapter 4: *The structure of bovine F₁-ATPase inhibited with ADP and magnesium fluoride*

half-closed state. However, this twisting does not entirely explain the presence of the half closed state. Superimposition of the β_{TP} and β_{DP} subunits from the $(ADP AlF_4^-)_2-F_1$ structure and the reference and other structures shows they are very similar, implying that the large movements seen in the half-closed state can occur without accompanying large changes to the other β subunits. In another unpublished crystal structure of F_1 -ATPase, both the open and half closed states are observed in the β_E subunit (Bartoschek, S., Contessi, S., Montgomery, M. G., Leslie, A. G. W. and Walker, J. E. unpublished results). As the crystals were grown under the standard conditions used for growing the crystals for determining the reference structure, it appears to be easy for the β_E subunit to convert between the open and half closed states.

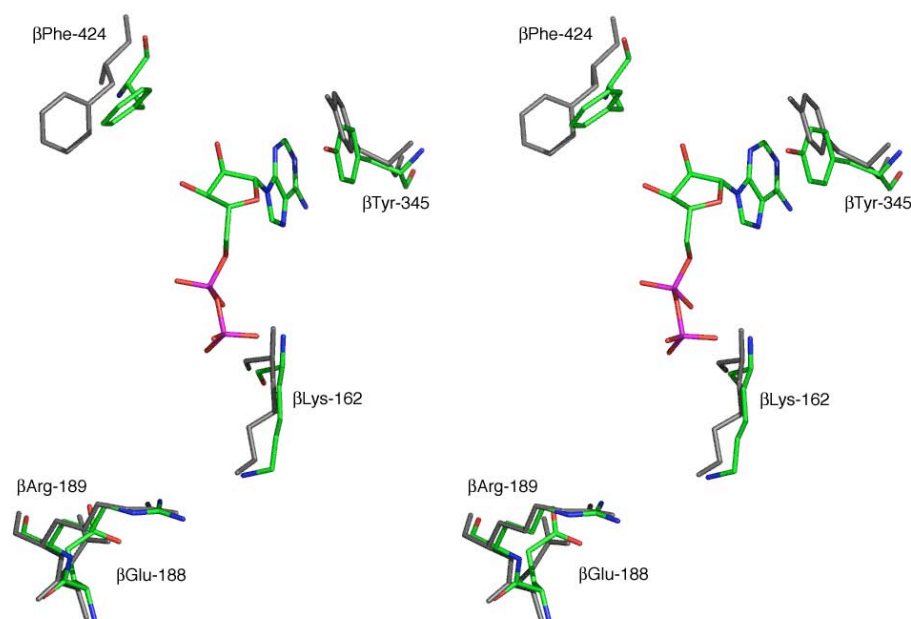


Figure 4.18 Stereo image of the superimposed β_E subunits of the reference structure (grey) and the $F_1-MgF_3^-$ structure (coloured). The residues align closely apart from β Phe-424 and β Tyr-345. In the $F_1-MgF_3^-$ β_E subunit these residues are closer, and aligned with, the adenine ring of ADP.

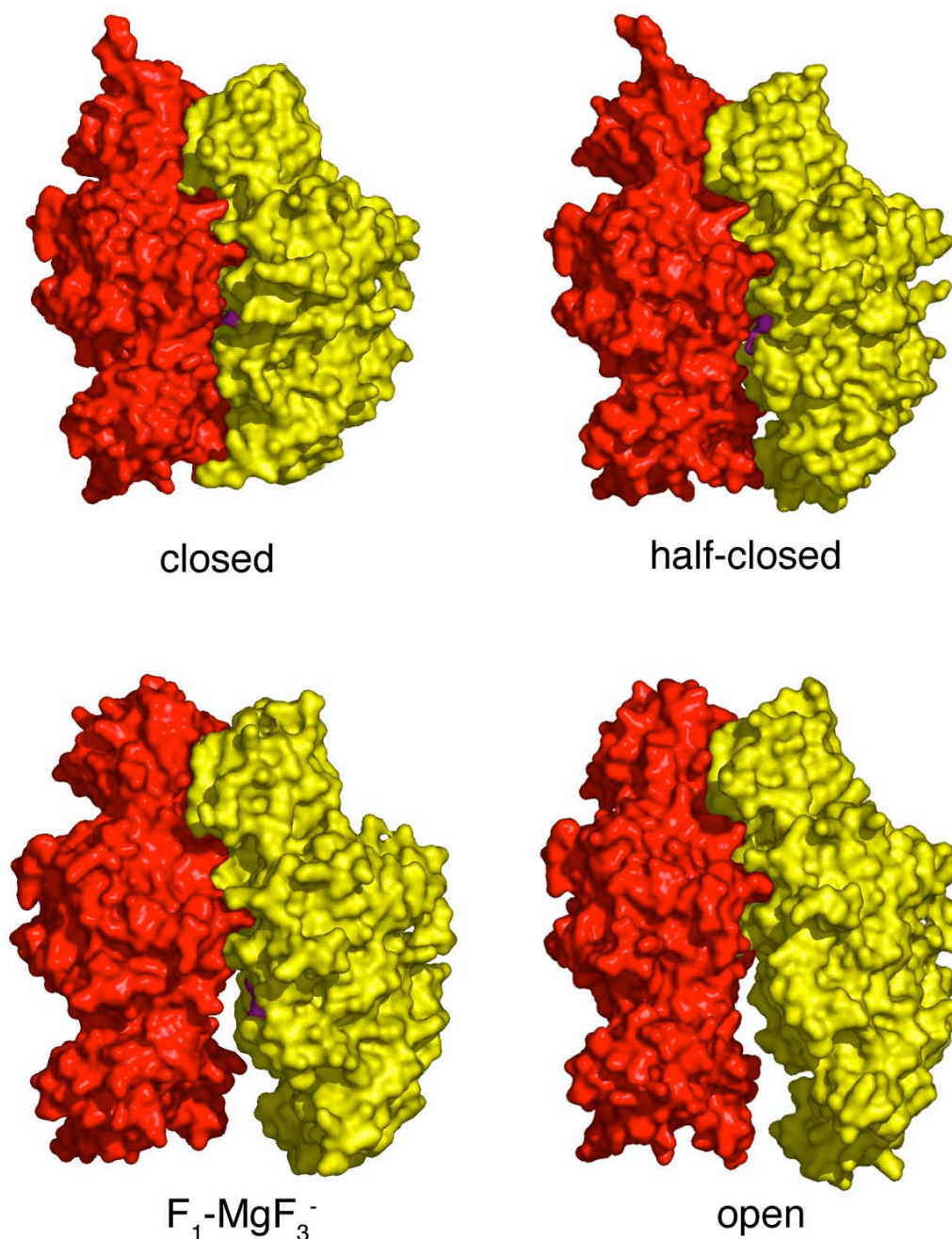


Figure 4.19 Surface representation of the interfaces between α and β subunits in various structures of bovine mitochondrial F_1 -ATPase. The α subunits are red and the β subunits are yellow, the nucleotide surface is coloured magenta. The transition between closed and open states is shown. The closed state is the α_{DP} - β_{DP} interface from the reference structure. The half-closed state is the α_E - β_E interface from the $(\text{ADP AlF}_4^-)_2\text{-F}_1$ structure. The $F_1\text{-MgF}_3^-$ state is the α_E - β_E interface from the $F_1\text{-MgF}_3^-$ structure, where the nucleotide binding pocket is slightly more occluded than in the open state. The open state is represented by the α_E - β_E interface in the reference structure.

Chapter 4: The structure of bovine F_1 -ATPase inhibited with ADP and magnesium fluoride

The twisting observed in the γ subunit of the $(\text{ADP AlF}_4^-)_2\text{-F}_1$ structure may be caused by lattice contacts. In the $\text{F}_1\text{-DCCD}$ structure, a rotation of 20° is seen in the γ subunit. As this crystal also has a shrunken cell, it may be the cause of the rotation of the γ subunit. The γ subunit in the $\text{F}_1\text{-MgF}_3^-$ structure adopts essentially the same conformation as in the reference structure. Despite the shrunken cell, the lower portion of the γ subunit was disordered and no corresponding electron density was observed for it. Because the a dimension of the unit cell has increased by ca 3 Å it may be that the γ subunit has freedom to adopt a range of conformations in this region.

As the γ subunit has the same conformation as the reference structure, it is not immediately obvious how it could affect the β_E subunit and lead to it binding nucleotide. The reference, $\text{BeF}_3^-\text{-F}_1$ and $\text{F}_1\text{-MgF}_3^-$ structures were aligned on their six N-terminal domains (which vary very little between structures). The rms deviations were about 1 Å. Comparison of the β_E subunits from these structures after this alignment showed that they were very similar. However, there are subtle differences in the structures of β_E subunits (Figures 4.18 and 4.19), most notably a 2.4° rotation, relative to the reference structure, of the C-terminal α -helical region of the β_E subunit towards the γ subunit.

Two of the residues that form the adenine binding pocket have different positions in the $\text{F}_1\text{-MgF}_3^-$ structure relative to the β_E subunit of the reference structure. In the $\text{F}_1\text{-MgF}_3^-$ structure the side chain of $\beta\text{Tyr-345}$ is twisted towards and aligned with the adenine ring. The side chain and main chain atoms of $\beta\text{Phe-424}$ are much closer than in the reference structure to the adenine ring, providing a hydrophobic binding pocket. Whether these residues have moved closer to the adenine ring as a result of structural changes in the β_{DP} and β_{TP} subunits or whether the fit is induced by the presence of ADP cannot be determined at present. Surface representations of α and β subunit interfaces are shown in Figure 4.19. From these figures it can be seen that the interface is slightly more occluded in the $\text{F}_1\text{-MgF}_3^-$

Chapter 4: The structure of bovine F_1 -ATPase inhibited with ADP and magnesium fluoride

structure than in the reference structure. This is due to a 2.4° rotation of the C-terminal α -helices towards the γ subunit. The same domain is rotated 16° in the $(\text{ADP AlF}_4^-)_2\text{-F}_1 \beta_E$ subunit relative to the reference structure β_E subunit and by 13° relative to the $\text{F}_1\text{-MgF}_3^- \beta_E$ subunit. This small rotation of the C-terminal domain leads to a slightly tighter $\alpha_E\text{-}\beta_E$ interface and may increase the affinity of the β_E subunit for nucleotide.

In all previously solved structures of bovine mitochondrial F_1 -ATPase, a sulphate has been found bound to the β_E subunit in a position normally occupied by the β phosphate of nucleotide in the other subunits. The sulphate in this site could compete with nucleotide as the concentration is much higher (20 mM) than ADP (50 μM). The $\text{F}_1\text{-MgF}_3^-$ structure is the first to be solved in the absence of sulphate. Therefore, it is possible that the sulphate in the β_E subunit of the previously solved structures is preventing ADP binding. Further experiments will be required to test this hypothesis.

4.2.4 Implications for the catalytic mechanism

Does the $\text{F}_1\text{-MgF}_3^-$ structure represent a step in the catalytic mechanism of F_1 -ATPase and, if so, how does it fit into the catalytic schemes proposed based on crystallographic evidence and on other methods? That the three sites can bind nucleotide simultaneously has been shown by a variety of methods (Menz *et al.*, 2001b; Nishizaka *et al.*, 2004; Weber *et al.*, 1996). The $\text{F}_1\text{-MgF}_3^-$ structure can be interpreted as representing a new step in the catalytic cycle immediately following the half-closed step when ADP and Pi are bound (represented by the β_E subunit of the $(\text{ADP AlF}_4^-)_2\text{-F}_1$ structure). The present structure might suggest that phosphate is released before ADP, but as no phosphate or analogue was present in the crystallisation buffers, this is a tentative suggestion requiring more experimental investigation. A sulphate was found bound in the β_E subunit of many of the previously solved

Chapter 4: The structure of bovine F_1 -ATPase inhibited with ADP and magnesium fluoride

structures, but it is bound to the site occupied by the β phosphate of ADP, rather than in a site associated with the γ phosphate.

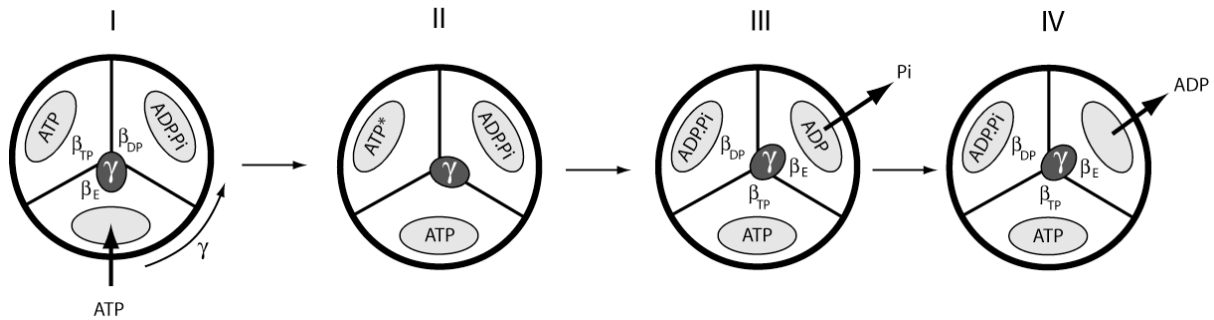


Figure 4.20 A possible reaction scheme for ATP hydrolysis taking the F_1 - MgF_3^- structure into account. The F_1 -ATPase is viewed from the membrane. Only the β and γ subunits are shown. I: Binding of ATP causes an 80° rotation of the γ subunit committing the ATP in the β_{TP} subunit to hydrolysis (ATP^*). II: A further rotation of the γ subunit (40°) hydrolyses ATP and causes the conversion of the β_{DP} subunit to the β_E subunit. III: Phosphate is released before ADP (represented by the F_1 - MgF_3^- structure). IV: Further catalytic events, and possible movements of the γ subunit, lead to the release ADP. [After (Kagawa *et al.*, 2004)].

A sequence of states in the catalytic cycle, based on solved structures, has been proposed [Figure 4.20 (Kagawa *et al.*, 2004)]. State I is represented most closely by the $(ADP \cdot AlF_3)$ - F_1 structure (Braig *et al.*, 2000) which contains AMP-PNP in the β_{TP} subunit and ADP and AlF_3 in the β_{TP} subunit. The distances between the AlF_3 and the attacking water and β phosphate oxygen are quite large (3.4 \AA). State II was proposed to be represented by the $(ADP \cdot AlF_4^-)$ - F_1 structure. However, as the γ subunit in this structure is twisted, relative to the reference structure, it also represents state III to some extent (with ADP and P_i bound). Thus, the structure probably represents a state intermediate between II and III. The two sites

Chapter 4: The structure of bovine F_1 -ATPase inhibited with ADP and magnesium fluoride

occupied by ATP in state II may, therefore, be better represented by the β_{TP} and β_{DP} subunits of the F_1 - MgF_3^- structure. The γ subunit is not twisted in this structure and the MgF_3^- mimics the transition state between ATP and ADP and phosphate accurately. In state III, partly represented by the $(ADP AlF_4^-)_2$ - F_1 structure, the next step is the opening of the half closed state. This opening is achieved by the rotation of the C-terminal α -helical region of the β_E subunit by 16° . Bound phosphate and magnesium may be released first, as the rotation removes α Arg-373 and β Arg-189, which coordinate the γ -phosphate, from the nucleotide binding site (Figure 4.16). Subsequent catalytic changes or movement in the γ subunit would then lead to the ADP remaining in the β_E subunit to being released (state IV).

4.3 Conclusion

The crystallisation of bovine F_1 -ATPase with ADP and magnesium fluoride has shown, for the first time, the nature of the catalytic sites when an accurate analogue of phosphoryl transfer is present. This structure has also revealed a new sub-step in the catalytic cycle of the enzyme, after ATP hydrolysis and release of phosphate and magnesium, but before ADP release. It will be interesting to see if crystallisation of the ADP and magnesium fluoride inhibited enzyme in the presence of phosphate (or an analogue) produces the half-closed state of the β_E subunit seen in the $(ADP AlF_4^-)_2$ - F_1 structure. The major sub-step within the cycle yet to be resolved is that with the γ subunit in an intermediate state between states I and II in Figure 4.20. Further experiments with different inhibitors and reaction

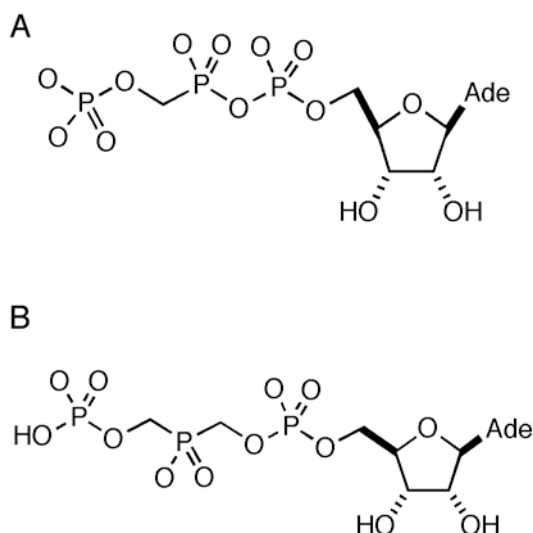


Figure 4.21 Stable transition state analogues of ATP. **A:** ATP analogue with the β - γ phosphate bridging oxygen replaced by a CH₂-O group. **B:** An ATP analogue with both the α - β and β - γ bridging oxygens replaced by CH₂-O groups. The species are larger than ATP but the β -subunit catalytic sites would probably accommodate the extra bond lengths. [Figure courtesy of Prof. M. Blackburn, Krebs Institute, Department of Chemistry, University of Sheffield.]

intermediate analogues may reveal the crystal structure of this part of the catalytic cycle. It is still unclear how cooperativity between the β -subunit catalytic sites is mediated. Communication occurs via the γ and α subunits but the mechanism must be extremely subtle. A film, currently being produced, morphing together the crystal structures that represent steps in the catalytic cycle, may demonstrate the structural basis of this communication.

Many analogues and inhibitors remain to be co-crystallised with bovine mitochondrial F₁-ATPase. These include stable analogues of ATP that may mimic a transition state (Figure 4.21). The introduction of a carbon between the β and γ phosphates [and between the α and β phosphates (Figure 4.21 B)] prevents hydrolysis of the phosphates but retains the stereochemistry of ATP. These molecules are larger than ATP but the β -subunit catalytic

Chapter 4: The structure of bovine F_1 -ATPase inhibited with ADP and magnesium fluoride

sites appear to be able to accommodate many different sizes of nucleotide analogues. Crystallisation with other phosphate analogues, such as nitrate [which has been shown to mimic a metaphosphate reaction intermediate (Cook *et al.*, 2002) and has been shown to inhibit ATP hydrolysis by F_1 -ATPase (Ebel and Lardy, 1975)] or pyrophosphate, may reveal further insights into how the process of generation of mechanical energy from chemical energy is achieved.

Appendix A: Crystallographic theory

A.1 Introduction

The interpretation of the diffraction patterns of X-rays by metals and salts by Max von Laue and Peter Ewald instituted the study of molecular structure by X-ray diffraction. The work of Lawrence and William Bragg (Bragg and Bragg, 1913) on the reflection of X-rays by crystals produced ‘Bragg’s law’ (Equation A.1, discussed in Section A.5) and led to the solution of inorganic salt structures.

$$2d \sin \theta = \lambda \quad (A.1)$$

The analysis of biological molecules by X-ray diffraction began with W. T. Astbury’s investigations of fibrous molecules (wool, silk and keratin); the classification of the diffraction into either α or β patterns was the first glimpse of the secondary structure of proteins (Astbury, 1933). At this time the methods used to purify globular proteins had become sophisticated enough to allow sufficient purity for crystallisation, the most famous example being haemoglobin. The initial analysis of these crystals, by Max Perutz, led to the prediction of the presence of α -helical rods (Boyes-Watson *et al.*, 1947) and the development of isomorphous replacement, the technique that enabled the first structure of a globular protein to be solved (Green *et al.*, 1954). The structure of myoglobin followed in 1957 (Kendrew *et al.*, 1958) and lysozyme, the first enzyme structure, was solved in 1965 (Blake *et al.*, 1965). Since then, the development of recombinant protein techniques combined with advances in structural analysis such as molecular replacement (Rossman and Blow, 1962),

anomalous dispersion (Hendrickson, 1991) and synchrotron radiation, have allowed the number of structures solved per year to increase almost exponentially.

A.2 X-ray sources

A.2.1 Rotating anode X-ray tubes

Most 'in-house' X-ray diffraction experiments are performed on a rotating anode X-ray tube that produces copper K_{α} X-rays (Figure A.1).

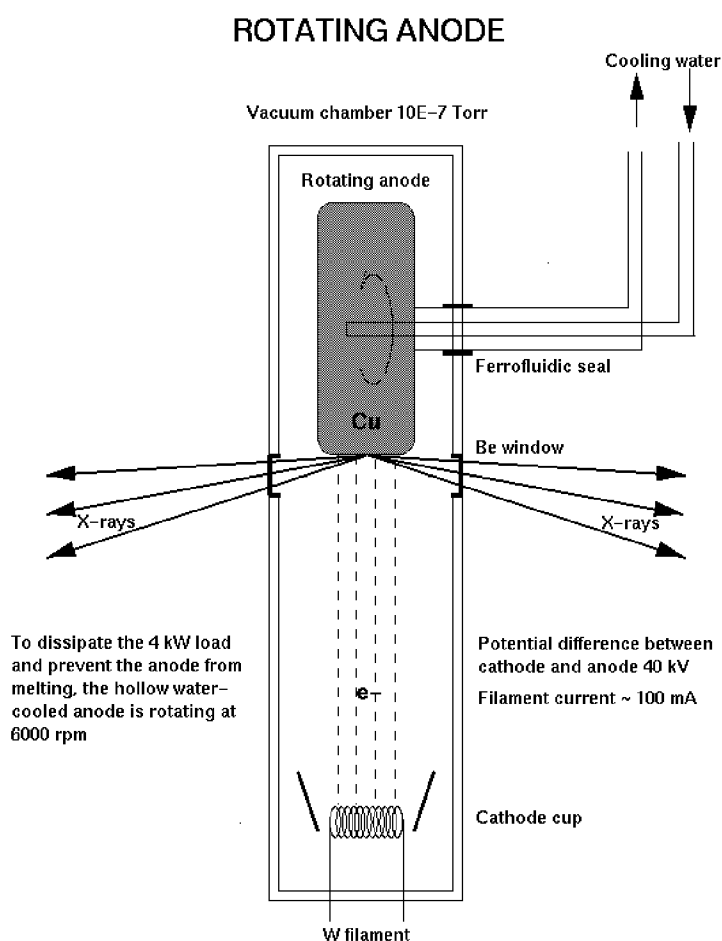


Figure A.1 Schematic of a rotating anode X-ray tube. Electrons are emitted towards the anode and strike at a high speed. Most energy is released as heat and is removed by cooling the anode with water. The remaining energy is emitted as X-rays.

X-rays are produced by firing electrons from a tungsten cathode at a copper anode. As the electrons strike the anode, most of the energy is dissipated as heat (anodes require water cooling) but some electrons displace copper electrons to higher orbitals. As other electrons move down to replace the displaced electrons, energy is released in the form of X-rays with characteristic wavelengths: K_{α} and K_{β} X-rays (Figure A.2). The anode is rotated to constantly present a fresh surface to the electron beam, so that more electrons can be fired at the target leading to higher brilliance of the X-rays emitted. Rotation is necessary as water cooling cannot remove heat quickly enough from the focal spot. Without rotation the anode would melt.

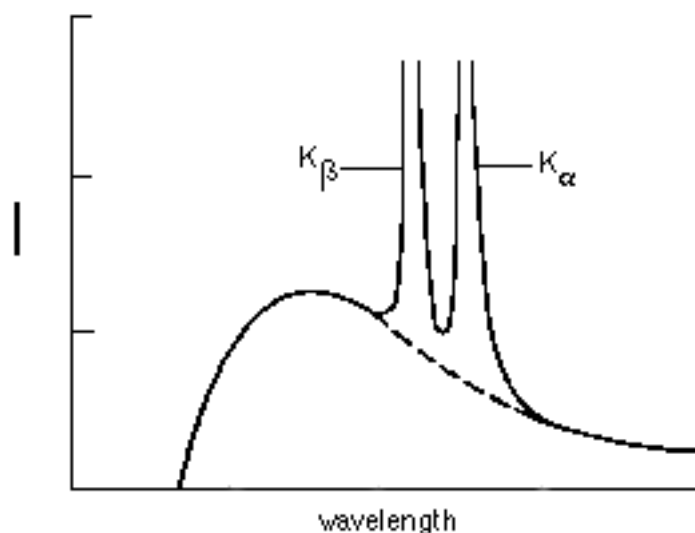


Figure A.2 The X-ray spectrum generated by a copper anode bombarded with electrons. X-rays are emitted over a range of wavelengths, but there are two high intensity peaks (the K_{α} and K_{β} peaks). I is intensity on an arbitrary scale.

Only the K_{α} doublet ($\lambda=1.5418 \text{ \AA}$) is used for diffraction experiments. The K_{β} radiation is removed by passing the beam through a nickel filter. Alternatively, the X-rays are then passed through a monochromator. In rotating anode generators, this is usually

graphite. The planes of carbon atoms reflect X-rays with a wavelength of 1.5418 Å. This produces a beam of X-rays at a single wavelength. Modern generators contain X-ray mirrors (made of highly polished glass or quartz covered in a thin layer of either gold or platinum) that both focus and monochromatise the beam.

A.2.2 Synchrotron radiation

Synchrotron radiation has many advantages over in-house X-rays. The beams produced are more intense than rotating anode generators by several orders of magnitude. Synchrotrons circulate charged particles (usually electrons) in a large ring. Originally used as particle colliders to study, for example, electron positron elimination, it was found that when the charged particles change direction, radiation is emitted. This radiation was a by product of the collider experiments, but the potential of this radiation in structural biology was harnessed by the construction of synchrotrons specifically for this radiation (Rosenbaum *et al.*, 1971). The ring is more accurately described as short, straight sections, with the direction being changed by bending magnets (Figure A.3). The rings have a diameter between 10 and 100 meters. There are four types of magnet in a synchrotron:

1. Bending magnets – These magnets guide the electrons around the ring and produce radiation in the process. Other magnets are placed in the straight sections and are referred to as insertion devices (2 to 4).
2. Wavelength shifters – These magnets introduce a sharper bend in the particle trajectory and a stronger magnetic field than bending magnets before returning particles to their original trajectory. The beam produced is generally more intense and has a shorter wavelength.

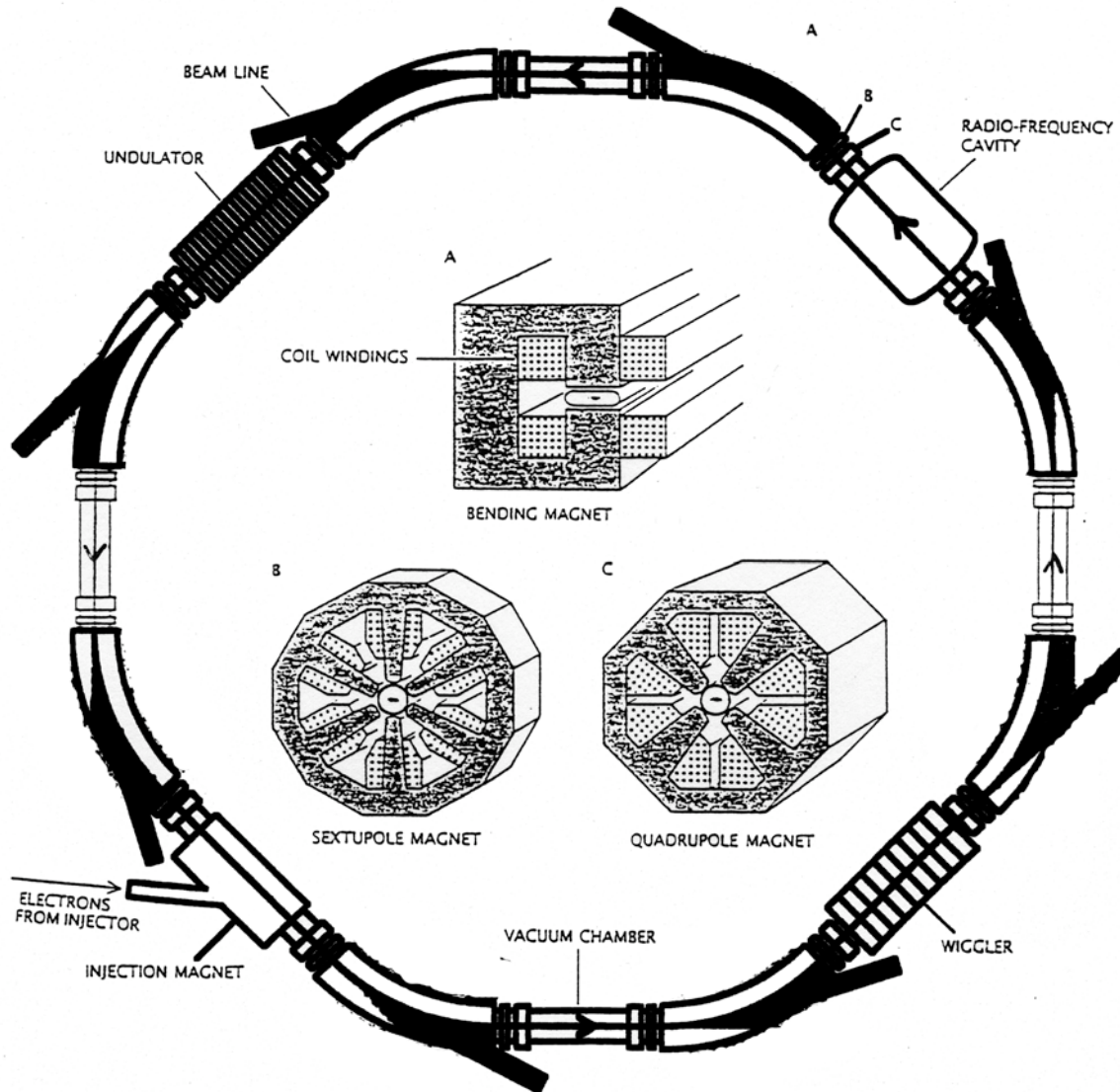


Figure A.3 Schematic of the electron storage ring of a synchrotron. Bending magnets (corners) keep the electrons in a circular path. As the electrons change direction synchrotron radiation, utilised at beamlines, is emitted. Insertion devices (undulators, wigglers and wavelength shifters) are placed between bending magnets and they also emit radiation.

3. Wigglers – They are essentially many wavelength shifters in a row. The beams produced have a higher flux. Constructive interference between the radiation emitted at each change of direction produces a broad band of wavelengths. Wavelengths can be selected by using different monochromators.
4. Undulators – These devices are wigglers with lower magnetic field strength, but with a larger number of poles at more frequent intervals. The radiation produced is more intense, tuneable and has lower beam divergence. The wavelength is changed by changing the gap between the magnets above and below the beam.

Synchrotron radiation has many advantages over in-house generators, the greatest of which is the intensity of the beam. This is extremely useful for protein crystallography where crystals generally diffract weakly. The other advantage of synchrotron radiation is the tunability of the wavelength; this function is used in Multiple wavelength Anomalous Dispersion (MAD) experiments (see Section A.7).

A.3 X-ray detectors

A.3.1 Image plates

Image plates consist of a thin layer of inorganic phosphor [usually BaFBr(Eu)²⁺] placed on a flat base (Figure A.4). Incident X-ray photons excite the europium creating defects in the phosphor lattice. This produces a latent image of the incident X-rays and is read by stimulating the phosphor with laser light, resulting in fluorescent emission. Plates are usually scanned with a laser in the red region of visible light ($\lambda=633$ nm). The emitted light is in the blue region ($\lambda=390$ nm) and is measured by a photomultiplier. The light emitted is approximately proportional to the number of X-ray photons to which a specific area has been

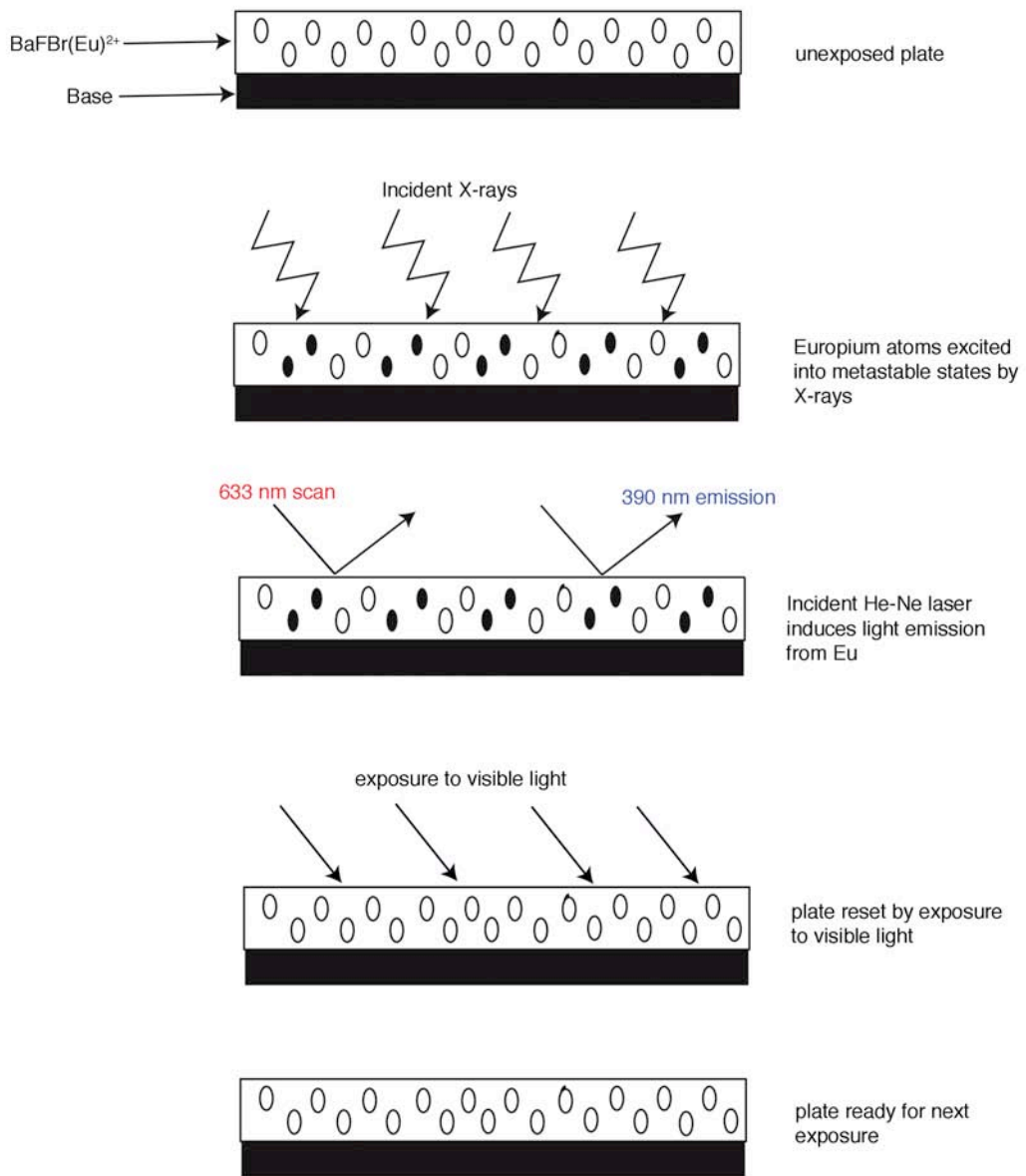


Figure A.4 Principle of operation of an image plate detector. Incident X-rays excite the phosphor to metastable states. The stored energy is released by exposure to red light. The energy is released as blue light and read by a photomultiplier. The plate is reset by exposure to visible light.

exposed. Image plate detectors are the most commonly found ‘in-house’ for detecting X-rays.

A.3.2 CCD Detectors

The most commonly found detector at synchrotron radiation sources is the charge coupled device (CCD) detector. These detectors have extremely fast readout times, low background levels and a high maximum count rate (particularly useful with the intense beams produced by synchrotrons). X-ray photons interact with a phosphor (in the ADSC Quantum detectors this is gallium arsenide doped with europium ions). The interaction of the X-ray photon with the phosphor converts, and magnifies, the signal to light photons (500 to 700 light photons are released per X-ray photon). The light signal is then passed through a fibre optic taper to demagnify the active area to the size of the CCD chip. The CCD chip converts the light signal to an electronic signal, which is digitised and, after corrections for non-uniformity of response and spatial distortion, is converted into an image file (Figure A.5).

The light that hits the CCD chip frees an electron from the silicon, creating a charge proportional to the number of incident photons. The electrons released by incident light are kept within the pixel by maintaining high potential around the pixel. This is performed by gate electrodes (Figure A.6). Once the exposure is over, the gate electrodes are changed to release the charge, which is read for each pixel sequentially and produces a charge associated with each pixel. This charge is amplified and converted to an image that represents the number of X-ray photons incident on the detector surface.

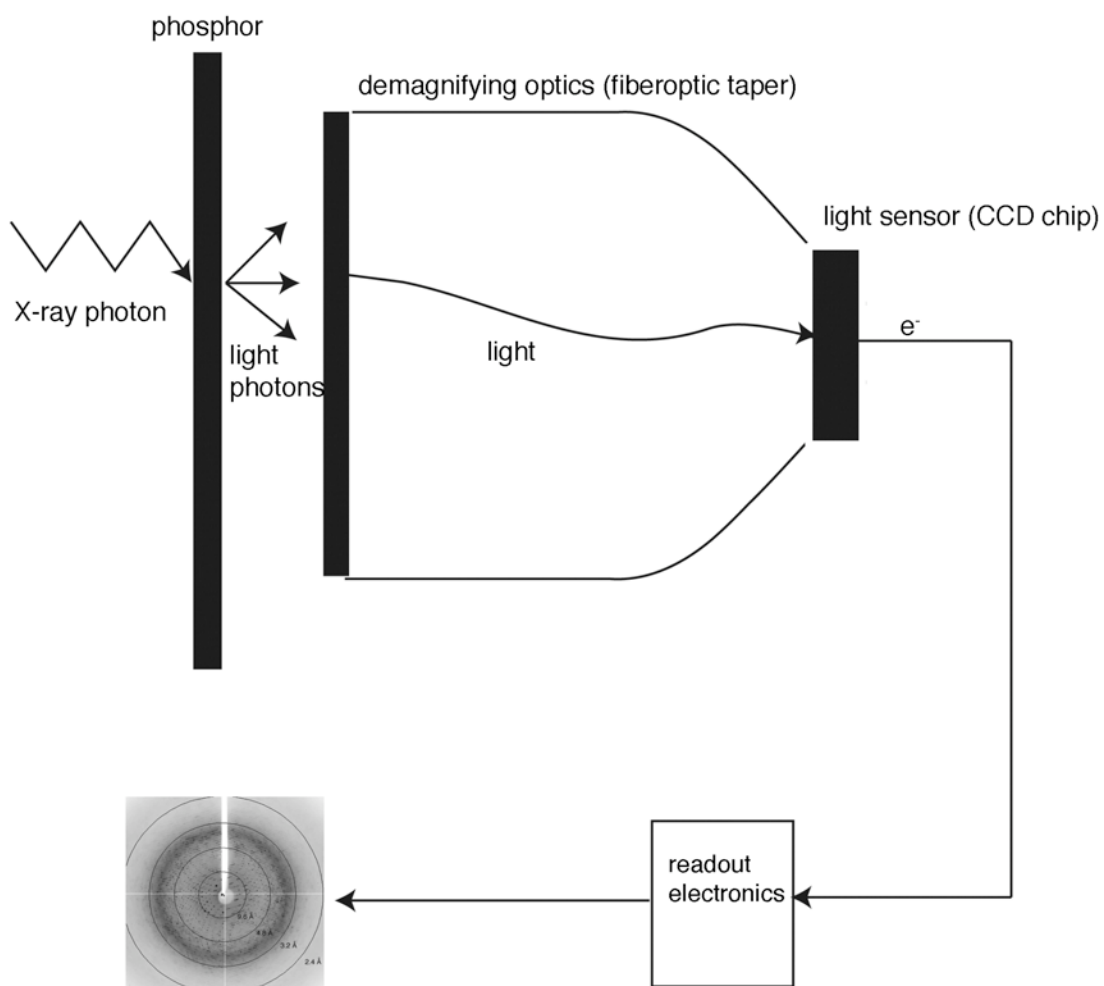


Figure A.5 Schematic of a CCD detector. X-ray photons interact with the phosphor converting the signal to light photons. Demagnifying optics reduce the light image to the size of the CCD chip which detects the light image as an electrical charge image. This information is then converted into an image file similar to those produced by other types of detector.

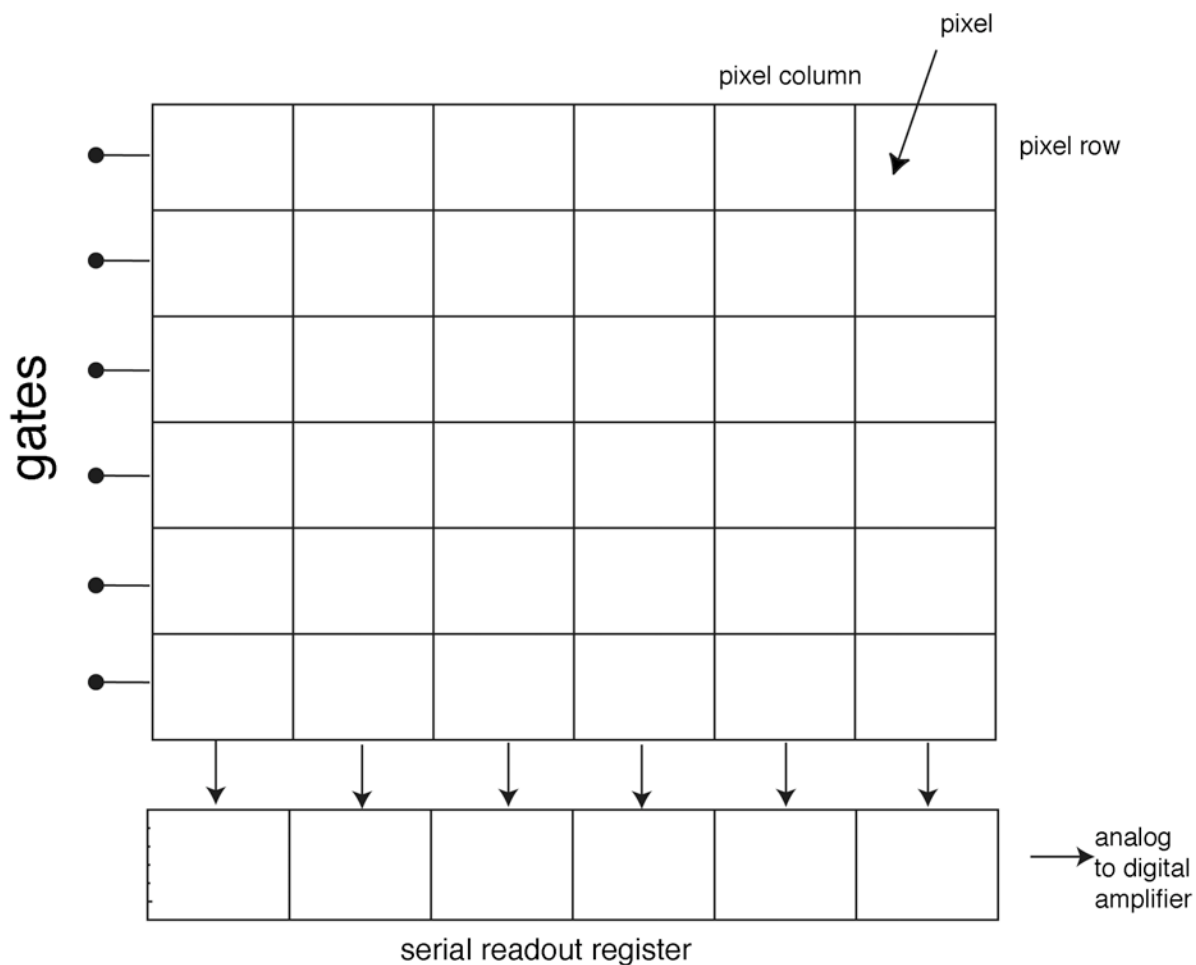


Figure A.6 Schematic of a CCD chip. The diagram is viewed from the point of view of an incident photon. Photons release electrons from the silicon in a pixel. The charge is maintained within the pixel, until the exposure is over, by surrounding high potentials created by the gate electrodes. The charge from each pixel is then moved sequentially to the serial readout register where the charge is amplified and converted to a digital signal.

A.4. Crystals

Crystals are three-dimensional ordered arrays of ions or molecules. When molecules precipitate from solution, they attempt to reach the lowest possible energetic state. Often this can be the regular packing found in crystals. This applies as much to small molecules as to

complex macromolecules. The size and shape of macromolecules means the crystal packing leads to large spaces between molecules. The contacts between molecules also tend to be rather small. Therefore, crystals of macromolecules tend to have a high solvent content and be rather more fragile than crystals of ions or small molecules. Protein crystals usually contain 50% protein and 50% mother liquor (values can range from 27% to 80% solvent). These crystals are far from ideal. Single crystals and the diffraction patterns observed are the sum of the patterns from numerous mosaic blocks, within the crystal, that all have slightly different orientations (Figure A.7).

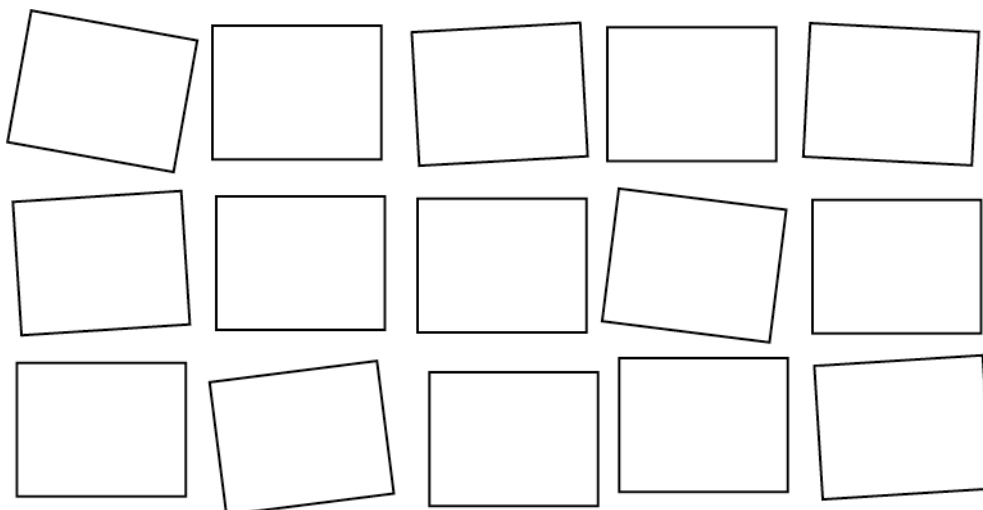


Figure A.7 Schematic of the mosaicity of protein crystals. Macromolecular crystals are imperfect and are made up of mosaic blocks, all in a slightly different orientation. The schematic is grossly exaggerated.

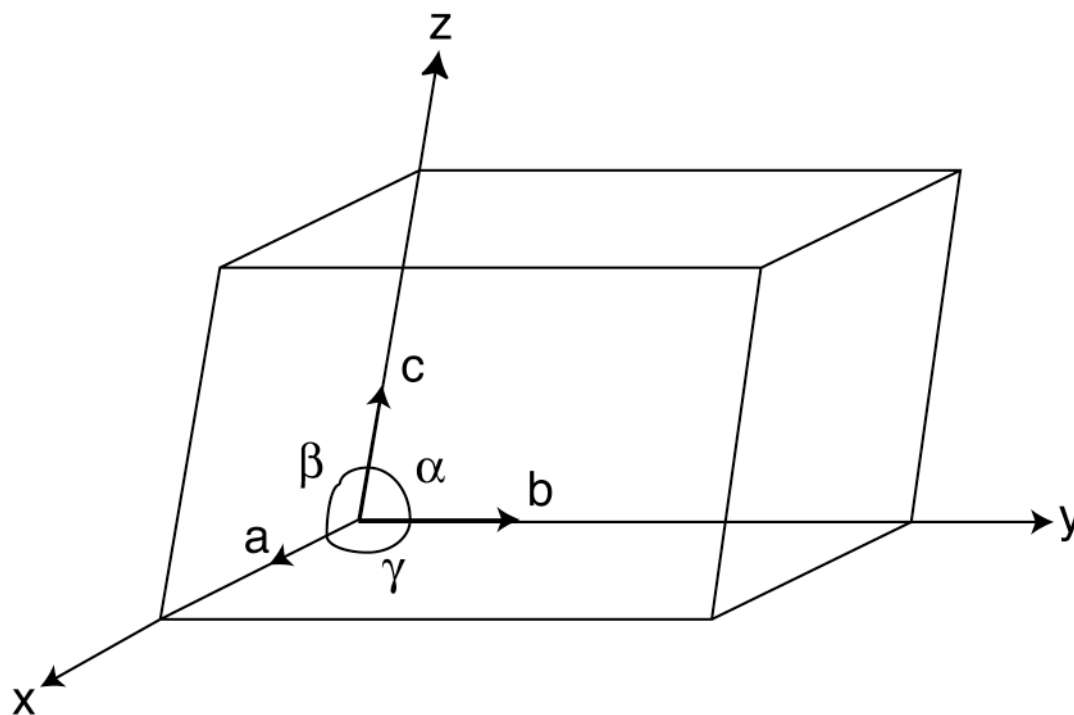


Figure A.8 A unit cell within a crystal lattice. The unit cell is defined by three cell edges a , b and c and three angles α , β and γ . The coordinates x , y and z are measured along a , b and c respectively.

The unit cell of a crystal is the smallest unit that can repeat in all directions. It is defined by three lattice translations: a , b and c , which have a length and direction, and by the angles between them α , β and γ (Figure A.8). The unit cell with minimum volume is termed the primitive cell, the crystal lattice is composed of the primitive cell stacked in three dimensions in the same orientation. As biological molecules are composed of L-amino acids, crystals cannot contain mirror plane symmetry. Therefore, protein crystals are based on 2, 3, 4, or 6 fold rotation symmetries, the requirements for these systems are shown in Table A.1.

Table A.1 The seven crystal systems

Crystal system	Symmetry requirement	Axes	Angle and length constraints
Triclinic	None	No constraints	None
Monoclinic	One 2-fold axis	b parallel to 2-fold axis, a and c perpendicular to 2-fold axis	α and $\gamma = 90^\circ$
Orthorhombic	Three perpendicular 2-fold axes	a, b and c parallel to 2-fold axes	α , β and $\gamma = 90^\circ$
Trigonal	One 3-fold axis	c parallel to 3-fold axis, a and b perpendicular to 3-fold axis	α and $\beta = 90^\circ$ $\gamma = 120^\circ$ $a = b$
Tetragonal	One 4-fold axis	c parallel to 4-fold axis, a and b perpendicular to 4-fold axis	α , β and $\gamma = 90^\circ$ $a = b$
Hexagonal	One 6-fold axis	c parallel to 6-fold axis, a and b perpendicular to 6-fold axis	α and $\beta = 90^\circ$ $\beta = 120^\circ$ $a = b$
Cubic	Four 3-fold axis	a, b and c related by 3-fold axis	α , β and $\gamma = 90^\circ$ $a = b = c$

The entire symmetry of a crystal lattice is described by its space group. The space group defines the symmetry operations that generate the crystal lattice. The smallest unit that can be rotated and translated to generate one unit cell, using only the symmetry operators allowed by the crystallographic symmetry, is called the asymmetric unit (as it requires no symmetry itself). An example space group is shown in Figure A.9. The space group $P2_12_12_1$ has three 2-fold screw axes (Figures A.9 and A.10). This relates molecules within the unit cell by a rotation and a translation.

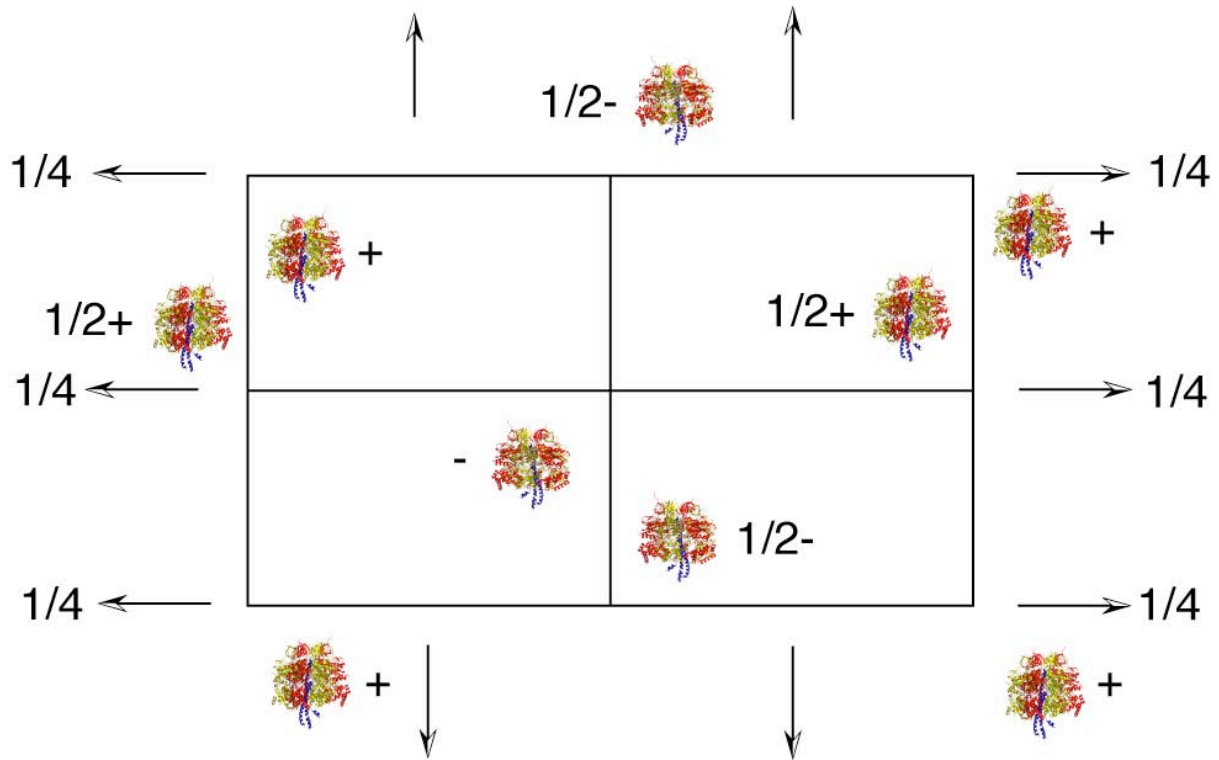


Figure A.9 The projection of a $P2_12_12_1$ unit cell. The unit cell contains four asymmetric units. The F_1 -ATPase complexes represent identical particles related by the symmetry of the space group. The plus sign (+) indicates that that the particle is a certain distance (z) above the bottom plane of the unit cell and $1/2+$ at z above the mid-plane. The minus sign (-) designates the particle is at z below the bottom plane and $1/2-$ at z below the mid-plane. The screw axes $1/4$ are at height $1/4$ and $3/4$ of the unit cell. The third set of screw axes are not shown and are normal to the plane of the paper. N.B the F_1 -ATPase complex is shown for illustrative purposes only and should not be interpreted as representing the true crystal packing. [After (Drenth, 1999)].

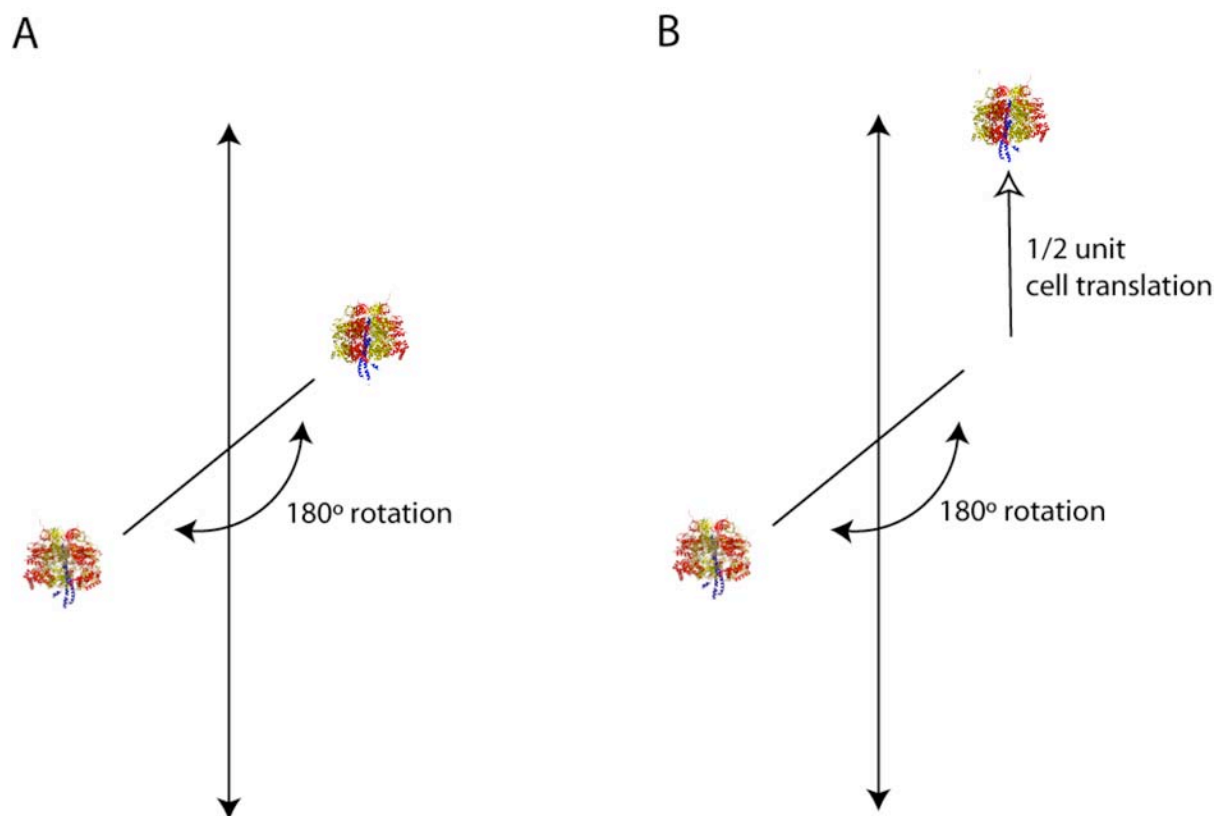
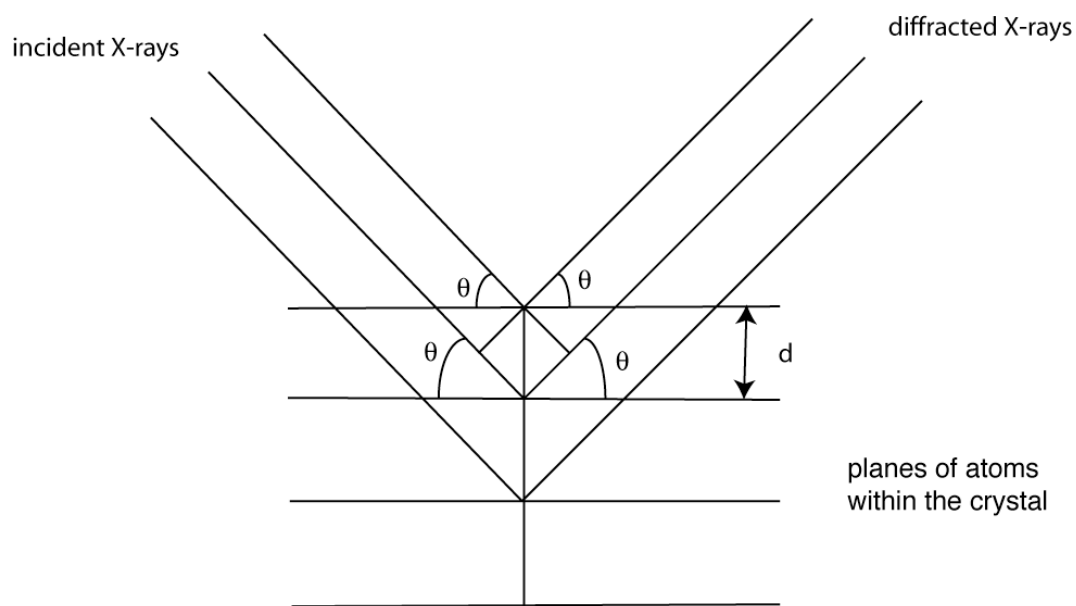


Figure A.10 A 2-fold axis (A) and a 2-fold screw axis (B). The 2-fold axis relates the molecules by a 180° rotation. The 2-fold screw axis relates the two molecules by a 180° rotation and a translation over half the unit cell length.

A.5 Scattering of X-rays by protein crystals

The majority of X-rays pass through a crystal mounted in an X-ray beam. However, some are scattered by the electrons of the molecules within the crystal. The diffraction of X-rays by crystals can be viewed as reflections from a series of planes (Figure A.11 A). Parallel X-rays are reflected from the parallel planes of the crystal. The angle of incidence is equal to

A



B

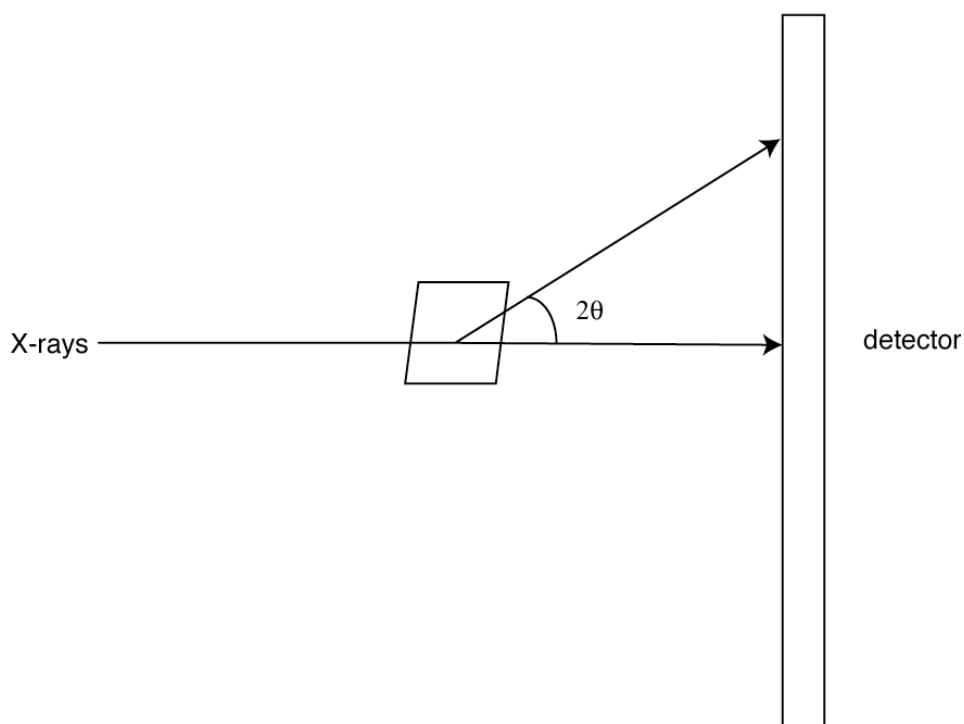


Figure A.11 Bragg's theory of diffraction of X-rays by crystals. **A:** Four lattice planes are shown separated by a distance d . The incident and reflected beams arrive, and leave, at an angle θ to the lattice planes. Therefore, the beam is reflected by an angle 2θ relative to its incident direction (**B**).

the angle of reflection, θ and the beam is reflected by an angle 2θ relative to its incident direction (Figure A.11 B). Constructive interference will occur between X-rays, reflected from different planes within the crystal, when the difference in the pathlength (the distance travelled by the X-ray) is an integral number of wavelengths. The difference in the distance travelled by reflected X-rays is $2 d \sin\theta$, this can be applied to all reflected X-rays and gives Bragg's Law (equation A.2).

$$2d \sin\theta = n \lambda \quad (A.2)$$

where d is the distance between planes in the crystal, θ is the angle of incidence of the X-rays, n is an integer and λ is the wavelength of the X-rays. This law determines where a diffraction spot will be observed; the spacing of the spots is inversely proportional to the spacing of crystal planes. The intensity of the spots is not governed by this law and depends on the electrons that scatter the X-ray. Therefore the intensity arises from the structure of the molecule in the crystal and the position of the spot arises from the positions of the molecules within the crystal lattice.

The planes of the crystal that give rise to the diffraction are defined by the Miller indices h , k and l . These indices define the series of planes that intersect the lattice points. The h index gives the number of planes in one unit cell repeat along the x axis and the k and l indices give the number of planes in one unit cell repeat along the y and z axes.

The spacing of spots in the diffraction pattern varies with the spacing of molecules within the lattice. Specifically, there is an inverse relationship; so large unit cells produce tightly spaced spots in a diffraction pattern and vice versa. The spacing of the reflections is called the reciprocal lattice as it is the inverse of the real lattice.

A.6 The Ewald sphere and reciprocal space

The Ewald sphere is a construction to visualise which planes within a crystal are in the correct orientation to diffract X-rays. The sphere has a radius of $1/\lambda$ and represents the wavelength in reciprocal space, with its centre at the crystal origin. A reciprocal lattice point must be in contact with the sphere in order satisfy Bragg's law and produce a reflection (Figure A.12).

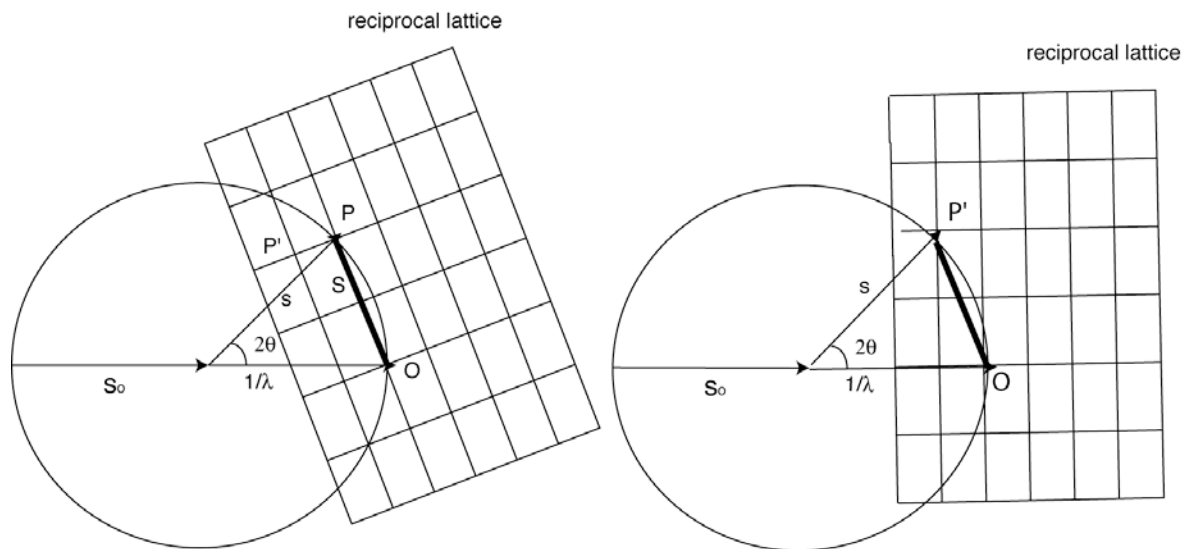


Figure A.12 A two-dimensional representation of the Ewald sphere. The sphere has a radius of $1/\lambda$, s_0 is the direction of the incident X-rays and s the direction of the scattered beam. The sphere has its origin at the crystal position. The origin of the reciprocal lattice is O , where the X-ray beam exits the Ewald sphere. The lattice point P is in contact with the sphere and will produce a reflection. For another lattice point P' to produce a reflection, the reciprocal lattice must be rotated about its origin O . In practice this means rotating the crystal in the X-ray beam.

As all lattice points cannot be in contact with the sphere at any time, the crystal must be rotated in the beam in order for all lattice points to be in contact with the sphere and to measure all possible reflections. The angle by which the beam is diffracted can be between 0° and 180° and be in any direction, the vector representing the diffracted ray ends anywhere on the surface of the sphere of radius $1/\lambda$, the Ewald sphere.

A.7 Structure solution and the phase problem

The intensity of each of the spots in a diffraction pattern depends on the distribution of the electron density within the unit cell. The intensity of the diffracted beam is proportional to the square of the amplitude of the structure factor, F_{hkl} . The structure factor equation is shown (Equation A.3):

$$F_{hkl} = \sum_{j=1}^n f_j e^{2\pi i(hx_j + ky_j + lz_j)} \quad (A.3)$$

The contribution of each atom (j) to the structure factor is shown. The amplitude of the atomic scattering factor (f_j) is determined by the type of atom and the phase is determined by its position within the unit cell (x_j , y_j and z_j); n is the number of atoms within the unit cell. The electron density and the structure factors are the Fourier transform of one another and the electron density can be written as a Fourier series (Equation A.4):

$$\rho(x, y, z) = \frac{1}{V} \sum_h \sum_k \sum_l F_{hkl} e^{-2\pi i(hx + ky + lz)} \quad (A.4)$$

where $\rho(x,y,z)$ is the electron density function for a given position (xyz) in the unit cell, V is the volume of the unit cell, F_{hkl} is the structure factor and hkl are the Miller indices (Section A.5).

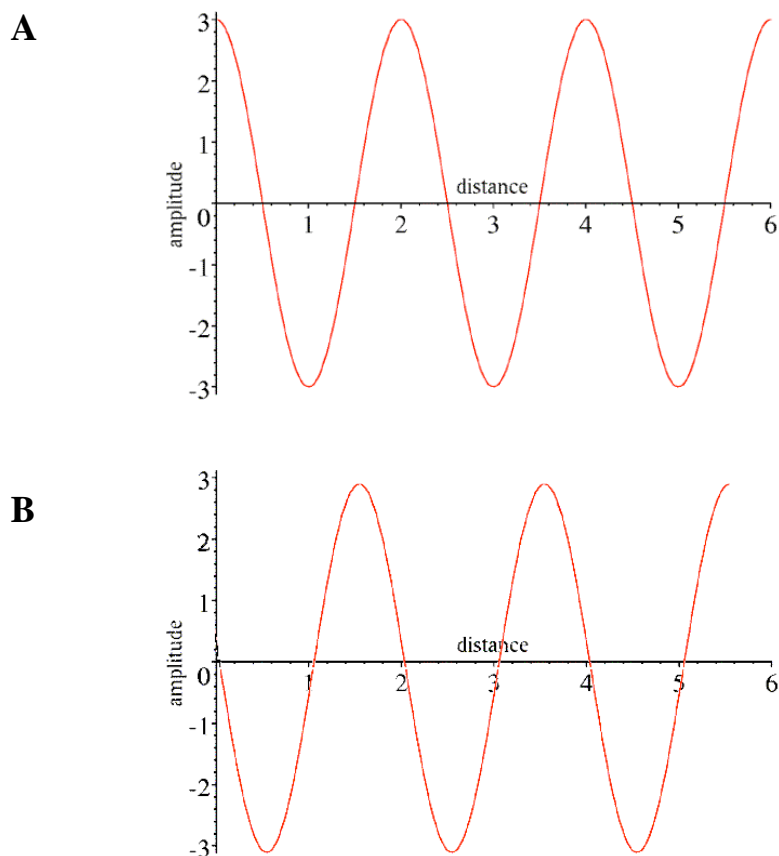


Figure A.13 Two simple waves that are out of phase with respect to each other. Wave A has maximum amplitude at a distance of zero whereas wave B has maximum amplitude at a distance of 1.5; therefore, the phase difference between the waves is 1.5. Phases and differences are expressed in degrees, in this case 270° .

The amplitude of the structure factor can be calculated from the observed intensities. However, the detector records no information on the phases. The phase of a wave is the relative position of the waveform with respect to an origin from which the X-rays are

scattered (Figures A.13 and A.14). Without the phases the electron density within the unit cell cannot be calculated, this is the 'phase problem'.

Different methods have been derived to overcome this problem. The amplitudes and phases are determined by the structure of the molecule in the crystal. Therefore, any knowledge of the electron density or structure can be used to estimate the phases of the structure factors. The simplest method is assign trial phases to a small set of reflections. Phase relationships are then used to generate phases of other reflections. This method (so called direct methods) requires very high resolution data ($<1.2 \text{ \AA}$) and is generally only applicable to small molecules but has been used to solve the structures of some small proteins.

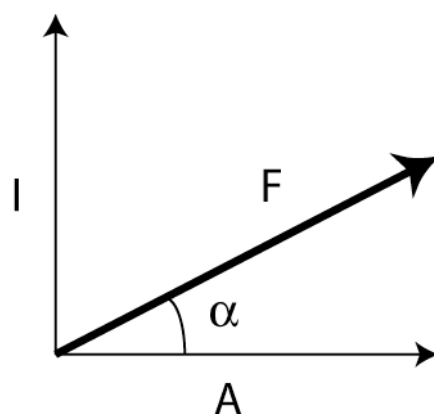


Figure A.14 The structure factor. The structure factor can be represented as a vector F . The length of the vector is proportional to $I^{1/2}$ (the square root of the intensity) and the angle α is the phase.

If the structure of a homologous protein is known the model can be used to estimate the phases. This process is called molecular replacement. Molecular replacement uses the

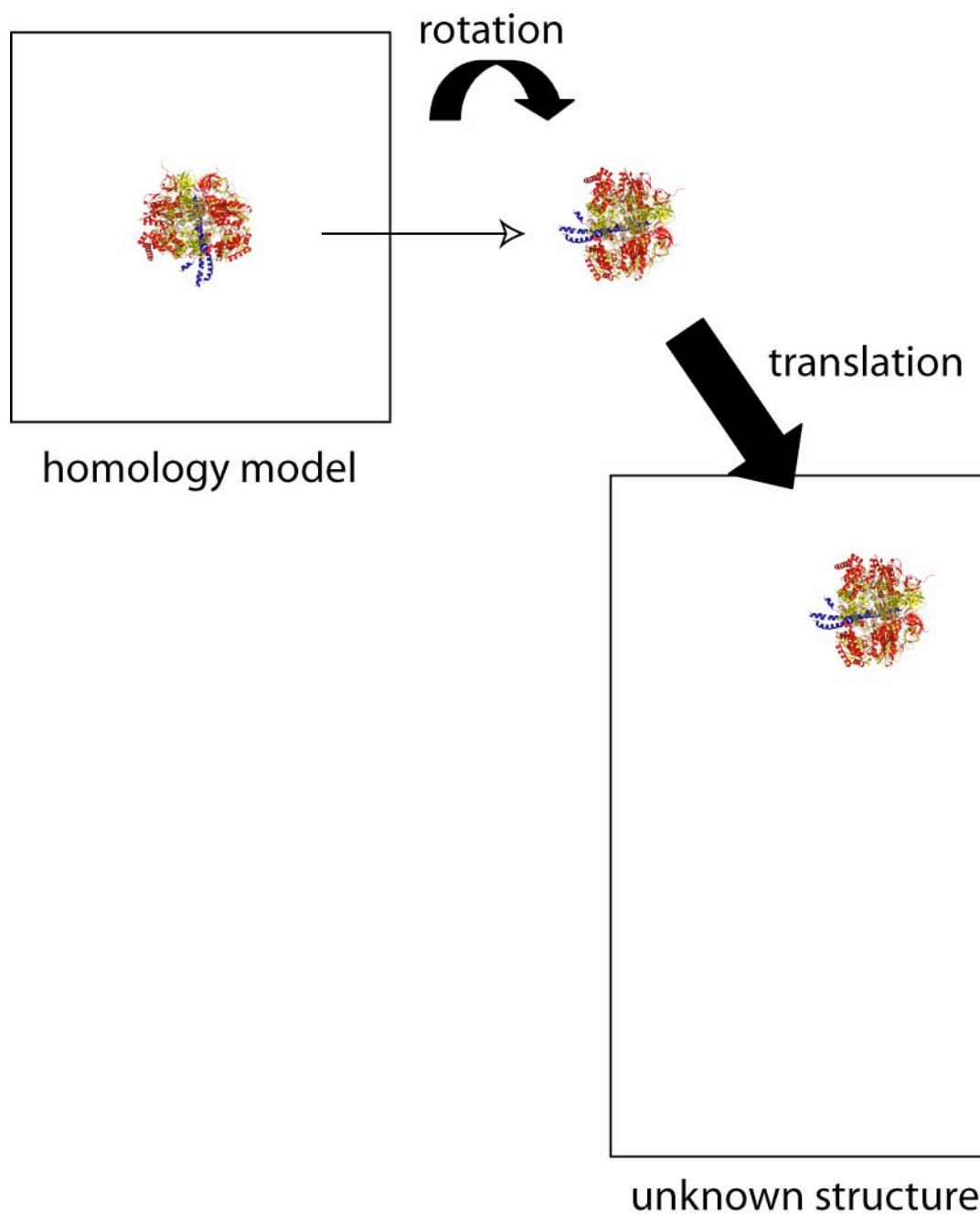


Figure A.15 The processes of molecular replacement. The orientation of the unknown structure is found by the rotation function and its position within the new unit cell by the translation function.

Patterson maps (the Fourier transform of the intensities) to find the orientation of the new molecule in the unit cell and then the position of the new protein relative to the origin of the new unit cell (Figure A.15 and Section 2.2.17.4). The Patterson maps from the model and

new structure are compared; peaks within the Patterson maps from intramolecular vectors only depend on the orientation of the structure in the unit cell. Therefore, peaks for approximately $\frac{2}{3}$ of the volume of the molecule are looked at and matching the peaks from the Patterson maps will find the orientation of the new structure within the unit cell. The search for the position of the molecule looks at the intermolecular vector peaks in the Patterson map. These peaks arise from any pair of atoms in different molecules related by crystal symmetry. The intramolecular peaks are subtracted from the Patterson and only peaks due to intermolecular vectors are matched. This places the molecule within the unit cell.

Once the position of the molecule in the new unit cell is known, phases can be determined from the model, and electron density maps calculated using measured amplitudes for the unknown structure and calculated phases from the model placed in the unit cell of the unknown structure.

In cases where no homology model exists other methods must be employed to estimate the phases. The first method developed was isomorphous replacement (Green *et al.*, 1954). In this method, heavy metal atoms (such as mercury, platinum or gold) are introduced into the crystals that bind to specific residues (mercury binds to cysteines, platinum to methionines), naturally present or introduced into the protein, to create heavy atom derivative (i.e. crystals with the same unit cell and orientation of protein). As heavy atoms are electron rich, the diffraction of the incident X-rays will differ from the diffraction from the native crystals. This leads to measurable differences in the intensity as the structure factors are different. The locations of the heavy atoms can then be determined from the difference Patterson maps and this allows calculation of the protein phases.

Isomorphous replacement can often fail as introducing heavy atoms to the protein can cause changes in unit cell dimensions and protein conformation. The technique of multiplexwavelength anomalous dispersion [MAD (Hendrickson, 1991)] overcomes many of

these problems. This technique also requires the presence of a heavy atom, either naturally present, soaked in or by replacing natural amino acids with those containing a heavy atom (seleno-methionine is equivalent to a methionine where the sulphur is replaced by a selenium atom). MAD takes advantage of the wavelength dependence of the atomic scattering factor of an element at wavelengths close to its absorption edge, together with the ability to tune the wavelength of synchrotron radiation. First, the absorption peak of the atom is found by a fluorescence scan of the crystal. This establishes the peak for the atom in its current environment. Then three data sets are collected, at the absorption peak, the point of inflection of the absorption curve and a remote wavelength. As data are collected on a single crystal, there is no problem with isomorphism. The scattering factors of the anomalously scattering atoms are different, and therefore, the intensities of reflections will be different for each wavelength at which a data set is taken. The presence of the heavy atom also breaks Friedel's Law [that ($I_{hkl} = I_{-h-k-l}$)] and leads to different intensities of Friedel related reflections. Comparison of the intensities of the Friedel pairs can be used to estimate the phases.

A.8 The molecular model

After phases have been estimated and electron density maps calculated, the model can be built. The electron density is interpreted and a molecular model is built to fit the density. The atomic coordinates and temperature factors of the molecule are refined against the observed amplitudes. As the model improves, the theoretical amplitudes calculated from the model should converge with the observed amplitudes. The measure of this convergence is called the R factor (Equation A.5):

$$R = \frac{\sum_{hkl} \left| |F_{obs}| - k|F_{calc}| \right|}{\sum_{hkl} |F_{obs}|} \quad (A.5)$$

where F_{obs} are the observed amplitudes, F_{calc} are the calculated amplitudes from the model and k is the scale factor.

However, the refinement process may make adjustments to the model that reduce the R factor but do not represent realistic changes to the model. To avoid this pitfall the Free R Factor is used. A small set of reflection (usually 5%) are removed from the data before refinement. These reflections are then used to calculate an R factor called the Free R Factor (Equation A.6):

$$R_{free} = \frac{\sum_{hkl \in T} \left| |F_{obs}| - k|F_{calc}| \right|}{\sum_{hkl \in T} |F_{obs}|} \quad (A.6)$$

where T is the test set of reflections removed from the data set. Reducing the Free R Factor gives an unbiased estimate of the improvement in the model, as the model has not been refined against these data.

Appendix B: Supplementary figures

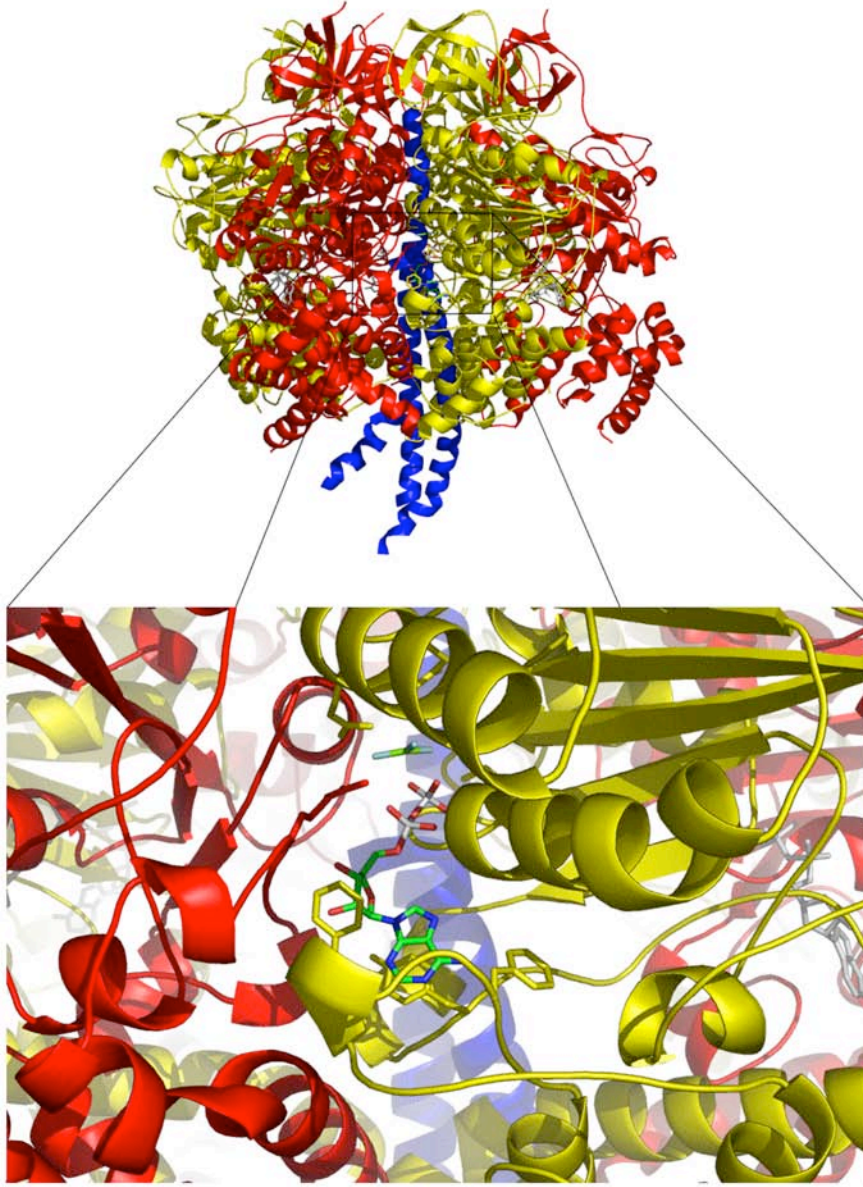


Figure B.1 The structure of F₁-MgF₃⁻ viewed from the ‘standard’ orientation with a magnification of the β_{TP} catalytic site. The catalytically important residue side chains are displayed.

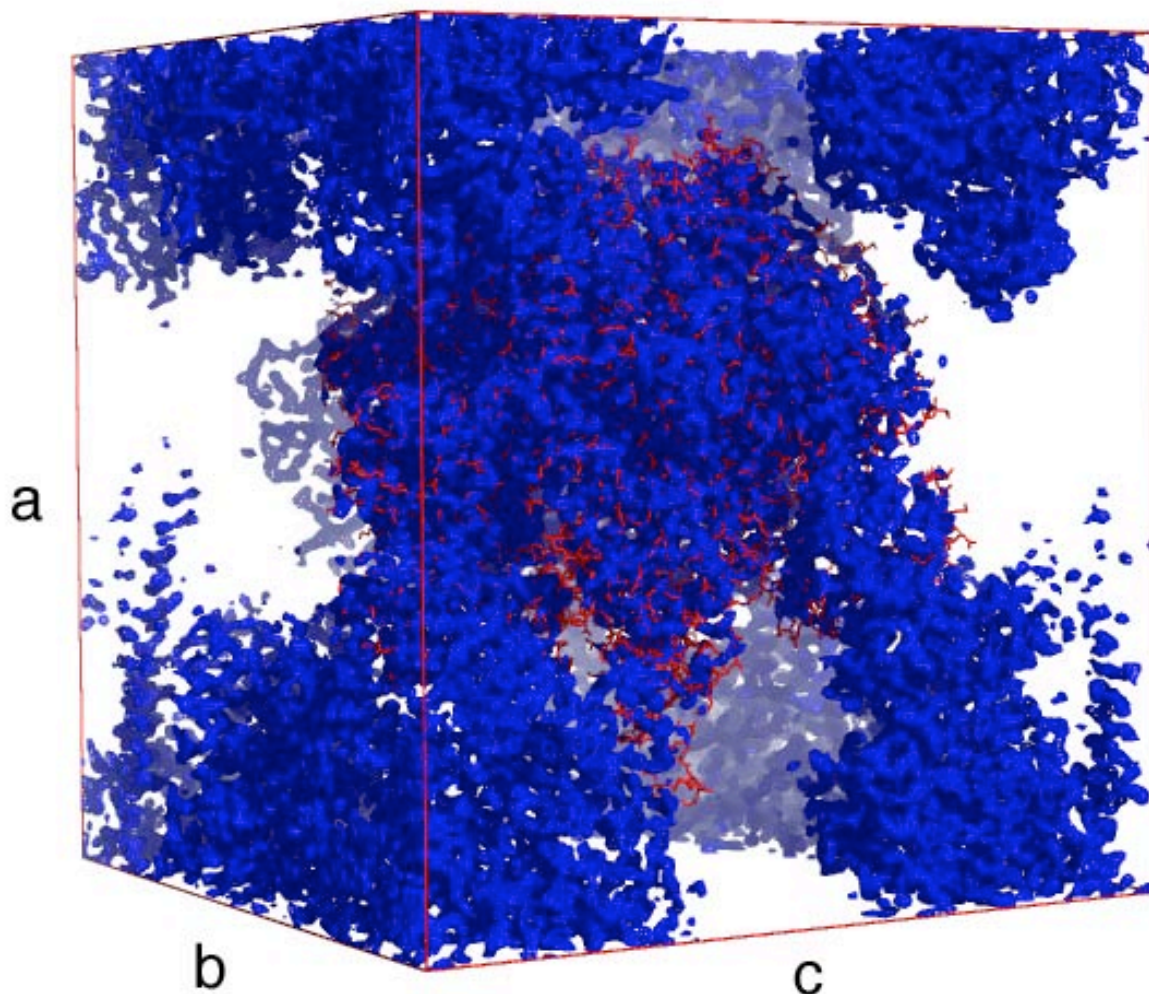


Figure B.2 The asymmetric unit of the $F_1\text{-MgF}_3^-$ structure. The atomic model of $F_1\text{-MgF}_3^-$ and the unit cell edges are shown in red and the electron density for the model and symmetry related molecules is shown as a blue mesh (contoured at 1σ). The decrease in the a axis by up to 16 \AA increases the order of the crystals

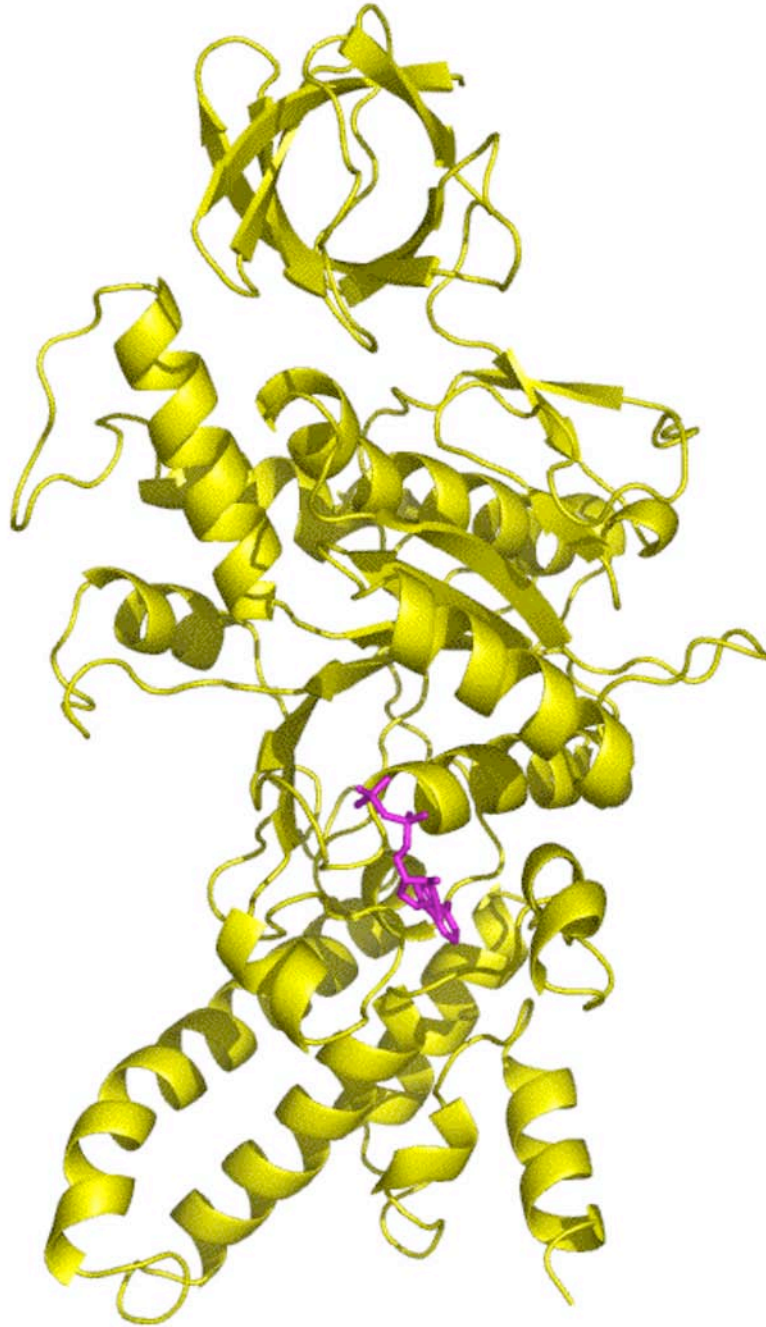


Figure B.3 The β_E subunit of bovine F_1 -ATPase inhibited with ADP and magnesium fluoride (F_1 - MgF_3^-). The subunit is essentially in the open conformation observed in the reference structure but binds ADP (magenta).

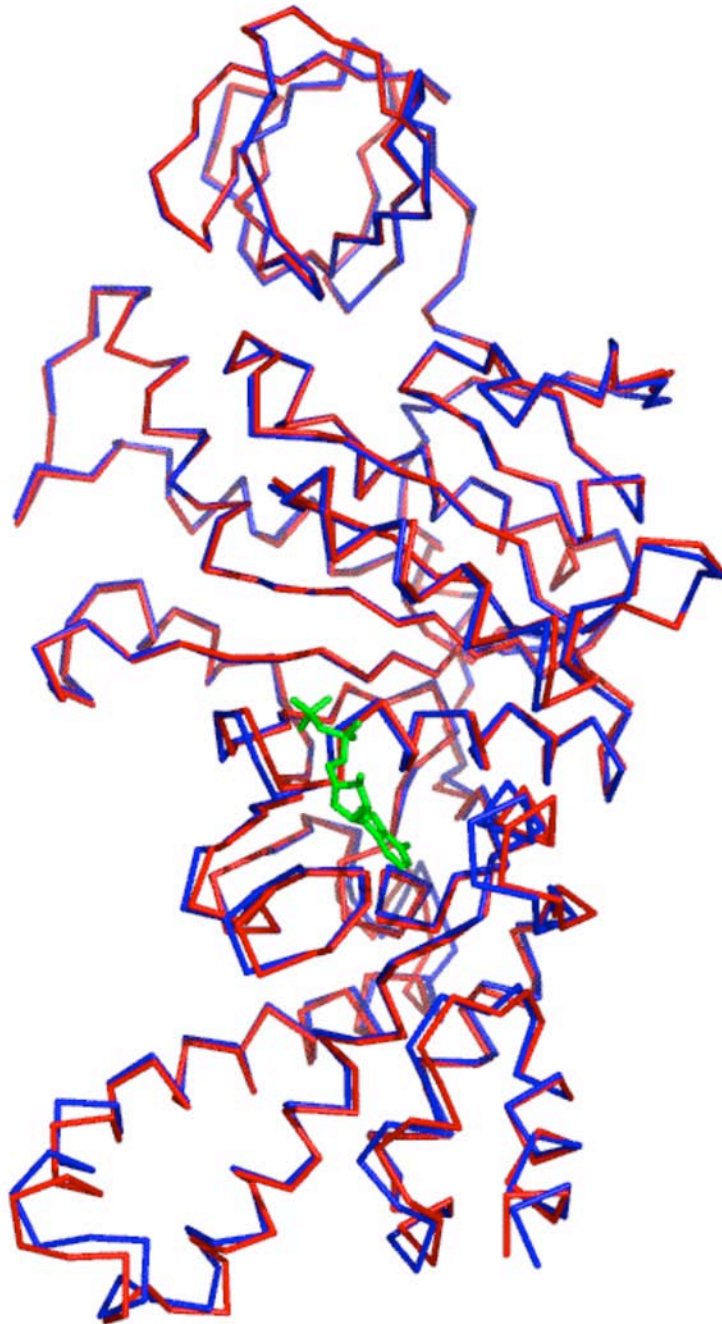


Figure B.4 Ribbon representation of the $F_1\text{-MgF}_3^- \beta_E$ subunit (blue) superimposed on the N-terminal β -sheet domain of the reference structure β_E subunit. The structures are in essentially the same conformation but there is a 2.4° rotation of the C-terminal domain and a tightening of the hydrophobic pocket. ADP is shown (green)

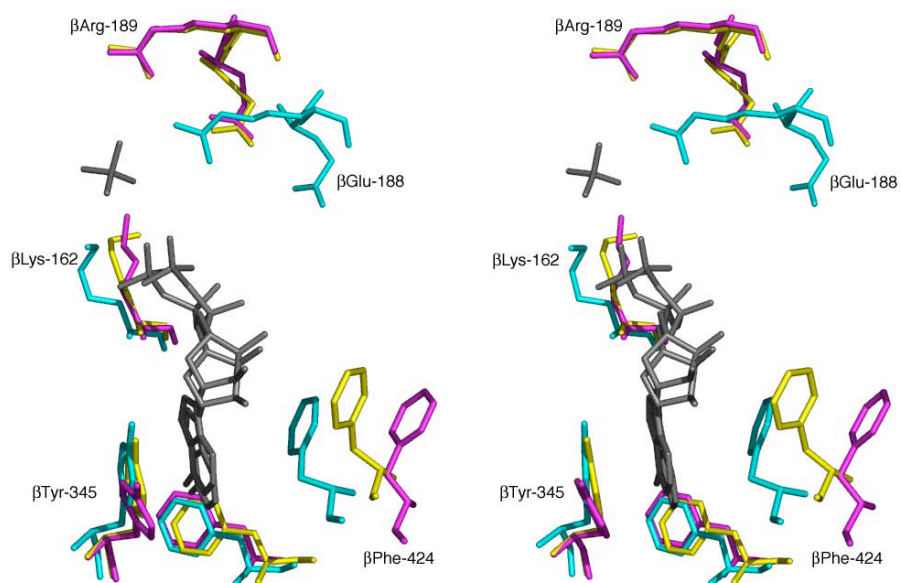


Figure B.5 The progression from open to half-closed, the view is in stereo. The β_E subunits of the reference (magenta), $F_1\text{-MgF}_3^-$ (yellow) and $(\text{ADP-AlF}_4^-)_2\text{-F}_1$ (cyan) structures were superimposed on their P-loops (residues 155-165). Initial binding of ADP is accompanied by a movement of the $C\alpha$ and side chain of $\beta\text{Phe-424}$ towards the adenine ring forming a hydrophobic binding pocket. The transition from open (ADP bound) to half closed involves a tightening of the hydrophobic pocket and a rotation and movement of $\beta\text{Arg-189}$ closer to the β phosphate as it coordinates a phosphate (also coordinated by $\beta\text{Lys-162}$). The transition from half closed to closed involves no further tightening of the hydrophobic pocket but the movement of $\beta\text{Arg-189}$ towards the β phosphate and the alignment of $\beta\text{Glu-188}$ with the phosphate intermediate to present the attacking water (see next figure)

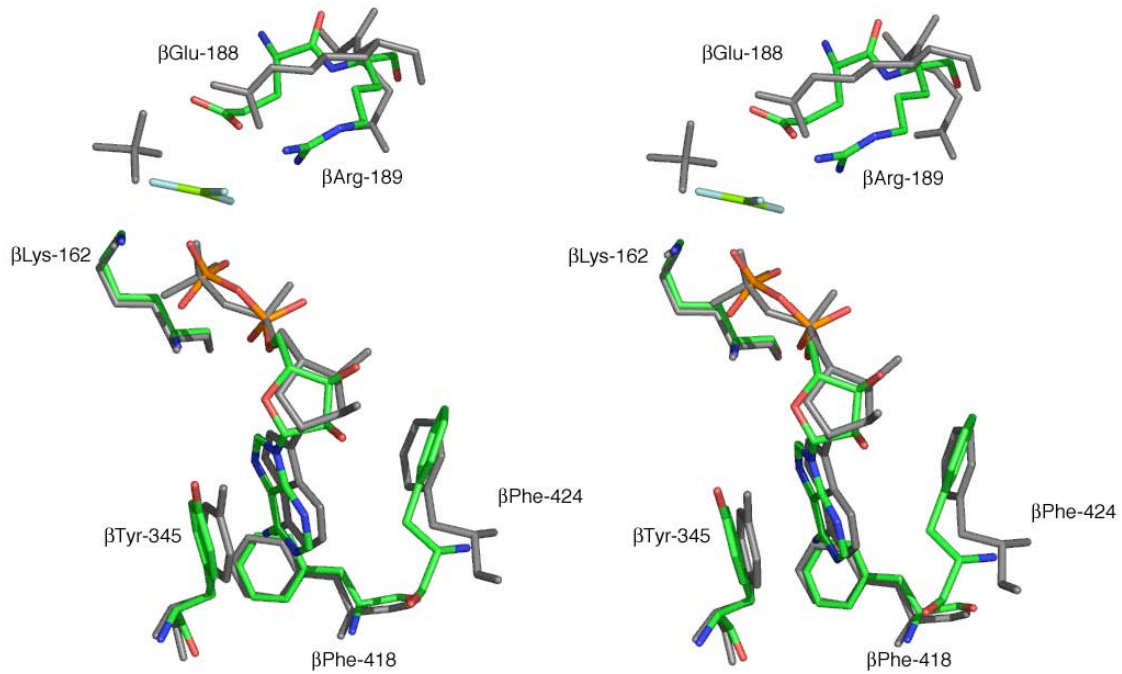


Figure B.6 Superimposition of the β_E subunit from the $(\text{ADP-AIF}_4)_2\text{-F}_1$ structure (grey) and the β_{TP} subunit from the $\text{F}_1\text{-MgF}_3^-$ subunit (coloured). The transition from half closed to loose. Structures were superimposed on their P-loops (residues 155-165).

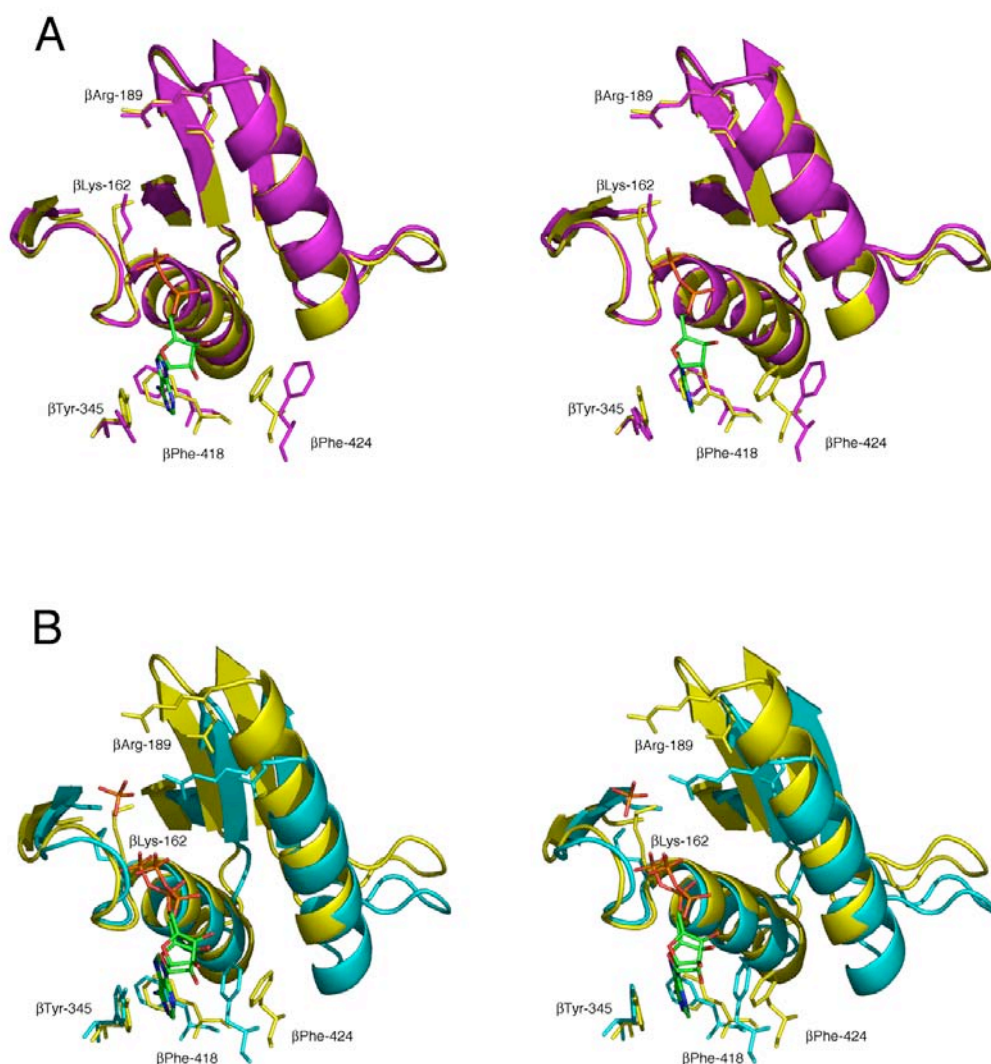


Figure B.7 Nucleotide binding in the β_E subunit. The β_E subunits of the reference (magenta), $F_1\text{-MgF}_3^-$ (yellow) and $(\text{ADP-AlF}_4^-)_2\text{-F}_1$ (cyan) structures were superimposed on their P-loops (residues 155-165). **A:** Initial binding of ADP is accompanied by a movement of the $C\alpha$ and side chain of $\beta\text{Phe-424}$ towards the adenine ring forming a hydrophobic binding pocket. **B:** The transition from open (ADP bound) to half closed involves a tightening of the hydrophobic pocket and a rotation and movement of $\beta\text{Arg-189}$ closer to the β phosphate as it coordinates a phosphate (also coordinated by $\beta\text{Lys-162}$)

References

- Ablooglu, A. J., Till, J. H., Kim, K., Parang, K., Cole, P. A., Hubbard, S. R. and Kohanski, R. A. (2000). Probing the catalytic mechanism of the insulin receptor kinase with a tetrafluorotyrosine-containing peptide substrate. *J. Biol. Chem.* **275**: 30394-30398.
- Abrahams, J. P., Buchanan, S. K., Van Raaij, M. J., Fearnley, I. M., Leslie, A. G. W. and Walker, J. E. (1996). The structure of bovine F₁-ATPase complexed with the peptide antibiotic efrapeptin. *Proc. Natl. Acad. Sci. U. S. A.* **93**: 9420-9424.
- Abrahams, J. P., Leslie, A. G. W., Lutter, R. and Walker, J. E. (1994). Structure at 2.8 Å resolution of F₁-ATPase from bovine heart mitochondria. *Nature* **370**: 621-628.
- Adachi, K., Yasuda, R., Noji, H., Itoh, H., Harada, Y., Yoshida, M. and Kinosita, K., Jr. (2000). Stepping rotation of F₁-ATPase visualized through angle-resolved single-fluorophore imaging. *Proc. Natl. Acad. Sci. U. S. A.* **97**: 7243-7247.
- Admiraal, S. J. and Herschlag, D. (1995). Mapping the transition state for ATP hydrolysis: implications for enzymatic catalysis. *Chem. Biol.* **2**: 729-739.
- Akashi, A., Yoshida, Y., Nakagoshi, H., Kuroki, K., Hashimoto, T., Tagawa, K. and Imamoto, F. (1988). Molecular cloning and expression of a gene for a factor which

- stabilizes formation of inhibitor-mitochondrial ATPase complex from *Saccharomyces cerevisiae*. *J. Biochem. (Tokyo)* **104**: 526-530.
- Altmann, R. (1890). Die Elementarorganismen und ihre Beziehungen zu den Zellen. Viet, Leipzig.
- Ansorge, W. (1985). Fast and sensitive detection of protein and DNA bands by treatment with potassium permanganate. *J. Biochem. Biophys. Meth.* **11**: 13-20.
- Aqvist, J., Kolmodin, K., Florian, J. and Warshel, A. (1999). Mechanistic alternatives in phosphate monoester hydrolysis: what conclusions can be drawn from available experimental data? *Chem. Biol.* **6**: R71-80.
- Arana, J. L. and Vallejos, R. H. (1982). Involvement of sulfhydryl groups in the activation mechanism of the ATPase activity of chloroplast coupling factor 1. *J. Biol. Chem.* **257**: 1125-1127.
- Arnold, I., Pfeiffer, K., Neupert, W., Stuart, R. A. and Schagger, H. (1998). Yeast mitochondrial F₁F₀-ATP synthase exists as a dimer: identification of three dimer-specific subunits. *EMBO J.* **17**: 7170-7178.
- Arselin, G., Vaillier, J., Salin, B., Schaeffer, J., Giraud, M. F., Dautant, A., Brethès, D. and Velours, J. (2004). The modulation in subunits e and g amounts of yeast ATP synthase modifies mitochondrial cristae morphology. *J. Biol. Chem.* **279**: 40392-40399.
- Astbury, W. T. (1933). Fundamentals of fibre structure, Oxford University Press.

- Beechey, R. B., Hubbard, S. A., Linnett, P. E., Mitchell, A. D. and Munn, E. A. (1975). A simple and rapid method for the preparation of adenosine triphosphatase from submitochondrial particles. *Biochem. J.* **148**: 533-537.
- Berman, H. M., Westbrook, J., Feng, Z., Gilliland, G., Bhat, T. N., Weissig, H., Shindyalov, I. N. and Bourne, P. E. (2000). The Protein Data Bank. *Nucleic. Acids. Res.* **28**: 235-242.
- Bianchet, M. A., Hullihen, J., Pedersen, P. L. and Amzel, L. M. (1998). The 2.8 Å structure of rat liver F₁-ATPase: configuration of a critical intermediate in ATP synthesis/hydrolysis. *Proc. Natl. Acad. Sci. U. S. A.* **95**: 11065-11070.
- Blackburn, G. M., Williams, N. H., Gamblin, S. J. and Smerdon, S. J. (2003). Comment on "The pentacovalent phosphorus intermediate of a phosphoryl transfer reaction". *Science* **301**: 1184; author reply 1184.
- Blake, C. C. F., Koenig, D. F., Mair, G. A., North, A. C. T. and Phillips, D. C. (1965). Structure of hen egg white lysozyme. A three dimensional Fourier synthesis at 2 Å resolution. *Nature* **206**.
- Boyer, P. D. (1975). A model for conformational coupling of membrane potential and proton translocation to ATP synthesis and to active transport. *FEBS Lett.* **58**: 1-6.
- Boyer, P. D. (1979). Membrane bioenergetics. Reading, MA, Addison-Wesley.
- Boyer, P. D. (1993). The binding change mechanism for ATP synthase-some probabilities and possibilities. *Biochim. Biophys. Acta* **1140**: 215-250.

- Boyer, P. D., Stokes, B. O., Wolcott, R. G. and Degani, C. (1975). Coupling of "high-energy" phosphate bonds to energy transductions. *Fed. Proc.* **34**: 1711-1717.
- Boyes-Watson, J., Davidson, E. and Perutz, M. F. (1947). An X-ray study of horse methaemoglobin I. *Proc. Roy. Soc. A* **191**: 83-192.
- Bradford, M. M. (1976). A rapid and sensitive method for the quantitation of microgram quantities of protein utilizing the principle of protein-dye binding. *Anal. Biochem.* **72**: 248-254.
- Bragg, W. H. and Bragg, W. L. (1913). The reflection of X-rays in crystals. *Proc. Roy. Soc. A* **88**: 428-438.
- Braig, K., Menz, R. I., Montgomery, M. G., Leslie, A. G. W. and Walker, J. E. (2000). Structure of bovine mitochondrial F₁-ATPase inhibited by Mg²⁺ ADP and aluminium fluoride. *Structure Fold. Des.* **8**: 567-573.
- Bushnell, G. W., Louie, G. V. and Brayer, G. D. (1990). High-resolution three-dimensional structure of horse heart cytochrome c. *J. Mol. Biol.* **214**: 585-595.
- Böttcher, B., Bertsche, I., Reuter, R. and Graber, P. (2000). Direct visualisation of conformational changes in EF₀F₁ by electron microscopy. *J. Mol. Biol.* **296**: 449-457.
- Cabezón, E., Arechaga, I., Butler, P. J. G. and Walker, J. E. (2000a). Dimerization of bovine F₁-ATPase by binding the inhibitor protein, IF₁. *J. Biol. Chem.* **275**: 28353-28355.

- Cabezón, E., Butler, P. J., Runswick, M. J., Carbajo, R. J. and Walker, J. E. (2002). Homologous and heterologous inhibitory effects of ATPase inhibitor proteins on F-ATPases. *J. Biol. Chem.* **277**: 41334-41341.
- Cabezón, E., Butler, P. J., Runswick, M. J. and Walker, J. E. (2000b). Modulation of the oligomerization state of the bovine F₁-ATPase inhibitor protein, IF₁, by pH. *J. Biol. Chem.* **275**: 25460-25464.
- Cabezón, E., Montgomery, M. G., Leslie, A. G. W. and Walker, J. E. (2003). The structure of bovine F₁-ATPase in complex with its regulatory protein IF₁. *Nature Struct. Bio.* **10**: 744-750.
- Cabezón, E., Runswick, M. J., Leslie, A. G. W. and Walker, J. E. (2001). The structure of bovine IF₁, the regulatory subunit of mitochondrial F-ATPase. *EMBO J.* **20**: 6990-6996.
- Carbajo, R. J., Silvester, J. A., Runswick, M. J., Walker, J. E. and Neuhaus, D. (2004). Solution structure of subunit F₆ from the peripheral stalk region of ATP synthase from bovine heart mitochondria. *J. Mol. Biol.* **342**: 593-603.
- Choe, J. Y., Iancu, C. V., Fromm, H. J. and Honzatko, R. B. (2003). Metaphosphate in the active site of fructose-1,6-bisphosphatase. *J. Biol. Chem.* **278**: 16015-16020.
- Cintron, N. M. and Pedersen, P. L. (1979). A protein inhibitor of the mitochondrial adenosine triphosphatase complex of rat liver. Purification and characterization. *J. Biol. Chem.* **254**: 3439-3443.

Collaborative Computational Project Number 4 (1994). The CCP4 suite: programs for protein crystallography. *Acta Cryst. D Biol. Cryst.* **50**: 760-763.

Collinson, I. R., Fearnley, I. M., Skehel, J. M., Runswick, M. J. and Walker, J. E. (1994a). ATP synthase from bovine heart mitochondria: identification by proteolysis of sites in F_0 exposed by removal of F_1 and the oligomycin-sensitivity conferral protein. *Biochem. J.* **303**: 639-645.

Collinson, I. R., Runswick, M. J., Buchanan, S. K., Fearnley, I. M., Skehel, J. M., van Raaij, M. J., Griffiths, D. E. and Walker, J. E. (1994b). F_0 membrane domain of ATP synthase from bovine heart mitochondria: purification, subunit composition, and reconstitution with F_1 -ATPase. *Biochemistry* **33**: 7971-7978.

Collinson, I. R., Skehel, J. M., Fearnley, I. M., Runswick, M. J. and Walker, J. E. (1996). The F_1F_0 -ATPase complex from bovine heart mitochondria: the molar ratio of the subunits in the stalk region linking the F_1 and F_0 domains. *Biochemistry* **35**: 12640-12646.

Collinson, I. R., van Raaij, M. J., Runswick, M. J., Fearnley, I. M., Skehel, J. M., Orriss, G. L., Miroux, B. and Walker, J. E. (1994c). ATP synthase from bovine heart mitochondria. In vitro assembly of a stalk complex in the presence of F_1 -ATPase and in its absence. *J. Mol. Biol.* **242**: 408-421.

Cook, A., Lowe, E. D., Chrysina, E. D., Skamnaki, V. T., Oikonomakos, N. G. and Johnson, L. N. (2002). Structural studies on phospho-CDK2/cyclin A bound to nitrate, a transition state analogue: implications for the protein kinase mechanism. *Biochemistry* **41**: 7301-7311.

- Cozens, A. L. and Walker, J. E. (1987). The organization and sequence of the genes for ATP synthase subunits in the cyanobacterium *Synechococcus* 6301. Support for an endosymbiotic origin of chloroplasts. *J. Mol. Biol.* **194**: 359-383.
- Cramer, P., Bushnell, D. A., Fu, J., Gnatt, A. L., Maier-Davis, B., Thompson, N. E., Burgess, R. R., Edwards, A. M., David, P. R. and Kornberg, R. D. (2000). Architecture of RNA polymerase II and implications for the transcription mechanism. *Science* **288**: 640-649.
- Cross, R. L. (1981). The mechanism and regulation of ATP synthesis by F₁-ATPases. *Ann. Rev. Biochem.* **50**: 681-714.
- Cross, R. L. and Boyer, P. D. (1975). The rapid labeling of adenosine triphosphate by ³²P-labeled inorganic phosphate and the exchange of phosphate oxygens as related to conformational coupling in oxidative phosphorylation. *Biochemistry* **14**: 392-398.
- Del Rizzo, P. A., Bi, Y., Dunn, S. D. and Shilton, B. H. (2002). The "second stalk" of *Escherichia coli* ATP synthase: structure of the isolated dimerization domain. *Biochemistry* **41**: 6875-6884.
- DeLano, W. L. (2002). The PYMOL molecular graphics System.
- Di Pancrazio, F., Mavelli, I., Isola, M., Losano, G., Pagliaro, P., Harris, D. A. and Lippe, G. (2004). *In vitro* and *in vivo* studies of F₀F₁-ATP synthase regulation by inhibitor protein IF₁ in goat heart. *Biochim. Biophys. Acta* **1659**: 52-62.

- Dienhart, M., Pfeifer, K., Schagger, H. and Stuart, R. (2002). Formation of the yeast F₁F_o-ATP Synthase Dimeric Complex Does Not Require the ATPase inhibitor protein Inh1. *J. Biol. Chem.* **277**: 39289-39295.
- Dimroth, P., Matthey, U. and Kaim, G. (2000). Osmomechanics of the *Propionigenium modestum* F_o motor. *J. Bioenerg. Biomem.* **32**: 449-458.
- Dimroth, P., Wang, H., Grabe, M. and Oster, G. (1999). Energy transduction in the sodium F-ATPase of *Propionigenium modestum*. *Proc. Natl. Acad. Sci. U. S. A.* **96**: 4924-4929.
- Dmitriev, O., Jones, P. C., Jiang, W. and Fillingame, R. H. (1999). Structure of the membrane domain of subunit b of the *Escherichia coli* F_oF₁ ATP synthase. *J. Biol. Chem.* **274**: 15598-15604.
- Drenth, J. (1999). Principles of protein X-ray crystallography. New York; London, Springer.
- Dunn, S. D., McLachlin, D. T. and Revington, M. (2000). The second stalk of *Escherichia coli* ATP synthase. *Biochim. Biophys. Acta* **1458**: 356-363.
- Ebel, R. E. and Lardy, H. A. (1975). Stimulation of rat liver mitochondrial adenosine triphosphatase by anions. *J. Biol. Chem.* **250**: 191-196.
- Engelbrecht, S. and Junge, W. (1997). ATP synthase: a tentative structural model. *FEBS Lett.* **414**: 485-491.
- Esnouf, R. M., Ren, J., Garman, E. F., Somers, D. O., Ross, C. K., Jones, E. Y., Stammers, D. K. and Stuart, D. I. (1998). Continuous and discontinuous changes in the unit cell

- of HIV-1 reverse transcriptase crystals on dehydration. *Acta Cryst. D Biol. Cryst.* **54**: 938-953.
- Evans, P. R. (1997). Scaling of MAD data. *Joint CCP4 and ESF-EACBM Newsletter* **33**: 22-24.
- Falk, G., Hampe, A. and Walker, J. E. (1985). Nucleotide sequence of the *Rhodospirillum rubrum atp* operon. *Biochem. J.* **228**: 391-407.
- Fearnley, I. M. and Walker, J. E. (1986). Two overlapping genes in bovine mitochondrial DNA encode membrane components of ATP synthase. *EMBO J.* **5**: 2003-2008.
- Fernandez-Moran, H. (1962). Cell-membrane ultrastructure. Low-temperature electron microscopy and X-ray diffraction studies of lipoprotein components in lamellar systems. *Circulation* **26**: 1039-1065.
- Fletcher, J. I., Swarbrick, J. D., Maksel, D., Gayler, K. R. and Gooley, P. R. (2002). The structure of Ap₄A hydrolase complexed with ATP-MgF_x reveals the basis of substrate binding. *Structure (Camb)* **10**: 205-213.
- Foster, D. L. and Fillingame, R. H. (1982). Stoichiometry of subunits in the H⁺-ATPase complex of *Escherichia coli*. *J. Biol. Chem.* **257**: 2009-2015.
- French, S. and Wilson, K. S. (1978). *Acta Cryst.* **A34**: 517.
- Frey, T. G., Renken, C. W. and Perkins, G. A. (2002). Insight into mitochondrial structure and function from electron tomography. *Biochim. Biophys. Acta* **1555**: 196-203.

- Futai, M., Noumi, T. and Maeda, M. (1989). ATP synthase (H⁺-ATPase): results by combined biochemical and molecular biological approaches. *Ann. Rev. Biochem.* **58**: 111-136.
- Gao, Y. Q., Yang, W., Marcus, R. A. and Karplus, M. (2003). A model for the cooperative free energy transduction and kinetics of ATP hydrolysis by F₁-ATPase. *Proc. Natl. Acad. Sci. U. S. A.* **100**: 11339-11344.
- Garman, E. (1999). Cool data: quantity AND quality. *Acta Cryst. D Biol. Cryst.* **55**: 1641-1653.
- Garman, E. F. and Schneider, T. R. (1997). Macromolecular Cryocrystallography. *J. Appl. Cryst.* **30**: 211-237.
- Gibbons, C., Montgomery, M. G., Leslie, A. G. and Walker, J. E. (2000). The structure of the central stalk in bovine F₁-ATPase at 2.4 Å resolution. *Nature Struct. Bio.* **7**: 1055-1061.
- Gonzalez, L., Jr., Brown, R. A., Richardson, D. and Alber, T. (1996). Crystal structures of a single coiled-coil peptide in two oligomeric states reveal the basis for structural polymorphism. *Nature Struc. Bio.* **3**: 1002-1009.
- Gordon-Smith, D. J., Carbajo, R. J., Yang, J. C., Videler, H., Runswick, M. J., Walker, J. E. and Neuhaus, D. (2001). Solution structure of a C-terminal coiled-coil domain from bovine IF₁: the inhibitor protein of F₁-ATPase. *J. Mol. Biol.* **308**: 325-339.

- Graham, D. L., Lowe, P. N., Grime, G. W., Marsh, M., Rittinger, K., Smerdon, S. J., Gamblin, S. J. and Eccleston, J. F. (2002). MgF_3^- as a transition state analog of phosphoryl transfer. *Chem. Biol.* **9**: 375-381.
- Gray, M. W., Burger, G. and Lang, B. F. (1999). Mitochondrial evolution. *Science* **283**: 1476-1481.
- Gray, M. W. and Spenser, D. F. (1996). Evolution of microbial life. Cambridge, Cambridge University Press.
- Green, D. W., Ingram, V. M. and Perutz, M. F. (1954). The structure of Haemoglobin IV. *Proc. Roy. Soc. A* **225**: 287-387.
- Gresser, M. J., Myers, J. A. and Boyer, P. D. (1982). Catalytic site cooperativity of beef heart mitochondrial F_1 adenosine triphosphatase. Correlations of initial velocity, bound intermediate, and oxygen exchange measurements with an alternating three-site model. *J. Biol. Chem.* **257**: 12030-12038.
- Grigorieff, N. (1998). Three-dimensional structure of bovine NADH:ubiquinone oxidoreductase (complex I) at 22 Å in ice. *J. Mol. Biol.* **277**: 1033-1046.
- Groth, G. and Pohl, E. (2001). The structure of the chloroplast F_1 -ATPase at 3.2 Å resolution. *J. Biol. Chem.* **276**: 1345-1352.
- Haebel, P. W., Wichman, S., Goldstone, D. and Metcalf, P. (2001). Crystallization and initial crystallographic analysis of the disulfide bond isomerase DsbC in complex with the alpha domain of the electron transporter DsbD. *J. Struct. Biol.* **136**: 162-166.

- Hashimoto, T., Negawa, Y. and Tagawa, K. (1981). Binding of intrinsic ATPase inhibitor to mitochondrial ATPase-stoichiometry of binding of nucleotides, inhibitor, and enzyme. *J. Biochem. (Tokyo)* **90**: 1151-1157.
- Hausrath, A. C., Gruber, G., Matthews, B. W. and Capaldi, R. A. (1999). Structural features of the γ subunit of the *Escherichia coli* F₁-ATPase revealed by a 4.4 Å resolution map obtained by X-ray crystallography. *Proc. Natl. Acad. Sci. U. S. A.* **96**: 13697-13702.
- Hendrickson, W. A. (1991). Determination of macromolecular structures from anomalous diffraction of synchrotron radiation. *Science* **254**: 51-58.
- Higashijima, T., Ferguson, K. M., Sternweis, P. C., Ross, E. M., Smigel, M. D. and Gilman, A. G. (1987). The effect of activating ligands on the intrinsic fluorescence of guanine nucleotide-binding regulatory proteins. *J. Biol. Chem.* **262**: 752-756.
- Higgins, C. F., Hiles, I. D., Salmond, G. P., Gill, D. R., Downie, J. A., Evans, I. J., Holland, I. B., Gray, L., Buckel, S. D., Bell, A. W. and Hermodson, M. A. (1986). A family of related ATP-binding subunits coupled to many distinct biological processes in bacteria. *Nature* **323**: 448-450.
- Higuti, T., Negama, T., Takigawa, M., Uchida, J., Yamane, T., Asai, T., Tani, I., Oeda, K., Shimizu, M., Nakamura, K. and et al. (1988). A hydrophobic protein, chargerin II, purified from rat liver mitochondria is encoded in the unidentified reading frame A6L of mitochondrial DNA. *J. Biol. Chem.* **263**: 6772-6776.

- Hong, S. and Pedersen, P. L. (2002). ATP synthase of yeast: structural insight into the different inhibitory potencies of two regulatory peptides and identification of a new potential regulator. *Arch. Biochem. Biophys.* **405**: 38-43.
- Hoppe, J., Brunner, J. and Jorgensen, B. B. (1984). Structure of the membrane-embedded F_o part of F₁F_o-ATP synthase from *Escherichia coli* as inferred from labeling with 3-(Trifluoromethyl)-3-(m-[125]iodophenyl)diazirine. *Biochemistry* **23**: 5610-5616.
- Hoppe, J. and Sebald, W. (1984). The proton conducting F_o part of bacterial ATP synthases. *Biochim. Biophys. Acta* **768**: 1-27.
- Hunte, C., Koepke, J., Lange, C., Rossmann, T. and Michel, H. (2000). Structure at 2.3 Å resolution of the cytochrome bc₁ complex from the yeast *Saccharomyces cerevisiae* co-crystallized with an antibody F_v fragment. *Structure Fold. Des.* **8**: 669-684.
- Ichikawa, N., Karaki, A., Kawabata, M., Ushida, S., Mizushima, M. and Hashimoto, T. (2001). The region from phenylalanine-17 to phenylalanine-28 of a yeast mitochondrial ATPase inhibitor is essential for its ATPase inhibitory activity. *J. Biochem. (Tokyo)* **130**: 687-693.
- Ichikawa, N. and Ogura, C. (2003). Overexpression, purification, and characterization of human and bovine mitochondrial ATPase inhibitors: comparison of the properties of mammalian and yeast ATPase inhibitors. *J. Bioenerg. Biomemb.* **35**: 399-407.
- Issartel, J. P., Dupuis, A., Lunardi, J. and Vignais, P. V. (1991). Fluoroaluminum and fluoroberyllium nucleoside diphosphate complexes as probes of the enzymatic mechanism of the mitochondrial F₁-ATPase. *Biochemistry* **30**: 4726-4733.

- Itoh, H., Takahashi, A., Adachi, K., Noji, H., Yasuda, R., Yoshida, M. and Kinosita, K. (2004). Mechanically driven ATP synthesis by F_1 -ATPase. *Nature* **427**: 465-468.
- Iwata, S., Lee, J. W., Okada, K., Lee, J. K., Iwata, M., Rasmussen, B., Link, T. A., Ramaswamy, S. and Jap, B. K. (1998). Complete structure of the 11-subunit bovine mitochondrial cytochrome bc_1 complex. *Science* **281**: 64-71.
- Jensen, R. E. and Dunn, C. D. (2002). Protein import into and across the mitochondrial inner membrane: role of the TIM23 and TIM22 translocons. *Biochim. Biophys. Acta.* **1592**: 25-34.
- Jiang, W., Hermolin, J. and Fillingame, R. H. (2001). The preferred stoichiometry of c subunits in the rotary motor sector of *Escherichia coli* ATP synthase is 10. *Proc. Natl. Acad. Sci. U. S. A.* **98**: 4966-4971.
- Jones, P. C., Hermolin, J., Jiang, W. and Fillingame, R. H. (2000). Insights into the rotary catalytic mechanism of F_0F_1 -ATP synthase from the cross-linking of subunits b and c in the *Escherichia coli* enzyme. *J. Biol. Chem.* **275**: 31340-31346.
- Jones, T. A., Zou, J. Y., Cowan, S. W. and Kjeldgaard, M. (1991). Improved methods for building protein models in electron density maps and the location of errors in these models. *Acta Cryst. A* **47**: 110-119.
- Joshi, S., Cao, G. J., Nath, C. and Shah, J. (1996). Oligomycin sensitivity conferring protein of mitochondrial ATP synthase: deletions in the N-terminal end cause defects in interactions with F_1 , while deletions in the C-terminal end cause defects in interactions with F_0 . *Biochemistry* **35**: 12094-12103.

Junge, W., Lill, H. and Engelbrecht, S. (1997). ATP synthase: an electrochemical transducer with rotatory mechanics. *Trends Biochem. Sci.* **22**: 420-423.

Kagawa, R., Montgomery, M. G., Braig, K., Leslie, A. G. W. and Walker, J. E. (2004). The structure of bovine F₁-ATPase inhibited by ADP and beryllium fluoride. *EMBO J.* **23**: 2734-2744.

Kagawa, Y. and Racker, E. (1966a). Partial resolution of the enzymes catalyzing oxidative phosphorylation. VIII. Properties of a factor conferring oligomycin sensitivity on mitochondrial adenosine triphosphatase. *J. Biol. Chem.* **241**: 2461-2466.

Kagawa, Y. and Racker, E. (1966b). Partial resolution of the enzymes catalyzing oxidative phosphorylation. X. Correlation of morphology and function in submitochondrial particles. *J. Biol. Chem.* **241**: 2475-2482.

Kagawa, Y. and Racker, E. (1966c). Partial resolution of the enzymes catalyzing oxidative phosphorylation. IX. Reconstruction of oligomycin-sensitive adenosine triphosphatase. *J. Biol. Chem.* **241**: 2467-2474.

Karrasch, S. and Walker, J. E. (1999). Novel features in the structure of bovine ATP synthase. *J. Mol. Biol.* **290**: 379-384.

Kendrew, J. C., Bodo, G., Dintzis, H. M., Parrish, R. G., Wyckoff, H. and Phillips, D. C. (1958). A three dimensional model of the myoglobin molecule obtained by X-ray analysis. *Nature* **181**: 662-666.

- Klabunde, T., Strater, N., Frohlich, R., Witzel, H. and Krebs, B. (1996). Mechanism of Fe(III)-Zn(II) purple acid phosphatase based on crystal structures. *J. Mol. Biol.* **259**: 737-748.
- Knowles, J. R. (1980). Enzyme-catalyzed phosphoryl transfer reactions. *Annu. Rev. Biochem.* **49**: 877-919.
- Kuo, A., Bowler, M. W., Zimmer, J., Antcliff, J. F. and Doyle, D. A. (2003). Increasing the diffraction limit and internal order of a membrane protein crystal by dehydration. *J. Struct. Biol.* **141**: 97-102.
- Laemmli, U. K. (1970). Cleavage of structural proteins during the assembly of the head of bacteriophage T4. *Nature* **227**: 680-685.
- Lahiri, S. D., Zhang, G., Dunaway-Mariano, D. and Allen, K. N. (2003). The pentacovalent phosphorus intermediate of a phosphoryl transfer reaction. *Science* **299**: 2067-2071.
- Lange, C. and Hunte, C. (2002). Crystal structure of the yeast cytochrome bc₁ complex with its bound substrate cytochrome c. *Proc. Natl. Acad. Sci. U. S. A.* **99**: 2800-2805.
- Laskowski, R. A., MacArthur, M. W., Moss, D. S. and Thornton, J. M. (1992). PROCHECK - A program to check the stereochemical quality of protein structures. *J. Appl. Cryst.* **26**: 283-291.
- Laue, T. M., Shah, B. D., Ridgeway, T. M. and Pelletier, S. L. (1992). Analytical Ultracentrifugation in Biochemistry and Polymer Science. S. E. Harding, Rowe, A. J. and Horton, J. C. Cambridge, UK, Royal Society of Chemistry: 90-125.

- Leslie, A. G. W. (1992). Recent changes to the MOSFLM package for processing film and image plate data. *Joint CCP4 and EACMB Newsletter on Protein Crystallography* **26**: Warrington: Daresbury Laboratory.
- Lindqvist, Y., Schneider, G. and Vihko, P. (1994). Crystal structures of rat acid phosphatase complexed with the transition-state analogs vanadate and molybdate. Implications for the reaction mechanism. *Eur. J. Biochem.* **221**: 139-142.
- Lithgow, T. (2000). Targeting of proteins to mitochondria. *FEBS Lett.* **476**: 22-26.
- Lodish, H., Berk, A., Zipursky, L. S., Matsudaira, P., Baltimore, D. and Darnell, J. (2000). *Molecular cell biology*. New York, W. H. Freeman.
- Lolkema, J. S. and Boekema, E. J. (2003). The A-type ATP synthase subunit K of *Methanopyrus kandleri* is deduced from its sequence to form a monomeric rotor comprising 13 hairpin domains. *FEBS Lett.* **543**: 47-50.
- Lunardi, J., Dupuis, A., Garin, J., Issartel, J. P., Michel, L., Chabre, M. and Vignais, P. V. (1988). Inhibition of H⁺-transporting ATPase by formation of a tight nucleoside diphosphate-fluoroaluminate complex at the catalytic site. *Proc. Natl. Acad. Sci. U. S. A.* **85**: 8958-8962.
- Lutter, R., Abrahams, J. P., van Raaij, M. J., Todd, R. J., Lundqvist, T., Buchanan, S. K., Leslie, A. G. W. and Walker, J. E. (1993). Crystallization of F₁-ATPase from bovine heart mitochondria. *J. Mol. Biol.* **229**: 787-790.
- Mannella, C. A., Marko, M. and Buttle, K. (1997). Reconsidering mitochondrial structure: new views of an old organelle. *Trends Biochem. Sci.* **22**: 37-38.

- Martin, R. B. (1988). Ternary hydroxide complexes in neutral solutions of Al^{3+} and F.
Biochem. Biophys. Res. Commun. **155**: 1194-1200.
- Matsubara, H., Hase, T., Hashimoto, T. and Tagawa, K. (1981). Amino acid sequence of an intrinsic inhibitor of mitochondrial ATPase from yeast. *J. Biochem. (Tokyo)* **90**: 1159-1165.
- Mayer, M. P. (2004). Timing the catch. *Nat. Struct. Mol. Biol.* **11**: 6-8.
- Mendel-Hartvig, J. and Capaldi, R. A. (1991). Structure-function relationships of domains of the δ subunit in *Escherichia coli* adenosine triphosphatase. *Biochim. Biophys. Acta* **1060**: 115-124.
- Menz, R. I., Leslie, A. G. W. and Walker, J. E. (2001a). The structure and nucleotide occupancy of bovine mitochondrial F_1 -ATPase are not influenced by crystallisation at high concentrations of nucleotide. *FEBS Lett.* **494**: 11-14.
- Menz, R. I., Walker, J. E. and Leslie, A. G. W. (2001b). Structure of bovine mitochondrial F_1 -ATPase with nucleotide bound to all three catalytic sites: implications for the mechanism of rotary catalysis. *Cell* **106**: 331-341.
- Miroux, B. and Walker, J. E. (1996). Over-production of proteins in *Escherichia coli*: mutant hosts that allow synthesis of some membrane proteins and globular proteins at high levels. *J. Mol. Biol.* **260**: 289-298.
- Mitchell, P. (1961). Coupling of phosphorylation to electron and hydrogen transfer by a chemi-osmotic type of mechanism. *Nature* **191**: 144-148.

- Mitome, N., Suzuki, T., Hayashi, S. and Yoshida, M. (2004). Thermophilic ATP synthase has a decamer c-ring: indication of noninteger 10:3 H⁺/ATP ratio and permissive elastic coupling. *Proc. Natl. Acad. Sci. U. S. A.* **101**: 12159-12164.
- Mueller, D. M., Puri, N., Kabaleeswaran, V., Terry, C., Leslie, A. G. and Walker, J. E. (2004). Ni-chelate-affinity purification and crystallization of the yeast mitochondrial F₁-ATPase. *Protein exp. purif.* **37**: 479-485.
- Murshudov, G. N., Vagin, A. A. and Dodson, E. J. (1997). Refinement of macromolecular structures by the maximum-likelihood method. *Acta Cryst. D Biol. Cryst.* **53**: 240-255.
- Nalin, C. M. and McCarty, R. E. (1984). Role of a disulfide bond in the γ subunit in activation of the ATPase of chloroplast coupling factor 1. *J. Biol. Chem.* **259**: 7275-7280.
- Navaza, J. (1994). AMoRe: an automated package for molecular replacement. *Acta Cryst. A* **50**: 157-163.
- Nicholls, D. G. and Ferguson, S. J. (2002). *Bioenergetics 3*. Amsterdam; London, Academic Press.
- Nishio, K., Iwamoto-Kihara, A., Yamamoto, A., Wada, Y. and Futai, M. (2002). Subunit rotation of ATP synthase embedded in membranes: α or β subunit rotation relative to the c subunit ring. *Proc. Natl. Acad. Sci. U. S. A.* **99**: 13448-13452.

- Nishizaka, T., Oiwa, K., Noji, H., Kimura, S., Muneyuki, E., Yoshida, M. and Kinoshita, K., Jr. (2004). Chemomechanical coupling in F₁-ATPase revealed by simultaneous observation of nucleotide kinetics and rotation. *Nat. Struct. Mol. Biol.* **11**: 142-148.
- Noji, H., Yasuda, R., Yoshida, M. and Kinoshita, K., Jr. (1997). Direct observation of the rotation of F₁-ATPase. *Nature* **386**: 299-302.
- Norling, B., Tourikas, C., Hamasur, B. and Glaser, E. (1990). Evidence for an endogenous ATPase inhibitor protein in plant mitochondria. Purification and characterization. *Eur. J. Biochem.* **188**: 247-252.
- Okada, Y., Hashimoto, T., Yoshida, Y. and Tagawa, K. (1986). Existence of stoichiometric amounts of an intrinsic ATPase inhibitor and two stabilizing factors with mitochondrial ATP synthase in yeast. *J. Biochem. (Tokyo)* **99**: 251-256.
- Orriss, G. L., Leslie, A. G. W., Braig, K. and Walker, J. E. (1998). Bovine F₁-ATPase covalently inhibited with 4-chloro-7-nitrobenzofurazan: the structure provides further support for a rotary catalytic mechanism. *Structure* **6**: 831-837.
- Ostermeier, C., Harrenga, A., Ermler, U. and Michel, H. (1997). Structure at 2.7 Å resolution of the *Paracoccus denitrificans* two-subunit cytochrome c oxidase complexed with an antibody Fv fragment. *Proc. Natl. Acad. Sci. U. S. A.* **94**: 10547-10553.
- Palade, G. E. (1953). An electron microscope study of the mitochondrial structure. *J. Histochem. Cytochem.* **1**: 188-211.
- Paschen, S. A. and Neupert, W. (2001). Protein import into mitochondria. *IUBMB Life* **52**: 101-112.

- Paumard, P., Arselin, G., Vaillier, J., Chaignepain, S., Bathany, K., Schmitter, J. M., Brethès, D. and Velours, J. (2002a). Two ATP synthases can be linked through subunits i in the inner mitochondrial membrane of *Saccharomyces cerevisiae*. *Biochemistry* **41**: 10390-10396.
- Paumard, P., Vaillier, J., Couлары, B., Schaeffer, J., Soubannier, V., Mueller, D. M., Brethès, D., di Rago, J. P. and Velours, J. (2002b). The ATP synthase is involved in generating mitochondrial cristae morphology. *EMBO J.* **21**: 221-230.
- Paumard, P., Vaillier, J., Napias, C., Arselin, G., Brethès, D., Graves, P. V. and Velours, J. (2000). Environmental study of subunit i, a F₀ component of the yeast ATP synthase. *Biochemistry* **39**: 4199-4205.
- Pebay-Peyroula, E., Dahout-Gonzalez, C., Kahn, R., Trezeguet, V., Lauquin, G. J. and Brandolin, G. (2003). Structure of mitochondrial ADP/ATP carrier in complex with carboxyatractyloside. *Nature* **426**: 39-44.
- Philo, J. S. (2000). A method for directly fitting the time derivative of sedimentation velocity data and an alternative algorithm for calculating sedimentation coefficient distribution functions. *Anal. Biochem.* **279**: 151-163.
- Pullman, M. E. and Monroy, G. C. (1963). A naturally occurring inhibitor of mitochondrial adenosine triphosphatase. *J. Biol. Chem.* **238**: 3762-3769.
- Pullman, M. E., Penefsky, H., Datta, A. and Racker, E. (1960). Partial resolution of the enzymes catalysing oxidative phosphorylation. Purification and properties of soluble, dinitrophenol-stimulated adenosine triphosphatase. *J. Biol. Chem.* **238**: 3322-3329.

- Ramachandran, G. N., Ramakrishnan, C. and Sasisekharan, V. (1963). Stereochemistry of polypeptide chain configurations. *J. Mol. Biol.* **7**: 95-99.
- Ramakrishnan, C. and Ramachandran, G. N. (1965). Stereochemical criteria for polypeptide and protein chain conformations. II. Allowed conformations for a pair of peptide units. *Biophys. J.* **5**: 909-933.
- Rastogi, V. K. and Girvin, M. E. (1999). Structural changes linked to proton translocation by subunit c of the ATP synthase. *Nature* **402**: 263-268.
- Richter, M. L., Hein, R. and Huchzermeyer, B. (2000). Important subunit interactions in the chloroplast ATP synthase. *Biochim. Biophys. Acta* **1458**: 326-342.
- Rodgers, A. J. and Wilce, M. C. (2000). Structure of the gamma-epsilon complex of ATP synthase. *Nature Struct. Bio.* **7**: 1051-1054.
- Rosenbaum, G., Holmes, K. G. and Witz, J. (1971). Synchrotron radiation as a source for X-ray diffraction. *Nature* **230**: 434-437.
- Rossmann, M. G. and Blow, D. M. (1962). The detection of subunits within the crystallographic asymmetric unit. *Acta Cryst.* **16**.
- Roudeau, S., Spannagel, C., Vaillier, J., Arselin, G., Graves, P. V. and Velours, J. (1999). Subunit f of the yeast mitochondrial ATP synthase: topological and functional studies. *J. Bioenerg. Biomembr.* **31**: 85-94.
- Rouslin, W. (1983). Protonic inhibition of the mitochondrial oligomycin-sensitive adenosine 5'-triphosphatase in ischemic and autolyzing cardiac muscle. Possible mechanism for

- the mitigation of ATP hydrolysis under nonenergizing conditions. *J. Biol. Chem.* **258**: 9657-9661.
- Rubinstein, J., Kane Dickson, V., Runswick, M. J. and Walker, J. E. (2004). ATP synthase from *Saccharomyces cerevisiae*: Location of subunit h in the peripheral stalk region. *J. Mol. Biol.* **345**: 513-520.
- Rubinstein, J. and Walker, J. (2002). ATP synthase from *Saccharomyces cerevisiae*: location of the OSCP subunit in the peripheral stalk region. *J. Mol. Biol.* **321**: 613-619.
- Rubinstein, J. L., Walker, J. E. and Henderson, R. (2003). Structure of the mitochondrial ATP synthase by electron cryomicroscopy. *EMBO J.* **22**: 6182-6192.
- Saiki, R. K., Scharf, S., Faloona, F., Mullis, K. B., Horn, G. T., Erlich, H. A. and Arnheim, N. (1985). Enzymatic amplification of beta-globin genomic sequences and restriction site analysis for diagnosis of sickle cell anemia. *Science* **230**: 1350-1354.
- Sambongi, Y., Iko, Y., Tanabe, M., Omote, H., Iwamoto-Kihara, A., Ueda, I., Yanagida, T., Wada, Y. and Futai, M. (1999). Mechanical rotation of the c subunit oligomer in ATP synthase (F₀F₁): direct observation. *Science* **286**: 1722-1724.
- Saraste, M. (1999). Oxidative phosphorylation at the *fin de siècle*. *Science* **283**: 1488-1493.
- Schagger, H. and Pfeiffer, K. (2000). Supercomplexes in the respiratory chains of yeast and mammalian mitochondria. *EMBO. J.* **19**: 1777-1783.

- Schmidt, R. A., Qu, J., Williams, J. R. and Brusilow, W. S. (1998). Effects of carbon source on expression of F_o genes and on the stoichiometry of the c subunit in the F_1F_o -ATPase of *Escherichia coli*. *J. Bacteriol.* **180**: 3205-3208.
- Schlichting, I. and Reinstein, J. (1997). Structures of active conformations of UMP kinase from *Dictyostelium discoideum* suggest phosphoryl transfer is associative. *Biochemistry* **36**: 9290-9296.
- Schneider, E. and Altendorf, K. (1985). All three subunits are required for the reconstitution of an active proton channel (F_o) of *Escherichia coli* ATP synthase (F_1F_o). *EMBO J.* **4**: 515-518.
- Schnizer, R., Van Heeke, G., Amaturio, D. and Schuster, S. M. (1996). Histidine-49 is necessary for the pH-dependent transition between active and inactive states of the bovine F_1 -ATPase inhibitor protein. *Biochim. Biophys. Acta* **1292**: 241-248.
- Schwarz, O., Schurmann, P. and Strotmann, H. (1997). Kinetics and thioredoxin specificity of thiol modulation of the chloroplast H^+ -ATPase. *J. Biol. Chem.* **272**: 16924-16927.
- Schägger, H. and Pfeiffer, K. (2000). Supercomplexes in the respiratory chains of yeast and mammalian mitochondria. *EMBO J.* **19**: 1777-1783.
- Seelert, H., Poetsch, A., Dencher, N. A., Engel, A., Stahlberg, H. and Müller, D. J. (2000). Structural biology. Proton-powered turbine of a plant motor. *Nature* **405**: 418-419.
- Shirakihara, Y., Leslie, A. G. W., Abrahams, J. P., Walker, J. E., Ueda, T., Sekimoto, Y., Kambara, M., Saika, K., Kagawa, Y. and Yoshida, M. (1997). The crystal structure of

- the nucleotide free $\alpha_3\beta_3$ subcomplex of F_1 -ATPase from the thermophilic *Bacillus* PS3 is a symmetric trimer. *Structure* **5**: 825-836.
- Smith, J. B. and Sternweis, P. C. (1977). Purification of membrane attachment and inhibitory subunits of the proton translocating adenosine triphosphatase from *Escherichia coli*. *Biochemistry* **16**: 306-311.
- Smith, P. K., Krohn, R. I., Hermanson, G. T., Mallia, A. K., Gartner, F. H., Provenzano, M. D., Fujimoto, E. K., Goeke, N. M., Olson, B. J. and Klenk, D. C. (1985). Measurement of protein using bicinchoninic acid. *Anal. Biochem.* **150**: 76-85.
- Sondek, J., Lambright, D. G., Noel, J. P., Hamm, H. E. and Sigler, P. B. (1994). GTPase mechanism of G proteins from the 1.7 Å crystal structure of transducin α -GDP-AIF₄. *Nature* **372**: 276-279.
- Sorensen, T. L., Moller, J. V. and Nissen, P. (2004). Phosphoryl transfer and calcium ion occlusion in the calcium pump. *Science* **304**: 1672-1675.
- Soulimane, T., Buse, G., Bourenkov, G. P., Bartunik, H. D., Huber, R. and Than, M. E. (2000). Structure and mechanism of the aberrant ba_3 -cytochrome c oxidase from *Thermus thermophilus*. *EMBO J.* **19**: 1766-1776.
- Stahlberg, H., Müller, D. J., Suda, K., Fotiadis, D., Engel, A., Meier, T., Matthey, U. and Dimroth, P. (2001). Bacterial Na^+ -ATP synthase has an undecameric rotor. *EMBO Rep.* **2**: 229-233.

- Sternweis, P. C. and Gilman, A. G. (1982). Aluminum: a requirement for activation of the regulatory component of adenylate cyclase by fluoride. *Proc. Natl. Acad. Sci. U. S. A.* **79**: 4888-4891.
- Stock, D., Leslie, A. G. W. and Walker, J. E. (1999). Molecular architecture of the rotary motor in ATP synthase. *Science* **286**: 1700-1705.
- Studier, F. W. and Moffatt, B. A. (1986). Use of bacteriophage T7 RNA polymerase to direct selective high-level expression of cloned genes. *J. Mol. Biol.* **189**: 113-130.
- Svensson-Ek, M., Abramson, J., Larsson, G., Tornroth, S., Brzezinski, P. and Iwata, S. (2002). The X-ray crystal structures of wild-type and EQ(I-286) mutant cytochrome c oxidases from *Rhodobacter sphaeroides*. *J. Mol. Biol.* **321**: 329-339.
- Süss, K.-H. and Schmidt, O. (1982). Evidence for an α_3 , β_3 , γ , δ , I, II, ϵ , III₅ subunit stoichiometry of chloroplast ATP synthetase complex (CF₁-CF₀). *FEBS Lett.* **144**: 213-218.
- Teng, T.-Y. (1990). Mounting of crystals for macromolecular crystallography in a free-standing thin-film. *J. Appl. Cryst.* **23**: 387-391.
- Thomas, D. R., Morgan, D. G. and DeRosier, D. J. (1999). Rotational symmetry of the C ring and a mechanism for the flagellar rotary motor. *Proc. Natl. Acad. Sci. U. S. A.* **96**: 10134-10139.
- Thompson, J. D., Higgins, D. G. and Gibson, T. J. (1994). CLUSTAL W: improving the sensitivity of progressive multiple sequence alignment through sequence weighting,

- position-specific gap penalties and weight matrix choice. *Nucleic Acids Res.* **22**: 4673-4680.
- Toyoshima, C. and Mizutani, T. (2004). Crystal structure of the calcium pump with a bound ATP analogue. *Nature* **430**: 529-535.
- Toyoshima, C., Nakasako, M., Nomura, H. and Ogawa, H. (2000). Crystal structure of the calcium pump of sarcoplasmic reticulum at 2.6 Å resolution. *Nature* **405**: 647-655.
- Toyoshima, C. and Nomura, H. (2002). Structural changes in the calcium pump accompanying the dissociation of calcium. *Nature* **418**: 605-611.
- Toyoshima, C., Nomura, H. and Tsuda, T. (2004). Lumenal gating mechanism revealed in calcium pump crystal structures with phosphate analogues. *Nature* **432**: 361-368.
- Tsunoda, S. P., Rodgers, A. J., Aggeler, R., Wilce, M. C., Yoshida, M. and Capaldi, R. A. (2001). Large conformational changes of the ϵ subunit in the bacterial F_1F_0 ATP synthase provide a ratchet action to regulate this rotary motor enzyme. *Proc. Natl. Acad. Sci. U. S. A.* **98**: 6560-6564.
- Tybulewicz, V. L., Falk, G. and Walker, J. E. (1984). *Rhodospseudomonas blastica atp* operon. Nucleotide sequence and transcription. *J. Mol. Biol.* **179**: 185-214.
- Vaillier, J., Arselin, G., Graves, P. V., Camougrand, N. and Velours, J. (1999). Isolation of supernumerary yeast ATP synthase subunits e and i. Characterization of subunit i and disruption of its structural gene ATP18. *J. Biol. Chem.* **274**: 543-548.

- Valiyaveetil, F. I. and Fillingame, R. H. (1998). Transmembrane topography of subunit a in the *Escherichia coli* F₁F_o ATP synthase. *J. Biol. Chem.* **273**: 16241-16247.
- van Raaij, M. J., Abrahams, J. P., Leslie, A. G. and Walker, J. E. (1996a). The structure of bovine F₁-ATPase complexed with the antibiotic inhibitor aurovertin B. *Proc. Natl. Acad. Sci. U. S. A.* **93**: 6913-6917.
- van Raaij, M. J., Orriss, G. L., Montgomery, M. G., Runswick, M. J., Fearnley, I. M., Skehel, J. M. and Walker, J. E. (1996b). The ATPase inhibitor protein from bovine heart mitochondria: the minimal inhibitory sequence. *Biochemistry* **35**: 15618-15625.
- van Walraven, H. S., Gravesen, M. and Kraayenhof, R. (1984). Purification of a high molecular weight membrane protein by fast protein liquid chromatography: the ATPase complex of a thermophilic cyanobacterium. *J. Biochem. Biophys. Met.* **9**: 163-169.
- van Walraven, H. S., Lutter, R. and Walker, J. E. (1993). Organization and sequences of genes for the subunits of ATP synthase in the thermophilic cyanobacterium *Synechococcus* 6716. *Biochem. J.* **294**: 239-251.
- van Walraven, H. S., Strotmann, H., Schwarz, O. and Rumberg, B. (1996). The H⁺/ATP coupling ratio of the ATP synthase from thiol-modulated chloroplasts and two cyanobacterial strains is four. *FEBS Lett.* **379**: 309-313.
- Velours, J. and Arselin, G. (2000). The *Saccharomyces cerevisiae* ATP synthase. *J. Bioenerg. Biomembr.* **32**: 383-390.

- Venard, R., Brèthes, D., Giraud, M. F., Vaillier, J., Velours, J. and Haraux, F. (2003). Investigation of the role and mechanism of IF₁ and STF₁ proteins, twin inhibitory peptides which interact with the yeast mitochondrial ATP synthase. *Biochemistry* **42**: 7626-7636.
- von Heijne, G. (1986). Mitochondrial targeting sequences may form amphiphilic helices. *EMBO J.* **5**: 1335-1342.
- Vonck, J., von Nidda, T. K., Meier, T., Matthey, U., Mills, D. J., Kühlbrandt, W. and Dimroth, P. (2002). Molecular architecture of the undecameric rotor of a bacterial Na⁺-ATP synthase. *J. Mol. Biol.* **321**: 307-316.
- Wada, T., Long, J. C., Zhang, D. and Vik, S. B. (1999). A novel labeling approach supports the five-transmembrane model of subunit a of the *Escherichia coli* ATP synthase. *J. Biol. Chem.* **274**: 17353-17357.
- Walker, J. E. (1994). The regulation of catalysis in ATP synthase. *Curr. Opin. Struct. Biol.* **4**: 912-918.
- Walker, J. E. (1998). ATP synthesis by rotary catalysis (Nobel lecture). *Angewandte Chemie - international edition* **37**: 2309-2319.
- Walker, J. E., Falk, G., Gay, N. J. and Tybulewicz, V. L. (1984a). Genes for bacterial and mitochondrial ATP synthase. *Biochem. Soc. Trans.* **12**: 234-235.
- Walker, J. E., Fearnley, I. M., Gay, N. J., Gibson, B. W., Northrop, F. D., Powell, S. J., Runswick, M. J., Saraste, M. and Tybulewicz, V. L. (1985). Primary structure and

- subunit stoichiometry of F₁-ATPase from bovine mitochondria. *J. Mol. Biol.* **184**: 677-701.
- Walker, J. E., Gay, N. J., Powell, S. J., Kostina, M. and Dyer, M. R. (1987). ATP synthase from bovine mitochondria: sequences of imported precursors of oligomycin sensitivity conferral protein, factor 6, and adenosinetriphosphatase inhibitor protein. *Biochemistry* **26**: 8613-8619.
- Walker, J. E., Lutter, R., Dupuis, A. and Runswick, M. J. (1991). Identification of the subunits of F₁F₀-ATPase from bovine heart mitochondria. *Biochemistry* **30**: 5369-5378.
- Walker, J. E. and Runswick, M. J. (1993). The mitochondrial transport protein superfamily. *J. Bioenerg. Biomembr.* **25**: 435-446.
- Walker, J. E., Saraste, M. and Gay, N. J. (1984b). The *unc* operon. Nucleotide sequence, regulation and structure of ATP synthase. *Biochim. Biophys. Acta* **768**: 164-200.
- Walker, J. E., Saraste, M., Runswick, M. J. and Gay, N. J. (1982). Distantly related sequences in the α and β subunits of ATP synthase, myosin, kinases and other ATP-requiring enzymes and a common nucleotide binding fold. *EMBO J.* **1**: 945-951.
- Webb, M. R., Grubmeyer, C., Penefsky, H. S. and Trentham, D. R. (1980). The stereochemical course of phosphoric residue transfer catalyzed by beef heart mitochondrial ATPase. *J. Biol. Chem.* **255**: 11637-11639.

- Weber, J., Bowman, C. and Senior, A. E. (1996). Specific tryptophan substitution in catalytic sites of *Escherichia coli* F₁-ATPase allows differentiation between bound substrate ATP and product ADP in steady-state catalysis. *J. Biol. Chem.* **271**: 18711-18718.
- Weber, J., Dunn, S. D. and Senior, A. E. (1999). Effect of the ϵ subunit on nucleotide binding to *Escherichia coli* F₁-ATPase catalytic sites. *J. Biol. Chem.* **274**: 19124-19128.
- Weber, J. and Senior, A. E. (2000). ATP synthase: what we know about ATP hydrolysis and what we do not know about ATP synthesis. *Biochim. Biophys. Acta* **1458**: 300-309.
- Webster, C. E. (2004). High-energy intermediate or stable transition state analogue: theoretical perspective of the active site and mechanism of β -phosphoglucomutase. *J. Am. Chem. Soc.* **126**: 6840-6841.
- Weissmann, G. and Claiborne, R. (1975). Cell membranes: biochemistry, cell biology, & pathology. New York, HP Publishing Co.
- Westheimer, F. H. (1981). Monomeric metaphosphates. *Chem. Rev.* **4**: 313-326.
- Wiedemann, N., Pfanner, N. and Ryan, M. T. (2001). The three modules of ADP/ATP carrier cooperate in receptor recruitment and translocation into mitochondria. *EMBO J.* **20**: 951-960.
- Wilkins, S. and Capaldi, R. A. (1998). Electron microscopic evidence of two stalks linking the F₁ and F_o parts of the *Escherichia coli* ATP synthase. *Biochim. Biophys. Acta* **1365**: 93-97.

- Wilkins, S., Rodgers, A., Ogilvie, I. and Capaldi, R. A. (1997). Structure and arrangement of the δ subunit in the *E. coli* ATP synthase (ECF_1F_0). *Biophys. Chem.* **68**: 95-102.
- Wolf, E., Kim, P. S. and Berger, B. (1997). MultiCoil: a program for predicting two- and three-stranded coiled coils. *Protein Sci.* **6**: 1179-1189.
- Yankovskaya, V., Horsefield, R., Tornroth, S., Luna-Chavez, C., Miyoshi, H., Leger, C., Byrne, B., Cecchini, G. and Iwata, S. (2003). Architecture of succinate dehydrogenase and reactive oxygen species generation. *Science* **299**: 700-704.
- Yasuda, R., Noji, H., Yoshida, M., Kinosita, K., Jr. and Itoh, H. (2001). Resolution of distinct rotational substeps by submillisecond kinetic analysis of F_1 -ATPase. *Nature* **410**: 898-904.
- Yoshikawa, S., Shinzawa-Itoh, K., Nakashima, R., Yaono, R., Yamashita, E., Inoue, N., Yao, M., Fei, M. J., Libeu, C. P., Mizushima, T., Yamaguchi, H., Tomizaki, T. and Tsukihara, T. (1998). Redox-coupled crystal structural changes in bovine heart cytochrome c oxidase. *Science* **280**: 1723-1729.
- Zhang, P., Toyoshima, C., Yonekura, K., Green, N. M. and Stokes, D. L. (1998). Structure of the calcium pump from sarcoplasmic reticulum at 8 Å resolution. *Nature* **392**: 835-839.